

IL
NUOVO CIMENTO

ORGANO DELLA SOCIETÀ ITALIANA DI FISICA

SOTTO GLI AUSPICI DEL CONSIGLIO NAZIONALE DELLE RICERCHE

VOL. I, N. 5

Serie decima

1° Maggio 1955

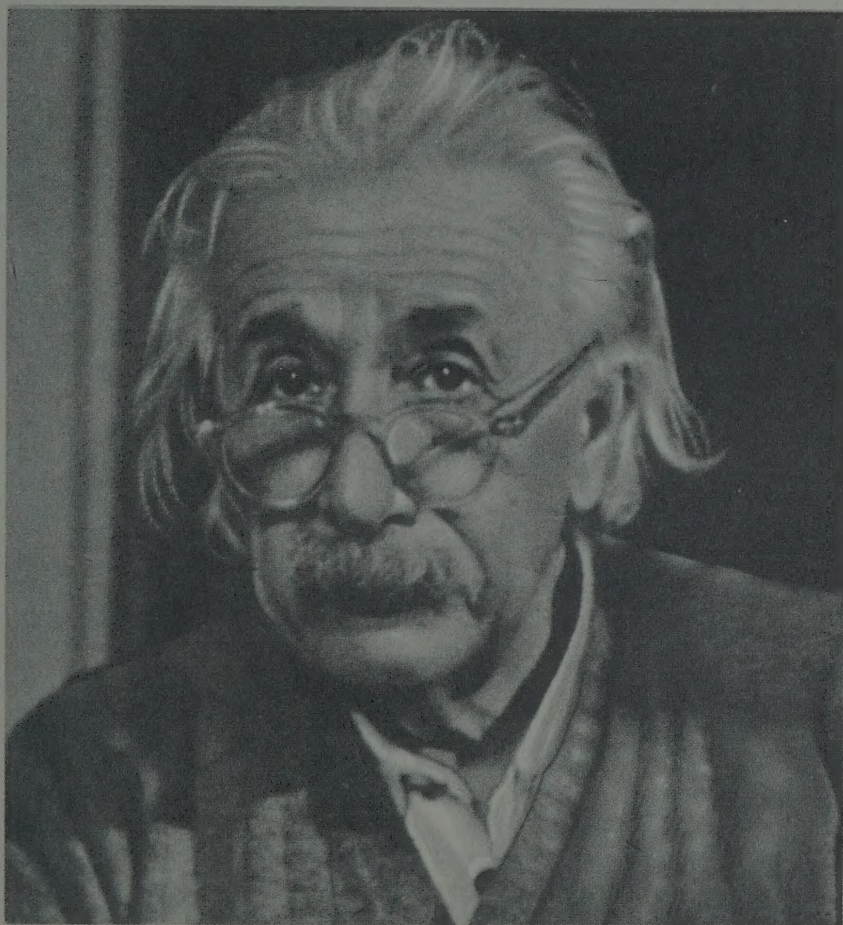
████████████████████

ALBERT EINSTEIN

È MORTO

IL GIORNO 18 APRILE 1955

████████████████████



ALBERT EINSTEIN

* Ulm, 14 Marzo 1879

† Princeton, N. J., 18 Aprile 1955



STAMPATO IN ITALIA
DALLA TIPOGRAFIA "L'ESPRESSO"
VIA MONTENAPOLEONE, 10 - 00187 ROMA

SOCIETÀ ITALIANA DI FISICA
SCUOLA INTERNAZIONALE DI FISICA

Sotto gli auspici del Ministero della Pubblica Istruzione
e del Consiglio Nazionale delle Ricerche

CORSO ESTIVO A VARENNA, SUL LAGO DI COMO

17 Luglio - 6 Agosto 1955

- 1) Quest'anno, 1955, con il contributo del Ministero della Pubblica Istruzione, del Consiglio Nazionale delle Ricerche, del Comitato Nazionale per le Ricerche Nucleari, dell'Università di Milano, delle Autorità e di Enti, Società e privati della Provincia di Como, la Scuola Internazionale di Fisica della Società Italiana di Fisica terrà a Varenna, sul Lago di Como, nella Villa Monastero — messa gentilmente a disposizione, insieme con il parco annesso, dall'Ente Villa Monastero, — il 3° *Corso estivo* nel quale verranno trattate, in modo organico, approfondito e critico, le seguenti *questioni di Fisica Nucleare*:

- *Struttura e modelli del nucleo, con particolare riguardo a quelli a shell e collettivi*;
- *Nuove specie di atomi: positonio, atomi mesici; tecniche relative*;
- *Ottica Neutronica*;
- *Momenti nucleari*;
- *Questioni generali e particolari della Fisica del reattore.*

Le lezioni saranno affidate rispettivamente ai seguenti professori:

AAGE BOHR, professore all'Università di Copenhagen,

SERGIO DE BENEDETTI, professore al Carnegie Institute of Technology, Pittsburgh Penn. (U.S.A.),

GEORGE PLACZEK, Professore alla Columbia University, New-York (U.S.A.);

I. ISIDOR RABI, professore alla Columbia University, New York (U.S.A.),

ALVIN M. WEINBERG, direttore delle ricerche al Oak Ridge National Laboratory (U.S.A.).

Infine seminari e conferenze su questioni connesse con quelle che costituiscono l'oggetto del Corso saranno tenute da eminenti fisici di varie nazionalità.

Le lezioni, i seminari, le conferenze e le discussioni saranno di regola tenuti in inglese o in francese

- 2) La Direzione del Corso è affidata al professore CARLO SALVETTI, professore di Radioattività all'Università di Milano.
- 3) Il corso avrà la durata di 21 giorno: si inizierà alle ore 18 di Domenica 17 Luglio, e si chiuderà il pomeriggio di Sabato 6 Agosto con la solenne commemorazione di Enrico Fermi a Varenna e al Tempio Voltiano a Como,
- Le lezioni, i seminari, le conferenze saranno distribuiti dal Direttore tra le 8,30 e le 11 della mattina e le 17,30 e le 19,30 del pomeriggio di tutti i giorni salvo le domeniche e i pomeriggi di Sabato 23 e 30 Luglio.

È fatto obbligo agli allievi di frequentare regolarmente il Corso in tutta la sua attività.

- 4) Il numero totale degli allievi è di 30.

Chi desidera frequentare il Corso, dovrà entro il 10 Giugno 1955 farne pervenire domanda al

Prof. CARLO SALVETTI
Società Italiana di Fisica

Via Saldini, 50

MILANO (Italia)

fornendo, ben chiaramente, le seguenti informazioni:

- a) Nome e Cognome.
- b) Data e luogo di nascita.
- c) Indirizzo attuale.
- d) Titoli di studio universitari ottenuti e presso quale Università.
- e) Professione attuale.
- f) Elenco bibliografico dei lavori di Fisica già pubblicati.
- g) Quale conoscenza orale e scritta ha dell'inglese e del francese.
- h) Se verrà a Varenna da solo o accompagnato da familiari; nel caso che venga da solo, se è disposto a prendere alloggio in camera in comune con altro allievo; nel caso che venga accompagnato da familiari, quale è il grado di parentela di questi.

Inoltre, il richiedente deve allegare alla domanda una lettera di presentazione, rilasciata da un professore universitario di Fisica, il quale assicuri che il richiedente ha interesse per i suoi studi a frequentare il Corso e che possiede già adeguata preparazione.

L'accettazione delle domande è decisa dalla Presidenza della Società unitamente alla Direzione del Corso tenendo conto dei documenti presentati dai singoli richiedenti e di una equa ripartizione dei posti tra le varie nazioni cui questi appartengono. Le comunicazioni delle deliberazioni saranno inviate agli interessati entro il 15 Giugno 1955.

- 5) Gli allievi saranno alloggiati o nella foresteria della Villa Monastero o in alberghi di Varenna, vicino alla Villa, in camere da 1 o 2 letti.
Nella Villa o in un albergo di Varenna sarà organizzata la mensa della Scuola.
6. Grazie alle sovvenzioni di cui la Scuola dispone, la spesa totale che ogni allievo deve sostenere per la frequenza al Corso, alloggio e vitto alla mensa della Scuola, è limitata a L. 25 000, se egli prende alloggio in camera, da solo, e a L. 20 000, se prende alloggio in camera con altro allievo o con familiari. Dette somme sono da versarsi, non più tardi del 24 Luglio, all'Amministrazione della Scuola, a Varenna, in moneta italiana.
Borse di studio, in numero limitatissimo, potranno essere accordate a quegli allievi che ne giustifichino il bisogno.
- 7) Per gli allievi che desiderino portare con loro i familiari, la Scuola, su richiesta che l'allievo dovrà unire alla domanda per frequentare il Corso, cercherà, entro le possibilità locali (che sono però assai limitate causa la stagione balneare), di trovare una sistemazione adeguata in alberghi di Varenna.
I familiari possono essere accolti, insieme con l'allievo, alla mensa della Scuola. Tutte le spese per alloggio, vitto, ecc., relative ai familiari sono da computarsi a parte e totalmente a carico dell'allievo: esse, per trattamento uguale a quello fatto all'allievo, si aggirano intorno a L. 3 000 per giorno e per persona adulta, e dovranno essere regolate direttamente dall'allievo con l'albergatore.
- 8) Per ogni informazione relativa al Corso rivolgersi direttamente al Direttore di questo.

Milano, 25 Aprile 1955

Il Segretario della S.I.F.: G. C. DALLA NOCE Il Direttore del Corso: C. SALVETTI

Il Presidente della S.I.F.: G. POLVANI

Remarks on the Operation of the Diffusion Cloud Chamber (I) (*).

P. E. ARGAN (+) and N. D'ANGELO (++)

Istituto di Fisica dell'Università - Roma
Istituto Nazionale di Fisica Nucleare - Sezione di Roma

A. GIGLI

Istituto di Fisica dell'Università - Genova

(ricevuto il 10 Gennaio 1955)

Summary. — A theoretical study has been carried out on a diffusion cloud chamber operating with methyl-alcohol vapor in air at normal pressure, and with a strong temperature gradient. Temperature distribution, vapor pressure and supersaturation have been calculated as functions of the number of ions formed per cm^3/s in the interior of the chamber. The calculated height of the sensitive layer is consistent with the experimental observations. The study has been extended to the case in which the various quantities depend on both vertical and horizontal coordinates. Information has been obtained about the perturbation of the structure of the sensitive layer as the result of introducing plates inside the chamber with a certain temperature distribution; in particular the approximate distance from these plates (or from the side walls of the chamber) at which tracks of ionizing particles are still observable has been determined.

1. — Introduction.

In 1939 LANGSDORF ⁽¹⁾ considered for the first time, both from a theoretical and experimental point of view, the operation of a diffusion cloud chamber of permanent sensitivity. More recently the problem has been taken up by

(*) This work was supported in part by a grant from the I.N.F.N. - Sezione Acceleratore.

(+) Present address: Istituto di Fisica della Università - Genova.

(++) Present address: Laboratorio di Fisica dell'Istituto Superiore di Sanità, Roma.

(1) A. LANGSDORF Jr.: *Rev. Scient. Inst.*, **10**, 91 (1939).

various authors ⁽²⁾, but only in the last few years have satisfactory results been obtained ⁽³⁾. At present, diffusion cloud chambers, working at normal or high (20-30 atmospheres) pressure are successfully in use for the study of various problems ⁽⁴⁾.

The principle of operation of this instrument is well known. Usually it consists of an air-tight chamber containing an inert gas. An organic liquid (methyl, propyl, ethyl-alcohol) at a temperature $T_2 \cong 293^\circ\text{K}$ is placed in a suitable tray in the upper part of the chamber. Organic vapor diffuses in the inert gas towards the bottom which is maintained at a temperature $T_1 < T_2$ ($T_1 \cong 213^\circ\text{K}$). Near the bottom, a permanent condition of supersaturation of the vapor exists, which, by a convenient choice of the gas-vapor mixture and of the values T_1 and T_2 , can be such as to allow the condensation of organic vapor on electrically charged centers. Tracks of ionizing particles are therefore observable in a horizontal sensitive layer of a few cm height ($4 \div 6$) from the bottom of the chamber.

In his theory LANGSDORF neglected the effect of vapor condensation on both electrically charged and uncharged centers of condensation on the temperature and vapor pressure distributions. In this way he was able to obtain only an approximate picture of the actual behavior of a diffusion chamber as a result of ignoring heat production and the attenuation of the vapor flux. The Kuusinen ⁽⁵⁾ isothermal diffusion equations were assumed to be valid even in the presence of a strong temperature gradient. Moreover, the diffusing vapor, even when supersaturated, was treated as a perfect gas. Finally, the effects due to the presence of the side walls of the chamber were not taken into consideration; the problem thus became a one-dimensional one, i.e. temperature, vapor pressure and supersaturation of the vapor were considered to depend only on the distance from the bottom of the chamber.

Recently SHUTT ⁽³⁾ has developed a one-dimensional theory in which the

⁽²⁾ E. W. COWAN: *Rev. Scient. Inst.*, **21**, 991 (1950); T. NEEDELS and G. NIELSEN: *Rev. Scient. Inst.*, **21**, 976 (1950); G. NIELSEN, T. NEEDELS and O. WEDDLE: *Rev. Scient. Inst.*, **22**, 673 (1951).

⁽³⁾ R. P. SHUTT: *Rev. Scient. Inst.*, **22**, 730 (1951); C. SUCCI and G. TAGLIAFERRI: *Nuovo Cimento*, **9**, 1092 (1952); A. LOVATI and C. SUCCI: *Nuovo Cimento*, **11**, 963 (1953); A. R. BEVAN: *Journ. Scient. Inst.*, **31**, 45 (1954); M. H. ALSTON, A. V. CREVE and W. H. EVANS: *Rev. Scient. Inst.*, **25**, 547 (1954); W. B. FOWLER, R. P. SHUTT, A. M. THORNDIKE and W. L. WHITTEMORE: *Rev. Scient. Inst.*, **25**, 996 (1954).

⁽⁴⁾ E. C. FOWLER, W. B. FOWLER, R. P. SHUTT, A. M. THORNDIKE and W. L. WHITTEMORE: *Phys. Rev.*, **91**, 135 (1953); W. B. FOWLER, R. P. SHUTT, A. M. THORNDIKE and W. L. WHITTEMORE: *Phys. Rev.*, **93**, 861 (1954) and *Phys. Rev.*, **95**, 1026 (1954); E. L. FIREMAN and D. SHWARZER: *Phys. Rev.*, **94**, 385 (1954); M. H. ALSTON, A. V. CREWE, W. H. EVANS, L. L. GREEN and J. C. WILLMOTT: *Proc. Phys. Soc.*, **67**, 657 (1954).

⁽⁵⁾ J. KUUSINEN: *Ann. der Phys.*, **14**, 445 (1935).

attenuation of the vapor flux by condensation on the charged centers is taken into account and the growth of the drops is considered according to the vapor and heat diffusion equations, with spherical symmetry. The assumption is also made that the rate of fall of the drops is governed by Stoke's law.

More recently, SUCCI and TAGLIAFERRI⁽³⁾ have taken up the theory of Langsdorf and evaluated, by a successive approximation procedure, the distribution of the supersaturation when the effect of the condensation of the vapor on electrically charged centers penetrating from above the sensitive layer is not negligible.

In these last few months we have taken up the theoretical study of the diffusion cloud chamber, searching for a simple approach to some of the questions not yet treated by other authors. Our theory is treated in §§ 2 and 3 of this paper, after presenting some fundamental relations (§ 2'1). In § 2 the problem is treated by considering that the various quantities involved depend only on the distance from the bottom of the chamber (one-dimensional treatment). At first (§ 2'2) the operation of a diffusion cloud chamber is considered without taking into account the condensation of the vapor on electrically charged centers; later (§ 2'3) the height of the sensitive layer is evaluated by taking the condensation into account.

In § 3 the same problem is treated two-dimensionally, i.e. the physical quantities involved are considered to depend on both a vertical and a horizontal coordinate, in order to take into account the influence on the volume and shape of the sensitive layer of a given temperature distribution on the side walls of the chamber, as well as on the plates of various materials introduced vertically inside.

2. - Fundamental relations and one-dimensional treatment of the problem.

2'1. - In the following, the indices 1 and 2 refer to vapor and gas respectively. Further, the following notations will be used:

- c concentration (expressed in moles)
- v average velocity (or drift velocity)
- p partial pressure
- T temperature
- A specific heat at constant pressure
- D diffusion coefficient
- K coefficient of heat conductivity of the gas-vapor mixture.

We indicate by $I_1 = c_1 v_1$ and $I_2 = c_2 v_2$ the current vectors of the vapor and gas respectively, assuming that A and K do not depend on the temperature.

By a suitable generalization of Fick's ⁽⁶⁾ first law to the case in which a temperature gradient is present we can write:

$$(1) \quad I_i = \frac{c_1 v_1 + c_2 v_2}{c_1 + c_2} c_i - \frac{D}{RT} \text{grad } p_i, \quad (i = 1, 2).$$

The first term of the second member of equation (1) represents the convection contribution to I_i ; the second term is the diffusion contribution. Neglecting heat radiation, we obtain the following equations (Appendix I, 1) ⁽⁷⁾:

$$(2) \quad \left\{ \begin{array}{l} a) \quad \text{div } I_1 = 0, \\ b) \quad \text{div } I_2 = 0, \\ c) \quad \text{div } \{-K \text{ grad } T + T(A_1 I_1 + A_2 I_2)\} = 0, \\ d) \quad I_1 = c_1 v_1 = \frac{c_1 v_1 + c_2 v_2}{c_1 + c_2} c_1 - \frac{D}{RT} \text{grad } p_1, \\ e) \quad I_2 = c_2 v_2 = \frac{c_1 v_1 + c_2 v_2}{c_1 + c_2} c_2 - \frac{D}{RT} \text{grad } p_2, \end{array} \right.$$

with the hypothesis that

$$(3) \quad \left\{ \begin{array}{l} p_i = R c_i T \\ p_1 + p_2 = P = \text{const.} \end{array} \right. \quad (i = 1, 2)$$

when considering stationary operation.

The diffusion coefficient depends on the temperature in the following manner:

$$(4) \quad D = D_1 \left(\frac{T}{T_1} \right)^n,$$

where D_1 is the diffusion coefficient of the organic vapor in the gas at atmospheric pressure and at temperature T_1 . In the particular case to be discussed of methyl alcohol vapors diffusing in air at atmospheric pressure, $D_1 = 0.0809$ CGS units and $n = 2$ ⁽⁸⁾.

Equations (2) take a very simple form if D does not depend on the temper-

⁽⁶⁾ A. FICK: *Pogg. Ann.*, **94**, 59 (1855).

⁽⁷⁾ N. D'ANGELO: *Thesis* (Rome, 1953).

⁽⁸⁾ *International Critical Tables*, vol. V, p. 62.

ature. This assumption has facilitated treatment of the two-dimensional problem, as we will see later.

2.2. - As a first approach, let us schematize the diffusion chamber as a system of two infinitely large horizontal sheets, separated by a distance h ; the upper one is at a temperature T_2 and the lower one at a temperature $T_1 < T_2$. In this hypothesis the various quantities involved will only be functions of the distance from the lower plate. Clearly, in the one-dimensional treatment of the problem under stationary conditions, $I_1 = \Phi = \text{constant}$ for symmetry reasons; moreover the gas must be macroscopically at rest, i.e. $I_2 \equiv 0 \equiv v_2$.

The temperature distribution is determined by equations $a)$, $b)$ and $c)$ of (2). With the above hypothesis, equations $a)$ and $b)$ are automatically fulfilled and equation $c)$ can be written in the following form

$$\frac{d^2 T}{dy^2} + \frac{A_1 \Phi}{K} \frac{dT}{dy} = 0.$$

The solution of this equation, taking into account that $T(0) = T_1$ and $T(h) = T_2$, is

$$(5) \quad T(y) = T_1 + \frac{1 - \exp[-ay]}{1 - \exp[-ah]} (T_2 - T_1),$$

in which by a we mean the quantity $A_1 \Phi / K$. Φ is such that the function $T(y)$ does not depart much from linearity, as will be seen in the following.

Equations $d)$ and $e)$ of (2) combined with (3) and assuming the temperature dependence of D to be given by Eq. (4), give the distribution of the vapor pressure $p_1(y)$ (Appendix I, 2):

$$(6) \quad p_1(y) = P \{1 - B^{\gamma/A} (Ay + B)^{-\gamma/A}\}$$

where the meaning of γ , A and B are the following:

$$(7) \quad \gamma = \frac{R \Phi T_1^2}{P D_1},$$

$$(8) \quad A = \frac{T_2 - T_1}{h}, \quad B = T_1.$$

The distribution of the supersaturation $S(y)$ becomes therefore:

$$(9) \quad S(y) = \frac{p_1(y)}{p_{1s}(y)} = P \frac{1 - B^{\gamma/A} (Ay + B)^{-\gamma/A}}{p_{1s}[T(y)]}.$$

In equation (6) the vapor flux Φ is included in the constant γ . Under ordinary working conditions, that is, when the vapor flux Φ is not externally fixed, its value will be that corresponding to the saturated vapor pressure $p_{1s}(h) = p_1(h)$ for $y = h$; this allows an immediate evaluation of the coefficient γ and consequently the distribution of the vapor pressure $p_1(y)$. By introducing values which satisfy the equation of Clausius-Clapeyron for the saturated vapor pressure $p_{1s}[T(y)]$, the distribution of the supersaturation $S(y)$ has been calculated.

The calculations have been carried out for a chamber operating by diffusion of methyl alcohol in air at normal pressure, with the source of organic vapor at a temperature $T_2 = 293^\circ\text{K}$, and the bottom of the chamber at $T_1 = 213^\circ\text{K}$. A value of $h = 20$ cm was used. The results have been plotted in Fig. 1. From the intersection of the curve of supersaturation $S_0(y)$ with the curve of critical supersaturation I , we obtain 17 cm as the height of the sensitive layer. It can be seen that, by equations *d*) and *e*) of (2) and assuming that the diffusion coefficient D does not depend on the temperature, one obtains a distribution of the supersaturation $S(y)$ which, for very small values of y differs strongly from that given by Eq. (9); for y sufficiently large, however, this difference tends rapidly to zero, so that the height of the sensitive layer is to be considered to be almost unaffected by this simpler assumption.

The results which we have obtained in this section are not very different from those established previously by LANGSDORF. It seemed particularly advantageous to use the Langsdorf hypothesis as a starting point, and to write an equation system, (2), which represents the

physical problem in the most general way possible, even after introducing some very rough approximations. This representation is favorable for taking into account the condensation of the vapor on electrically charged centers (§ 2'3) and for the two-dimensional treatment of the problem (§ 3).

2'3. — Taking the results obtained in § 2'1 and 2'2 as a starting point, we can now try to see how the distribution of the supersaturation is modified by the formation of ion pairs in the chamber from cosmic radiation, radioactive contamination or other external causes. It is shown that the height

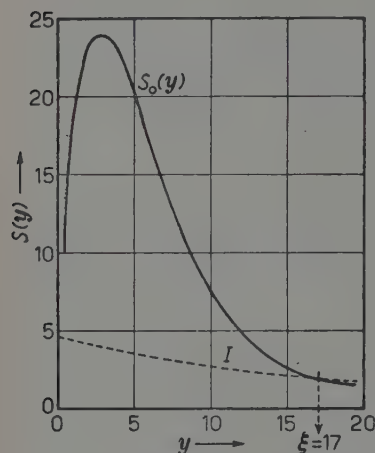


Fig. 1. — The curve $S_0(y)$ represents the distribution of the supersaturation (one dimensional treatment) as a function of the height, neglecting the effect of condensation on charged centers (formula (9)). Curve I is the distribution of the critical supersaturation

of the sensitive layer as a function of the number of ions formed per cm^3/s can be evaluated.

Equations *d*) and *e*) of system (2) using the same hypothesis than above (Appendix I, 2), enable us to write the following relation for the current vector:

$$(10) \quad I_1 = - \frac{P}{P - p_1} \frac{D}{RT} \text{grad } p_1.$$

In order to take account of the attenuation of the vapor flux by condensation, we have replaced the vector I by the vector

$$(11) \quad I^* = (\varepsilon + \varepsilon'y)I,$$

which represents the new current vector only for values of y between 0 and ξ , where ξ is the height of the sensitive layer.

Similarly we can write the new temperature distribution in the following way:

$$(12) \quad T^* = (\eta + \eta'y)T.$$

For the constants ε , ε' , η and η' we make the following assumptions:

a) the temperature T^* reduces to T_1 at the bottom of the chamber ($y = 0$), i.e.

$$(13) \quad \eta = 1.$$

b) The continuity condition must be fulfilled by the vapor flux at the top of the sensitive layer ($y = \xi$); thus it follows that

$$(14) \quad \varepsilon + \varepsilon'\xi = 1.$$

c) The same condition must be fulfilled by the vapor pressure; this gives a relation between ε' and η' .

d) From (11) it can easily be deduced that

$$(15) \quad (I - I^*)_{y=0} = I(1 - \varepsilon),$$

the term $1 - \varepsilon$ represents therefore the fractional reduction of the vapor flux at the bottom of the chamber and, consequently, ε depends on the number of ions formed per cm^3/s .

The following relations are obtained after some detailed calculations shown

in Appendix II:

$$(16) \quad \varepsilon' \left(\frac{A}{B} \xi - 1 \right) + \eta' (1 - \varepsilon' \xi) = 0$$

and

$$(17) \quad \ln \frac{P - p_1^*}{P - p_{1s}(T_1)} = -\beta B y \left[(1 - \varepsilon' \xi) + y \left(\varepsilon' - \frac{1}{2} \frac{A}{B} \right) \right].$$

Equation (16) establishes a relation between ε' , η' and ξ , while (17) relates the new vapor pressure $p_1^*(y)$ to the vapor flux Φ ($\beta = R\Phi/PD_1$), the height y , the height of the sensitive layer ξ and the parameter ε' which, by Eq. (14), depends on the number of ions formed per cm^3/s inside the chamber.

Our problem is reduced to that of finding a relation between the value of ε and the height of the corresponding sensitive layer ξ . From equations (12), (14), (16), (17), the equation of Clausius-Clapeyron, and Thompson's law, one would think it possible to obtain the analytical relation between ε and ξ directly. This, however, is not possible explicitly; for this reason we have used a method of successive approximations by which we obtain pairs of values of ε and ξ which are solutions of the problem.

The temperature and vapor pressure distributions calculated by means of Eqs. (5) and (6) of the preceding paragraph have enabled us to draw the curve of supersaturation $S_0(y)$ as shown in Fig. 1 and therefore to obtain the value ξ_0 of the height of the sensitive layer when the effect of condensation is considered to be negligible.

Once the value of $\varepsilon = \varepsilon_0$ has been appropriately fixed, one obtains the corresponding value of $\varepsilon' = \varepsilon'_0$ for $\xi = \xi_0 = 17$ cm by the use of relation (14). Putting $\xi = \xi_0$ and $\varepsilon' = \varepsilon'_0$, Eq. (16) gives the value of η' which, introduced into Eq. (12), because of Eq. (13), gives the new temperature distribution $T^*(y)$. Relation (17), with the same substitutions, gives the vapor pressure $p_{11}^*(y)$. In this manner it is possible to obtain a new distribution of the supersaturation $S_1(y)$ and consequently a new value of the height of the sensitive layer.

The procedure is repeated using this value of ξ_1 and assuming the relation

$$(18) \quad \frac{1 - \varepsilon_0}{1 - \varepsilon_1} = \frac{\xi_0}{\xi_1},$$

which gives a new value of $\varepsilon = \varepsilon_1$, which, combined with ξ_1 is the starting point for the successive application of the same procedure. This approximation method converges very rapidly; a few successive applications are sufficient to determine the height ξ_r of the sensitive layer with an uncertainty of $2 \div 3$ mm.

As one sees from Eq. (18), the value of ε' does not vary from one stage to another in the approximation procedure. This means that for each value of $\xi = \xi_i$ the continuity condition of the vapor flux is automatically fulfilled, and thus it is possible to find immediately the pair of values ε and ξ which satisfy the condition that ε' has a given value.

The final distributions of the supersaturation $S(y)$, corresponding to $\varepsilon_0 = 0.6, 0.7$ and 0.8 have been plotted in Fig. 2; they have been obtained from the approximation procedure described above. From the intersection of $S(y)$ with the critical supersaturation curve I , for the three cases under consideration, one obtains values for the heights of the sensitive layer $\xi_f = 4.5, 5.8$, and 7.8 cm respectively.

In Fig. 3 we have plotted the height of the sensitive layer ξ_f versus ε_0 ; in Fig. 4 the final value of ε_f versus ε_0 . Varying the value of ε_0 , ε_f is always found between 1 and ~ 0.85 as can be seen from Fig. 4; in the interval $0.6 \lesssim \varepsilon_0 \lesssim 0.8$ ($0.89 \lesssim \varepsilon_f \lesssim 0.91$) ε_f can be considered constant. This approximation is also valid for values of $\varepsilon_0 < 0.6$, as can be seen on the same graph, and gives a direct relation between ε_0 and ξ_f :

$$(19) \quad \xi_f = \xi_0 \frac{1 - \varepsilon_f}{1 - \varepsilon_0}.$$

Eq. (19) gives, at least to a first approximation, a simple analytical extension down to values of $\varepsilon_0 < 0.5$ of ξ_f in Fig. 3.

The order of magnitude of the values of ε_0 used to calculate the distribution of the supersaturation as shown in Fig. 2 has been established by using some simple physical considerations which relate this parameter to the fractional attenuation of the vapor flux at the bottom of the chamber due to condensation.

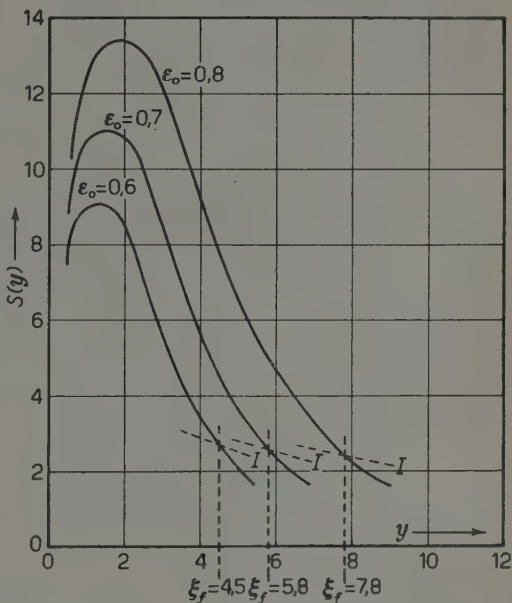


Fig. 2. -- The three curves represent the distribution of the supersaturation (one-dimensional treatment) obtained taking into consideration the condensation on charged centers, and for the values indicated of the parameter ε_0 . Curve I represents the distribution of the critical supersaturation for the three cases considered.

Relation (15) can be written in the following way:

$$(20) \quad \Delta\Phi_{(y=0)} = \Phi(1 - \varepsilon_f).$$

Once the value of γ is established with the criteria already discussed in

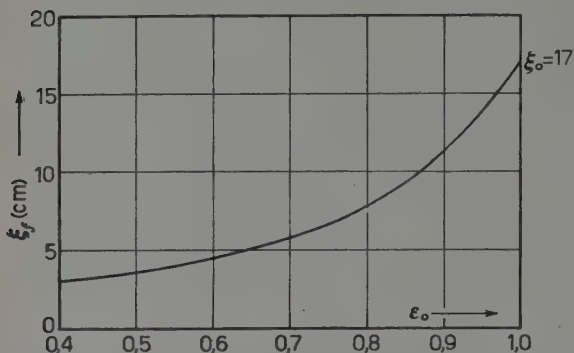


Fig. 3. — The dependence of the height of the sensitive layer ξ_f on the parameter ε_0 .

§ 2'2, we can find the numerical value of the vapor flux Φ from relation (7); assuming $p_1(h) = p_{1s}(h) = 100$ mm Hg, $\gamma = 1.74$ from Eq. (6). The value for Φ thus found is:

$$\Phi = 3.70 \cdot 10^{-8} \text{ mole/cm}^2\text{s}.$$

It can be assumed that the amount of organic liquid deposited in the form of drops per cm^2/s at the bottom of the chamber is proportional to

the number n of ions created per cm^3/s and to the height of the sensitive layer ξ_f . Therefore

$$(21a) \quad \Delta\Phi_{(y=0)} = n\xi_f \frac{4}{3} \pi \bar{r}^3 \frac{\delta}{M} = \Phi(1 - \varepsilon_f),$$

having indicated with \bar{r} the mean radius of the methyl alcohol drops which reach the bottom of the chamber, with δ and M the density and the molecular weight of the methyl alcohol. The average radius \bar{r} depends on the height of the sensitive layer and the following relation can be considered to be valid for each drop on reaching the bottom of the chamber:

$$(21b) \quad r^2 = \frac{K}{v} y_s;$$

y_s is the height at which a droplet begins to grow, K is a practically constant quantity ⁽¹⁾ and v is the velocity of fall which is also a constant.

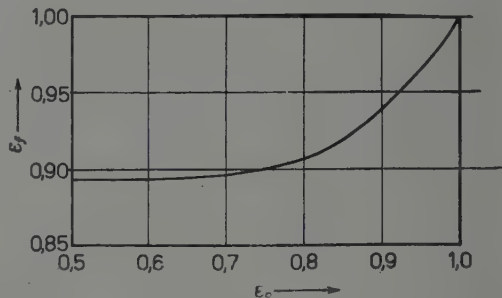


Fig. 4. — The dependence of the parameter ε_f on the parameter ε_0 .

(1) J. G. WILSON: *The Principle of Cloud-Chamber Technique* (Cambridge, 1951).

Integrating (21*b*) between 0 and ξ , and dividing by ξ , we find \bar{r} to be proportional to $\xi^{\frac{1}{2}}$. Thus, from (21*a*) we find that $\Delta\Phi_{(v=0)}$ is proportional to $\xi^{\frac{5}{2}}$.

Introducing the numerical values of the various quantities into (21*a*) ($\delta = 0.79$ g/cm³, $M = 32.04$) and utilizing the graphs in Figs. 3 and 4, it is possible to represent the dependence of the height of the sensitive layer on $n\bar{r}^3$. This dependence is shown in Fig. 5; it can be easily seen that the height of

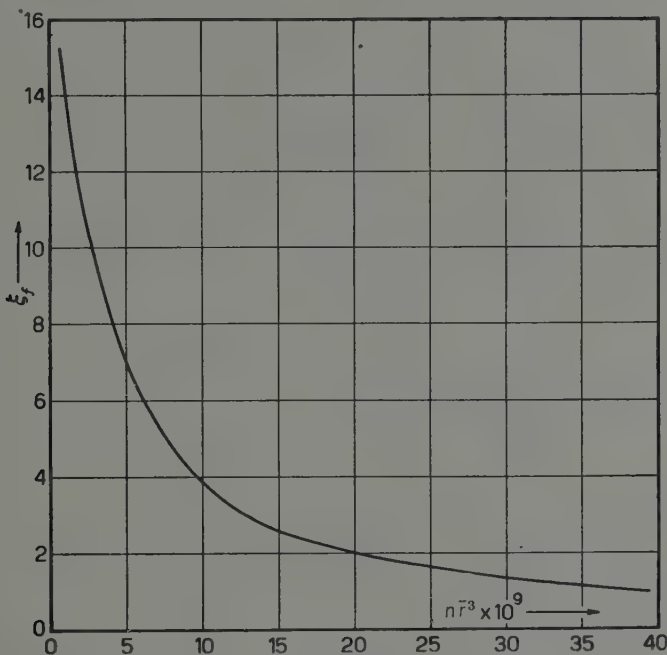


Fig. 5. — The dependence of the height of the sensitive layer ξ_f on $n\bar{r}^3$.

the sensitive layer is 8 to 4 cm, if the number of ions n (*) lies between 1 and 10, and if one assumes for \bar{r} a value of 1 to $2 \cdot 10^{-3}$ cm ⁽¹⁰⁾ and therefore a value of ε_0 between 0.8 and 0.6. This result is consistent with the experimental observations.

3. — Two-dimensional treatment of the problem.

3.1. — We now propose to demonstrate how, starting from the system of equations (2) and (3) of § 2.1, it is possible to determine the distribution of

(*) It must be noted that the values for n we are using are contained in the interval usually accepted for air at normal pressure and at sea level.

⁽¹⁰⁾ N. N. DAS GUPTA and S. K. GHOSH: *Rev. Mod. Phys.*, **18**, 225 (1946); R. L. LANDER and C. E. NIELSEN: *Rev. Scient. Inst.*, **24**, 20 (1953).

the temperature and of the vapor pressure when these quantities depend on both the height and a horizontal coordinate. The problem is essentially that of determining the structure of the sensitive layer of a diffusion cloud chamber, which is infinite in only one direction, whose intersection with the x, y plane is shown in Fig. 6. AC and BD represent the side walls of the chamber or plates of any material put inside, with a given temperature distribution. AB and CD are the bottom and top plates at temperatures T_1 and T_2 respectively.

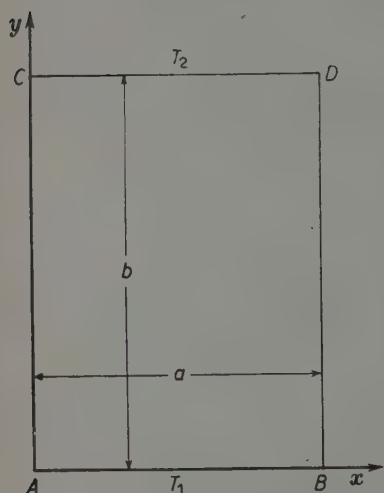


Fig. 6. - The parallelogram $ABCD$ represents the area d taken for the integration, of the equation system (24).

We take first the case, as before, in which the effect of the condensation on the charged centers is negligible; later, although it is impossible to apply directly the procedure described in § 2'3, it is still possible to obtain information about the reduction of the sensitive layer as a function of the number of ions per cm^3/s at least in the center of the chamber.

Equations (2) and (3) constitute a system of 12 independent equations with 13 unknowns. We have already seen that this is sufficient to describe the behaviour of the vapor-gas mixture in the one-dimensional treatment; the elimination of I_2 and v_2 from the unknowns reducing the system to 7 independent equations and 7 unknowns, the solutions of which were found.

In order to avoid excessive complications in the two-dimensional treatment, the simplifying hypothesis $I_2 = 0 = v_2$ has been introduced. It should be noted that this hypothesis will not in general be valid (it means in fact, that the gas is macroscopically at rest, and it is clear that for some of the conditions to be imposed concerning the vapor pressure p_1 and the temperature T at the boundary of the parallelogram $ABCD$, it is impossible to avoid the motion of the gas). Nevertheless, for properly chosen boundary conditions, it can be shown that the approximation introduced is reasonable. Experimental observations bear out this point.

The system therefore reduces to 8 independent equations with 8 unknowns.

From (2) and (3) one obtains immediately:

$$(22) \quad \begin{cases} I_1 = - \frac{P}{P - p_1} \frac{D}{RT} \text{grad } p_1, \\ \text{div } I_1 = 0, \\ \text{div } \{-K \text{grad } T + A_1 T I_1\} = 0, \end{cases}$$

which, if we put

$$(23) \quad \alpha = \frac{A_1 P D}{K R} = \text{const.}; \quad p = P - p_1; \quad u = \ln p,$$

is reduced to the following differential system:

$$(24) \quad \begin{cases} T \cdot \Delta_2 u - \text{grad } T \times \text{grad } u = 0, \\ \Delta_2 T - \alpha \cdot \Delta_2 u = 0. \end{cases}$$

The distributions of the vapor pressure p_1 and of the temperature T are determined by Eqs. (24) when the boundary conditions are given for the parallelogram $ABCD$ of Fig. 6.

The integration of the system has recently been carried out by the « Istituto Nazionale per le Applicazioni del Calcolo, del C.N.R. » with the following boundary conditions:

for the function $T(xy)$

$$(25a) \quad \begin{cases} T(x, 0) = 213^\circ \text{K} & T(x, b) = 293^\circ \text{K} \\ T(0, y) = T(a, y) = \begin{cases} 213 + 8y & \text{for } 0 \leq y \leq b/2 \\ 293 & \text{for } b/2 \leq y \leq b; \end{cases} \end{cases}$$

for the vapor pressure, the boundary values have been given by the following relation:

$$(25b) \quad \begin{cases} T (^\circ \text{K}) & p_1 (\text{dyne/cm}^2) \\ 229 & 0.133 \cdot 10^4 \\ 257 & 1.330 \cdot 10^4 \\ 278 & 5.320 \cdot 10^4 \\ 294 & 13.300 \cdot 10^4 \\ 323 & 53.200 \cdot 10^4 \\ 338 & 101.000 \cdot 10^4 \end{cases}$$

The values of p_1 satisfy the equation of Clausius-Clapeyron for the given temperatures. These boundary conditions correspond, for example, to a diffusion cloud chamber whose side walls are covered by velvet saturated with alcohol.

At present the integration of the differential system (24) for boundary

conditions corresponding to experimental conditions which can be easily realized is in progress.

Tables I and II give the values of $T(x, y)$ and $p_1(x, y)$ as calculated from (24) using the boundary conditions given above.

The curves drawn in Fig. 7 represent the temperature distribution on horizontal planes at various heights; the curves in Fig. 8 give the values of

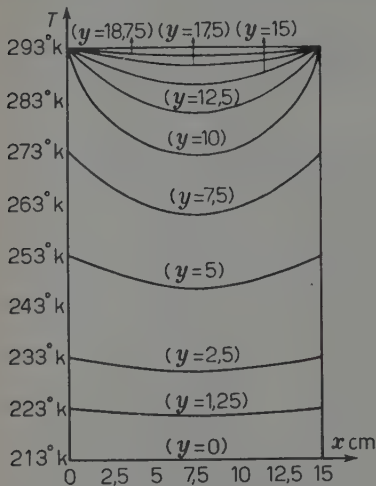


Fig. 7. - The temperature distribution on horizontal planes at different heights as derived from the integration of the equation system (24) with the boundary conditions as discussed in the text.

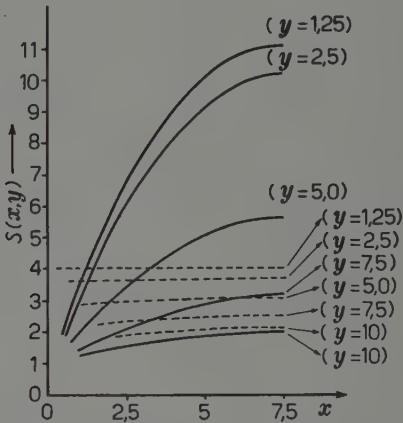


Fig. 8. - Distribution of the supersaturation on horizontal planes at different heights, derived from the integration of the equation system (24) with the boundary conditions given in the text. The dotted curves represent the distribution of the critical supersaturation on planes at corresponding heights.

TABLE I. - Numerical values of $T(x, y)$.
Solution of Eqs. (24) with boundary conditions (25a) and (25b).

$y \backslash x$	0	1.25	2.50	5.00	7.50
1	2	3	4	5	6
0.00	213	213.00	213.00	213.00	213.00
1.25	223	222.68	222.38	221.92	221.74
2.50	233	232.32	231.67	230.68	230.32
5.00	253	251.30	249.71	247.39	246.58
7.50	273	269.40	266.25	262.17	260.86
10.00	293	283.92	279.10	273.85	272.30
12.50	293	289.24	286.02	281.88	280.57
15.00	293	291.13	289.43	286.99	286.15
17.50	293	292.20	291.47	290.38	289.99
18.75	293	292.62	292.26	291.73	291.55
20.00	293	193.00	293.00	293.00	293.00

TABLE II. — Numerical values of $p_1(x, y)$ (+).
Solution of Eqs. (24) with boundary conditions (25a) and (25b).

y	x	0	1.25	2.50	5.00	7.50
1	2	3	4	5	6	
0.00	0.0005	0.0005	0.0005	0.0005	0.0005	0.0005
1.25	0.0028	0.0306	0.0492	0.0700	0.0746	0.0746
2.50	0.0121	0.0677	0.1046	0.1437	0.1551	0.1551
5.00	0.0931	0.1985	0.2622	0.3231	0.3366	0.3366
7.50	0.3882	0.4905	0.5303	0.5479	0.5479	0.5479
10.00	1.2692	0.9631	0.8658	0.7868	0.7674	0.7674
12.50	1.2692	1.1628	1.0981	0.9799	0.9547	0.9547
15.00	1.2692	1.2223	1.1742	1.1133	1.0926	1.0926
17.50	1.2692	1.2509	1.2305	1.2018	1.1936	1.1936
18.75	1.2692	1.2631	1.2529	1.2386	1.2346	1.2346
20.00	1.2692	1.2733	1.2733	1.2733	1.2733	1.2733

(+) The numerical values in this table are to be multiplied by 10^5 .

the supersaturation $S(x, y)$ on the same horizontal planes. It is possible to construct the top surface of the sensitive layer from the intersection of the supersaturation curve (full line) with the critical supersaturation curve (dotted line) corresponding to the same horizontal plane; this is shown in Fig. 9. The sensitive layer has a maximum $\xi_{00} = 9.4$ cm and its structure is symmetrical with respect to a vertical plane at equal distance from AC and BD . The presence of an insensitive zone near the walls is evident; the order of magnitude of this zone is the same as that observed in an experimental arrangement where the conditions were very close to those given by (25a) and (25b) ⁽¹¹⁾.

These results were obtained by introducing the following numerical values in the first relation of (23):

$$A_1 = 8.00 \quad \text{cal/mole } ^\circ\text{K}$$

$$P = 1.01 \cdot 10^6 \quad \text{dyne/cm}^2$$

$$R = 8.3 \cdot 10^7 \quad \text{erg/mole } ^\circ\text{K}$$

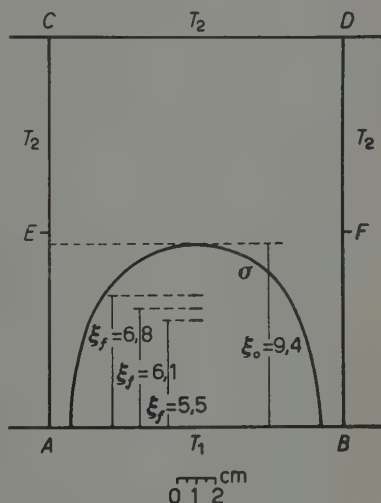


Fig. 9. — The curve σ represents the structure of the top of the sensitive layer; it has been obtained using the results of the integration of the equation system (24). The values of ξ_f give a measure of the height of the top of the sensitive layer corresponding to three different values of ξ_0 .

⁽¹¹⁾ P. E. ARGAN, N. D'ANGELO and A. GIGLI: *Ric. Scient.*, 24, 1006 (1954).

and assuming for D and K an average value in the temperature interval considered. This assumption is justified by the fact that the solution of the differential system (24) is not very sensitive to the value of the constant α ⁽¹²⁾; in fact, by an a posteriori verification, the effect on the final results in varying D and K within the limits imposed by our operating conditions is entirely negligible. Another important consequence of this fact is the following: if one assumes for the ratio D/\bar{K} the value $2.31 \cdot 10^3$ which in our conditions of operation describes the mixture of methyl alcohol and air, and the value $2.80 \cdot 10^3$ which in the same conditions describes the mixture of methyl alcohol and carbon-dioxide, the difference in the temperature distributions is only some tenths of a degree. This fact is particularly interesting, because we can assume our conclusions to be valid, at least to a first approximation, for all those mixtures having methyl alcohol like organic component, whose ratio D/K may even depart sensibly from the values given above.

Finally, we observe ⁽¹²⁾ that, after establishing properly chosen boundary conditions, the distribution of the partial pressure $p_1(x, y)$ does not depend on the value of α , while the temperature distribution $T(x, y)$ depends linearly on α , as can be deduced from the solution of eqs. (24). For a chamber operating at high pressure, it is therefore not necessary to calculate $p_1(x, y)$, but only the temperature distribution $T(x, y)$.

3.2. - The procedure outlined in § 2.3, in the one-dimensional treatment, cannot be applied directly to the results which we have obtained, in § 3.1, if one wishes to take into account the condensation of the vapor on electrically charged centers; the particular symmetry conditions are not present which made the application of the above procedure feasible. In the theory which was developed for a chamber infinite in the x direction, symmetry reasons and stationary conditions gave the two conditions $I_1 = \Phi = \text{const.}$, and $I_2 = 0 = v_2$. Now, while the second of these still seems acceptable, the first is certainly unapplicable as can clearly be seen from the boundary conditions which we have imposed for the integration of Eqs. (24). Nevertheless, for symmetry reasons it is possible to evaluate approximately the lowering of the sensitive layer in the center of the chamber by assuming an average value for the vapor flux vector. This average value can easily be calculated using the numerical values given in column 6 of Tables I and II and making use of Eq. (10). One obtains:

$$\bar{I}_{x=7.5}^{(y)} = \bar{\Phi} = 5 \cdot 10^{-8} \text{ mole/cm}^2\text{s}.$$

The assumption, in this case, that D is a constant equal to its average value,

⁽¹²⁾ Report of the Istituto Nazionale per le Applicazioni del Calcolo del C.N.R., Rome, May 1954 (unpublished).

has brought about a notable simplification in eq. (16) which relates the quantities ε' and η' .

The relation, in fact, reduces to

$$(26) \quad \varepsilon' = \eta',$$

from which, because of (18), it follows that η' is invariant in the successive stages of the approximation procedure. Consequently, the possibility of determining the temperature distribution for $0 \leq y \leq \xi$ is evident.

As in the one-dimensional case, we have assumed that the reduction of the vapor flux due to condensation at the bottom of the chamber, is proportional to $\xi^{\frac{5}{2}}$. This determines the value of the parameter ε_0 .

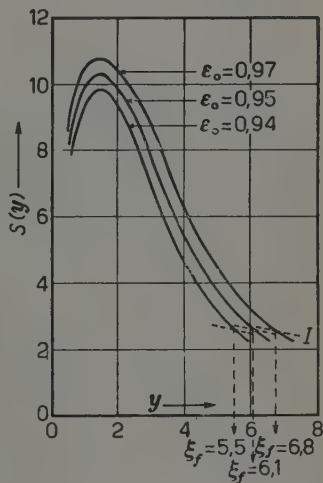
Indicating magnitudes in the one-dimensional theory with the index u , and those of the two-dimensional theory with the index b , we can write the following relation:

$$(27) \quad \frac{\bar{\Phi}_b(1 - \varepsilon_{0b})}{\bar{\Phi}_u(1 - \varepsilon_{0u})} = \left(\frac{\xi_{0b}}{\xi_{0u}} \right)^{\frac{5}{2}}.$$

We now introduce in (27) the values already given for $\bar{\Phi}_b$, $\bar{\Phi}_u$, ξ_{0b} and ξ_{0u} and the values 0.6, 0.7, and 0.8 which were used for ε_{0u} in the one-dimensional calculation, and thus get the corresponding values for ε_{0b} .

The final distributions of the supersaturation at the center of the chamber are shown in Fig. 10 for the above three values of ε_{0b} . From the intersection of these curves with those which represent the distribution of the critical supersaturation I , one obtains the corresponding values of the maximum height of the sensitive layer to be $\xi_f = 5.5, 6.1, 6.8$ cm respectively.

Fig. 10. - The three curves shown represent the distribution of the supersaturation (two-dimensional treatment), for the center of the chamber and as a function of the height, taking account of the condensation of vapor on electrically charged centers, for the values as indicated for the parameter ε_0 . The curves I represent the distribution of the critical supersaturation for the three cases considered.



4. - Conclusions.

With the theory elaborated in this paper we think we have answered in an adequate and simple way some of the questions, which, from our point of view, are very important for certain particular performances which might

be expected of a diffusion cloud chamber. Because of its extremely small dead time, and the particular geometry of the zone which is sensitive to ionizing radiation, this instrument would normally be used in accelerator experiments. For such experiments, it is important to know, with the greatest possible precision, the structure and the volume of the sensitive zone as a function of the ion load, as well as any possible effects on the sensitivity due to the arrangement and temperature of the walls or plates, especially in the vicinity of these structures. It seems possible to draw the following conclusions:

1) Although in both the one-dimensional and two-dimensional theories given here, the calculations have been carried out for methyl-alcohol and air at normal pressure, the equations are sufficiently general to permit the calculation of other combinations of organic and inert gases at different pressures and with other temperature gradients. Some of these possibilities are at present being calculated.

2) The results obtained in the one-dimensional treatment are consistent with the experimental observations regarding the height of the sensitive layer as a function of the number of ions per cm^3/s . It was not necessary in our picture to assume an excessive ion load (C. SUCCI and G. TAGLIAFERRI⁽³⁾) in order to obtain a good accord between theory and experiment.

3) Given a known ionic load, it is possible to determine the height of the sensitive layer to a good approximation, from the curve in Fig. 5.

4) The evaluation of the deformation of the sensitive layer in the neighborhood of the plates placed inside the chamber or near the walls of the chamber itself is not easy. Analytically, the problem can be confronted with the hypothesis that the gas is macroscopically at rest, i.e. that $\mathbf{I}_2 \equiv 0 \equiv \mathbf{v}_2$ and neglecting the condensation of the vapor on charged centers. The realization of the first condition should not create great experimental difficulties if the temperature distribution on the plates or walls is chosen opportunely.

5) The analytical difficulties which arise in the evaluation of the lowering of the sensitive layer in the presence of condensation centers, are considerable in the two-dimensional treatment. We think that the criteria adopted for the evaluation of the top surface of the layer is sufficient for all practical needs. Experiments have confirmed the existence of an insensitive zone near the plates or the walls of the chamber which corresponds in size with the one predicted by our theory.

Acknowledgements.

We wish to express our appreciation to Prof. E. AMALDI and to Prof. E. PANCINI for the interest shown in this work, and for having made possible the collaboration between the Institutes of Physics of the Universities of Rome and Genoa.

We are very grateful to Prof. M. PICONE, Director of the Istituto Nazionale per le Applicazioni del Calcolo del C.N.R., who has given us permission to carry out the integration of the differential equation system (24) at his Institute.

Our particular thanks go to Prof. M. AGENO for his kind interest in this work.

APPENDIX I

(A1.1). Let us suppose that a non-homogeneous mixture of two gases is enclosed in a container at constant temperature and pressure. The mutual diffusion of the two gases will tend to make the concentrations uniform within the container. The motion of the two gases at a time t and in a point P inside the container can be described by two diffusion vectors \mathbf{I}_1 and \mathbf{I}_2 defined so that

$$(A1.1) \quad \mathbf{I}_i \times \mathbf{n} dS \quad (i = 1, 2)$$

represents the quantity of gas 1 or 2 which crosses the area dS per unit time. The vectors \mathbf{I}_1 and \mathbf{I}_2 are functions of the concentration gradient of gas 1 and 2 respectively.

With these hypotheses, the following relations are valid for the first law of FICK:

$$(A1.2) \quad \mathbf{I}_1 = -D \text{grad } c_1, \quad \mathbf{I}_2 = -D \text{grad } c_2.$$

Since the diffusion coefficient D is the same for both relations,

$$(A1.3) \quad \mathbf{I}_1 + \mathbf{I}_2 = 0.$$

Instead of (A1.2), when the total pressure is a constant, but the temperature gradient may be different from zero, we write:

$$(A1.4) \quad \begin{cases} \mathbf{I}_1 = -\frac{D}{RT} \text{grad } p_1, \\ \mathbf{I}_2 = -\frac{D}{RT} \text{grad } p_2, \end{cases}$$

while the relation (A1.3) is still valid.

(A1.4) represent a useful extension of the equations of Fick to the case characterized by a non-uniform temperature distribution and with $P = p_1 + p_2 = \text{const.}$ For $T = \text{const.}$ eqs. (A1.4) reduce to eqs. (A1.2.) of FICK.

The preceding equations now enable us to write the equations (2) of the text which are starting point for the solution of the problem. In fact, we write:

$$(A1.5) \quad I_1 = c_1 v_1; \quad I_2 = c_2 v_2$$

and in the presence of convection motion, we introduce for the total velocity in P at the time t , the quantity

$$(A1.6) \quad v = \frac{c_1 v_1 + c_2 v_2}{c_1 + c_2};$$

the vectors

$$I_1^{(d)} = c_1(v_1 - v), \quad I_2^{(d)} = c_2(v_2 - v)$$

represent the current vectors of the vapor and the gas for an observer travelling with a velocity v , at the time t , in the point P .

By definition:

$$(A1.7) \quad I^{(d)} = I_1^{(d)} + I_2^{(d)} = 0$$

and the above observer sees only the mutual diffusion of the vapor and the gas, characterized by the vectors $I_1^{(d)}$ and $I_2^{(d)}$ the sum of which is equal to zero

Consequently:

$$(A1.8) \quad \begin{cases} I_1^{(d)} = -\frac{D}{RT} \text{grad } p_1 \\ I_2^{(d)} = -\frac{D}{RT} \text{grad } p_2. \end{cases}$$

Under stationary conditions, the equations of the conservation of matter can be written in the following way:

$$(A1.9) \quad \text{div } I_1 = 0, \quad \text{div } I_2 = 0$$

and, taking account of only the conduction and convection phenomena, the following relation

$$(A1.10) \quad \text{div} \{-K \text{grad } T + T(A_1 I_1 + A_2 I_2)\} = 0$$

expresses the conservation of heat.

These considerations lead to the system of equations (2) of the text.

(A1.2). It is not difficult to obtain the vapor pressure distribution in a one-dimensional treatment, using equations *d*) and *e*) of system (2) together with (3) as a consequence of the fact $I_1 = \Phi = \text{const.}$ and $I_2 = 0 = v_2$.

We can, in fact, write d) and e) in the form:

$$(A1.11) \quad \begin{cases} -\Phi = \frac{c_1}{c_1 + c_2} c_1 v_1 - \frac{D}{RT} \frac{dp_1}{dy} \\ 0 = \frac{c_2}{c_1 + c_2} c_1 v_1 + \frac{D}{RT} \frac{dp_1}{dy} \end{cases}$$

Assuming an expression of the type $T(y) = Ay + B$ with $A = (T_2 - T_1)/h$ and $B = T_1$, and a temperature dependence of the type (4) for the diffusion coefficient D , it follows from (A1.11) that

$$(A1.12) \quad p_1 - P = c(Ay + B)^{-\gamma/A} \quad (c = \text{const.})$$

with $\gamma = R\Phi T_1^2 / PD_1$.

For $y = 0$, p_1 must assume the value of the saturated vapor pressure $p_{1s}(0)$ at the temperature T_1 ; it follows that

$$(A1.13) \quad p_1 = P - (P - p_{1s}(0)) B^{\gamma/A} (Ay + B)^{-\gamma/A}.$$

If one observes that under ordinary working conditions of a diffusion cloud chamber $P \gg p_{1s}(0)$, this relation reduces to (6) of the text.

APPENDIX II

(AII.1). In § 2.3 we have formulated some hypotheses in order to evaluate the deformation of the distribution of the supersaturation $S_0(y)$ by taking account of the condensation of vapor on electrically charged centers. We are going to give the calculation in some detail starting from these assumptions and from the four conditions a), b), c) and d) discussed in the text.

The expression

$$(A2.1) \quad I^* = - \frac{D(T^*)P}{(P - p_1^*)RT^*} \frac{dp_1^*}{dy},$$

is the direct extension of (10) which represents the flux vector in the one-dimensional theory, if the effects of condensation are considered negligible.

Supposing in (A2.1) that $D(T^*) \cong D(T)$, apart from a factor DP/R , and from (10) and (11), one can write I^* in one of the two following ways:

$$(A2.2) \quad \frac{\varepsilon + \varepsilon' y}{T} \frac{d \ln (P - p_1)}{dy}$$

or

$$(A2.3) \quad \frac{1}{T^*} \frac{d \ln (P - p_1^*)}{dy},$$

which, when set equal, give

$$(A2.4) \quad (\varepsilon + \varepsilon'y)(\eta + \eta'y) \frac{d \ln (P - p_1)}{dy} = \frac{d \ln (P - p_1^*)}{dy},$$

from which one obtains

$$(A2.5) \quad \int_{P-p_{1s}(T_1)}^{P-p_1^*} d \ln (P - p_1^*) = - \gamma \int_0^y (\varepsilon + \varepsilon'y)(\eta + \eta'y) \frac{dy}{Ay + B}$$

remembering from (A1.13) Appendix I, that

$$(A2.6) \quad \ln (P - p_1) = \ln (P - p_{1s}(T_1)) - \frac{\gamma}{A} \ln \frac{Ay + B}{B}.$$

The integration limits for the first member of (A2.5) have been chosen as $y = 0$, $p_1 = p_{1s}(T_1)$. This means that, at the bottom of the chamber p_1 and p_1^* coincide with the saturated vapor pressure p_{1s} at the temperature T_1 .

Integration of (A2.5) gives

$$(A2.7) \quad \ln \frac{P - p_1^*}{P - p_{1s}(T_1)} = - \frac{\gamma}{B} [y],$$

in which the significance of the symbol $[y]$ is evident.

If we substitute in place of η and ε the values 1 and $1 - \varepsilon'\xi$ ((13) and (14)) in the term $[y]$, this reduces to a function of y and ξ :

$$(A2.8) \quad F(y, \xi) = \left[1 - \varepsilon'\xi - \frac{1}{2} \frac{A}{B} y + \frac{1}{2} \frac{A}{B} \varepsilon'\xi y + \frac{1}{2} \eta'y - \frac{1}{2} \varepsilon'\eta'\xi y + \frac{1}{2} \varepsilon'y \right] y.$$

Let us now impose the condition

$$(A2.9) \quad p_1^*(\xi) = p_1(\xi),$$

which means that the vapor pressure p_1^* for $y = \xi$ is continuous.

From eqs. (A2.6), (A2.7), and (A2.9) it follows that:

$$(A2.10) \quad \ln \frac{P - p_1^*(\xi)}{P - p_{1s}(T_1)} = - \frac{\gamma}{B} F(\xi, \xi) = \ln \frac{P - p_1(\xi)}{P - p_{1s}(T_1)} = - \frac{\gamma}{B} \left(\xi - \frac{1}{2} \frac{A}{B} \xi^2 \right),$$

that is

$$(A2.11) \quad F(\xi, \xi) = \xi - \frac{1}{2} \frac{A}{B} \xi^2.$$

This expression is easily simplified and reduced to

$$(A2.12) \quad \varepsilon' \left(\frac{A}{B} \xi - 1 \right) + \eta' - \varepsilon' \eta' \xi = 0,$$

which constitutes the relation sought between ε' , η' and ξ (formula (16) in the text).

Formula (17) of the text is easily obtained by substituting in (A2.8) for the term $\varepsilon' \eta' \xi$, the expression given by (A2.12).

APPENDIX III

The integration of the equation system (24) in the rectangular area (indicated in the following with the letter d) shown in Fig. 6 and with various boundary conditions (the boundary is indicated in the following with fd) is being carried out.

The conditions chosen by us correspond to a physical situation which is not difficult to realize experimentally. The simplest, as has already been discussed in the next, is to assume a properly chosen temperature distribution on all fd and to create conditions on the walls AC and BD for which the pressure assumes, point by point, a value which, for a given temperature, satisfies the equation of Clausius-Clapeyron (this, for instance, could easily be realized by covering the walls with alcohol saturated velvet). The saturated vapor pressure could also be imposed for only certain zones of the walls, but this certainly is not easily realizable experimentally: in fact it would mean prohibiting the condensation of the vapor on zones in which one does not desire that condition to be satisfied.

We call these last, « impenetrable zones » for the vapor; because of (10) we therefore can write that $\partial p_1 / \partial x = 0$.

The cases which we have taken under consideration, apart from those discussed in the text, are the following:

Case I.

$$T_{fd} \left\{ \begin{array}{ll} T(x, 0) = 213 & T(x, b) = 293. \\ T(0, y) = T(a, y) = \begin{cases} 213 + 8y, & 0 \leq y \leq b/2 \\ 293 & , \quad b/2 \leq y \leq b. \end{cases} \end{array} \right.$$

$$a) \quad p_{1fd} \left\{ \begin{array}{ll} p_1(x, b) = p_{1s}[T(x, b)], & p_1(x, 0) = p_{1s}[T(x, 0)] \\ p_1(0, y) = p_1(a, y) = p_{1s}[T(0, y)], & b/2 \leq y \leq b \\ \partial p_1(0, y) / \partial x = \partial p_1(a, y) / \partial x = 0, & 0 \leq y \leq b/2. \end{array} \right.$$

$$b) \quad p_{1fd} \left\{ \begin{array}{ll} p_1(x, b) = p_{1s}[T(x, b)], & p_1(x, 0) = p_{1s}[T(x, 0)] \\ \partial p_1(0, y) / \partial x = \partial p_1(a, y) / \partial x = 0. & \end{array} \right.$$

Case II.

$$T_{fa} \begin{cases} T(x, 0) = 213, & T(x, b) = 293. \\ T(0, y) = T(a, y) = 213 + 4y. \end{cases}$$

$$a) \quad p_{1fa} \begin{cases} p_1(x, b) = p_{1s}[T(x, b)], & p_1(x, 0) = p_{1s}[T(x, 0)], \\ \partial p_1(0, y)/\partial x = \partial p_1(a, y)/\partial x = 0. \end{cases}$$

$$b) \quad p_{1fa} \begin{cases} p_1(x, b) = p_{1s}[T(x, b)], & p_1(x, 0) = p_{1s}[T(x, 0)], \\ p_1(0, y) = p_1(a, y) = p_{1s}[T(a, y)]. \end{cases}$$

Further, the possibility of resolving the system (24) with cylindrical coordinates is being studied for the purpose of comparing the greatest part of our experimental results using a cylindrical chamber with the theoretical results.

RIASSUNTO

Si studiano teoricamente le caratteristiche di una camera a nebbia a sensibilità permanente, funzionante per diffusione di vapori di alcool metilico in aria a pressione normale e sotto forte gradiente di temperatura. Vengono calcolate le distribuzioni di temperatura, di pressione di vapore e di sovrasaturazione in funzione del numero di ioni che si formano per cm^3/s nel volume racchiuso dalla camera. L'altezza dello strato sensibile alle radiazioni ionizzanti risulta in buon accordo con le osservazioni sperimentali. Lo studio è stato esteso anche al caso in cui le varie grandezze che intervengono nel problema si ritengono funzioni oltre che della quota a partire dal fondo della camera anche di una coordinata orizzontale. Se ne ricavano informazioni circa la perturbazione introdotta nella forma dello strato sensibile da setti di materiale posti nell'interno della camera con distribuzione di temperatura assegnata; in particolare si deduce l'ordine di grandezza della distanza minima dai setti (o dalle pareti laterali) a cui sono ancora osservabili tracce di particelle ionizzanti.

The Ring Focus in the Spiral Orbit Spectrometer.

L. MARQUEZ

Centro Brasileiro de Pesquisas Físicas - Rio de Janeiro, Brasil

(ricevuto il 18 Gennaio 1955)

Summary. — It is shown in this work that the spiral orbit spectrometer has a ring focus near the stable orbit. Taking advantage of this property by means of a cylindrical slit, the characteristics of the spiral orbit spectrometer can be greatly improved. For a particular case studied, the transmission as a function of the line width is given by $T = 0.7W^{\frac{1}{2}}$ for a point source.

1. — Introduction.

The spiral orbit spectrometer was first built by MIYAMOTO ⁽¹⁾, and its theory was developed by IWATA, MIYAMOTO, and KOTANI ⁽²⁾. Spiral orbit spectrometers have been built and used in Japan ⁽³⁾ and in Berkeley ⁽⁴⁾. SAKAI ⁽⁵⁾ has made a study comparing the three types of spectrometers known up to now, and in his work he arrives at the relation $T = 0.077W^{\frac{1}{2}}$ between the transmission and the line width for the spiral orbit spectrometer. In this paper we are going to show that there exists a ring focus in the spiral orbit spectrometer, and that by using this property the characteristics of the spiral orbit spectrometer can be improved about a factor of ten from the relation found by SAKAI.

Let us suppose that we have a cylindrically symmetric magnetic field which is radially decreasing, and let us call the median plane a plane perpendicular

⁽¹⁾ G. MIYAMOTO: *Proc. Phys. Mat. Soc. Japan*, **17**, 587 (1943).

⁽²⁾ G. IWATA, G. MIYAMOTO and M. KOTANI: *Journ. Phys. Soc. Japan*, **2**, 1 (1949).

⁽³⁾ M. SAKAI: *Journ. Phys. Soc. Japan*, **5**, 178 (1950).

⁽⁴⁾ R. SAGANE, W. L. GARDNER and H. W. HUBBARD: *Phys. Rev.*, **82**, 557 (1951).

⁽⁵⁾ M. SAKAI: *Journ. Phys. et Rad.*, **14**, 570 (1953).

to the axis of cylindrical symmetry and midway between the pole faces of the magnet that produces such field. We will use a system of cylindrical coordinates with the origin at the intersection of the median plane and the axis of cylindrical symmetry, with the z -axis coinciding with the axis of cylindrical symmetry and pointing upwards. In such a magnet the vertical component of the magnetic field in the median plane can be written as $H_z(r, 0) = H_0 f(r)$, where $f(r)$ is a function of r only and is equal to one when r is equal to 0, and H_0 is the value of the field at the origin.

Once the field is defined in the median plane, it can be computed anywhere else by the relations $\text{div } \mathbf{H} = 0$ and $\text{curl } \mathbf{H} = 0$. If the field is decreasing, one finds then that, for particles which are moving outside the median plane, the radial component of the magnetic field produces a restoring force that accelerates the particles towards the median plane. This force is the one that produces the ring focus.

If a source that emits monoenergetic electrons of mass m , charge e , and velocity v is placed in the origin, the electrons emitted in the median plane will approach asymptotically to a circle with its center at the origin if for large values of the time t , dr/dt and d^2r/dt^2 go to zero. These conditions imply that for a certain value R of r , the following relation holds $\int_0^R r f(r) dr = R^2 f(R)$,

and that H_0 should have a value H_s given by the relation $H_s = mvR/e \int_0^R r f(r) dr$.

The first of these two relations is the condition for the existence of a stable orbit, and R is the radius of the stable orbit. The condition of the field being radially decreasing is not sufficient for the existence of the stable orbit.

We can define a dimensionless parameter k by the relation $H_0 = kH_s$ and, if one makes a plot of the fraction of the number of electrons which are emitted from a monoenergetic source and received in the detector as a function of k , one obtains a curve called the line profile. The maximum value of this fraction in the line profile is called the transmission T , and the full width at half the maximum is called the line width W . For these and other definitions related to β -ray spectrometers we follow FRISCH ⁽⁶⁾.

2. - The Trajectories and the Ring Focus.

The difficulty studying the properties of this machine is due to the impossibility of expressing the solutions of the system of differential equations in terms of known or common functions. For this reason we decided to solve them numerically. We chose for $f(r)$ the function $f(r) = 1 - 2r^2/3R^2$ in the

⁽⁶⁾ O. R. FRISCH: *Progress in Nuclear Physics*, vol. 2 (London, 1952), p. 1.

region from r equal to zero to r equal to R , where R is a constant length. This function is mathematically simple for the numerical integrations, and it seems that it can be made by suitably shaped pole faces without too great difficulty.

With this field it can be shown that for electrons emitted in the median plane the stable orbit is given by $r = R$ and that $H_s = 3mv/eR$. We made $R = v = 1$ to simplify the equations. The vertical and the radial component of the field at any point are given respectively by $H_z = kH_s(1 - 2r^2/3 + 2z^2/3)$ and $H_r = -4kH_s r z/3$.

The differential equations for the trajectories were left in the following form:

$$\frac{d^2 r}{dt^2} = r \frac{d\theta}{dt} \left(\frac{d\theta}{dt} - 3kg \right),$$

$$\frac{d^2 z}{dt^2} = -4kzr^2 \frac{d\theta}{dt},$$

$$\left(\frac{dr}{dt} \right)^2 + \left(r \frac{d\theta}{dt} \right)^2 + \left(\frac{dz}{dt} \right)^2 = 1 \quad \text{with} \quad g = 1 - \frac{2r^2}{3} + \frac{2z^2}{3}.$$

The trajectories were integrated for various values of the angle β which the emitted electrons form with the median plane at the origin, and for several values of k . We calculated with $k = 1.0000$ trajectories with $\sin \beta$ equal to 0.0000, 0.0100, 0.0200, 0.0400, and 0.0600. We also calculated for these same angles and values of k ranging from 0.9950 to 1.0050. The remaining trajectories needed for the problem were found by interpolation. The numerical integrations were carried out by Milne's method starting with a Taylor's expansion. The interval of t used was 0.0500 or 0.1000 and we carried four decimal places.

In Fig. 1 are shown the stable orbit and several trajectories of different values of k and $\sin \beta$. Notice that for k greater than one all the trajectories come back towards the center of the machine. For k less than one, the trajectories come back towards the center if $1 - k$ is less than $\sin^2 \beta/2$; they approximately coincide with

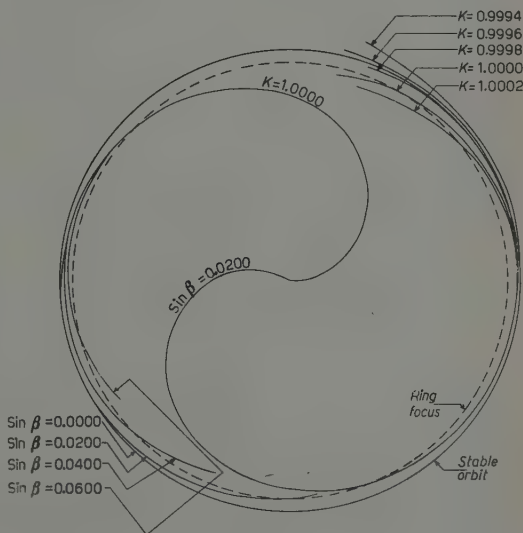


Fig. 1. — The projection of the trajectories in the median plane.

the stable orbit if $1 - k$ is equal to $\sin^2 \beta/2$; and they go beyond the stable orbit if $1 - k$ is greater than $\sin^2 \beta/2$. In Fig. 1 is also indicated the position of the ring focus.

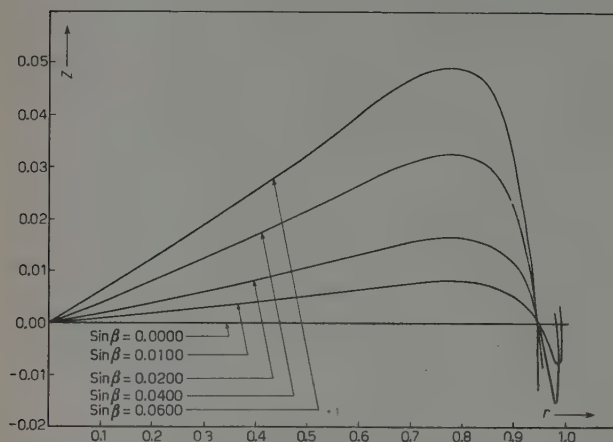


Fig. 2. — The projection of the trajectories in a rotating plane containing the cylindrical axis and the electron.

In Fig. 2 we show z as a function of r ; the ring focus is evident from this figure, being located between the values for r of 0.94 to 0.95. By examining closely the region of the ring focus, we found the optimum location of the ring focus and its aperture as a function of $\sin \beta$ that is allowed to pass, and they are shown in Table I.

TABLE I. — The optimum radius and aperture of the slit for ring focusing for several values of the maximum $\sin \beta$ allowed to pass. The radius of the stable orbit is unity.

Max $\sin \beta$	Radius (r)	Aperture ($2z$)
0.0300	0.9476	0.0006
0.0400	0.9463	0.0016
0.0500	0.9443	0.0034
0.0600	0.9419	0.0060

3. — The Characteristics of the Spectrometer.

In Fig. 3 we show schematically the spiral orbit spectrometer using ring focus, the aperture of the slit in the ring focus is narrower than shown. The pole faces should have such shape as to produce the desired field. The source is at the origin. The cylinders A define a slit which gives the maximum value of β that is allowed to pass. The spiral baffles B should extend from A to C . They should have the same shape as the trajectories in the median plane with k equal to 1; and there should be several of them symmetrically placed around the machine. They will serve to separate positrons from electrons. The hollow cylinders C define a slit that corresponds to the ring focus, its radius and aperture being those in Table I. We assume that the width of the detector

goes from the ring focus to the stable orbit and that its height covers the maximum value that z can have in this region. This maximum value of z is 0.047 for $\sin \beta$ equal to 0.0600 and it is approximately proportional to z .

We can see from Fig. 1 that many electrons are not received in the detector because they collide with the cylinders C . This situation can be improved by having two identical detectors at 180° , and we have made calculations for this case too. Of course the best case would be if one could have a ring

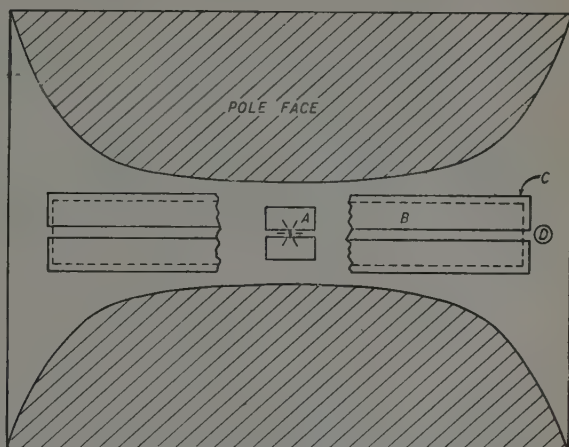


Fig. 3. - The spiral orbit spectrometer with ring focus, schematically. For description see text.

detector, a ring of some detector just slightly wider than the slit in the ring focus and placed around it. Such detector could possibly be made of a

scintillator plastic connected through a light pipe to a photomultiplier tube. We also made calculations for the ring detector.

In Fig. 4 are shown three line profiles calculated for one detector, two detectors and a ring detector when the maximum value of $\sin \beta$ is 0.0500. For the other maximum values of $\sin \beta$ the line profiles have similar shapes. The results of the transmission and line widths obtained are shown in Table II.

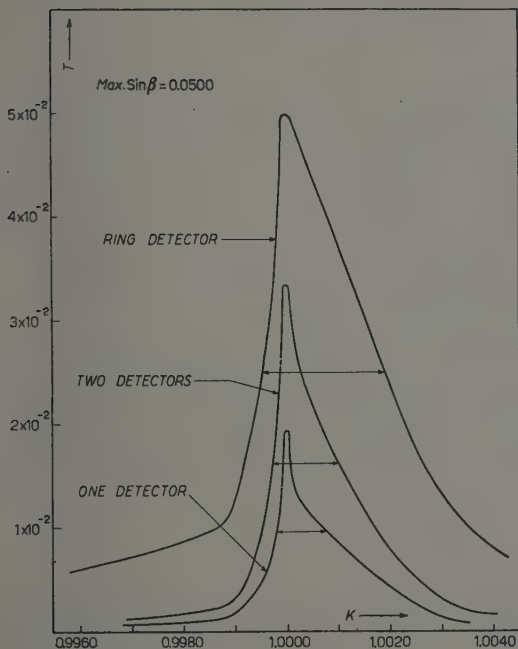


Fig. 4. - The line profiles of the spiral orbit spectrometer with ring focus, calculated with one detector, with two detectors and a ring detector.

TABLE II. — *The transmission and the line width for several values of the maximum $\sin \beta$ allowed to pass.*

Max $\sin \beta$	One detector		Two detectors		Ring detector	
	T	W	T	W	T	W
0.0300	0.0150	0.00033	0.0247	0.00052	0.0300	0.00072
0.0400	0.0174	0.00062	0.0296	0.00078	0.0400	0.00136
0.0500	0.0193	0.00091	0.0334	0.00116	0.0500	0.00232
0.0600	0.0206	0.00111	0.0360	0.00148	0.0600	0.00344

4. — Conclusions.

The relation between the transmission and the line width derived from the results in Table II is $T = 0.7W^{\frac{1}{2}}$ with one detector; $T = 1.0W^{\frac{1}{2}}$ with two detectors; and $T = 1.05W^{\frac{1}{2}}$ with a ring detector. This means that in this respect the spiral orbit spectrometer with ring focus when used with one detector is slightly below the machine of KOFOED-HANSEN (⁷) and better than all the other machines we know, including those in the review article of FRISCH (⁷). When the spiral orbit spectrometer with ring focus is used with two detectors or with a ring detector, it is also better than the machine of KOFOED-HANSEN (⁷) in the relation between the transmission and the line width.

The maximum transmissions that the spiral orbit spectrometer studied can give are 2.1% with one detector; 3.7% with two detectors; and 7.0% with a ring detector. These values depend on the value of β at which the trajectory is tangent to the ring focus, and on the probability of detection when the electron is between the ring focus and the stable orbit.

We have not examined the effect of the source size on the line width, nor have we examined other types of functions $f(r)$ which might possibly improve further the spiral orbit spectrometer with ring focus.

In regard to the possibility of this machine being successfully built, we would like to recall that to make a field with the exact $f(r)$ is not necessary, and the machine will work provided its radial dependence fulfills the condition stated in the introduction. However, the cylindrical symmetry of the field is much more critical for the functioning of the machine.

(⁷) O. KOFOED-HANSEN, J. LINDHARD and O. B. NIELSEN: *K. Danske Vidensk. Selsk. Mat. Fys. Medd.*, **25**, No. 16 (1950).

RIASSUNTO (*)

Si dimostra nel presente lavoro che lo spettrometro a orbita spirale ha un fuoco anulare in prossimità dell'orbita stabile. Sfruttando questa proprietà per mezzo di una fenditura cilindrica si può notevolmente migliorare la caratteristica dello spettrometro ad orbita spirale. Per un caso particolare studiato, la funzione di trasmissione in funzione dello spessore della traccia è data, per una sorgente puntiforme, da $T = 0,7 W^{\frac{1}{2}}$.

(*) Traduzione a cura della Redazione.

High Energy Neutron Reactions and the Nuclear Optical Model.

L. C. GOMES and J. LEITE LOPES

*Centro Brasileiro de Pesquisas Físicas and Faculdade Nacional de Filosofia
Rio de Janeiro, D.F.*

(ricevuto il 29 Gennaio 1955)

Summary. — Born's approximation is extended to the calculation of reaction and total cross sections. The results are compared with the experimental data on high energy neutron induced nuclear reactions under the assumption of a complex square well for the nuclear potential. This varies with the excitation energy but the values adjusted for the total cross section do not fit the angular distribution of the scattered neutrons.

Introduction.

Total cross-sections of neutron induced nuclear reactions have been measured for many elements and for different ranges of energy. The measures at about 90 MeV ⁽¹⁾ were satisfactorily described by the optical model proposed by FERNBACH, SERBER and TAYLOR ⁽²⁾.

In this model, a nucleus is represented by a partially transparent sphere endowed with an index of refraction and an absorption coefficient. This is equivalent to the assumption that the incident neutron is subjected by the nucleus to an average complex potential, the real part of which, U_0 , determines the refractive index of nuclear matter whereas the imaginary part, U_1 , is responsible for the partial neutron absorption. For 90 MeV neutrons, the experimental data were successfully described ⁽²⁾ by the following values of the constants.: $U_0 = 30.8$ MeV, $U_1 = 9.5$ MeV, with a nuclear radius $R = r_0 A^{1/3}$, $r_0 = 1.37 \cdot 10^{-13}$ cm.

This model was, however, not so successful in accounting for the measur-

⁽¹⁾ L. J. COOK, E. M. McMILLAN, J. M. PETERSON and D. C. SEWELL: *Phys. Rev.*, **75**, 7 (1949).

⁽²⁾ S. FERNBACH, R. SERBER and T. B. TAYLOR: *Phys. Rev.*, **75**, 1352 (1949).

ements at 156 MeV ⁽³⁾, 270 MeV ⁽⁴⁾ and 280 MeV ⁽⁵⁾. At the first of these energies, the nuclear potential U_0 required by the model would be 6 MeV. At 270 MeV, not even for $U_0 = 0$ are the experimental points brought into agreement with the curve predicted by the optical model. These results did not support the extrapolated hope that U_0 would be about the same as indicated by the low energy data.

More recently, an extension of the optical model to the description of low energy neutron induced reactions ⁽⁶⁾ was proposed by FESHBACH, PORTER and WEISSKOPF ⁽⁷⁾. The behaviour of the total cross-sections as a function of the energy, up to 3 MeV, indicates that the neutron wave is not completely absorbed by the nucleus — a suggestion that the latter could be conveniently described by a complex potential. The constants required by experiment are in this case ⁽⁸⁾:

$$U_0 = 42 \text{ MeV}, \quad U_1 = 2.1 \text{ MeV}, \quad r_0 = 1.45 \cdot 10^{-13} \text{ cm}.$$

The knowledge of U_0 , U_1 and r_0 for different energies is of interest. It may give some information to the question of velocity dependent nuclear forces and of the distribution of nucleons in nuclei at such energies.

A re-examination of the description of the high energy data by the optical model is reported in this note. In this energy region, some approximation method should be used for the calculation of the cross-sections involved. Our results are based on the use of the Born approximation. The computation of the elastic scattering cross-section in this approximation is well known. In § 1 we show that the Born method can be extended to the reaction cross-section, which enables one to evaluate the total cross-section in this approximation. In § 2, the formula is compared with experiment; the angular distribution of the elastically scattered neutrons is also given.

⁽³⁾ A. E. TAYLOR, T. G. PICKAVANCE, J. M. CASSELS and T. C. RANDLE: *Phil. Mag.*, **42**, 751 (1951).

⁽⁴⁾ J. DE JUREN: *Phys. Rev.*, **80**, 27 (1950).

⁽⁵⁾ R. FOX, C. LEITH, L. WOUTERS and K. R. MACKENZIE: *Phys. Rev.*, **80**, 23 (1950).

⁽⁶⁾ H. H. BARSCHALL: *Phys. Rev.*, **86**, 431 (1952); D. W. MILLER, R. K. ADAIR, C. K. BROCKELMAN and S. E. DARDEN: *Phys. Rev.*, **88**, 83 (1952).

⁽⁷⁾ H. FESHBACH, C. E. PORTER and V. F. WEISSKOPF: *Phys. Rev.*, **90**, 166 (1953).

⁽⁸⁾ R. K. ADAIR: *Phys. Rev.*, **94**, 737 (1954); V. F. WEISSKOPF: *Communication at the Glasgow Nuclear Physics Conference*, 1954.

1. - Reaction and Total Cross-Sections in Born Approximation.

The exact expressions for the elastic scattering cross-section σ_s and the reaction cross-section σ_r are respectively:

$$\sigma_s = \frac{4\pi}{k^2} \sum_l (2l+1) \exp[-2\eta_1^{(l)}] [\sin^2 \eta_0^{(l)} + \sinh^2 \eta_1^{(l)}],$$

$$\sigma_r = \frac{\pi}{k^2} \sum_l (2l+1) (1 - \exp[-4\eta_1^{(l)}]).$$

$\eta_0^{(l)} + i\eta_1^{(l)}$ is the l -th complex phase-shift corresponding to complex potential $V_0(r) + iV_1(r)$ in the single particle wave equation.

In Born's approximation, both parts $\eta_0^{(l)}$ and $\eta_1^{(l)}$ of the phase-shift are given by:

$$(1) \quad \begin{cases} \eta_{0,1}^{(l)} = -\frac{2mk}{\hbar^2} \int_0^\infty V_{0,1}(r) [f_l(r)]^2 r^2 dr, \\ f_l(r) = \left(\frac{\pi}{2kr}\right)^{\frac{1}{2}} J_{l+\frac{1}{2}}(kr), \end{cases}$$

and are to be inserted in the Born scattering cross-section:

$$(2) \quad \sigma_s = \frac{4\pi}{k^2} \sum_l (2l+1) (\eta_0^{(l)^2} + \eta_1^{(l)^2}).$$

Since the phase-shift occurs quadratically in (2), the reaction cross-section should have the following form, in Born's approximation:

$$(3) \quad \sigma_r = \frac{4\pi}{k^2} \sum_l (2l+1) (\eta_1^{(l)} - 2\eta_1^{(l)^2}).$$

We write the potential in the following way:

$$(4) \quad V_0(r) + iV_1(r) = (U_0 + iU_1)\Phi(r),$$

where U_0 and U_1 do not depend on r . The phase shifts are, from (1) and (4):

$$(5) \quad \eta_{0,1}^{(l)} = -\frac{2mk}{\hbar^2} U_{0,1} \zeta_l; \quad \zeta_l = \int_0^\infty \Phi(r) [f_l(r)]^2 r^2 dr.$$

The total cross-section is then:

$$(6) \quad \sigma_{\text{tot}} = \sigma_s + \sigma_r = \frac{4\pi}{k^2} \sum_l (2l+1) \eta_1^{(l)} + \frac{U_0^2 - U_1^2}{U_0^2 + U_1^2} \sigma_s,$$

where:

$$(7) \quad \left\{ \begin{array}{l} \sigma_s = 2\pi \int_0^\pi |f(\theta)|^2 \sin \theta \, d\theta, \\ f(\theta) = -\frac{2m}{\hbar^2} \int_0^\infty (U_0 + iU_1) \Phi(r) \frac{\sin Kr}{Kr} r^2 \, dr, \\ K = 2k \sin \frac{\theta}{2}. \end{array} \right.$$

The sum which appears in the right-hand side of (6) can be easily computed by means of (5) and of the following identity:

$$\sum_l (2l+1) [f_l(r)]^2 = 1,$$

which is the limit of:

$$\frac{\sin Kr}{Kr} = \sum_l (2l+1) [f_l(r)]^2 P_l(\cos \theta),$$

for $\theta \rightarrow 0$. One obtains:

$$\sum_l (2l+1) \eta_1^{(l)} = -\frac{2mkU_1}{\hbar^2} \int_0^\infty \Phi(r) r^2 \, dr.$$

Therefore (6) is:

$$\sigma_{\text{tot}} = -\frac{8\pi m}{\hbar^2 k} U_1 \int_0^\infty \Phi(r) r^2 \, dr + \frac{U_0^2 - U_1^2}{U_0^2 + U_1^2} \sigma_s.$$

An attractive square well potential is defined by:

$$\Phi(r) = \begin{cases} -1, & \text{for } r < R, \\ 0, & \text{for } r > R, \end{cases}$$

where $R = r_0 A^{\frac{1}{3}}$ is the nuclear radius. It gives rise to the following cross-sections:

$$\begin{aligned}\sigma_s &= \frac{2\pi m^2}{\hbar^4 k^2} (U_0^2 + U_1^2) R^4, \\ \sigma_r &= \frac{8\pi m U_1}{3\hbar^2 k} R^3 - \frac{4\pi m^2}{\hbar^4 k^2} U_1^2 R^4, \\ \sigma_{\text{tot}} &= \frac{8\pi m U_1}{3\hbar^2 k} R^3 + \frac{2\pi m^2}{\hbar^4 k^2} (U_0^2 - U_1^2) R^4.\end{aligned}$$

The dependence of the total cross-section with A has the following form:

$$\sigma_{\text{tot}} = \alpha A + \beta A^{\frac{4}{3}},$$

where

$$\alpha = \frac{8\pi m}{3\hbar^2 k} U_1 r_0^3, \quad \beta = \frac{2\pi m^2}{\hbar^4 k^2} (U_0^2 - U_1^2) r_0^4.$$

2. - Comparison with Experiment.

We see that the dependence of σ_{tot}/A with $A^{\frac{1}{3}}$ is linear. This is in agreement with the experimental results, which are plotted in Fig. 1 for 90 MeV and 410 MeV (*) and in Fig. 2 for 156, 270 and 280 MeV. The slopes of the straight lines are negative and this means that, at least in the Born approximation, the absorptive part of the potential U_1 is larger than the real part U_0 .

TABLE I.

r_0	Neutron energy							
	$E = 90 \text{ MeV}$		$E = 156 \text{ MeV}$		$E = 275 \text{ MeV}$		$E = 410 \text{ MeV}$	
	U_0	U_1	U_0	U_1	U_0	U_1	U_0	U_1
	MeV	MeV	MeV	MeV	MeV	MeV	MeV	MeV
1.3	25.0	29.3	12.4	20.8	15.8	24.4	25.2	29.7
1.4	19.4	23.4	9.7	16.7	11.2	19.5	19.5	23.8
1.5	15.2	19.1	6.0	13.6	7.7	15.9	11.8	19.4

In Table I are the values of U_0 and U_1 for the different incoming neutron energies and a few values of r_0 (in 10^{-13} cm unit). The potentials change with

(*) V. A. NEDZEL: *Phys. Rev.* **94**, 174 (1954).

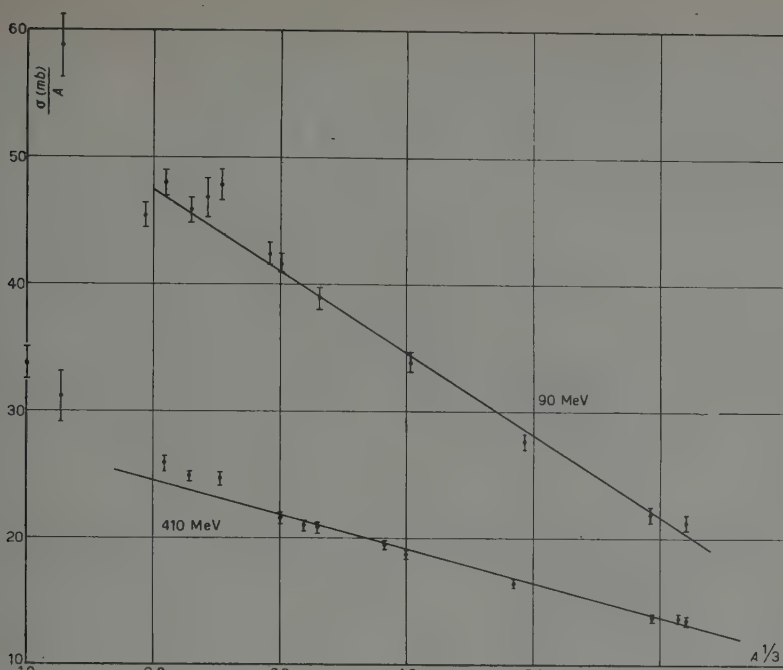


Fig. 1.

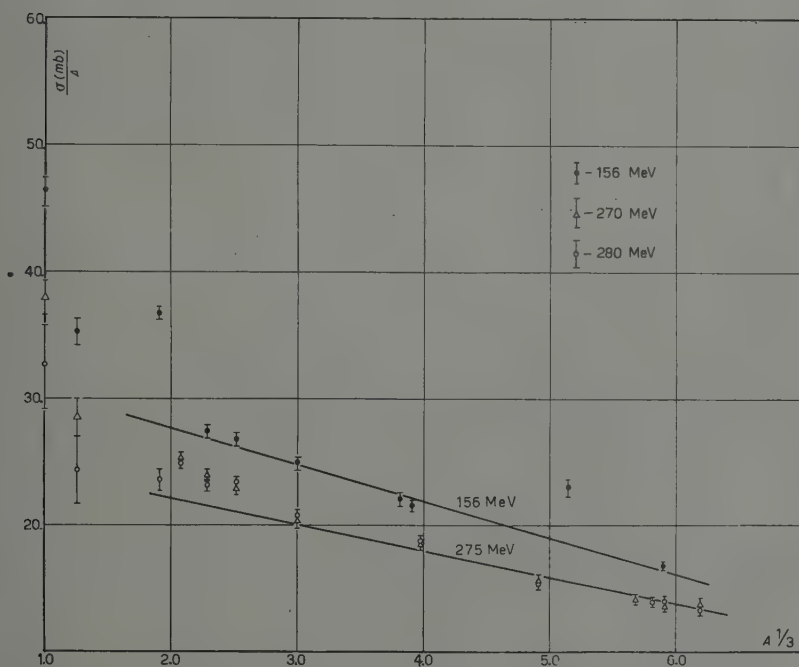


Fig. 2.

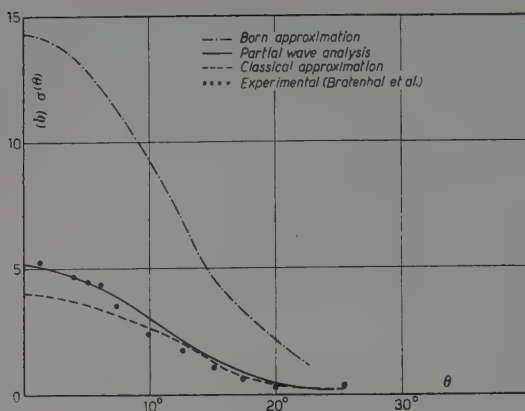


Fig. 3.

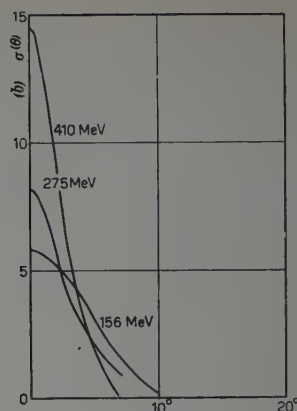


Fig. 4.

the excitation energy; this is visualized in Fig. 5. Whereas the value of U_0 required by the treatment of SERBER *et al.*, would be zero for 270 MeV neutrons ⁽⁴⁾, in the present approximation the corresponding value is about 16 MeV for $r_0 = 1.3 \cdot 10^{-13}$ cm.

These values of U_0 and U_1 , however, do not fit well the angular distribution of the elastically scattered neutrons. Fig. 3 reproduces the curve as predicted by Born's approximation at 90 MeV. It is about three times as large as the experimental points ⁽⁹⁾ which fit the partial wave analysis ⁽¹⁰⁾ for Aluminium. The curve predicted by the WKB approximation ⁽²⁾ is also shown in Fig. 3 and gives results of the opposite size as compared to

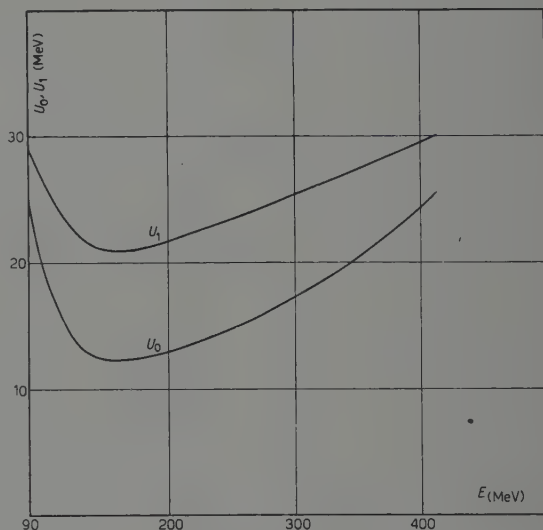


Fig. 5.

Born's approximation. Fig. 4 shows the angular distribution in Born's approximation for the higher energies. Experimental measurements of this distribution at such energies are not known to us. Another quantity which is not reproduced

⁽⁹⁾ A. BRATENHAL, S. FERNBACH, R. H. HILDEBRAND, C. E. LEITH and B. J. MOYER: *Phys. Rev.*, **77**, 597 (1950).

⁽¹⁰⁾ S. PASTERNAK and H. S. SNYDER: *Phys. Rev.*, **80**, 921 (1950).

by Born's approximation in the present model is the ratio of reaction to total cross-section (*). This ratio is about one half and independent of the nucleus, as indicated experimentally (⁴). This is not reproduced by the present treatment; the ratio σ_r/σ_{tot} is smaller than 0.5 and is not independent of A . This is essentially the reason why we did not add a spin-orbit coupling to the complex potential, as suggested previously by FERMI (¹¹) in treating the high energy polarization of protons. This additional potential would increase only the elastic cross-section and would decrease the ratio of reaction to total cross-section still more (assuming the absorption to be spin independent).

The results show that the Born approximation, as extended to encompass the inelastic processes, is not a good tool to decide about the validity of the optical model at the energies investigated. Indeed, the phase shift for $l=0$ and at 90 MeV, as computed by formula (1) with the potentials of Table I is about 1.4.

A preliminary calculation which employs the first 14 terms of the Faxen-Holtmark series, the phase-shifts being still evaluated by the integral (1), gives a complex potential equal to $(19.5 + i17)$ MeV, if the total cross-section is adjusted for Al and Pb.

The authors had several stimulating conversations with L. MARQUEZ on the subject of this paper.

(*) We are indebted to Dr. L. MARQUEZ for calling our attention to this question.

(¹¹) E. FERMI: *Nuovo Cimento*, **11**, 407 (1954).

RIASSUNTO (*)

Si estende l'approssimazione di Born al calcolo delle sezioni d'urto di reazione e totali. Si confrontano i risultati coi dati sperimentali per le reazioni nucleari provocate da neutroni di alta energia, nell'ipotesi di una buca rettangolare di potenziale nucleare. Il potenziale varia con la energia di eccitazione, ma i valori adattati per le sezioni d'urto totali non soddisfano la distribuzione angolare dei neutroni diffusi.

(*) Traduzione a cura della Redazione.

Structural Effects in the Ultrasonic Absorption of Liquid Mixtures (*).

D. SETTE

Istituto Nazionale di Ultracustica « O. M. Corbino » - Roma

(ricevuto il 9 Febbraio 1955)

Summary. — Experiments have been performed to clarify the behavior of those binary liquid mixtures where the ultrasonic absorption coefficient has a maximum at an intermediate concentration. Measurements on water-methyl alcohol mixtures at -10°C and -32°C have shown that a maximum of the absorption coefficient is present just as in the other water-alcohol systems. This corroborates Storey's theory that the losses are caused by relaxation phenomena due to alteration of the molecular association equilibrium produced by temperature variations. Research on mixtures of partially soluble liquids in the critical region permits an approximate calculation of the increase of viscosity losses produced by the density fluctuations in the liquid. This calculation shows that while the viscosity losses can be much greater than those given by Stokes' formula, they are not sufficient to explain the values of the experimental absorption coefficient. The relaxation phenomena in the equilibrium among mother phase and custers are the more important dissipative effects. The conclusion is reached that in all these mixtures having a maximum of the absorption coefficient, the losses are caused primarily by relaxation phenomena due to the variation of the equilibrium among different ways in which molecules of the two kinds can associate. The equilibrium is altered by the temperature variations produced by sound waves.

1. — Introduction.

The ultrasonic absorption of those binary liquid mixtures in which the coefficient reaches a maximum at an intermediate concentration, has been object of considerable research in these years. Such a behavior of the absorption

(*) The work has been partially carried out at the Physics Department of the Catholic University of America (Washington D.C.) and for that part it was aided by ONR contract.

coefficient was first found in some mixtures formed by water either with alcohols or with some other polar liquid like acetone ⁽¹⁾. More research has successively shown a similar behavior of the ultrasonic absorption coefficient in mixtures of other polar liquids such as the nitrobenzene-alcohol ⁽²⁾ and ether-alcohol systems, as well as in some mixtures of finite soluble liquids near the consolute temperature ⁽³⁾. It was moreover shown ⁽³⁾ that the absorption coefficient of such mixtures is frequency dependent and it decreases quickly with increasing temperature. The latter behavior points to the existence of dissipative phenomena which are strongly affected by thermal agitation.

The same results were found by L. R. O. STOREY ⁽⁴⁾ in water-ethyl alcohol mixtures. STOREY suggested an explanation for the losses in this system, and in those formed by polar molecules, which is based on the assumption that molecular associations are present in solution and that their equilibrium is altered by the temperature changes produced by sound waves.

STOREY's suggestion seems plausible as it allows for a satisfactory explanation of the behavior of the absorption coefficient in those water-alcohol systems which show a maximum. It is not clear however why the ultrasonic absorption in water-methyl alcohol behaves differently than in other water-alcohol systems.

In the present paper results are given of the work carried out to clarify the behavior of mixtures where dissipative phenomena bound to the particular structure of the liquid are present. In particular the water-methyl alcohol mixtures as well as mixtures of partially soluble liquids near the consolute temperature are studied.

2. - The Nature of the Dissipative Effects.

Fig. 1 shows the curves [due to C. J. BURTON ⁽⁵⁾] of the absorption coefficient vs composition for various water-alcohol systems obtained at about 25 °C. It is

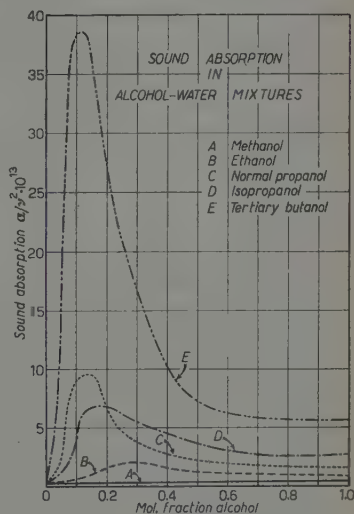


Fig. 1. - Ultrasonic absorption in water-alcohol mixtures at 25 °C.

⁽¹⁾ D. SETTE: *Suppl. Nuovo Cimento*, **6**, 1 (1949); G. W. WILLARD: *J.A.S.A.*, **12**, 438 (1941); F. H. WILLIS: *J.A.S.A.*, **19**, 242 (1947); C. J. BURTON: *J.A.S.A.*, **20**, 186 (1948).

⁽²⁾ D. SETTE: *J.A.S.A.*, **23**, 359 (1951).

⁽³⁾ D. SETTE: *Journ. Chem. Phys.*, **21**, 558 (1953).

⁽⁴⁾ L. R. O. STOREY: *Proc. Phys. Soc.*, B **65**, 943 (1952).

⁽⁵⁾ C. J. BURTON: *J.A.S.A.*, **20**, 186 (1948).

interesting to observe that while a maximum of the absorption coefficient is present in the systems formed either with ethyl alcohol or with a higher alcohol, in water-methyl alcohol mixtures the absorption coefficient is linearly dependent on concentration.

TABLE I - *Ultrasonic absorption in ethyl ether-ethyl alcohol and n-hexane-nitrobenzene mixtures at 8 MHz*

	Mole fraction second component	<i>T</i> (°C)	α (cm ⁻¹)	$(\alpha/\nu^2) \cdot 10^{17}$ (s ² cm ⁻¹)
Ethyl ether-ethyl alcohol	0	30	.035	54
	.166		.038	59
	.304		.040	62
	.453		.036	57
	.554		.035	55
	.743		.033	52
	.898		.033	52
	1		.033	52
n-hexane-nitrobenzene	0	25	.042	66
	.171		.065	101
	.293		.224	350
	.409		.435	680
	.500		.350	545
	.599		.155	240
	.709		.083	130
	.855		.048	76
	1		.046	72

In Figs. 2 and 3 similar curves are shown for the ethyl ether-ethyl alcohol and n-hexane-nitrobenzene mixtures. The measurements in these two systems were performed by means of an optical method ⁽⁶⁾ at a frequency of 8 MHz. The numerical results are given in Table I; (α is the amplitude absorption coefficient, ν the frequency).

The experimental values of the absorption coefficient for all the mixtures considered are much higher than the classical ones (i.e. due to viscosity and thermal conductivity), as normally happens in polyatomic pure liquids.

It is fairly well established that the excess of ultrasonic absorption in most liquids is caused by relaxation phenomena. These are bound to the existence in the liquid of equilibria which can be altered by sound waves and to the fact that a finite time is required by the system to pass from one equilibrium

⁽⁶⁾ D. SETTE: *Nuovo Cimento*, **7**, 55 (1950).

condition to another. In unassociated liquids it seems that the sound waves alter the energy distribution between translational and vibrational degrees of freedom. In such a case the temperature changes produced by sound waves are of importance and the phenomena can be described by assuming a frequency dependent specific heat. The relaxation frequencies are usually very high so that the parameter α/ν^2 remains constant in the frequency range of experiments. A characteristic of this type of relaxation phenomena is that the absorption coefficient of the liquid increases slightly with temperature.

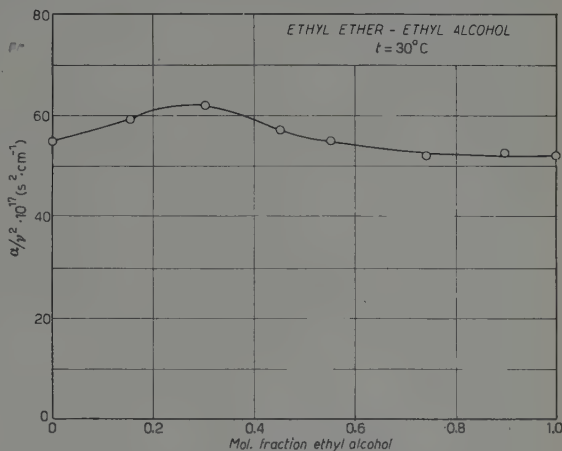


Fig. 2. - Ultrasonic absorption in ether-ethyl alcohol mixtures.

In strongly associated liquids, like water and alcohols the energy equipartition between external and internal degrees of freedom is attained very quickly, owing to the strong coupling among molecules.

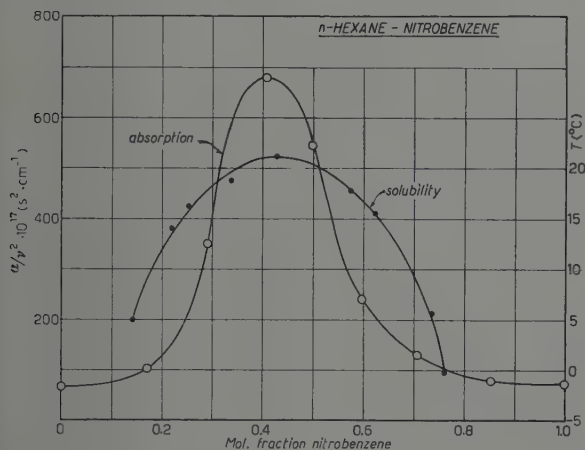


Fig. 3. - Ultrasonic absorption at 25°C and coexistence curve for n-hexane-nitrobenzene mixtures.

experimental range. The temperature dependence of the absorption coefficient produced by such relaxation phenomena (α_{β}) is very characteristic. It has been found experimentally that the absorption coefficient decreases very quickly when the temperature raises while the ratio $\alpha_{\text{exp}}/\alpha_c = (\alpha_{\beta} + \alpha_c)/\alpha_c$ (α_c , classical

The relaxation phenomena of interest in such liquids are those relative to equilibria between various structural forms which are present in the liquid and have different densities. The pressure changes produced by the sound waves are now responsible for the equilibrium variation and the phenomena can be described by means of a frequency dependent compressibility. Usually the relaxation frequencies are well above the ex-

absorption coefficient) remains practically constant for each liquid and generally has a value roughly between 1.5 and 3.

Another kind of relaxation phenomena still found in low viscosity liquids,

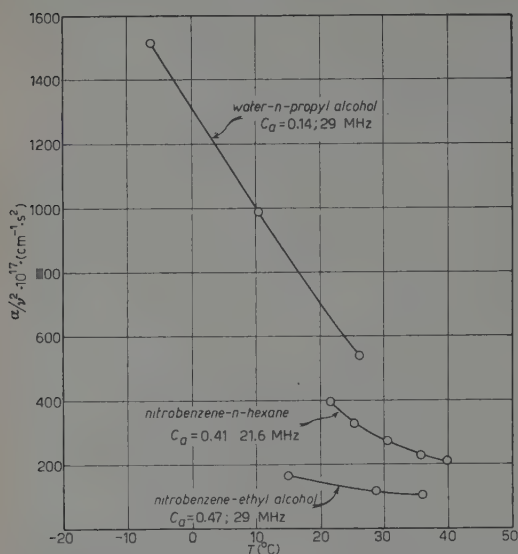


Fig. 4. — α/v^2 versus temperature for some mixtures.

the neighborhood of that for which the maxima of absorption occur in the systems: water-n-propyl alcohol, nitrobenzene-ethyl alcohol and nitrobenzene-n-hexane. The measurements were made at frequencies of 21.6 MHz and 29 MHz with a pulse method described elsewhere (7). In Table II are given the results of measurements in such mixtures as function of temperature and frequency (Fig. 5).

The rapid decrease of α/v^2 with temperature shows that the dissipative processes in all these systems are bound to structural equilibria destroyed by thermal agitation.

Similar and more extensive results have been obtained by L. R. O. STOREY (8) in the case of water-ethyl alcohol mixtures. He was able

refers to liquids in which a chemical equilibrium with a low rate constant is present. This is for instance the case of salt solutions. Many liquids of the last category have relaxation frequencies not too far from the accessible range so that α/v^2 at times does not remain constant with v . The temperature changes produced by the sound waves are important in these liquids and the phenomena can be described by means of a specific heat which is function of frequency. The change of chemical equilibrium with temperature has a very important influence on the variation of α with temperature.

Fig. 4 gives the ratio α/v^2 for mixtures whose composition is in

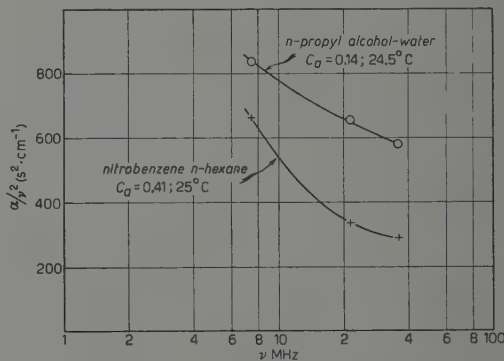


Fig. 5. — α/v^2 versus ν for some mixtures.

(7) D. SETTE: *Journ. Chem. Phys.*, **19**, 1337 (1951).

(8) See quotation (4).

TABLE II. — *Ultrasonic absorption in some binary mixtures.*

	Mole fraction second component	T (°C)	ν MHz	α cm ⁻¹	$(\alpha/\nu^2) \cdot 10^{17}$ (s ² cm ⁻¹)
Water-n-propyl	.139	24.5	7.5	.470	835
			21.8	3.11	655
		6.2	29	12.7	1515
		10.6		8.30	990
		26.2		4.50	536
		24.5	36.5	7.75	582
Ethyl alcohol- nitrobenzene	.474	15	29	1.36	165
		28.7		.983	117
		36		.875	104
n-hexane-nitro- benzene	.409	25.1	7.5	.371	660
		21.6	21.6	1.85	396
		25.1		1.53	328
		25.1	21.8	1.57	330
		30.6	21.6	1.26	270
		35.7		1.07	228
		39.8		.96	206
		25.1	36.3	3.79	287

to show that the ratio $\alpha_{\text{exp}}/\alpha_c$ does not remain constant when the temperature changes. Following a suggestion of E. BAUER⁽⁹⁾ for the explanation of the ultrasonic absorption in these mixtures, STOREY assumed that associations of different molecules are in solution and that the equilibrium among them is altered by temperature changes, as in liquids where a chemical equilibrium with a low rate of reaction is present. The specific heat would then be frequency dependent.

The reasons which suggested to BAUER and STOREY the idea that molecular associations could be in solution are the following: 1) the specific heats of water alcohol mixtures are not linear functions of the composition; 2) the freezing point curve has a discontinuity for a composition near that for which the sound absorption coefficient is maximum; 3) the heat of mixing is finite and it has a maximum for the same composition (Fig. 6). It seems to us that two more reasons can be added. The various water-alcohol systems which have a maximum of the absorption coefficient have also a maximum of the

(⁹) See quotation (4) and: J. M. M. PINKERTON: *International Conference on Ultrasonics*, pag. 126 (Koninklijke Vlaasme Acad. Brussels, 1951).

sound velocity. This has been explained by R. PARSHAD ⁽¹⁰⁾ on the basis of dynamic equilibria among different kinds of molecular associations. Moreover the viscosity as function of concentration in water-ethyl alcohol and water-n-propyl alcohol (Fig. 7), for which data are available ⁽¹¹⁾, presents a maximum

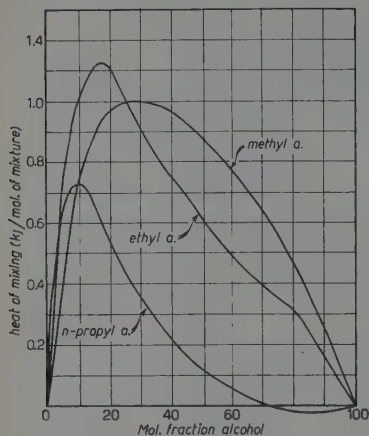


Fig. 6. — Heat of mixing for water-alcohol mixtures.

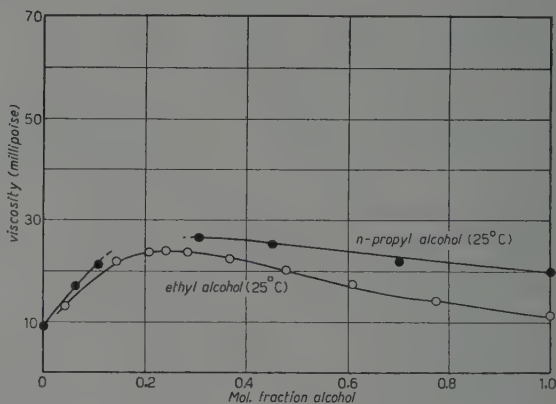


Fig. 7. — Viscosity in water-ethyl alcohol and water-n-propyl alcohol mixtures.

for a concentration near the one of maximum ultrasonic absorption. While it is still uncertain what the particular process is which causes such a behavior, it is well agreed that the viscosity maximum is bound to molecular associations ⁽¹²⁾.

The behavior of sound absorption in the mixtures of water and an alcohol where a maximum of the absorption coefficient occurs, can be easily explained by the hypothesis of existence of relaxation phenomena among molecular associations. The term association is used broadly in the sense that it includes any kind of short range order. It is evident that in such a system the absorption coefficient will attain a maximum for the concentration for which the number of those molecular associations which cause the relaxation phenomena is maximum. The fast temperature decrease of the absorption coefficient is, moreover, due to the destruction of associations by thermal agitation.

3. — Water-Methyl Alcohol Mixtures.

STOREY's suggestion seems to explain satisfactorily the experiments in those water-alcohol systems where a maximum of the absorption coefficient

⁽¹⁰⁾ P. PARSHAD: *Ind. Journ. Phys.*, **15**, 323 (1941); *J.A.S.A.*, **20**, 66 (1948).

⁽¹¹⁾ *International Critical Tables*, vol. V, pag. 22 (New York, 1928).

⁽¹²⁾ J. R. PARKINGTON: *Advanced Treatise on Physical Chemistry*, vol. II, pag. 115 (London, 1951).

has been found. It is to be observed however that the same phenomena which suggest the presence of associations in the mixture of water either with ethyl-alcohol or with a higher alcohol are present also in the water-methyl alcohol system. In particular: the heat of mixing (Fig. 6) has a maximum for a mole fraction of alcohol of about .25; the freezing point of the mixtures goes, in the part for which data are available, beyond the freezing point of either component; each of the sound velocity and the viscosity ⁽¹¹⁾ curves present a maximum. It seems therefore plausible to admit that the same kinds of associations are present in the water methyl-alcohol mixtures as in the other systems water-alcohol. Instead, as has been shown in Fig. 1, the absorption coefficient at 25 °C does not present a noticeable maximum.

This behavior could simply be due, as STOREY pointed out, to the fact that in the case of water-methyl alcohol mixtures the temperature of 25 °C at which the measurements were performed, is too high compared with the freezing point of the mixtures, to observe any effect of the molecular associations on the ultrasonic absorption. Moreover, it could be that a smaller fraction of the specific heat is involved in the phenomena in the case of methyl alcohol, than in those of the other alcohols.

In order to clarify the behavior of the ultrasonic absorption in the water-alcohol systems we have studied the water-methyl alcohol mixtures at temperature largely below the normal room temperature ⁽¹³⁾.

In Fig. 8, the experimental values of α/ν^2 at 23 MHz are plotted for the temperature of -32 °C and -10 °C. On the same figure a part of the solidification curve as a function of composition is shown.

The presence of a maximum of the absorption coefficient is evident at both temperatures. Its position changes slightly with temperature. The freezing point of the mixture of maximum absorption at -32 °C is not too much different from the temperature of the experiment, so that we can admit that

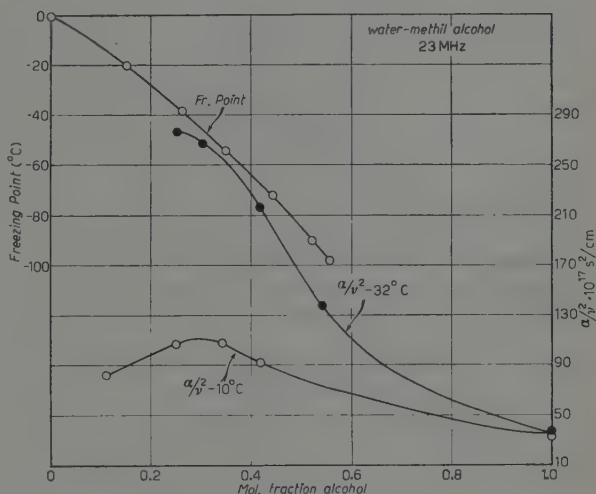


Fig. 8. - α/ν^2 versus composition at -10 °C and -32 °C and solidification curve for water-methyl alcohol mixtures.

⁽¹³⁾ D. SETTE: to be published on *Ricerca Scientifica*.

the prevalent associations have a mole fraction of alcohol 0.25, i.e. they are formed by 3 molecules of water and one of methyl alcohol. This result agrees with those of STOREY because he found an increase in the coordination number with the molecular weight of the alcohol: it would be 3 for methyl alcohol, 4 for ethyl alcohol; 9 for n-propyl alcohol.

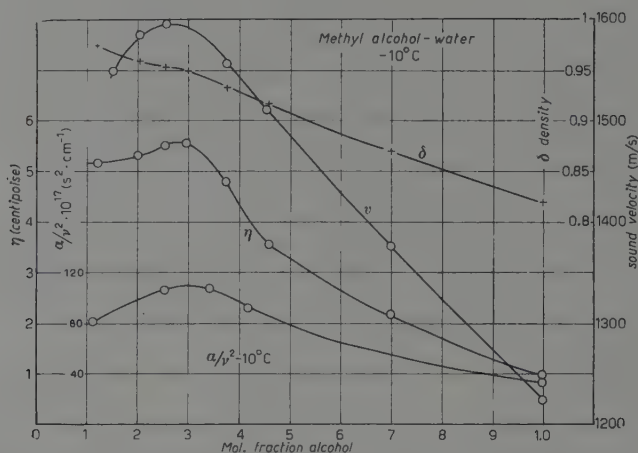


Fig. 9. — Density, viscosity, sound velocity and sound absorption in water-methyl alcohol mixtures.

In order to calculate the classical absorption coefficients at -10°C , measurements of velocity, density and viscosity were made⁽¹⁴⁾. The results are given in Fig. 9. α/v^2 vs composition has also been plotted to show the relative position of maxima in the curves relative to absorption, velocity, viscosity and density.

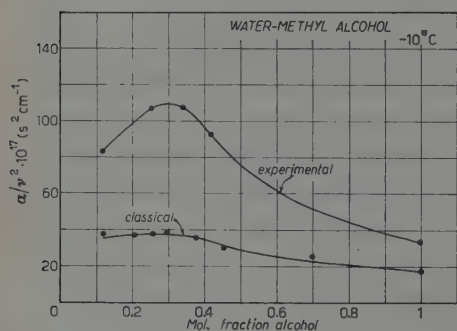


Fig. 10. — Experimental and classical values of α/v^2 in water-methyl alcohol mixtures at -10°C .

The experimental and classical values of α/v^2 at -10°C are shown in Fig. 10. In the calculation of α_c only the viscosity losses have been considered because they are normally in liquids much greater than those due to thermal conductivity. The difference of ordinates between the two curves gives the part of α_{exp}/v^2 ascribed to relaxation phenomena.

The temperature dependence of

⁽¹¹⁾ The author express his thanks to Dr. G. PISENT for helping him during these measurements.

$\alpha_{\text{exp}}/\nu^2$ for a mixture of composition 0.25, is shown in Fig. 11. The classical values of α_c/ν^2 calculated at temperature of -10°C and $+13.6^\circ\text{C}$ are indicated by points.

The ratio $\alpha_{\text{exp}}/\alpha_c$ is not independent from the temperature but it varies from 1.7 at 13.6°C to 2.7 at -10°C . Moreover, in contrast to what happens in the two pure components, the ratio $\alpha_{\text{exp}}/\nu^2$ in these mixtures changes with frequency, as shown in Fig. 12 for a mixture of alcohol mole fraction 0.34.

These results show, in agreement to what has been mentioned above, that the relaxation phenomena in the water-methyl alcohol mixtures are not exclusively of that structural kind which is present in the two pure components, i.e. due to the existence in the liquid of various structures of different densities and which produce a frequency dependent compressibility.

Together with phenomena of this kind which are probably present in the

mixtures as well as in the pure components, there are others produced by different equilibria as for instance the equilibrium among associations suggested by BAUER and STOREY. The latter relaxation phenomena are of the same nature as those found in liquids where a chemical equilibrium with a low rate constant is present and can be characterized by a frequency dependent specific heat.

The problem of separating the losses produced by each of the two kinds of phenomena is not an easy one. For the case of water-ethyl alcohol mixtures STOREY has assumed that the losses due to the first kind of phenomena (α_β), i.e., due to a frequency dependent compressibility, change linearly between the known values for the pure components. This approximation seems a little crude, however, if one considers that the viscosity in these systems is not a linear function of composition but has a maximum. This means that the classical

absorption coefficient does not change linearly with the composition and there is no reason why α_β should. It would seem a better hypothesis to assume

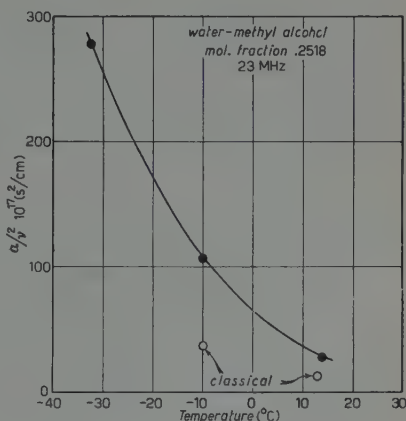


Fig. 11. — α/ν^2 versus temperature for a water-methyl alcohol mixture (alcohol mole fraction 0.25).

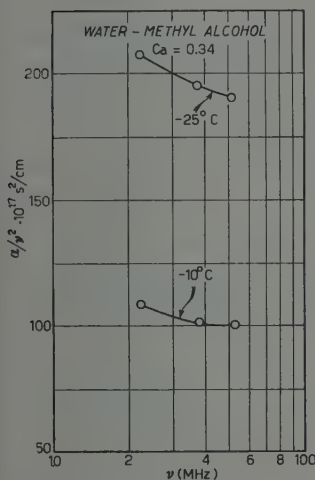


Fig. 12. — α/ν^2 versus ν for a water-methyl alcohol mixture (alcohol mole fraction 0.34).

a linear variation of the ratio $(\alpha_\beta + \alpha_c)/\alpha_c$ between the known values for the pure components where the ratio is temperature independent. The value of $\alpha_{\text{exp}}/\alpha_c = (\alpha_\beta + \alpha_c)/\alpha_c$ is 2 for methyl alcohol and 3 for water. If we assume that the same value 3 can be used for water at -10°C , a linear variation of $(\alpha_\beta + \alpha_c)/\alpha_c$ gives for the ratio itself the values 2.75 and 2.66 for the mixtures of mole fraction .25 and .34 for which we have measured the absorption coefficient as function respectively of temperature and frequency.

The experimental value of the ratio $\alpha_{\text{exp}}/\alpha_c$ for a mixture of 0.25 alcohol mole fraction is 1.73 at 13°C , i.e. much less than the value of $(\alpha_\beta + \alpha_c)/\alpha_c$ calculated with the above approximation (2.75). The same assumption applied to a the mixture of .34 alcohol mole fraction would give a value of $(\alpha_\beta + \alpha_c)/\nu^2 = 98 \cdot 10^{-17} \text{ s}^2 \text{ cm}^{-1}$ at -10°C , i.e. the relaxation phenomena of the kind present in the pure components would explain the largest part of the observed absorption coefficient because $\alpha_{\text{exp}}/\nu^2$ goes from $108 \cdot 10^{-7}$ to $100 \cdot 10^{-17} \text{ s}^2 \text{ cm}^{-1}$ between 23 and 53 MHz at -10°C . The contribution to the losses of the relaxation phenomena of the new kind would then be very small. Instead the opposite is indicated by the experimental results as, for instance, the temperature dependence of the ratio $\alpha_{\text{exp}}/\alpha_c$. It seems therefore that the same structural changes with composition which produce the appearance of the new process alter so greatly the structure of the liquid that no simple hypothesis can be at present done concerning the process bound to a frequency dependent compressibility.

The impossibility at present of separating the contributions of the two different phenomena does not allow one to make a reliable calculation of their relaxation frequencies.

The results of our experiments in water-methyl alcohol mixtures seem, however, to corroborate the idea of BAUER and STOREY that the maximum of absorption coefficient in water-alcohol systems is caused by relaxation phenomena due to the slowness with which equilibria of molecular associations follow the changes of temperature produced by sound waves. As mentioned above, to the term association must be given a broad meaning to include any kind of molecular state of order.

A similar explanation could be valid for the absorption in those mixtures of polar liquids like nitrobenzene-alcohol which have a maximum of the absorption coefficient.

4. - Absorption in Mixtures of Partially Soluble Liquids and Critical Phenomena.

The n-hexane-nitrobenzene system is a typical example of mixtures of two partially soluble liquids. In Fig. 2 the solubility ⁽¹⁵⁾ is shown together

⁽¹⁵⁾ *International Critical Tables*, vol. III, pag. 396 (New York, 1928).

with the sound absorption coefficient at 25 °C as function of composition. The consolute temperature 21.02 °C, and the temperature of the experiment differ only by a few degrees.

Similarly, a strong increase of sound absorption has been found in some other binary mixtures of partially soluble liquids when the temperature approaches the coexistence curve. A. G. CHYNOWETH and W. G. SCHNEIDER⁽¹⁶⁾ have studied a mixture water-triethylamine having 44.6 weight percent of amine (.126 amine mole fraction) and a mixture aniline-n-hexane with 74.6 weight percent of hexane.

It seems plausible to admit that the increase of sound losses in these mixtures in the critical region is bound to the critical phenomena which take place in the liquid. As is known the liquid in the critical region is no longer a homogeneous phase but is formed by a mother phase in which clusters of various sizes and compositions are dispersed⁽¹⁷⁾. An optical phenomenon, the critical opalescence, caused by the scattering of light produced by clusters shows that the their average size is of the order of magnitude of visible light wavelengths⁽¹⁸⁾.

The sound propagation in a heterogeneous medium of this kind undergoes losses of new types in addition to the classical one.

It is to be observed that since the sizes of the clusters are much smaller than the sound wave lengths ($0.3 \div 0.003$ cm), the scattering of sound energy is of no importance. This conclusion, based on the results of optical opalescence experiments, is confirmed by the sound absorption measurements at various frequencies. In fact scattering of sound energy produces a sound absorption coefficient (α_{sc}) which for spherical obstacles of compressibility β' and radius r , is given by the expression⁽¹⁹⁾

$$(1) \quad \alpha_{sc} = \frac{32\pi^5}{9} \frac{Nr^6}{u} \left(\frac{\beta' - \beta}{\beta} \right)^2 v^4,$$

N being the number of obstacles for volume unit, β the compressibility of the medium and u the sound velocity.

According to (1) the parameter α/v^2 for the scattering process had to increase with v^2 . Fig. 5 shows the experimental variation of α_{exp}/v^2 with v for a mixture nitrobenzene-n-hexane with nitrobenzene mole fraction .41. Fig. 13 gives the variation of α/v^2 with v for a mixture triethylamine-water with

⁽¹⁶⁾ A. G. CHYNOWETH and W. G. SCHNEIDER: *Journ. Chem. Phys.*, **19**, 1566 (1951).

⁽¹⁷⁾ J. H. H. HILDEBRAND and R. L. SCOTT: *The solubility of nonelectrolytes*. Appendix IV (New York, 1950).

⁽¹⁸⁾ R. L. KRISHMAN: *Proc. Ind. Acad. Sci.*, **1A**, 211, 915 (1935); **2A**, 221 (1935); **5A**, 577 (1937); **9A**, 303 (1939).

⁽¹⁹⁾ R. LUCAS: *Journ. Phys. et Rad.*, **8**, 41 (1937).

44.6 weight percent of amine. The point at 600 kHz is the one obtained by CHYNOWETH and SCHNEIDER, the others were obtained with a pulse method. The numerical results are given in Table III.

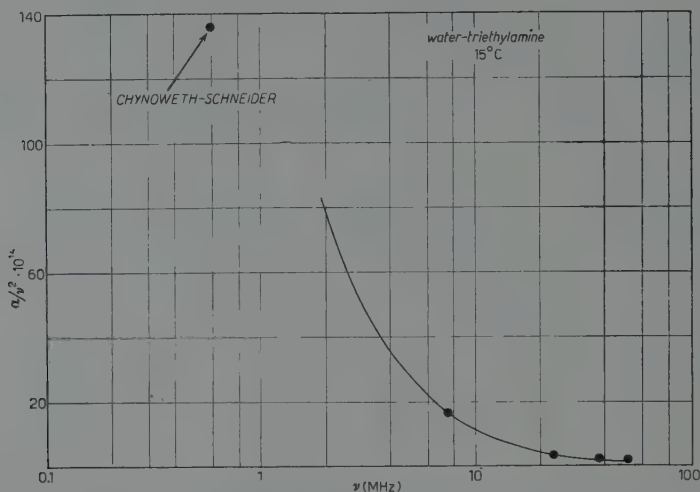


Fig. 13. — α/ν^2 versus ν for a water-triethylamine mixture at 15 °C (amine weight percent 44.6).

These experiments confirm that the scattering is not an important dissipative process in the mixtures examined.

TABLE III. — *Ultrasonic absorption in water triethylamine mixture having 45.6 amine weight percent (amine mole fraction .126) at 15 °C.*

MHz	α (cm ⁻¹)	$\alpha/\nu^2 \cdot 10^{15}$ s ² cm ⁻¹
0.6 (*)	0.49	1360
7.6	9.23	160
22.75	18.3	35.4
38.30	30.8	21
52.30	38.2	14

(*) Measured by Chynoweth and Schneider, quotation (15).

Therefore the increase of sound losses in mixtures in the critical region could be ascribed essentially to two causes:

- 1) increase of viscosity losses due to the heterogeneity of the liquid;
- 2) relaxation phenomena in the equilibrium of clusters.

The Stokes' calculation of the absorption coefficient due to viscosity, is

made using the hypothesis of a homogeneous fluid. R. LUCAS extended the calculations to the case of a liquid in which there are density fluctuations ⁽¹⁹⁾.

LUCAS assumed that the density fluctuations were time independent and isotropic and that the sound velocity did not vary along the direction of propagation. Moreover he maintained Stokes' relation between the two viscosity coefficients. It is then possible to get the following expression for the sound absorption coefficient due to viscosity in a liquid in which density fluctuations are present:

$$(2) \quad \alpha_{vis} = A\nu^2 + B,$$

where

$$(3) \quad A = \frac{8\pi^2}{3} \frac{\eta}{\varrho_0 u^3} \left(1 + \frac{1}{\tau} \int_0^\tau s^2 d\tau \right),$$

$$(4) \quad B = \frac{10}{9} \frac{\eta}{\varrho_0 u} \frac{1}{\tau} \int_0^\tau \left(\frac{\partial m}{\partial x} \right)^2 d\tau,$$

and ϱ_0 is the average density; ϱ the local density; $m = \sqrt{\varrho_0/\varrho}$; s , the condensation given by $\varrho = \varrho_0(1+s)$; η the viscosity coefficient; $d\tau = dx dy dz$, the volume element of the liquid and $r = \sqrt{x^2 + y^2 + z^2}$.

The equations (3) and (4) show that A and B depend upon the properties of the liquid and the density fluctuations in it, but that they are frequency independent.

As a consequence of the presence of density fluctuations the expression of the absorption coefficient has two corrective terms in addition to the Stokes' one. The first corrective term has the same frequency dependence of the Stokes'; the second is instead constant with frequency. The parameter α_{vis}/ν^2 therefore decreases with frequency. This is the general behavior of α_{exp}/ν^2 found in the mixtures n-hexane-nitrobenzene and water-triethylamine.

Unfortunately, however, a similar decrease of α/ν^2 with ν is expected also in the case of the other dissipative process: i.e. relaxation phenomena bound to the equilibrium among clusters. The clusters of different size and composition are in equilibrium among themselves and with the mother phase. This equilibrium depends upon the temperature and can therefore be altered by temperature variations produced by sound waves. The relaxation phenomena which arise are of the same kind of those found in liquids where a low rate chemical equilibrium is present and in those water-alcohol mixtures in which the association equilibrium is modified by the temperature variations. In the present case, the kinetics of the system is described by reactions which happen either among clusters of different kinds or between clusters and molecules of

the mother phase to generate clusters of a new composition. The relaxation phenomena produced by sound waves in these mixtures can be described by means of a specific heat function of frequency. Owing to the great number of equilibria present among clusters of different size and composition, a very broad distribution of relaxation times is to be expected, i.e. the decrease of α/ν^2 with frequency occurs more slowly and it extends to a broader range of frequencies than if only one relaxation time were present.

The fact that the general behavior of α/ν^2 versus ν to be expected for either one of the two dissipative phenomena is of the same kind, makes it impossible at present to use the experimental results of the frequency dependence of the absorption coefficient, in order to separate the contributions of the two phenomena to the absorption coefficient itself.

In order to have some indication on the relative importance of the phenomena of the two kinds it is necessary to make an independent calculation of the absorption coefficient due to viscosity. This requires the determination of coefficients A and B of equation (2). A and B , as shown by (4) and (5) depend upon the physical properties of the liquid.

A calculation of A and B therefore, requires a previous study of the density fluctuations inside the liquid. In fact, as mentioned above, the liquid in the critical region is not a homogeneous one, but can be considered as a solution formed by a mother phase in which a large number of clusters of different size and composition are dissolved. The density fluctuations which we are going to consider are only those bound to this heterogeneity of the liquid.

J. FRENKEL⁽²⁰⁾ has given a theory of pretransition phenomena in one component system which allows one to calculate the distribution function of embryos of the instable phase in the stable one (for instance liquid embryos in a vapor near the saturation point). Such theory can be extended to binary systems in the critical region. Reiss' calculations for such a case⁽²¹⁾ yield the following expression for the number of embryos of certain size and composition, i.e. formed by a molecules of component A and b molecules of component B :

$$(5) \quad N(a, b) = F \exp \left\{ - \frac{[a(\lambda_a - \mu_a) + b(\lambda_b - \mu_b) + \gamma(av_a + bv_b)^{\frac{2}{3}}]}{kT} \right\}$$

F is the total numbers of molecules (including molecular embryos of a given size and composition as a definite species of molecules); λ_a and λ_b are the partial molecular free energies of A and B in a solution having the same composition as the embryo, while μ_a and μ_b are the partial molecular free energy

⁽²⁰⁾ J. FRENKEL: *Kinetic Theory of Liquids* (Oxford, 1946), pag. 382.

⁽²¹⁾ H. REISS: *Journ. Chem. Phys.*, **18**, 840 (1950).

of molecules A and B in the mother phase. v_a and v_b are the partial molecular volumes of the molecules in the embryo. γ depends on the surface tension of the embryo.

The numerator of the exponent in (5) represents the reversible work necessary to form an embryo having the numbers a and b of molecules A and B from molecules A and B in the mother phase.

In order to use equation (5) in the calculation of the density fluctuations in the liquid it is necessary to know both the variation of partial molecular free energies, i.e. chemical potentials, of molecules A and B when they go from the mother phase to mixtures of compositions equal to those of the clusters and the values of surface tension between clusters and mother phase.

Unfortunately however equation (5) can not be used with advantage in the case which interest us owing to the uncertainty still present concerning the thermodynamics in the critical region. According to the more recent work the coexistence or solubility curve (temperature versus composition of the two phases in equilibrium) can have either a round or a flat top McMILLAN and MAYER⁽²²⁾ believe that the isotherms (either fugacity or chemical potential of one component vs composition) have a horizontal portion extending over a range of compositions at temperatures just above (or below) the critical one, in the region where there is apparently complete miscibility.

No information on the isotherms of the system nitrobenzene-*n*-hexane were found in the literature. On the contrary research has been done in the system water-triethylamine for which ultrasonic data are also available.

The water-triethylamine is a system with a lower critical temperature of 18.4 °C. Below this temperature one homogeneous phase should be present. For temperatures not much lower than the consolute one and for composition of the mixture not too much different than that of the critical mixture, the critical phenomena appear. L. D. ROBERTS and J. E. MAYER⁽²³⁾ have experimentally studied with great care the thermodynamic behavior of the system water-triethylamine. That part of their results which we are interested in can be summarised by saying that the isotherm lines of chemical potential vs composition have an horizontal portion in the critical region. At a temperature of 15 °C the horizontal segment of the isotherm extends from a composition of about 20 weight percent of amine to compositions of about 50 percent.

It is clear that under these circumstances it is not possible to use directly equation (5) for the calculations of both density fluctuations in the liquid and increase of ultrasonic absorption due to viscosity.

In order to have an approximate estimation of the increase of the absorption coefficient due to viscosity in the heterogeneous medium and an indication

(22) W. G. McMILLAN and J. E. MAYER: *Journ. Chem. Phys.*, **13**, 276 (1945).

(23) L. D. ROBERTS and J. E. MAYER: *Journ. Chem. Phys.*, **9**, 852 (1941).

of its importance compared to the absorption coefficient due to the relaxation phenomena we have used a different approach.

In the region where the isotherms are horizontal the system is formed essentially by a mother phase having a composition equal to the average composition of the mixture and clusters having all the compositions in the range of the horizontal portion of the isotherms themselves. If however we consider the system in a less specific way the fact that the thermodynamical status becomes independent from one more variable (composition) in a certain range of composition, means, according to the phase-rule, that we are no longer dealing with an one phase system but two phases are present whose compositions can be calculated from the extreme points of the horizontal portion of the isotherms. We think that the application of this general rule to the critical region is an approximation useful for our purposes especially if we deal with a mixture whose composition is near to one of the extremes of the mentioned horizontal portion of the isotherms. Such is our case. The ultrasonic absorption coefficient was studied as function of frequency at 15 °C in a mixture water-triethylamine having 44.6 weight percent of amine, while the isotherms are horizontal between 20 and 50 amine weight percent.

In accordance with the above, we can assume that our system is formed by two phases of which: 1) has a composition of 50 weight percent of amine and constitutes the 82 weight percent of the system and 2) (in form of clusters) has the composition of 20 weight percent of amine and constitutes the 17 weight percent of the system.

In this calculation we assume that the clusters are spheres of the same radius. As value of the diameter we have taken $2r = 5.5 \cdot 10^{-5}$ cm, which is the medium wavelength of visible light, because light scattering measurements have indicated that such is the average size of clusters in the critical region.

In such conditions it is possible to calculate A and B to be used in equation (2).

The densities of the two phases are ⁽²⁴⁾: $\rho_1 = .8850$ and $\rho_2 = .9625$; and the volume percent respectively $v_1 = 83.20\%$; $v_2 = 16.80\%$. Owing to the large difference in volume of the two phases we can assume that the clusters (phase 2) are dispersed in phase 1. This means that for the calculation of the integrals in (3) and (4) we can consider each cluster by itself. The number of clusters would be $N = 1.93 \cdot 10^{12}$ per cm^3 .

The integral in eq. (3) breaks into two parts each of them referring to one of the two phases, and can be easily calculated because the condensation, s , is constant in each phase. The average density is $\rho_0 = 0.90$ and the value of the integral is 0.001. This shows (eq. (2)) that the first correction to the Stokes' expression of the absorption coefficient due to viscosity is very small compared to the normal Stokes' term.

The integral of eq. (4) becomes equal to the product of the number of

clusters for volume unity (N) and the value of the integral itself over the volume c , of a single cluster. The evaluation of this integral requires the knowledge of $\partial m / \partial x$. If we consider only one spherical cluster of density ρ_2 located at the origin of axes and in a medium of density ρ_1 , the change of density along any axis through the origin is that shown in Fig. 14a.

In such $\partial m / \partial x$ when it is not zero goes to infinity. It is to be observed however that such a density diagram is roughly approximate and that the phenomena in the critical region are better represented assuming a continuous change of ρ from ρ_1 , to ρ_2 . We have assumed therefore for the calculation of integral (4) a variation of ρ according to Fig. 14b, i.e. given by a Gaussian law

$$(6) \quad \rho = \rho_1 + (\rho_2 - \rho_1) \exp[-h^2(x^2 + y^2 + z^2)];$$

h has been chosen in such a way to have

$$c(\rho_2 - \rho_1) = \int (\rho - \rho_1) d\tau.$$

being, the integral calculated over all space.

We obtain

$$h = \frac{1.1}{r} = 4 \cdot 10^4 \text{ cm}^{-1}.$$

Since $m = \sqrt{\rho_0 / \rho}$ and letting $\chi = (\rho_2 - \rho_1) / \rho_1$, we obtain

$$(7) \quad \left(\frac{\partial m}{\partial x} \right)^2 = \frac{\rho_0}{\rho_1} \chi^2 h^4 \frac{x^2 \exp[-2h^2(x^2 + y^2 + z^2)]}{\{1 + \chi \exp[-h^2(x^2 + y^2 + z^2)]\}^3}.$$

Using the series expansion of $1/(1+x)^3$ and ignoring all terms above the square term, one gets

$$(8) \quad \int \left(\frac{\partial m}{\partial x} \right)^2 d\tau = \frac{\rho_0}{\rho_1} \chi^2 h^4 \iiint x^2 \exp[-2h^2(x^2 + y^2 + z^2)] \cdot \\ \cdot \{1 - 3\chi \exp[-h^2(x^2 + y^2 + z^2)] + 6\chi^2 \exp[-2h^2(x^2 + y^2 + z^2)]\} dx dy dz$$

The range of variability of x, y, z in the integral on the right side, is obviously $-\infty$ to $+\infty$.

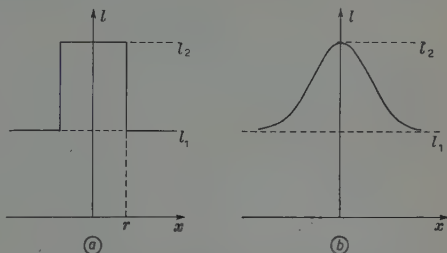


Fig. 14. - Density variation across a cluster.

The result is:

$$(9) \quad \int_c \left(\frac{\partial m}{\partial x} \right)^2 d\tau = \frac{\rho_0}{\rho_1} \frac{\chi^2}{h} \pi^{\frac{1}{2}} \left(\frac{1}{8\sqrt{2}} - \frac{\chi}{6\sqrt{3}} + \frac{6\chi}{76} \right),$$

and the numerical value for the case we are considering is:

$$\int_c \left(\frac{\partial m}{\partial x} \right)^2 d\tau = 8.7 \cdot 10^{-3}.$$

Consequently:

$$(10) \quad \frac{1}{\tau} \int_0^{\tau} \left(\frac{\partial m}{\partial x} \right)^2 d\tau = N \int_c \left(\frac{\partial m}{\partial x} \right)^2 d\tau = 16.8 \cdot 10^4.$$

Assuming for u and η respectively the values 1350 m/s and $4.66 \cdot 10^{-2}$ dynes/cm² given for the mixture water triethylamine having 44.6 weight percent amine respectively by CHYNOWETH and SCHNEIDER ⁽¹⁶⁾ and TSAKALOTOS ⁽²⁴⁾ we can calculate A and B with equations (3) and (4):

$$A = 55.3 \cdot 10^{-17} (1 + 0.001)$$

$$B = 71.4 \cdot 10^{-3}$$

and

$$(11) \quad \frac{\alpha_{\text{vis}}}{\nu^2} = 55.3 \cdot 10^{-17} + 71.4 \cdot 10^{-3} \frac{1}{\nu^2}.$$

In Table IV are recorded the values of $\alpha_{\text{vis}}/\nu^2$ for the five frequencies for which we have experimental data, $\alpha_{\text{exp}}/\nu^2$.

TABLE IV. - Ultrasonic absorption in the water triethylamine mixture having 44.6 amine weight percent.

ν MHz	$(\alpha_{\text{exp}}/\nu^2) \cdot 10^{17}$ s ² cm ⁻¹	$(\alpha_{\text{vis}}/\nu^2) \cdot 10^{17}$ s ² cm ⁻¹	$(\alpha_{\text{rel}}/\nu^2) \cdot 10^{17}$ s ² cm ⁻¹	α_{rel} cm ⁻¹	$\frac{\alpha_{\text{vis}}}{\alpha_c}$	$\frac{\alpha_{\text{exp}}}{\alpha_{\text{vis}}}$
.6	136 000	20 000	116 000	.417	360	6.8
7.6	16 000	302	15 700	8.49	5.5	53
22.75	3 540	69	3 470	18.0	1.24	51
38.3	2 100	60	2 040	30.0	1.08	35
52.3	1 400	58	1 342	36.7	1.05	24

(24) TSAKALOTOS: *Zeits. Phys. Chem.*, **68**, 32 (1909).

The value of α_c/ν^2 is $55.3 \cdot 10^{-17} \text{ s}^2 \text{ cm}^{-1}$ where α_c is the normal viscosity absorption coefficient according to Stokes' formula.

The ratio, $\alpha_{\text{vis}}/\alpha_c$ between corrected and Stokes' viscosity absorption coefficients decreases quickly with the frequency. At 600 kHz it is rather high, about 360. The experimental absorption coefficient is however still much higher than α_{vis} at the lower frequency of the range examined. Moreover the frequency behavior of α_{vis} and α_{exp} is quite different.

According to these calculations, therefore, and in the limit of accuracy of the assumptions made, it seems that while the increase of ultrasonic absorption coefficient due to viscosity as a consequence of heterogeneity of the liquid in the critical region, can have a certain importance at low frequencies, the observed large values of the ultrasonic absorption coefficient are essentially due to relaxation phenomena, at least in the megacycles region.

The relaxation phenomena as mentioned above, are bound to the equilibria of clusters of different sizes and compositions among themselves and with the mother phase. These equilibria are affected by the temperature variations produced by sound waves, just as happens for the equilibria of molecular associations in water-alcohol systems.

As already mentioned, it is to be expected that these relaxation phenomena occur with a wide distribution of relaxation times, since the differences in sizes and compositions of the clusters are very large and therefore the equilibria involved are very numerous.

In a relaxation phenomenon occurring with a single relaxation time (τ) the absorption coefficient is expressed by

$$(12) \quad \alpha_r = A\nu^2 \frac{1}{1 + (\nu/\nu_r)^2},$$

where $\nu_r = 1/2\pi\tau$ is the relaxation frequency and A is a parameter which depends on temperature but does not change with frequency.

Equation (12) can be rewritten in the form

$$(13) \quad \frac{\alpha_r}{\nu^2} + \frac{1}{\nu_r^2} \alpha_r = A,$$

which shows that a plot of α_r/ν^2 versus α_r should give a straight line of slope $1/\nu_r^2$.

A plot of α_r/ν^2 vs α_r for the mixture water triethylamine examined before deviates quite radically from a straight line (Fig. 15).

This seems to confirm the existence of a wide distribution of relaxation times. This conclusion should not be affected by the low accuracy in the calculation of α_{vis} which we were able to carry out, because the calculation seems to indicate that the relaxation phenomena are by far the more important dissipation processes in the mixtures.

The slopes of the line α_r/ν^2 vs α_r at the lower and higher ends of the α range studied, if they were the slopes of straight lines, would correspond to relaxation

phenomena with the relaxation frequency respectively of 2.5 MHz and 30 MHz.

This can be taken as a very vague indication of what may be the range of the relaxation frequencies involved in the phenomena.

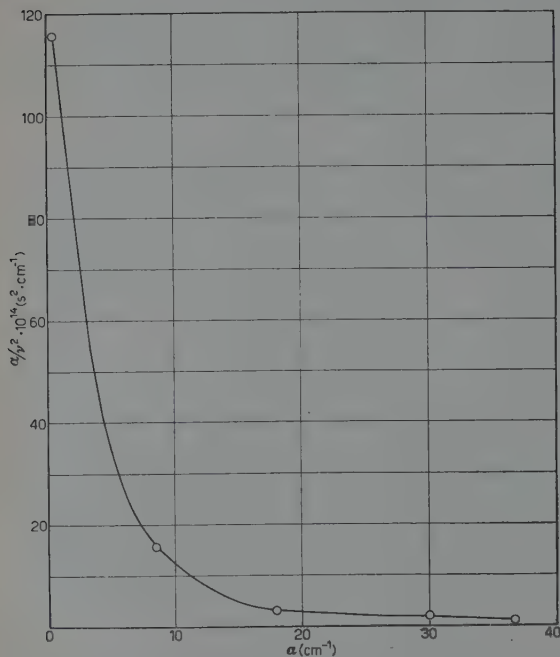


Fig. 15. — α_r/ν^2 versus α_r for a water-triethylamine mixture (amine weight percent 44.6)

5. — Conclusions.

The experimental results obtained for the ultrasonic absorption coefficient in those binary mixtures where a maximum of the coefficient has been found, lead to a conclusion valid for all systems, i.e. the main cause of losses remains in the fact that the molecules of the two components can associate in different ways and the result-

ing equilibria are altered by the temperature changes produced by sound waves. A finite time is needed to go from one equilibrium position to another.

One important class of this type of mixtures is formed by water-alcohol systems. The results in water-methyl alcohol mixtures, where a maximum of the absorption coefficient has been found at temperatures below the normal room temperature, remove an apparent anomaly in the behavior of water-alcohol mixtures and give credit to Storey's theory for the explanation of experiments on the basis of relaxation phenomena in the equilibrium among different molecular associations.

The same cause of losses can explain experiment in those binary mixtures which present a maximum of the absorption coefficient and are formed by two polar liquids.

In the mixtures of partially soluble liquids in the critical region the molecules of the two components can be found either in the mother phase or in clusters of various sizes and compositions. It is the distribution of molecules in the mother phase and in the clusters which is affected by the temperature changes produced by sound waves and gives rise to relaxation phenomena.

An approximate calculation has shown that the increase of viscosity losses due to density fluctuations in the liquid in the critical region is much smaller than the absorption observed in the megacycles region.

Acknowledgment.

The Author expresses his thanks to Professor K. F. HERZFELD for useful discussions and to Professor R. LUCAS for having exchanged views with him.

RIASSUNTO

Una indagine sperimentale ed alcuni calcoli teorici sono stati condotti allo scopo di chiarire le cause di assorbimento ultrasonoro in alcune mescolanze liquide binarie nelle quali si è riscontrato che il coefficiente di assorbimento presenta un massimo in funzione della concentrazione. Una importante categoria di mescolanze di questo tipo è costituita da sistemi formati da acqua ed alcuni alcool. Una apparente anomalia era costituita dal fatto che l'assorbimento ultrasonoro nel sistema acqua-alcool metilico sembrava presentare un andamento, in funzione della concentrazione, diverso da quello che esso ha nelle mescolanze di acqua e di uno degli alcool etilico, propilico, etc.. Ricerche a temperature notevolmente inferiori a quella ambiente hanno mostrato che nella mescolanza acqua-alcool metilico un massimo del coefficiente di assorbimento si presenta come nelle altre mescolanze acqua-alcool. Tali risultati confermano la teoria proposta da L. R. O. STOREY per spiegare il massimo del coefficiente di assorbimento ultrasonoro nei sistemi formati da liquidi polari. Secondo tale teoria esisterebbero nel liquido associazioni molecolari formate da molecole dei due tipi ed il loro equilibrio verrebbe alterato dalle variazioni di temperatura che accompagnano le onde sonore. Si originano così fenomeni di rilassamento che conducono a dissipazioni energetiche. Si è indagato inoltre sull'assorbimento ultrasonoro in mescolanze di liquidi parzialmente miscibili, nella regione critica. Il liquido è qui costituito da una madre fase nella quale sono dispersi agglomerati (clusters) di molecole dei due tipi in numero e rapporto differenti. È stato condotto un calcolo approssimato dell'aumento delle dissipazioni per viscosità causate dalla eterogeneità del liquido. Tali dissipazioni, pur potendo in certi campi di frequenza, superare notevolmente quelle indicate dalla formula di Stokes per liquidi omogenei, non sono sufficienti a spiegare il coefficiente di assorbimento ultrasonoro trovato sperimentalmente. Anche in tali mescolanze pertanto, la causa principale delle dissipazioni energetiche è da individuarsi in fenomeni di rilassamento prodotti dalle variazioni di temperatura che accompagnano le onde e che alterano gli equilibri degli agglomerati sia fra loro che con la madre fase. Si giunge quindi alla conclusione che, in tutti i sistemi binari del tipo esaminato, le dissipazioni sono essenzialmente prodotte da fenomeni di rilassamento dovuti alla variazione dell'equilibrio fra varie forme nelle quali molecole dei due componenti possono trovarsi unite. La variazione dell'equilibrio è causata dalle variazioni di temperatura che accompagnano il propagarsi delle onde ed i fenomeni possono essere descritti per mezzo di un calore specifico variabile con la frequenza.

Indefinite Metrics and Multi-Mass Field Theories.

R. J. N. PHILLIPS

Trinity College - Cambridge, England

(ricevuto il 21 Febbraio 1955)

Summary. — An analysis of quantum-theoretical scalar products is made, and a philosophy for treating indefinite scalar products is developed. This is applied in a study of positive-energy multi-mass fields. It is found that in general the multi-mass formalism confers no improved convergence; although convergent theories can be constructed in principle, it is not possible to do so in practice. The theories that can be used are at least as divergent as in the single-mass formalism.

1. — Introduction.

This paper treats two topics in quantum theory, each of interest in itself, which are to some extent interdependent in treatment and therefore best presented together. Thus our work on multi-mass fields presupposes our conclusions on indefinite metrics, and at the same time provides a good illustration of their application.

The use of indefinite scalar products as a basis for physical interpretation by present-day rules leads to the well known difficulty of negative « probabilities ». By an analysis of what underlies the definition of a scalar product, we show that both definite and indefinite scalar products can be used with any quantum theoretical scheme of state vectors and operators, subject to certain reasonable assumptions. Each scalar product corresponds to a different « physical » system, with different properties, but with the same sets of eigen-values and expectation values of energy, momentum and angular momentum. Since the use of indefinite scalar products is thus unnecessary, and causes trouble, this suggests that we reject them as a matter of principle for use in physical interpretation. This means rejecting not the mathematical scheme, but certain physical interpretations of it. If one prefers to hope that

some new interpretation of indefinite scalar products may exist, this can be left an open question; however it remains true that the positive definite scalar products, to which we restrict ourselves here, provide perfectly legitimate physical interpretations of the mathematical schemes.

The subsequent application of these ideas is simple. When faced, for example, by a mathematical scheme, with the desired energy-eigen-values but an indefinite scalar product, we make the latter positive definite with the help of a suitable indefinite metric before making physical interpretations. This of course involves changing the nature of the physical system described: for instance, the operators with real expectation values will not all be the same. However, we now have a reasonable physical picture where previously we had none.

Multi-mass fields which satisfy free field equations of the types


$$(1.1) \quad \prod_i (\square - \kappa_i^2) \varphi(x) = 0$$

$$(1.2) \quad \prod_j (\gamma_\mu \partial_\mu + \kappa_j) \psi(x) = 0$$

(for Bose and Fermi statistics respectively), have aroused interest in the past because of the opportunities they offer for constructing convergent theories. Investigations were brought to a head, however, in a paper by PAIS and UHLENBECK ⁽¹⁾, which dealt with such fields and also with fields satisfying equations with more involved functions of the d'Alembertian and Dirac operator.

Considering real fields φ and real, distinct mass roots κ_j , they showed that fields of type (1.1) are an assembly of single-mass «root fields», of both positive and negative energies, and are thus physically unacceptable. The case where certain of the mass roots are repeated is not so simple, but was taken by analogy with a one-dimensional example to be even more undesirable. When some of the κ_j are complex, an interpretation in terms of free particles is impossible. Similar results were found for Fermi fields of type (1.2), except that here they proposed to overcome the negative-energy difficulty by introducing anti-particles.

Their method was to decompose the multi-mass Lagrangian into a sum of root field Lagrangians. In our work, on the other hand, we use a Hamiltonian approach, which gives greater insight into the structure of the multi-mass fields, since it involves constructing them explicitly from root fields. In particular, we see how to express multi-mass fields with complex or multiple mass

 ⁽¹⁾ A. PAIS and G. E. UHLENBECK: *Phys. Rev.*, **79**, 145 (1950). See this too for references to earlier work.

roots in terms of *interacting* root fields. However, this technique is unwieldy in a general case, and once the insight has been gained it is simpler to use the Lagrangian method.

Our purpose is to complete the work of PAIS and UHLENBECK by investigating the positive-energy solutions of (1.1) and (1.2) which can be found if ψ is not assumed real, nor $\bar{\psi}$ assumed the adjoint of ψ . For Bose fields, these correspond to our re-interpretation of the well known indefinite-metric modifications of the indefinite-energy solutions ⁽²⁾. For Fermi fields we agree with DARLING ⁽³⁾ in finding no negative-energy difficulty. There is, however, an indefinite scalar product which must be treated in the light of our earlier work.

Interactions are then considered, and it is found to be impossible in practice to use «compensating» interactions which lead to better convergence. This is because we cannot find explicitly a suitable indefinite metric with which to introduce a positive definite scalar product, in these cases, although such indefinite metrics exist in principle. Thus our compensation theories appear to be mathematical curiosities and no more. Other interactions, which we can handle, lead to problems at least as divergent as in the single-mass formalism, and there is no advantage from this point of view in using multi-mass fields.

We do not consider higher-spin fields in detail, but it seems likely that compensation theories using such fields will meet with similar difficulties.

2. — Indefinite Metrics.

2.1. *Theoretical basis.* — This is not an exhaustive treatment of the theoretical basis of the topic, but rather a review of a possible logical sequence of assumptions and deductions which leads to the definition of a scalar product in the space of quantum states.

Bra and ket vectors. The states of a dynamical system are supposed represented by the directions of ket vectors $|A\rangle$ in an abstract linear space over the field of complex numbers. Another abstract linear space over the same field is formed, that of bra vectors $\langle B|$, isomorphic to the first. Corresponding vectors are denoted by the same label. This isomorphism implies an automorphism of the field of complex numbers, which we choose to be

$$(2.1) \quad c \rightarrow \bar{c}$$

where c , \bar{c} are conjugate complex numbers. Thus

$$(2.2) \quad \bar{c}\langle A| \sim c|A\rangle$$

⁽²⁾ See for example P. T. MATTHEWS: *Proc. Camb. Phil. Soc.*, **45**, 441 (1949).

⁽³⁾ B. T. DARLING: *Phys. Rev.*, **92**, 1547 (1953).

where \sim denotes the bra-ket correspondence rule. A state of our dynamical system can now be specified by either a bra or a ket.

Linear operators. We now introduce linear operators, which act on kets to produce other kets. An operator is considered completely defined if its effect on every ket is known. The adjoint α^\dagger , of a linear operator α which acts on kets, is defined as that operator which has the corresponding effect on bras. Thus

$$(2.3) \quad \langle A | \alpha^\dagger \sim \alpha | A \rangle$$

for all vectors $|A\rangle$. However, we can as yet attach no meaning to the operation on bras of an operator like α , defined in terms of kets.

A certain kind of matrix representation of operators is now possible. We introduce any basis $|e_i\rangle$ (supposed for convenience to be discrete) of the ket space. The effect of any linear operator α can be written

$$(2.4) \quad \alpha |e_i\rangle = \sum_j \alpha_{ji} |e_j\rangle$$

where the α_{ji} are numerical coefficients, forming a matrix. The usual rules of matrix multiplication apply.

A similar representation can be set up for linear operators which act on bras. The matrix representing α^\dagger , with respect to the corresponding basis of bras is the Hermitian conjugate of that representing α .

Among linear operators of physical interest are the infinitesimal operator of the time transformation, H ,

$$(2.5) \quad i\hbar \frac{d}{dt} |A\rangle = H |A\rangle \quad (\text{in Schrödinger representation}),$$

and the infinitesimal displacement operators of the Orthogonal Group P_i and M_i ($i=1, 2, 3$), defined in an analogous way.

Scalar product. We now introduce the scalar product $\langle B | A \rangle$ of a bra $\langle B |$ and a ket $|A\rangle$. It is a scalar bilinear function of the two vectors; we shall later need to restrict it further.

We can now give meaning to the acting of any linear operator on both bras and kets, by means of the postulate

$$(2.6) \quad \langle B | \{ \alpha | A \rangle \} = \{ \langle B | \alpha \} | A \rangle.$$

We shall want to associate certain linear operators ω , whose eigenvectors span the state-vector spaces, with physical observables, and to interpret the

quantities $\langle A | \omega | A \rangle$ as the expectation values of these observables in the (suitably normalized) state $|A\rangle$.

In particular, we shall associate H , P_i , and M_i with the Total Energy, Momentum, and Angular Momentum of the system. Since the latter are in principle observable, we must require each of the corresponding operators to have a complete set of eigenvectors.

We shall also interpret $\langle A | \delta_{\xi a} | A \rangle$ as the (relative) probability that an observable ξ has the value a in the state $|A\rangle$, where $\delta_{\xi a}$ is the function of ξ that has the value 1 when ξ takes the value a , and is zero otherwise.

We now investigate the effect of these assumptions on the form of the scalar product.

Taking the particular observable $\omega = 1$, we see that $\langle A | A \rangle$ must be real. This can be assured by assuming

- (i) The scalar product is Hermitian.

$$(2.7) \quad \langle B | A \rangle = \langle A | \bar{B} \rangle.$$

(Although not a strictly necessary assumption, it is always made in practice for its great convenience).

We can now define orthogonality. $|A\rangle$ and $|B\rangle$ are orthogonal if $\langle A | B \rangle = 0$. A similar definition can be made for bras. The analysis of a state vector in terms of an orthogonal basis is thus equivalent to the analysis of the state into physically exclusive states. Orthogonal bases thus have a particular significance.

Since $\langle A | A \rangle$ is real, all operators representing real physical observables must have real eigenvalues. In particular, we must add to our assumptions that H , P_i , M_i , have real eigenvalues.

For physically sensible results, we must further require that $\langle A | A \rangle$ is invariant with respect to the time transformation and the transformations of the Orthogonal Group. This implies that $\langle A | B \rangle$ is so invariant. Consequently we must assume

- (ii) The operators H , P_i , M_i are self-adjoint in our definition of the scalar product.

Construction of the scalar product. Suppose first that H , P_i , M_i form a complete set of observables. Choose a basis of H -eigenkets $|H'\alpha'\rangle$, with eigenvalues H' (where the α' are other labels). Set up a matrix representation of H , P_i , M_i , in the manner of (2.4). Since the P_i and M_i commute with H , their non-zero elements lie in square submatrices which correspond to the sets of basic vectors with the same H -eigenvalues. Each of these sets of basic vectors thus provides a matrix representation of the operators P_i and M_i .

Now any finite representation of the Orthogonal Group is known to be equivalent to a unitary representation; therefore if the above sets are finite we may choose the basic vectors in such a way that the P_i , M_i are Hermitian. We assume this is true also for the infinite representations and continuous representations in which we shall be interested.

Since H is diagonal in this representation, and has real eigenvalues, it is Hermitian too. We can of course now diagonalize sets of commuting observables such as the P_i , or P_1 , M_1 , without destroying the Hermitian character of any of the operators.

We can now define a positive definite scalar product which satisfies all our postulates, by means of

$$(2.8) \quad \langle e_i | e_j \rangle = \delta_{ij}$$

where the $|e_j\rangle$ are the basic kets defined above, supposed for convenience to form a discrete set. The generalization to the case of continuous ranges of basic kets follows the usual course.

Any other acceptable scalar product $\langle B | A \rangle^0$ may clearly be written in terms of this first scalar product, in the form

$$(2.9) \quad \langle B | A \rangle^0 = \langle B | \theta | A \rangle$$

where θ is an Hermitian operator which commutes with H , P_i and M_i . It must therefore be a function of H , P^2 , and M^2 .

If θ is positive definite, we have another positive definite scalar product. But if θ is indefinite, $\langle A | A \rangle^0$ may be either positive or negative. This means that in the usual physical interpretation, both positive and negative « probabilities » appear.

We have been assuming that the P_i , M_i and H form a complete set. If this is not so, there are fresh observables which commute with them and which we can add to form a complete set. These new observables describe new freedoms of motion of our dynamical system, and we assume that there are good physical reasons for restricting the definition of the scalar product with respect to these new freedoms. Thus certain infinitesimal displacement operators ω of these freedoms must be self-adjoint. The observables ω are chosen to commute with H , P_i and M_i . To construct a scalar product we proceed as before, but treating H and the ω together. We construct a basis of simultaneous eigenvectors of H and ω in such a way that the P_i and M_i are Hermitian, and so on. θ is now a function of H , P^2 , M^2 , and ω .

Matrix representations. With a positive definite scalar product, we may choose bases $|\xi_i\rangle$, normalized according to

$$(2.10) \quad \langle \xi_i | \xi_j \rangle = \delta_{ij}.$$

In consequence

$$(2.11) \quad \sum_i |\xi_i\rangle \langle \xi_i| = 1$$

and the quantities

$$(2.12) \quad \alpha_{ij} = \langle \xi_i | \alpha | \xi_j \rangle$$

may be considered the elements of matrices, which multiply in the usual way. This is of course simply a representation of type (2.4).

With an indefinite scalar product, however, the best we can do is to choose a basis $|\zeta_i\rangle$ such that

$$(2.13) \quad \langle \zeta_i | \zeta_j \rangle = \delta_{ij} \eta_i \quad (\text{not summed})$$

where η_i is either $+1$ or -1 . The matrices defined by an equation like (2.12) do not multiply in the usual way, for the analogue of (2.11) does not hold. Instead we have the multiplication rule

$$(2.14) \quad (\alpha\beta)_{ij} = \sum_k \alpha_{ik} \eta_k \beta_{kj}.$$

In view of this, we might fairly call η_i a diagonal metric tensor. However, for a given indefinite scalar product, each choice of basis defines such a tensor (diagonal in that particular representation), and we prefer to reserve the term «indefinite metric» for the operator θ by which an indefinite scalar product is defined in terms of a particular positive definite scalar product.

2.2. *The natural picture.* — We have seen that, subject to certain reasonable assumptions (most of which are always made), we can use either a definite or an indefinite scalar product with any quantum theoretical scheme.

The usual physical interpretation can be made consistently with a positive definite product (with trivial changes for a negative definite one), but breaks down otherwise because negative probabilities appear. Attempts have been made to reconcile the latter with experience but without general success⁽²⁾. However, a perfectly consistent interpretation of any mathematical scheme which uses an indefinite scalar product can be made if we first introduce a suitable indefinite metric into the scalar product to make it positive definite. Since this can always be done, it suggests that we formulate a specific physical principle: «For physical interpretation, a positive definite scalar product must be used».

This scalar product we call the Natural Product, and the mathematical picture in which it is used the Natural Picture. We have seen that there are many possible positive definite scalar products. The choice is made unique in practice by further assumptions (e.g. that a certain operator is self-adjoint), which specify more closely what «physical» system is being described. Our principle requires us to reject any such assumptions that imply an indefinite scalar product, which means in effect that we reject the corresponding physical systems.

We thus regard any mathematical scheme in an «indefinite picture» as having been transformed from some physically significant Natural Picture. Since there are generally many possible Natural Pictures, such a scheme can represent any one of many physical systems. The same of course is true of any scheme already in a positive definite picture. Clearly the postulates that fix the Natural Picture need have no relation to those that fix the original picture.

If one prefers not to reject the indefinite scalar products altogether, this can be left an open question, but the interpretations we have indicated still remain perfectly legitimate.

It is possible in particular cases to retain an indefinite scalar product and to avoid negative probabilities in practice by certain devices. This is a feature of Gupta's electrodynamics ⁽⁴⁾, in which an auxiliary condition is combined with the rather unsatisfactory assumption that the interaction must be considered switched off before any observation, to secure positive observed probabilities. Again, the infinite auxiliary masses of the «formalistic» regulator theories ⁽⁵⁾ ensure that no «negative-probability» particles can be observed in free states. However, neither of these devices provides a general rule, applicable in all cases.

2'3. Physical application. — Given a quantum mechanical situation stated in an indefinite picture, we may (at any rate in principle) identify the indefinite metrics θ which link this picture with different possible Natural Pictures, by diagonalizing H and the other commuting observables ω referred to in 2'1. θ is the diagonal operator which makes the $\langle A | \theta^{-1} | A \rangle$ positive and equal to the corresponding quantities $\langle A | A \rangle$ in the Natural Picture.

If θ has a particularly simple form, it may be easy to transform at once to the Natural Picture. On the other hand, it may well lead to greater formal simplicity to remain in the indefinite picture, and to use the Natural Products $\langle A | \theta^{-1} | B \rangle$ when making physical interpretations. To illustrate how this is done, we study transition probabilities.

⁽⁴⁾ S. N. GUPTA: *Proc. Phys. Soc.*, A **63**, 681 (1950).

⁽⁵⁾ E.g. S. N. GUPTA: *Proc. Phys. Soc.*, A **66**, 129 (1953).

Suppose that at time $t = t_0$ a dynamical system is observed to be in the state $|B\rangle$, in the Schrödinger representation. Then at time t it is in the state $T(t, t_0)|B\rangle$, where $T(t, t_0)$ is the time transformation operator. The (relative) probability amplitude that the system will be found at time t to be in the state $|A\rangle$ is thus

$$(2.15) \quad \langle A | \theta^{-1} T(t, t_0) | B \rangle.$$

If the vectors $|f_i\rangle$ form an orthonormal basis in the Natural Picture, and are therefore physically exclusive, we have

$$(2.16) \quad \sum_i |f_i\rangle \langle f_i| \theta^{-1} = 1$$

in the indefinite picture. Therefore (2.15) can be written

$$(2.17) \quad \sum_i \langle A | \theta^{-1} T(t, t_1) | f_i \rangle \langle f_i | \theta^{-1} T(t_1, t_0) | B \rangle$$

where t_1 is some time between t_0 and t . Transition probabilities can thus be decomposed in terms of other transition probabilities in a physically reasonable way. This is obvious in the Natural Picture.

For the transition to the interaction representation, we distinguish two cases. The first, in which θ commutes with both H_0 and H_1 , goes over quite simply. The second, in which θ commutes with neither H_0 nor H_1 (although of course it commutes with $H_0 + H_1$) is the case in which H_0 is not self-adjoint in the Natural Picture. There is nothing essentially wrong in this; H_0 has eigenstates that describe free particles, and it does not need to have real expectation values for $H_0 + H_1$ to be thought of as describing interacting particles. However, if we wish to switch off the interaction, we must notice that this implies changes in θ , and hence in the Natural Product. Since switching-off is never more than a purely formal device, there is no inconsistency here.

3. — Multi-Mass Field Theories.

3.1. *Spin 0 Bose fields.* — For the sake of simplicity, we study here the case of a field $\varphi(x)$ which satisfies

$$(3.1) \quad (\square - \kappa_1^2)(\square - \kappa_2^2)\varphi(x) = 0$$

where $\kappa_2^2 > \kappa_1^2$, and both « masses » are real. The treatment of higher-order equations follows the same lines.

Equation (3.1) can be derived from the Lagrangian density

$$(3.2) \quad \mathcal{L} = -\frac{1}{2}\{\Box\varphi \cdot \Box\varphi + (\kappa_1^2 + \kappa_2^2)\varphi_\mu\varphi_\mu + \kappa_1^2\kappa_2^2\varphi^2\}.$$

We introduce the new variable $A = \partial\varphi/\partial t$, and express (3.2) in terms of φ , A , their spatial derivatives, and $\partial A/\partial t$. Adding the term

$$(3.3) \quad \lambda[\partial\varphi/\partial t - A],$$

where λ is an undetermined multiplier, we treat φ and A as independent, and derive in the usual way the Hamiltonian density

$$(3.4) \quad \mathcal{H} = \pi A - B^2/2 + B\nabla^2\varphi + \frac{1}{2}(\kappa_1^2 + \kappa_2^2)[\nabla\varphi \cdot \nabla\varphi - A^2] + \frac{1}{2}\kappa_1^2\kappa_2^2\varphi^2,$$

where π and B are the momenta conjugate to φ and A respectively.

That this is a covariant formulation may be shown by the lengthier but more rigorous methods of Dirac's covariant Hamiltonian formalism ⁽⁶⁾, introducing the new field $A_\mu = \partial_\mu\varphi$, and eliminating the (redundant) spatial components.

Incidentally the well known methods of OSTROGRADSKY ⁽⁷⁾ can be generalized to treat fields, and lead to the same Hamiltonian.

To find the energy-eigenvalues, we expand φ as a superposition of plane wave solutions of (3.1), and try to deduce the coefficients, which are operators of course. From the properties required of these coefficients, we find that it is equivalent to expand φ in terms of single-mass field operators φ_1 and φ_2 , which obey

$$(3.5) \quad (\Box - \kappa_i^2)\varphi_i = 0 \quad (i = 1, 2)$$

and whose Fourier decompositions are well known. We shall adopt the latter approach for its compactness, and write

$$(3.6) \quad \varphi(x) = a_1\varphi_1(x) + a_2\varphi_2(x)$$

where the a_i are numerical coefficients.

Since we are primarily interested in physically recognizable fields, we suppose first that the φ_i are both real and described by positive definite Hamil-

⁽⁶⁾ P. A. M. DIRAC: *Can. Journ. Math.*, **2**, 129 (1950); **3**, 1 (1951).

⁽⁷⁾ See for example E. T. WHITTAKER: *Analytical Dynamics*, 4th ed. (London, 1937).

tonians, so that we may put

$$(3.7) \quad \frac{\partial}{\partial t} \varphi_i(x) = \pi_i(x), \quad (i = 1, 2)$$

where the π_i are the conjugate momenta. But from (3.4) we find

$$(3.8) \quad \begin{cases} A = \frac{\partial \varphi}{\partial t} \\ B = \square \varphi \\ \pi = (\kappa_1^2 + \kappa_2^2 - \square) \frac{\partial \varphi}{\partial t} \end{cases}$$

Thus, in order that the correct commutation relations shall hold between φ , π , A and B , the coefficients must satisfy

$$(3.9) \quad \begin{cases} a_1^2 + a_2^2 = 0 \\ \kappa_1^2 a_1^2 + \kappa_2^2 a_2^2 = -1 \end{cases}$$

When the solutions are substituted in (3.6) and (3.8), the Hamiltonian reduces to the sum of the two positive definite single-mass Hamiltonians, as indeed we might expect from the way this solution for φ has been constructed. It is thus positive definite and describes two fields of free bosons with rest-masses $\hbar \kappa_i$.

The fact that φ is not real (since a_2 is imaginary) is no drawback, for the Energy, Momentum, etc., are real.

In the case of n distinct root fields, (3.9) is replaced by

$$(3.10) \quad \begin{cases} \sum_i \kappa_i^{2r} a_i^2 = 0 \\ \sum_i \kappa_i^{2n-2} a_i^2 = (-1)^{n-1} \end{cases} \quad (r = 0, 1, \dots, n-2)$$

and the coefficients a_i are alternately imaginary and real.

We can find a solution in which all the a_i are real if we postulate that alternate root fields have negative-energy Hamiltonians. In the two-mass case above, we assume that φ_2 is so described, and therefore that

$$(3.11) \quad \frac{\partial \varphi_2}{\partial t} = -\pi_2.$$

The equations (3.9) are replaced by

$$(3.12) \quad \begin{cases} a_1^2 - a_2^2 = 0 \\ \kappa_1^2 a_1^2 - \kappa_2^2 a_2^2 = -1, \end{cases}$$

which have real solutions for a_1 and a_2 . The multi-mass Hamiltonian reduces to the sum of the two single-mass Hamiltonians, and is indefinite.

In the n -mass case too, all the a_i are real, but the energy is indefinite.

In physical terms, we have been seeking superpositions of single-mass fields which form multi-mass fields. Such superpositions are the basis of theories in which the divergences arising from different interactions are made to compensate. The «regularization» procedure of PAULI and VILLARS⁽⁸⁾ is an example; in effect a multi-mass field is substituted for a single-mass field in the interaction, leading to a convergent S -matrix. PAIS and UHLENBECK, who obtained our real solutions, pointed out that the use of regulators implied the introduction of unphysical fields of negative-energy bosons. This difficulty can be overcome by using our positive-energy fields in an indefinite picture. However, as we remark later, it proves impossible in practice to pass to the corresponding Natural Picture, and this procedure is of academic interest only. There remains the possibility of remaining in the indefinite picture, and letting the masses of the «auxiliary fields» tend to infinity, so that they are unobservable in practice and no negative probabilities appear. This however is a purely formal device.

Our Hamiltonian treatment, though easy to employ for a low number of root fields, is unwieldy in a general case. Here the Lagrangian approach of PAIS and UHLENBECK and earlier workers is much better. It leads directly to our real solutions, and the non-real (positive energy) solutions can be obtained from these as follows.

Consider a harmonic oscillator, with coordinate q and conjugate momentum p , described by the Hamiltonian

$$(3.13) \quad H = \frac{1}{2}(q^2 + p^2).$$

If q and p are self-adjoint and Hermitian, this has the usual positive eigenvalues. But if, on the other hand, q and p are self-adjoint and anti-Hermitian, PAULI⁽⁹⁾ has shown quite simply that the energy eigenvalues are reversed in sign, and that the scalar product is indefinite. We can identify the indefinite metric as that with elements $(-1)^n$ in the H -eigenstate of n quanta, in

⁽⁸⁾ W. PAULI and F. VILLARS: *Rev. Mod. Phys.*, **21**, 434 (1949).

⁽⁹⁾ W. PAULI: *Rev. Mod. Phys.*, **15** 175 (1943).

the usual Fock representation. When this is used to transform to a Natural Picture, q and p become anti-self-adjoint, and represent pure imaginary variables. Extending this to Bose fields, we can replace the negative-energy real root fields by positive-energy imaginary fields.

3.2. *Spin $\frac{1}{2}$ Fermi fields.* — As in the previous subsection, we restrict ourselves to a simple example. Consider the equation

$$(3.14) \quad (\gamma_\mu \partial_\mu + \kappa_1 (\gamma_\mu \partial_\mu + \kappa_2) \psi(x) = 0,$$

where $\kappa_2 > \kappa_1$, and both are assumed real and positive. This can be derived from the Lagrangian density

$$(3.15) \quad \mathcal{L} = -(\hbar/2) \{ \bar{\psi} \square \psi + (\kappa_1 + \kappa_2) \bar{\psi} \gamma_\mu \partial_\mu \psi + \kappa_1 \kappa_2 \bar{\psi} \psi \}$$

together with the «charge-conjugate» expression, where we make the usual connection with the charge-conjugate spinors $\psi'(x)$, $\bar{\psi}'(x)$:

$$(3.16) \quad \begin{cases} \psi'(x) = c\psi(x), & \bar{\psi}'(x) = c^{-1}\bar{\psi}(x) \\ \gamma_\mu^T = -c^{-1}\gamma_\mu c \\ c^T = -c, & c^* = c^{-1}. \end{cases}$$

The treatment now proceeds very much as in the Bose field case, with the help of Dirac's Hamiltonian formalism⁽⁶⁾. We introduce the new variables $\Psi = \gamma_\mu \partial_\mu \psi$ and $\bar{\Psi} = \gamma_\mu^T \partial_\mu \bar{\psi}$, rewrite the Lagrangian density in terms of ψ , $\bar{\psi}$, Ψ , $\bar{\Psi}$, their first derivatives, and certain undetermined multipliers. We then proceed to a Hamiltonian in terms of ψ , $\bar{\psi}$ and their conjugate momenta, eliminating all other (redundant) variables by a redefinition of Poisson Brackets. The theory can now be quantized without inconsistency.

As before, we express ψ and $\bar{\psi}$ in terms of single-mass root fields ψ_i . For the root fields, it is convenient to let $\bar{\psi}_i$ be the spinor adjoint of ψ_i , so that $\bar{\psi}_i = \psi_i^* \gamma_4$. Suppose first that this holds for the multi-mass field too. Then we have

$$(3.17) \quad \begin{cases} \psi(x) = \sum_i a_i \psi_i(x) \\ \bar{\psi}(x) = \sum_i \bar{a}_i \bar{\psi}_i(x). \end{cases}$$

This leads to the equations (stated for the general n -mass case),

$$(3.18) \quad \left\{ \begin{array}{l} \sum_i \kappa_i^r |a_i|^2 = 0 \quad (r = 0, 1, \dots, n-2) \\ \sum_i \kappa_i^{n-1} |a_i|^2 = (-1)^{n-1}, \end{array} \right.$$

for which there are no solutions.

To obtain solutions, there are two courses open to us. Either we may alter the commutation rules, or we may relax the rule $\bar{\psi} = \psi^* \gamma_4$.

Taking the latter course first, we alter (3.17) to

$$(3.19) \quad \left\{ \begin{array}{l} \psi(x) = \sum_i a_i \psi_i(x) \\ \bar{\psi}(x) = \sum_i \bar{a}_i (-1)^{i+1} \bar{\psi}_i(x). \end{array} \right.$$

This leads to real solutions for all the a_i . The Hamiltonian reduces to the sum of the positive definite single-mass Hamiltonians.

This solution is somewhat like the non-real solutions we found for Bose fields, for $\bar{\psi}$ is not the adjoint of ψ , and we cannot therefore use this field directly to regularize a single-mass field problem. However, as before, the physically important operators are self-adjoint, so there is nothing wrong with this solution.

Looking at this physically, we have found how to put together physically familiar Fermi fields to form a multi-mass field.

Returning to methods of solution, we now try altering the anticommutation rules of the root fields. If we assume that ψ_2 , (and in general, alternate root fields), is described by a Lagrangian which is the negative of the usual one, we are lead to the same real solutions for the a_i as before.

Let us examine these Fermi fields described by «negative-sign Lagrangians». The Hamiltonian, expressed in terms of conjugate variables, is formally the same as the usual one, so that the energy-eigenvalues are unchanged. However, the anti-commutation rule changes sign and becomes

$$(3.20) \quad [\psi_\alpha^*(r, t), \psi_\beta(r', t)]_+ = -\delta_{\alpha\beta} \delta(r - r').$$

The scalar product is thus indefinite.

The obvious indefinite metric to identify is that with elements $(-1)^n$ corresponding to the states of n quanta. If we use this to transform to a Natural Picture, the spinor adjoint of ψ becomes $-\bar{\psi}$. We are thus lead to precisely our first solution.

The Lagrangian approach leads directly to a decomposition in terms of root fields with Lagrangians of alternating signs. We have seen how the physical meaning can be found.

PAIS and UHLENBECK appear to have concluded that reversing the sign of a root field Lagrangian implies reversing the sign of the Hamiltonian eigenvalues. As we have seen, this is not so for fermions. The only difficulty is that of the indefinite metric.

3.3. *Multiple mass roots.* — So far we have only considered real distinct « root masses » $\hbar\kappa_i$. When two or more κ_i are the same, our earlier treatment breaks down, for we can no longer hope to express the multi-mass field as a linear superposition of free single-mass fields, with constant coefficients. PAIS and UHLENBECK have quantized a one-dimensional example, and have found the energy-levels exactly: they are continuous and indefinite, and it is not clear how positive-energy systems can be found. This treatment cannot be carried over to fields. However, the Hamiltonian approach suggests another way of gaining physical insight to repeated-mass fields.

Consider two interacting « positive energy » scalar Bose fields $\varphi_1(x)$ and $\varphi_2(x)$, described by the Hamiltonian density

$$(3.21) \quad \mathcal{H} = \sum_i \frac{1}{2}(\pi_i^2 + \nabla\varphi_i \cdot \nabla\varphi_i + \kappa_i^2\varphi_i^2) - ig\varphi_1\varphi_2$$

where $g = \frac{1}{2}(\kappa_2^2 - \kappa_1^2) > 0$. Each field satisfies

$$(3.22) \quad (\square - \kappa^2)^2\varphi_i(x) = 0$$

where $\kappa^2 = \frac{1}{2}(\kappa_1^2 + \kappa_2^2)$. This suggests that we try to express a two-mass field $\varphi(x)$, with repeated root mass $\hbar\kappa$, in the form

$$(3.23) \quad \varphi(x) = a_1\varphi_1(x) + a_2\varphi_2(x).$$

By means of (3.8), suitably modified, we can express A , B and π also, in terms of the φ_i and π_i . Hence we derive equations for the a_i , which have the solution $a_1 = a_2 = (4g)^{-\frac{1}{2}}$. Using this, the two-mass Hamiltonian density reduces to (3.21). Since g can be chosen as small as we please, this is a « positive-energy » solution. An indefinite-energy solution with real coefficients a_i can be found by letting φ_2 be a real negative-energy field, and suitably modifying the interaction term.

This treatment generalizes quite simply. Where there is an n -fold mass root κ , we introduce n interacting fields φ_i , each of which satisfies

$$(3.24) \quad (\square - \kappa^2)^n\varphi_i(x) = 0$$

(when the others have been eliminated), and express the multi-mass field as a linear superposition of such sets of fields together with free fields corresponding to the simple mass roots.

Had g in (3.21) had some other value, we could have used φ_1 and φ_2 to describe a two-mass field of distinct masses, which might even be complex. This provides a new way of looking at the case of complex roots.

3.4. Interactions. — Consider first interaction Hamiltonians H_1 which are self-adjoint in the Natural Picture. We pass to the Interaction Representation in this picture; it is simplest to do this *in the single-mass formalism*. We now take any self-adjoint Interaction Hamiltonian, and re-write it in terms of the multi-mass fields. Unfortunately, we find in practice that a problem, when thus re-stated, is at least as divergent as before, and in general more divergent.

For example, take the two-mass Fermi field $\psi(x)$, constructed from the two single-mass fields $\psi_i(x)$ in the manner of 3.2, interacting with a real scalar field $\varphi(x)$ through terms of the type

$$(3.25) \quad \mathcal{H}_1 = \alpha_{ij} \bar{\psi}_i(x) \psi_j(x) \varphi(x).$$

From equation (3.18) (modified) we find that

$$(3.26) \quad \psi_1(x) = (\kappa_2 - \kappa_1)^{-\frac{1}{2}} (\gamma_\mu \partial_\mu + \kappa_2) \psi(x)$$

with similar expressions for ψ_2 , $\bar{\psi}_1$, $\bar{\psi}_2$. Hence in general H_1 contains terms with two derivatives of ψ , and the S -matrix elements are more divergent than in the single-mass formalism. Further, since H_1 is self-adjoint, we have $\alpha_{ij} = \bar{\alpha}_{ji}$ and there is not enough freedom in choosing these coefficients to construct a case with better convergence in the multi-mass form.

Looking at this in another way, it is easy to write down multi-mass interaction terms, such as $g\bar{\psi}\psi\varphi$, which would give better convergence but which are not self-adjoint. To make them so, we must add terms with derivatives of $\bar{\psi}$, ψ and the improvement is lost.

It appears to be a general rule, although no simple proof has been found, that interaction terms of this first type (self-adjoint in the Natural Picture) do not give compensation effects and better convergence. There seems no advantage from this point of view in using the multi-mass formalism in these cases.

A multi-mass Fermi theory of this type, introduced in connection with a theory of fundamental length, is that of DARLING⁽³⁾. Like PAIS and UHLENBECK, he removes the indefinite product in effect without seeming to recognize its presence, by a particular choice of adjoints. His criticism that the commutation rules of PAIS and UHLENBECK are inconsistent with the form of their

Lagrangian arises because they have not made an explicit transformation to the Natural Picture, and have therefore not rewritten the Lagrangian in terms of the new adjoints.

On the other hand, returning to general interactions, it is possible to construct compensation theories in an indefinite picture. Take for example a five-mass Fermi field $\psi(x)$, interacting with a real scalar field $\varphi(x)$ through the term

$$(3.27) \quad \mathcal{H}_1 = g \bar{\psi}(x) \psi(x) \varphi(x),$$

which is self-adjoint in the usual indefinite picture. Using the Feynman-Dyson⁽¹⁰⁾ graphical methods, we find that all S -matrix graph contributions are convergent.

Unfortunately, neither in this nor in any other compensation theory of a similar kind does it seem possible to find a Natural Picture explicitly without diagonalizing $H_0 + H_1$, and this is beyond the power of present-day mathematics (*). Indeed, if this could be done, there would remain no divergence difficulties at all, for one could express any state in terms of eigenstates of $H_0 + H_1$. Thus, although we now know that these compensation theories exist in principle, we cannot use them in practice, and they remain mathematical curiosities and no more.

There might possibly be some value in a series approximation to θ , but it is clear that any approximation used in practice would have to commute with the total Hamiltonian.

Finally we remark that it is possible that some of our earlier assumptions are violated by some or all of the fields with compensating interactions; there is no means of checking this. It may even be that there are no positive definite scalar products associated with such fields. If this were so, our present interpretation of these fields would break down, and we would have to reject them altogether as unphysical, in accordance with the principle of section 2.2.

3.5. Higher-spin fields. — We have not investigated closely theories with higher-spin fields or mixtures of fields of different spins, but it appears that similar results will hold for them too.

For example, STÜCKELBERG's⁽¹¹⁾ well known expression of the Proca field in terms of a 4-vector and a scalar field shows us at once how to set up theories with compensation effects between neutral vector mesons, scalar mesons, and

⁽¹⁰⁾ F. J. DYSON: *Phys. Rev.*, **75**, 486, 1736 (1949); R. P. FEYNMAN: *Phys. Rev.*, **76** 749, 769 (1949).

(*) It is by no means certain that it will be within the power of future mathematics but our conventions allow us to suppose it can be done.

⁽¹¹⁾ E. C. G. STÜCKELBERG: *Helv. Phys. Acta*, **11**, 299 (1938).

photons, arranging separate compensations for the scalar and 4-vector components. The same can be done for pseudovector and charged mesons too. Such a theory is the renormalizable mixture of pseudovector and pseudoscalar mesons ⁽¹²⁾. However, they all suffer either from indefinite energies, or indefinite scalar products which we cannot handle in practice.

For fields of non-integral spin, we can decompose a multi-mass Lagrangian in terms of single-mass Lagrangian densities of the form

$$(3.28) \quad \mathcal{L} = \pm \frac{\hbar}{2} \bar{\psi} \{ \alpha_{\mu} \partial_{\mu} + \kappa \} \psi .$$

As with spin- $\frac{1}{2}$ fields, this leads to an indefinite scalar product ⁽¹³⁾ which is easy to treat in the free-field case above, but which leads to difficulties for compensating interactions.

In conclusion, the author would like to thank Dr. K. V. ROBERTS for much encouragement and constructive criticism throughout this work, and Dr. P. T. MATTHEWS and Dr. A. SALAM for helpful conversations. He also gratefully acknowledges a maintenance grant from the Department of Scientific and Industrial Research.

⁽¹²⁾ D. B. BEARD and H. A. BETHE: *Phys. Rev.*, **83**, 1106 (1951). Feynman points out the indefinite energy in *Phys. Rev.*, **76**, 769 (1949).

⁽¹³⁾ This appears to be true also in Bhabha's special formalism. See K. J. LE COUTEUR: *Proc. Camb. Phil. Soc.*, **44**, 63 (1947).

RIASSUNTO (*)

Si fa un'analisi dei prodotti scalari nella teoria quantistica e si espone un pensiero filosofico da seguire nel trattamento dei prodotti scalari indefiniti. Si applica quanto precede a uno studio di campi di masse molteplici di energia positiva. Si trova che in generale il formalismo di masse molteplici non migliora la convergenza; per quanto in linea di principio si possano costruire delle teorie convergenti, ciò non è possibile in pratica. Le teorie di cui l'applicazione è possibile sono divergenti almeno come nel formalismo per masse singole.

(*) Traduzione a cura della Redazione.

Les forces spin-orbite et les durées de vie β de ^{12}B et ^8Li .

B. G. JANCOVICI

Laboratoire de Physique de l'École Normale Supérieure - Paris

(ricevuto il 25 Febbraio 1955)

Summary. — The unfavored β -transitions $^8\text{Li} \rightarrow ^8\text{Be}$ and $^{12}\text{B} \rightarrow ^{12}\text{C}$ are explained by a mixing of supermultiplets in ^8Be and ^{12}C through the spin-orbit force. This spin-orbit force can be estimated from the experimental ft values. In ^{12}C , an effective force $a(\mathbf{l} \cdot \mathbf{s})$, where $a \sim 5$ MeV, is obtained, in good agreement with the generally admitted numbers. On the other hand, in ^8Be , a value $|a| \sim 1.6$ MeV is obtained. This abnormally low value is discussed.

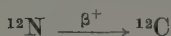
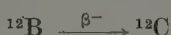
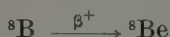
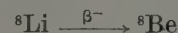
1. — Introduction.

Parmi les transitions β permises, il existe, pour les noyaux légers, une nette distinction entre les transitions favorisées ($\log ft \sim 3,5$) et les transitions non favorisées ($\log ft \sim 5$). Cette distinction, non prévue par le modèle des couches à couplage $j-j$, est par contre explicable dans le modèle des couches à couplage LS . Dans ce dernier modèle, une transition est favorisée ou non, selon que les états initial et final appartiennent ou n'appartiennent pas au même supermultiplet. La disparition progressive de la distinction entre transitions favorisées et non favorisées pour les noyaux plus lourds peut s'expliquer par l'importance croissante que prennent alors les forces de Coulomb et les forces non centrales qui mélangent les supermultiplets. Même pour les noyaux légers, les transitions non favorisées ne peuvent avoir une probabilité non nulle que grâce à un mélange partiel des supermultiplets. Les durées de vie β peuvent donc fournir des renseignements sur l'importance des forces non centrales ⁽¹⁾; c'est ce qu'on se propose d'étudier ici dans des cas particuliers.

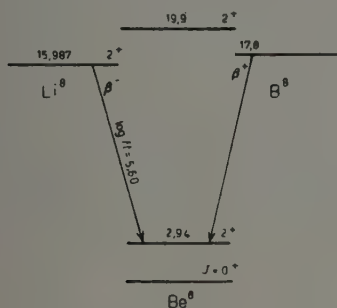
On peut attendre une transition non favorisée quand l'état final est un niveau bas d'un noyau léger pair-pair. En effet, un tel niveau appartient à

⁽¹⁾ Le rôle des forces de Coulomb est négligeable pour les noyaux légers.

un supermultiplet $(^2) (0, 0, 0)$, lequel ne contient qu'un seul état de charge possible, et l'état initial appartient forcément à un supermultiplet différent. En se bornant aux noyaux de la couche $1p$, on a comme désintégrations β de ce type les transitions



dont le schémas $(^3)$ sont donnés dans les figs. 1 et 2. La transition de ${}^8\text{Li}$ vers l'état de base ${}^8\text{Be}$ est interdite ($\Delta J = 2$) et l'on ne considérera que la transition



Flg. 1.

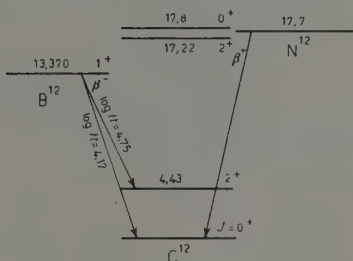


Fig. 2.

vers le premier état excité ${}^8\text{Be}^*$ ($\log ft = 5,60$); la transition miroir de ${}^8\text{B}$, moins bien connue expérimentalement, sera considérée comme analogue. On étudiera pour ${}^{12}\text{B}$ les deux transitions permises vers l'état de base de ${}^{12}\text{C}$ ($\log ft = 4,17$) et le premier état excité ${}^{12}\text{C}^*$ ($\log ft \approx 4,75$); la désintégration miroir de ${}^{12}\text{N}$ sera également considérée comme analogue.

On se propose donc d'interpréter les transitions ${}^8\text{Li} \rightarrow {}^8\text{Be}^*$, ${}^{12}\text{B} \rightarrow {}^{12}\text{C}$, et ${}^{12}\text{B} \rightarrow {}^{12}\text{C}^*$. Le chiffre le plus étonnant a priori est $\log ft = 4,17$ pour ${}^{12}\text{B} \rightarrow {}^{12}\text{C}$: cette valeur est nettement plus faible que le $\log ft \sim 5$ ou 6 qui caractérise d'ordinaire les transitions permises non favorisées. On montrera que, en fait, une force spin-orbite de grandeur raisonnable mélange assez les supermultiplets pour abaisser ainsi la durée de vie et que c'est au contraire la durée de vie de ${}^8\text{Li} \rightarrow {}^8\text{Be}^*$ qui semble trop longue quand on essaie de l'expliquer par la même théorie.

$(^2)$ E. P. WIGNER: *Phys. Rev.*, **51**, 106 (1937).

$(^3)$ F. AJZENBERG et T. LAURITSEN: *Rev. Mod. Phys.*, **24**, 321 (1952).

Le couplage intermédiaire décrit, mieux que les cas extrêmes des couplages LS ou $j-j$, les niveaux des noyaux légers ⁽⁴⁾. Cependant, pour les polyades $A = 4n$, le haut degré de symétrie favorise le couplage LS . Par contre, non seulement le couplage $j-j$ ne rend pas compte des niveaux d'énergie, mais encore il ne distingue pas les transitions favorisées et non favorisées, et il prévoit les durées de vie β trop courtes pour les transitions considérées (voir Appendice). On travaillera donc en couplage LS , les forces non centrales étant traitées comme une perturbation. Les configurations mises en jeu sont p^4 pour $A = 8$ et p^{-4} pour $A = 12$: elles donnent lieu à la même classification de niveaux.

2. — La force spin-orbite et le mélange des états.

Les états de la configuration p^4 ont été classés et leurs coefficients de parentage fractionnel $\langle n | n-1 \rangle$ et $\langle n | n-2 \rangle$ ont été calculés ^(5,6). Dans ⁸Be ou ¹²C, le niveau fondamental $J = 0^+$ et le niveau excité $J = 2^+$ sont vraisem-

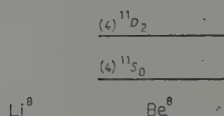
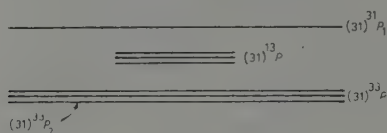


Fig. 3.

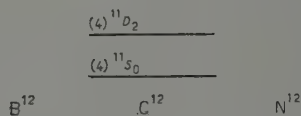
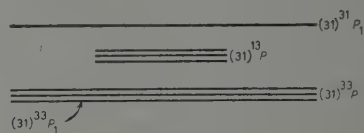


Fig. 4.

blablement de partition $[4]$, et on peut leur attribuer les états $[4]^{11}S_0$ et $[4]^{11}D_2$ ⁽⁴⁾ (fig. 3 et 4). Les niveaux fondamentaux de ⁸Li ou ¹²B doivent être de partition $[31]$, et on les supposera respectivement d'états $[31]^{33}P_2$ et $[31]^{33}P_1$.

Puisque les transitions β ne peuvent avoir lieu qu'entre niveaux d'un même supermultiplet, il faut admettre que les états finaux de la transition dans ⁸Be ou ¹²C contiennent un peu de supermultiplet $[31]P$. T et J étant de bons nombres quantiques, $[4]^{11}S_0$ ne peut être mélangé que de $[31]^{13}P_0$ et $[4]^{11}D_2$ de $[31]^{13}P_2$. Au premier ordre, ces mélanges ne peuvent être assurés que par une force spin-orbite (une force tenseur a des éléments de matrice nuls entre les états considérés).

⁽⁴⁾ D. R. INGLIS: *Rev. Mod. Phys.*, **25**, 390 (1953).

⁽⁵⁾ H. A. JAHN et H. VAN WIERINGEN: *Proc. Roy. Soc., A* **209**, 402 (1951).

⁽⁶⁾ J. P. ELLIOTT, J. HOPE et H. A. JAHN: *Phil. Trans. Roy. Soc., A* **246**, 241 (1953).

On considère que la force spin-orbite est due à des forces à deux corps:

$$(1) \quad \begin{cases} F = \sum_{i > j} F_{ij}, \\ F_{ij} = f(r_{ij}) [(\mathbf{r}_i - \mathbf{r}_j) \wedge (\mathbf{p}_i - \mathbf{p}_j/2)] \cdot (\mathbf{s}_i + \mathbf{s}_j). \end{cases}$$

L'interaction (1) entre un nucléon (ou un trou) et une couche fermée produit une force effective du type $a(\mathbf{l} \cdot \mathbf{s})$ ⁽⁷⁾. Dans le cas d'une configuration de n nucléons (ou trous) équivalents en dehors de couches fermées, l'interaction (1) peut donc s'écrire:

$$(1') \quad F = \sum_{i=1}^n a(\mathbf{l}_i \cdot \mathbf{s}_i) + \sum_{\substack{i, j=1 \\ i > j}}^n F_{ij}$$

où le premier terme représente l'interaction de ces n nucléons (ou trous) avec les couches fermées, et le deuxième terme représente l'interaction des n nucléons (ou trous) entre eux.

Tous les calculs sont grandement facilités si les fonctions d'onde à une particule sont les fonctions propres d'un puits oscillateur harmonique $V(r)$ ⁽⁸⁾. Tous les éléments de matrice de l'interaction (1) s'expriment alors en fonction des intégrales de Talmi de la fonction $f(r)$:

$$(2) \quad I_l = \int_0^\infty R_l^2(r) f(r) dr$$

où $R_l(r)$ est r fois la partie radiale de la première fonction propre de moment angulaire l d'un puits oscillateur harmonique $V(r) = \frac{1}{4}V(r)$. Ce formalisme se prête bien à l'étude des cas limites: forces à courte portée, pour lesquelles $I_{l+1} \ll I_l$; forces à longue portée pour lesquelles tous les I_l sont égaux. Les valeurs de a sont:

pour un nucléon $1p$ interagissant avec les 4 nucléons $1s$

$$(3) \quad a = 3I_1,$$

pour un trou $1p$ interagissant avec les 4 nucléons $1s$ et les 12 nucléons $1p$

$$(3') \quad a = -\frac{9}{2}I_1 - \frac{5}{2}I_2.$$

⁽⁷⁾ J. HUGHES et K. T. LECOUEUR: *Proc. Phys. Soc.*, A **63**, 1219 (1950).

⁽⁸⁾ I. TALMI: *Helv. Phys. Acta*, **25**, 185 (1952). L'expression correspondant à F_{ij} dans TALMI est deux fois trop grande. Je remercie le Dr. J. P. ELLIOTT pour m'avoir fait remarquer ce point.

Afin d'évaluer les mélanges dus à l'interaction (1'), on calcule les éléments de matrice du premier terme de (1') en utilisant les coefficients de parentage fractionnel $\langle n | n-1 \rangle$, et les éléments de matrice du deuxième terme en utilisant les coefficients de parentage fractionnel $\langle n | n-2 \rangle$ ⁽⁹⁾. On trouve ainsi:

$$(4) \quad \langle s^4 p^{\pm 4} [4]^{11} S_0 | \sum_{i=1}^4 a(\mathbf{l}_i \cdot \mathbf{s}_i) | s^4 p^{\pm 4} [31]^{13} P_0 \rangle = -\frac{2\sqrt{6}}{3} a,$$

$$(4') \quad \langle s^4 p^{\pm 4} [4]^{11} S_0 | \sum_{\substack{i,j=1 \\ i \neq j}}^4 F_{ij} | s^4 p^{\pm 4} [31]^{13} P_0 \rangle = -\frac{2\sqrt{6}}{3} I_2,$$

$$(4'') \quad \langle s^4 p^{\pm 4} [4]^{11} D_2 | \sum_{i=1}^4 a(\mathbf{l}_i \cdot \mathbf{s}_i) | s^4 p^{\pm 4} [31]^{13} P_2 \rangle = \frac{\sqrt{105}}{15} a,$$

$$(4''') \quad \langle s^4 p^{\pm 4} [4]^{11} D_2 | \sum_{\substack{i,j=1 \\ i \neq j}}^4 F_{ij} | s^4 p^{\pm 4} [31]^{13} P_2 \rangle = \frac{\sqrt{105}}{15} I_2,$$

d'où les éléments de matrice de F :

$$(5) \quad \langle s^4 p^{\pm 4} [4]^{11} S_0 | F | s^4 p^{\pm 4} [31]^{13} P_0 \rangle = -\frac{2\sqrt{6}}{3} (a + I_2),$$

$$(5') \quad \langle s^4 p^{\pm 4} [4]^{11} D_2 | F | s^4 p^{\pm 4} [31]^{13} P_2 \rangle = \frac{\sqrt{105}}{15} (a + I_2).$$

Le calcul des mélanges nécessite aussi la connaissance des différences d'énergies ΔE entre les termes à mélanger ^(3,4,10). Dans ^8Be , le niveau $[31]^{13}P_2$ pourrait être à 19,9 MeV; le niveau $[4]^{11}D_2$ est à 2,94 MeV: leur différence d'énergie est $\Delta E = 17$ MeV. Dans ^{12}C , les niveaux $[31]^{13}P_0$ et $[31]^{13}P_2$ pourraient être à 17,8 et 17,22 MeV respectivement; le niveau $[4]^{11}D_2$ est à 4,43 MeV: les différences d'énergies sont donc $\Delta E_{sp} = 17,8$ MeV, $\Delta E_{dp} = 12,79$ MeV. Toutes ces attributions ne sont pas certaines, mais les ordres de grandeur des énergies d'excitation doivent être corrects.

Les amplitudes de mélange sont alors données par

$$(6) \quad x = \frac{\langle F \rangle}{\Delta E}.$$

⁽⁹⁾ G. RACAH: *Phys. Rev.*, **63**, 367 (1943).

⁽¹⁰⁾ F. AJZENBERG et T. LAURITSEN: *Boston University, Quarterly Progress Report* no. 4, Appendix B, (September 30, 1954).

3. — Les transitions β .

Nous considérons que les transitions β ont lieu vers la partie $[31]^{13}P$ de l'état final. On doit donc considérer les transitions

$$(7a) \quad [31]^{33}P_2 \rightarrow [31]^{13}P_2 \quad \text{pour} \quad ^8\text{Li} \rightarrow ^8\text{Be}^*$$

$$(7b) \quad [31]^{33}P_2 \rightarrow [31]^{13}P_0 \quad \text{pour} \quad ^{12}\text{B} \rightarrow ^{12}\text{C}$$

$$(7c) \quad [31]^{33}P_1 \rightarrow [31]^{13}P_2 \quad \text{pour} \quad ^{12}\text{B} \rightarrow ^{12}\text{C}^*.$$

L'élément de matrice de l'opérateur de Fermi est nul entre états de spin isotopique total différent. Les trois transitions (7) sont donc uniquement dues à l'opérateur de Gamow-Teller. On calcule les éléments de matrice de cet opérateur grâce aux coefficients de parentage fractionnel $\langle n | n-1 \rangle$ ⁽¹¹⁾, et on trouve pour les trois transitions (7) les valeurs respectives:

$$\begin{aligned} (8a) & \\ (8b) & \\ (8c) & \end{aligned} \quad \left| \int \sigma \right|^2 = \begin{cases} 3 \\ 4/3 \\ 5/3 \end{cases}$$

ft est alors donné par ⁽¹²⁾:

$$(9) \quad ft = \frac{1}{|x|^2} \frac{4\,780}{\left| \int \sigma \right|^2}.$$

4. — Comparaison avec l'expérience. Conclusions.

Pour comparer les prévisions théoriques avec l'expérience, on utilise (8) et (9) pour déterminer $|x|^2$ à partir des valeurs expérimentales de ft . On en déduit ensuite par (5) et (6) les valeurs de $a + I_2$ qui conviennent dans chaque cas. Ces résultats sont donnés dans le tableau I.

La théorie rend compte correctement du rapport des durées de vie pour les deux transitions β $^{12}\text{B} \rightarrow ^{12}\text{C}$ et $^{12}\text{C}^*$, puisque ces deux transitions sont explicables par des valeurs voisines de $a + I_2$. La force spin-orbite correspondant est d'un ordre de grandeur satisfaisant: si les forces spin-orbite sont à portée courte devant le rayon nucléaire, $I_2 \ll I_1$, donc $I_2 \ll a$, et la transition vers l'état fondamental de ^{12}C , de ft mieux établi que celle vers l'état excité $^{12}\text{C}^*$

⁽¹¹⁾ I. TALMI: *Phys. Rev.*, **91**, 122 (1953).

⁽¹²⁾ J. B. GERHART: *Phys. Rev.*, **95**, 288 (1954).

fixe $a \sim 5,3$ MeV; au contraire, pour des forces à portée longue $I_2 = I_1$, et d'après (3'), $a = \frac{7}{8}(a + I_2) \sim 3,7$ MeV. On voit que a dépend peu de la portée de la force spin-orbite. Les valeurs ainsi trouvées pour a sont de l'ordre de celles qui résultent de l'étude des niveaux d'énergie de ^{12}C en couplage intermédiaire (4). Ce sont aussi les valeurs à attendre de la séparation $^2P_{\frac{1}{2}} - ^2P_{\frac{3}{2}}$ pour le trou $1p$ de ^{15}N ; cette séparation, qui est expérimentalement de 6,3 MeV et théoriquement de $(3/2)a$, fixerait $a \sim 4,2$ MeV.

TABLEAU I.

	$ x ^2$	$(a + I_2)$ MeV
$^8\text{Li} \rightarrow ^8\text{Be}^*$	0,040	— 1,6
$^{12}\text{B} \rightarrow ^{12}\text{C}$	0,24	5,3
$^{12}\text{B} \rightarrow ^{12}\text{C}^*$	0,051	4,4

Par contre, l'interprétation de $^8\text{Li} \rightarrow ^8\text{Be}$ ne semble pas très cohérente avec les résultats de $^{12}\text{B} \rightarrow ^{12}\text{C}$. Comme le paramètre du puits oscillateur harmonique de ^8Be et ^{12}C est sensiblement le même (13), les intégrales I_i ont des valeurs voisines dans les deux noyaux, et, d'après (3) et (3'), on attendrait pour ^8Be un $a + I_2$ égal aux $-\frac{2}{3}$ de celui de ^{12}C , soit $\sim -3,6$ MeV, au lieu du $-1,6$ MeV déduit du ft de ^8Li . Le mécanisme de force spin-orbite supposé prévoit donc un rapport

$$\left| \frac{(a + I_2) (^8\text{Be})}{(a + I_2) (^{12}\text{C})} \right|$$

nettement plus grand que celui suggéré par notre interprétation des durées de vie β .

Il semble donc que $\left| \frac{a(1p)}{a(1p^{-1})} \right|$ soit plus faible en réalité que la valeur attendue d'après (3) et (3'). Cela suggérerait peut-être d'adopter un modèle dans lequel la couche $1s$ serait de dimensions plus faibles par rapport à la couche $1p$ que dans le modèle de l'oscillateur harmonique. L'interaction ps deviendrait alors plus faible par rapport à l'interaction pp , et (3) pourrait diminuer par rapport à (3').

Cette interprétation aurait l'avantage de pouvoir expliquer ou au moins diminuer le désaccord (14) entre les valeurs du rayon nucléaire ($\sim 1,45 \cdot A^{\frac{1}{3}}$.

(13) B. C. CARLSON et I. TALMI: *Phys. Rev.*, **96**, 436 (1954).

(14) B. G. JANCOVICI: *Phys. Rev.*, **95**, 389 (1954). Comptes Rendus (sous presse).

$\cdot 10^{-13}$ cm) calculées à partir de la différence d'énergie entre noyaux miroirs, et celles ($\sim 1,2 \cdot A^{\frac{1}{3}} \cdot 10^{-13}$ cm) établies par la diffusion d'électrons rapides ou les rayons X des atomes μ -mésiques. La deuxième série de méthodes mesure le rayon quadratique moyen, et un modèle dans lequel les fonctions d'onde p s'étendent plus au dehors que les fonctions d'ondes s donnera, pour un rayon quadratique moyen déterminé, une différence d'énergie de Coulomb entre noyaux miroirs plus faible qu'une sphère uniforme; et donc le rayon coulombien apparent sera augmenté. Cet effet est cependant trop faible pour rendre compte des valeurs expérimentales, dans le modèle du puits oscillateur harmonique, alors qu'il sera augmenté si les dimensions de la couche $1s$ sont réduites.

D'autre part, un calcul relatif à ^{16}O , où l'on faisait varier deux paramètres représentant les diamètres respectifs des couches s et p , a montré que l'énergie était minimum pour une couche p plus étendue par rapport à la couche s que dans le modèle du puits oscillateur harmonique.

Cependant, même en supposant que l'effet ci-dessus existe et diminue $|a(1p)|$, il demeure le fait que la valeur $|a(1p)| \sim 1,6$ MeV dans ^8Be , suggérée par la durée de vie β de ^8Li , est plus faible que la valeur $|a(1p)| \sim 2$ MeV que semblent indiquer la séparation $^2P_{\frac{3}{2}} - ^2P_{\frac{1}{2}}$ de ^4He ou le spectre de ^6Li ⁽¹⁵⁾. Cette valeur anormalement faible d'un effet spin-orbite dans ^8Be est peut-être à rapprocher de la séparation, également anormalement faible, du doublet $^2P_{\frac{3}{2}} - ^2P_{\frac{1}{2}}$ dans ^7Li ou ^7Be . Il semble donc que le modèle des couches et l'interaction (1) prévoient des résultats incorrects pour $A=7$ ou 8 . Il est possible que les fonctions d'onde de ces noyaux soient sensiblement mélangées de celles d'un modèle à particules α (4). On peut aussi se demander si la force spin-orbite est bien due à une interaction du type (1) ou si elle ne résulte pas, au moins partiellement, d'autres forces, par exemple d'effets du 2^{ème} ordre d'une force tenseur ⁽¹⁶⁾.

Je remercie vivement M. le Professeur E. P. WIGNER pour m'avoir suggéré ce travail ainsi que pour l'aide et la direction constantes qu'il m'a apportées.

APPENDICE

Étude de ^{12}B et ^{12}C en couplage $j-j$.

On a également étudié ^{12}B et ^{12}C en couplage $j-j$, en suivant les méthodes de Racah et de Talmi.

On calcule au premier ordre la séparation des niveaux des configurations

⁽¹⁵⁾ A. M. LANE: communication privée.

⁽¹⁶⁾ E. P. WIGNER: *Conférence de Physique Nucléaire de Rio de Janeiro*.

$p_{\frac{3}{2}}^8$ et $p_{\frac{1}{2}}^7 p_{\frac{1}{2}}$ par une force centrale (1 ou P ou Q ou $-PQ$) $f(r)$, où P et Q sont respectivement les opérateurs d'échange d'espace et de spin; on a également calculé la séparation de ces niveaux par une force tenseur

$$\left[\frac{3(\sigma_1 \cdot r)(\sigma_2 \cdot r)}{r^2} - (\sigma_1 \cdot \sigma_2) \right] f(r).$$

Les énergies sont seulement données à une constante additive près ⁽¹⁷⁾, car le calcul a été fait pour des trous, et on n'a pas gardé l'énergie d'interaction, toujours la même, des trous p avec les couches fermées s et p , ou des couches fermées entre elles. Les énergies sont exprimées en fonction des intégrales de Talmi I_i de la fonction $f(r)$. Pour la force centrale, ces intégrales sont reliées à celles de Slater par:

$$I_1 = F_0 - 5F_2, \quad I_0 + I_2 = (2F_0 + F_2).$$

Les résultats sont donnés dans le tableau II; pour les forces centrales, on a donné les expressions à la fois en fonction des intégrales de Talmi et de celles de Slater.

Les déplacements de niveaux sont de l'ordre de quelques MeV au maximum et ne peuvent rendre compte des spectres de ^{12}B et ^{12}C , et en particulier de la grande séparation entre le premier niveau excité ($T=0$, $J=2$) de ^{12}C et le niveau fondamental ($T=1$, $J=1$) de ^{12}B .

Les éléments de matrice des transitions β sont:

$$\begin{aligned} {}^{12}\text{B}(p_{\frac{3}{2}}^7 p_{\frac{1}{2}}, T=1, J=1) &\rightarrow {}^{12}\text{C}(p_{\frac{3}{2}}^8, T=0, J=0) & \left| \int \sigma' \right|^2 = 16/9, \\ {}^{12}\text{B}(p_{\frac{3}{2}}^7 p_{\frac{1}{2}}, T=1, J=1) &\rightarrow {}^{12}\text{C}(p_{\frac{1}{2}}^7 p_{\frac{1}{2}}, T=0, J=2) & \left| \int \sigma \right|^2 = 5/9. \end{aligned}$$

Les durées de vie β qui en résultent sont beaucoup trop courtes.

Le couplage $j-j$ fournit donc une description beaucoup moins bonne que le couplage LS pour ^{12}B et ^{12}C .

Afin de mettre en évidence les différences entre le couplage LS et le couplage $j-j$, on a calculé les coefficients de la transformation $LS \leftrightarrow j-j$ pour les trois états mis en jeu; pour cela on a diagonalisé la matrice d'une interaction $\sum_i (\mathbf{l}_i \cdot \mathbf{s}_i)$, préalablement calculée par les coefficients de parentage fractionnel.

On a ainsi trouvé:

$$\begin{aligned} \Psi(p_{\frac{3}{2}}^8, T=0, J=0) &= \frac{\sqrt{5}}{9} \Psi([4] {}^{11}S_0) + \frac{2\sqrt{2}}{9} \Psi([22] {}^{11}S_0) + \\ &+ \frac{\sqrt{30}}{9} \Psi([31] {}^{13}P_0) + \frac{\sqrt{2}}{3} \Psi([211] {}^{13}P_0) - \frac{2\sqrt{5}}{9} \Psi([22] {}^{15}D_0), \end{aligned}$$

⁽¹⁷⁾ A cette constante additive près, on retrouve les résultats partiels de D. KURATH: *Phys. Rev.*, **88**, 804 (1952).

TABLEAU II.

Configuration	T	J	Force centrale				Force tenseur
			1	P	Q	-PQ	
$p^8_{\frac{3}{2}}$	0	0	$\frac{5}{2}(I_0 + I_2) + I_1$	$\frac{5}{2}(I_0 + I_2) - \frac{13}{3}I_1$	$\frac{8}{3}I_2$	0	$\frac{8}{3}I_1$
			$6F_0$	$\frac{2}{3}F_0 + \frac{80}{3}F_2$	$\frac{8}{3}F_0 - \frac{40}{3}F_2$	0	
	1	2	$\frac{25}{12}(I_0 + I_2) + \frac{11}{6}I_1$	$\frac{25}{12}(I_0 + I_2) - \frac{7}{2}I_1$	$-\frac{1}{3}(I_0 + I_2) + \frac{8}{3}I_1$	$\frac{1}{3}(I_0 + I_2) + \frac{4}{3}I_1$	$\frac{11}{5}I_1$
			$6F_0 - 5F_2$	$\frac{2}{3}F_0 + \frac{65}{3}F_2$	$2F_0 - 14F_2$	$2F_0 - 6F_2$	
$p^7_{\frac{3}{2}}p_1$	1	1	$\frac{25}{12}(I_0 + I_2) + \frac{11}{6}I_1$	$\frac{25}{12}(I_0 + I_2) - \frac{79}{18}I_1$	$\frac{22}{9}I_1$	$2I_1$	$\frac{7}{9}I_1 - \frac{5}{6}I_2$
			$6F_2 - 5F_2$	$-\frac{2}{9}F_0 + \frac{235}{9}F_2$	$\frac{22}{9}F_1 - \frac{110}{9}F_2$	$2F_0 - 10F_2$	
	0	2	$\frac{11}{4}(I_0 + I_2) + \frac{1}{2}I_1$	$\frac{11}{4}(I_0 + I_2) - \frac{7}{2}I_1$	$\frac{1}{2}(I_0 + I_2) + I_1$	$\frac{1}{2}(I_0 + I_2) + I_1$	$\frac{23}{10}I_1 - \frac{1}{2}I_2$
			$6F_0 + 3F_2$	$2F_0 + 23F_2$	$2F_0 - 4F_2$	$-6F_2$	
	0	1	$\frac{25}{12}(I_0 + I_2) + \frac{11}{6}I_1$	$\frac{25}{12}(I_0 + I_2) - \frac{71}{18}I_1$	$\frac{5}{6}(I_0 + I_2) + \frac{23}{9}I_1$	$-\frac{5}{6}(I_0 + I_2) + \frac{5}{3}I_1$	$\frac{1}{18}I_1 + \frac{5}{6}I_2$
			$6F_0 - 5F_2$	$\frac{2}{9}F_0 + \frac{215}{9}F_2$	$\frac{38}{9}F_0 - \frac{100}{9}F_2$	$-10F_2$	

$$\begin{aligned}
 \Psi(p_{\frac{7}{2}}^7 p_{\frac{1}{2}}, T=0, J=2) &= \frac{\sqrt{14}}{9} \Psi([4]^{11} D_2) - \frac{7\sqrt{30}}{90} \Psi([31]^{13} P_2) - \\
 &- \frac{2\sqrt{3}}{9} \Psi([31]^{13} D_2) + \frac{2\sqrt{105}}{45} \Psi([31]^{13} F_2) + \frac{2}{9} \Psi([22]^{15} S_2) - \\
 &- \frac{2\sqrt{2}}{9} \Psi([22]^{11} D_2) + \frac{\sqrt{7}}{9} \Psi([22]^{15} D_2) + \frac{\sqrt{2}}{6} \Psi([211]^{13} P_2), \\
 \Psi(p_{\frac{7}{2}}^7 p_{\frac{1}{2}}, T=1, J=1) &= -\frac{\sqrt{10}}{6} \Psi([31]^{33} P_1) + \frac{2\sqrt{3}}{9} \Psi([22]^{33} S_1) - \\
 &- \frac{\sqrt{15}}{9} \Psi([22]^{33} D_1) - \frac{2\sqrt{3}}{9} \Psi([211]^{31} P_1) + \frac{\sqrt{2}}{6} \Psi([211]^{33} P_1) + \\
 &+ \frac{\sqrt{15}}{9} \Psi([211]^{35} P_1).
 \end{aligned}$$

RIASSUNTO (*)

Le transizioni β non favorite ${}^8\text{Li} \rightarrow {}^8\text{Be}$ e ${}^{12}\text{Be} \rightarrow {}^{12}\text{C}$ si spiegano con una miscela di supermultipletti in ${}^8\text{Be}$ e ${}^{12}\text{C}$ tramite la forza spin-orbita. Tale forza spin-orbita può essere stimata dai valori ft sperimentali. Nel ${}^{12}\text{C}$ si ottiene una forza effettiva $a(\mathbf{l} \cdot \mathbf{s})$ dove $a \sim 5$ MeV, in buon accordo coi valori generalmente accettati. Nel ${}^8\text{Be}$, invece, si ottiene un valore $|a| \sim 1.6$ MeV. Si discute questo valore anormalmente basso.

(*) Traduzione a cura della Redazione.

On the Production of Secondary Electrons by High Energy μ -Mesons.

G. CAGLIOTI and S. SCIUTI

Istituto di Fisica dell'Università - Roma
Istituto Nazionale di Fisica Nucleare - Sezione di Roma

A. GIGLI

Istituto di Fisica dell'Università - Genova

(ricevuto il 1° Marzo 1955)

Summary. — With a counter hodoscope expressly designed for the study of secondary electrons, the generation of electronic secondaries in successive layers of material (Al or Pb) by μ -mesons has been studied. An examination of these results, in conjunction with hodoscope data already in part published, shows that the discrepancies between cloud chambers and hodoscope measurements can be fully explained.

1. — Introduction.

In recent years the interaction of high energy μ -mesons with matter has been studied by many authors using various experimental methods and nuclear techniques.

In this work we consider the production of secondary electrons ⁽¹⁻⁶⁾ generated by μ -mesons and, in particular, the problem concerning their generation in successive layers of dense material.

⁽¹⁾ W. E. HAZEN: *Phys. Rev.*, **64**, 7 (1943).

⁽²⁾ W. W. BROWN, A. S. MCKAY, and E. D. PALMATIER: *Phys. Rev.*, **76**, 506 (1949).

⁽³⁾ E. AMALDI, C. CASTAGNOLI, A. GIGLI and S. SCIUTI: *Nuovo Cimento*, **9**, 969 (1952).

⁽⁴⁾ M. L. T. KANNANGARA and M. ZIVKOVIC: *Phil. Mag.*, **44**, 797 (1953).

⁽⁵⁾ S. T. GOLDSACK and M. L. T. KANNANGARA: *Phil. Mag.*, **44**, 811 (1953).

⁽⁶⁾ W. D. WALKER: *Phys. Rev.*, **90**, 234 (1953).

In a preceding work, AMALDI and Coll. ⁽³⁾, operating with a counter hodoscope at a depth of 50 meters water equivalent, found that the mean number, per incident meson, of events selected as multiple electronic secondaries, that is, generated in successive layers of lead, was greater by about a factor of 2 than that evaluated by statistical methods, starting from the mean number, per incident meson, of events selected as single electronic secondaries.

Successively WOLFENDALE ⁽⁷⁾, reelaborating the data obtained in Wilson chamber ⁽⁸⁾, concluded that the result to which AMALDI and coll. had arrived was inconsistent with the cloud chamber measurements, and that their result was to be attributed to large statistical fluctuations. LOVATI and coll. ⁽⁹⁾ experimenting with a cloud chamber at 55 m w.e., arrived at a similar conclusion as that of WOLFENDALE.

The purpose of this work is to reexamine the situation and to demonstrate, both by results obtained with a counter hodoscope especially designed to study knock-ons (indicated in the following with *C*), and by a reelaboration of the data of experiments already in part published (to be indicated with *A*), that the discrepancies existing between the measurements with counters and cloud chambers can be completely explained.

2. - Experiments with Hodoscope A.

The counter hodoscope represented in Fig. 1 has been used in two experiments underground: Experiment A_1 ⁽³⁾ at 50 and Experiment A_2 ⁽¹⁰⁾ at 200 m w.e.

For all technical details reference should be made to the works A_1 and A_2 .

Among the various events registered by such a telescope we will consider the following for the study of electronic secondaries:

1) An alignment *ABCDE* plus a single counter discharged in a single tray *K* ($K = B, C, D, E$); this category will be indicated by *es* (*K*).

2) The events *des* (*H, K*) [*tes* (*H, K, J*); *qes* (*B, D, C, E*)] corresponding to the generation in the lead above of only two [three, four] trays *H* and *K* [*H, K, J*; *B, C, D, E*] of two [three, four] events of type *es* by a single incident meson.

⁽⁷⁾ A. W. WOLFENDALE: *Nuovo Cimento*, **10**, 1493 (1953).

⁽⁸⁾ H. J. J. BRADDICK, W. F. NASH and A. W. WOLFENDALE: *Phil. Mag.*, **42**, 1277 (1951).

⁽⁹⁾ A. LOVATI, A. MURA and C. SUCCI: *Nuovo Cimento*, **11**, 92 (1954).

⁽¹⁰⁾ P. E. ARGAN, A. GIGLI and S. SCIUTI: *Nuovo Cimento*, **11**, 530 (1954).

The selection of events of type $es(K)$ [$des(H, K)$; $tes(H, K, J)$] is now carried out by adding to the $es(K)$ [des, tes] defined above, those events which, as far as regards the tray K [the trays H, K ; H, K, J] in question, have only a single counter discharged besides the alignment $ABCDE$, and give rise, in some of the other trays, to a certain number of discharged counters, provided that the process which has produced this hodoscope picture, is clearly not correlated to the event es [des, tes] considered. For example, there will be included in the class of events of type $(H) es$ in a preassigned tray H , events $des(H, K)$, $tes(H, K, J)$ etc., and in the class $des(H, K)$, events of the type $tes(H, K, J)$ etc.

Naturally, in such generalizations, particular care must be taken for events of contiguous trays, in order to be able, if possible, to distinguish those having only one secondary that can cross (possibly by means of its products) 5 cm of lead (one layer) or 10 cm of lead (two layers) etc.. The percentage of such events, is, however, very low, as is shown by recent experiments with the cloud chamber (^{6,11,12}), according to which the number of knock-ons and their secondary showers capable of traversing 2 cm of Pb is less than 10% of the events of type es .

Therefore, we indicate with $\Sigma es(H)$, $\Sigma des(H, K)$ etc., the classes of events of type es , des etc., generalized in the above way, and with p_H , p_{HK} etc., the respective mean numbers per incident meson.

For reasons of intensity and ease of hodoscope interpretation, only events of type Σes and Σdes have been studied. These are the only ones occurring in numbers such as to permit relatively accurate statistics (*).

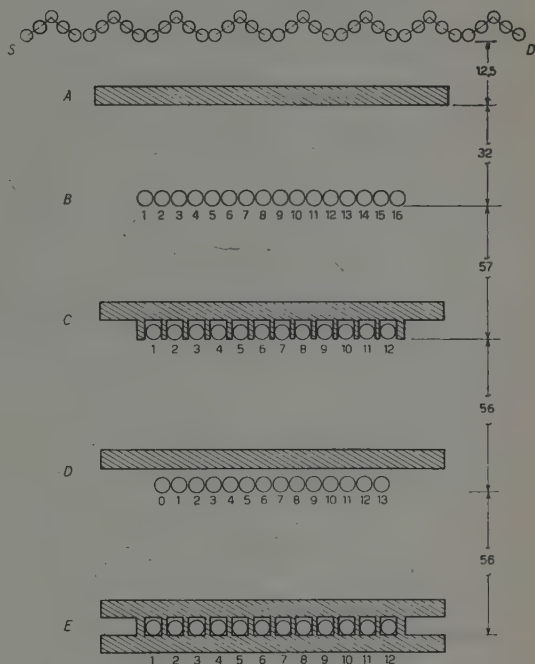


Fig. 1.

(¹¹) V. APPAPILLAI, A. W. MAILVAGANAM and W. A. WOLFENDALE: *Phil. Mag.*, **45**, 1059 (1954).

(¹²) H. J. J. BRADDICK and B. LEONTIC: *Phil. Mag.*, **45**, 1287 (1954).

(*) These definitions and criteria have also been adopted for hodoscope C.

The choice of trays H and K for the study of these events has been made with the following criteria:

- 1) the geometry of the two trays must be as identical as possible;
- 2) the two trays must be decoupled by an intermediate tray with an absorber above it.

In hodoscope A , constructed for other kind of experiments, trays C and E sufficiently satisfy these conditions. They are, in fact, the only ones that are exposed to the primary flux under practically identical conditions for the registration of the secondary electrons directly generated by the μ -mesons or by their secondaries. The trays in question have both the same number of counters (diameter 4 cm, length 80 cm); they are placed immediately under the layer of lead, and the counters are separated by lateral lead slats of 1 cm thickness (Fig. 1.).

In Table I are given the values of p_C , p_E , p_{CE} for the measurements at 50 m and 200 m w.e..

TABLE I.

Experiment	$p_C \cdot 10^2$	$p_E \cdot 10^2$	$p_{CE} \cdot 10^4$
A_1	0.60 ± 0.02	0.70 ± 0.06	0.73 ± 0.16
A_2	1.07 ± 0.03	1.08 ± 0.03	1.70 ± 0.41

From the numerical values of p and from a comparison between the hodoscope and a multiplate cloud chamber, it immediately seems that the production mechanism of events of type es is notably different in the two cases. In particular, the events studied in the cloud chamber, belong, for the majority, to the category of knock-on electrons; instead, these selected by trays C and E of hodoscope A seem essentially to be electronic showers produced in the lead above the counters and in the slats, of which at least one electron is able to discharge a counter different from that crossed by the primary. Further, a small contribution to such events is given by electron pairs generated directly by the μ -mesons or by secondary photons, of which at least one component discharges a counter not traversed by the primary.

The study of relativistic collisions between μ -mesons and knock-on electrons conclusively excludes the possibility that the trays C and E are sensitive to knock-on electrons (except for those few which, emitted at small angles, then scatter with a sufficiently large angle such as to strike a counter), in that the angular cut-off given by the geometry of the arrangement renders impossible

the direct registration of knock-on electrons emitted at relatively large angles, since such large angles are associated with a short range (*).

The above considerations are experimentally confirmed by the fact that, while secondary electrons starting from a very few MeV are revealed directly with a cloud chamber, this does not happen in the case of the hodoscope trays C and E (+), where the transfer of energy from the primary to the secondaries must be very high, as will be more fully demonstrated in the following.

3. — Experiment with Hodoscope C .

The obvious need of establishing a more direct comparison with the results of cloud chamber experiments led us to a complete modification (except for the electronics) of hodoscope A , giving one much better adapted for the study of knock-ons.

The following criteria were adopted in the planning of the new telescope:

a) to consider only two trays of counters, these to have as nearly as possible geometric symmetry with respect to the direction of any incident primary;

b) to increase the distance of the counter trays from the generator and to eliminate the lead slats between the counters, so as to obtain a greater angular resolution;

c) to vary the atomic number Z of the absorbers directly above the two trays so as to vary the mean number per incident meson of events whose production is proportional to Z/A (knock-on electrons) and of those whose rate of production increases with Z (events referred to at the end of § 2);

d) to study the possible dependence of p_H , p_K , p_{HK} on the thickness of the absorber between the two trays H and K , the cut-off energy E_c of the apparatus remaining constant.

The hodoscope constructed according to these criteria is represented in Fig. 2 (13).

(*) See, e.g., Fig. 3 in the previously cited work of M. L. T. KANNANGARA and M. ZIVKOVIC.

(+) The mean number p_C , p_E per incident meson are in good agreement with the corresponding cloud chamber data (small electronic showers, not including single knock-ons) obtained by WALKER (6) and WOLFENDALE (private communication).

(13) G. CAGLIOTI: *Tesi di Laurea, Roma* (1953).

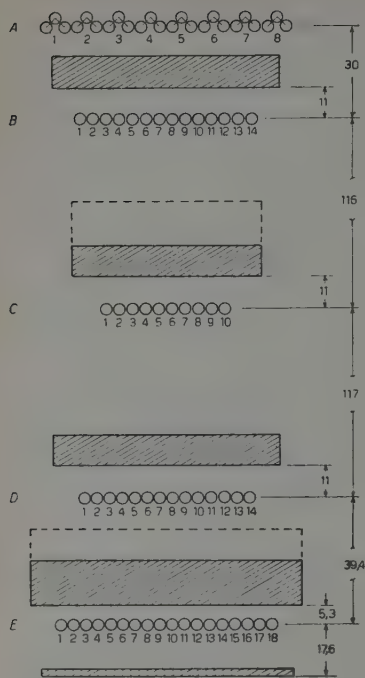


Fig. 2.

With it we have studied events of type Σes , Σdes in trays *B* and *D*. The apparatus was set up in the tunnel of the Castagnola (Tivoli) under 50 m w.e.. Measurements were initiated in the Autumn of 1953 and terminated in the Spring of 1954.

The mean numbers of events per incident meson for different experimental conditions (see Table II) are given in Table III.

The measurements α_1 , α_2 , α_3 were carried out according to the criterium given in *d*), while measurements β and γ were made to examine the dependence of m (see later) on thickness of the material above the trays *B* and *D*.

From various measurements in cloud chambers (^{11,12}) there is evidence that the penetration of the knock-ons is no greater than some tens of g/cm² on the average; it thus seems plausible to assume that the knock-ons observed are generated in the last few g/cm² of the absorber (¹⁴).

On the other hand, from the p 's in experiments α and β , it is deduced that, setting:

$$(1) \quad \bar{p}_{A1} = \frac{1}{2}(p_B + p_D)_\alpha,$$

$$(2) \quad \bar{p}_{Pb} = \frac{1}{2}(p_B + p_D)_\beta,$$

is:

$$(3) \quad \frac{\bar{p}_{A1}}{\bar{p}_{Pb}} = \frac{4.05 \cdot 10^{-2}}{3.34 \cdot 10^{-2}} = 1.21 \pm 0.03.$$

This value coincides exactly with the ratio:

$$(4) \quad \frac{(Z/A)_{A1}}{(Z/A)_{Pb}} = 1.21.$$

This equality is in agreement with the formula of БИЯВНА (¹⁵) if we suppose that the numbers of g/cm² effective in the production of measured knock-on electrons is the same in both cases.

(¹⁴) R. R. WILSON: *Phys. Rev.*, **84**, 100 (1951).

(¹⁵) B. ROSSI: *High Energy Particles* (New York, 1952).

TABLE II.

Experiment	Thickness of absorber (cm) above <i>B</i> and <i>D</i>		Absorber in <i>O</i> (g/cm ² Pb)	Time of observation (min)	Number of μ -mesons
	Al	Pb			
α_1	10	—	57	6 416	41 755
α_1	10	—	172	2 789	18 160
α_3	10	—	228	6829	43 863
$\alpha_1 + \alpha_2 + \alpha_3 \equiv \alpha$	10	—	> 57	16034	103 778
β	—	5	200	6388	40 506
γ ⁽¹⁾	—	0.62	228	7326	47 323

⁽¹⁾ The median plane of the Pb layer above *B* and above *D* is 16 cm from the median plane of the counter trays.

TABLE III.

Experiment	$p_B \cdot 10^2$	$p_D \cdot 10^2$	$p_{BD} \cdot 10^4$
α_1	4.22 ± 0.10	4.19 ± 0.10	20.6 ± 2.2
α_2	4.10 ± 0.15	3.96 ± 0.15	17.1 ± 3.0
α_3	4.02 ± 0.10	3.81 ± 0.10	20.1 ± 2.1
$\alpha_1 + \alpha_2 + \alpha_3 \equiv \alpha$	4.12 ± 0.06	3.99 ± 0.06	19.7 ± 1.4
β	3.46 ± 0.09	3.22 ± 0.09	11.6 ± 1.7
γ	3.35 ± 0.08	3.12 ± 0.08	11.2 ± 1.5

Finally we found in experiment β that the mean number per incident meson of events given by an alignment plus two or more discharged counters besides the primary in a certain tray (i.e. *B* or *D*) irrespective of what occurs in the other trays, with the usual limitations relative to the simplicity of the

hodoscope picture, is comparable with p_c and p_E of experiments A_1 at 50 m w.e. (*).

4. - Elaboration of the Experimental Data.

We consider the ratio:

$$(5) \quad m = \frac{p_{HK}}{p_H \cdot p_K}$$

where H and K are the two trays of counters used for studying events Σcs and Σdes . If the two trays are equal, one can put $p_H = p_K$ and (5) can be calculated, in those cases for which geometric factors can be disregarded, with the formula:

$$(6) \quad m = \frac{\int_{E_t}^{\infty} \mathcal{N}(E) \sigma^2(E) dE}{\left[\int_{E_t}^{\infty} \mathcal{N}(E) \sigma(E) dE \right]^2}$$

where $\mathcal{N}(E)$ is the differential spectrum normalized to one of the mesons incident on the hodoscope at the depth of the experiment, E_t is the cut-off energy of the apparatus and $\sigma(E) dE = dE \int_{E'_{\min}}^{E'_{\max}} \Phi(E, E') dE'$ is the probability that a meson of energy between E and $E + dE$ generates a knock-on electron of energy between E'_{\min} and E'_{\max} per g/cm² (+).

We would like to observe that (6), from the point of view of statistics is nothing but the ratio between the mean value of the square of the casual variable $\sigma(E)$ and the square of its mean value, $\mathcal{N}(E)$ being the probability density of σ :

$$(7) \quad m = \frac{\overline{\sigma^2}}{\bar{\sigma}^2}.$$

By a well known application of a formula of Lagrange on moments of inertia (¹⁶) to the calculus of probability, ratio (7) is greater than one and equal to unity when and only when $\sigma(E)$ is independent of E .

(*) Also at 200 m w.e., the frequency of events in tray B , with two or more counters discharged, besides the alignment, is of the same order of magnitude as the corresponding p_c and p_E .

(+) It should be noted that (6) is valid only within the limits for which the percent age loss of energy of the primary in crossing from tray H to tray K can be considered negligible.

(¹⁶) G. CASTELNUOVO: *Calcolo delle Probabilità* (Bologna, 1948), vol. I.

4'1. *Experiments A_1 and A_2 .* — As was noted in the introduction, in experiment A_1 a ratio analogous to (5), referred to the mean number per incident meson of the *es* and *des* (and not the respective Σ), was found to be $2.3 \pm .6$.

Reelaborating the data with the criterium given in § 2 and applying the same criterium to the experiment at 200 m.w.e.; we have obtained:

$$m = 1.7 \pm .4 \quad \text{at } 50 \text{ m.w.e.},$$

$$m = 1.5 \pm .4 \quad \text{at } 200 \text{ m.w.e.}.$$

From the examination of these results, one is thus led to conclude that in measurements with a hodoscope having trays of the type *C* and *E* of experiment *A*, the *m* departs rather notably from 1.

A quantitative justification of this results can be obtained from the properties of (7) which are applicable to the present case. According to the physical situation of trays *C* and *E* (§ 2), we can summarize by supposing that all knock-ons of energy E' less than a certain lower limit $E^{*'}$ have zero probability of being counted, while those above this limit will have a probability different from zero, which is practically constant and equal to one in virtue of the fact that they produce an electronic shower.

According to this scheme, in the calculation of *m*, the geometric factors which should be considered can be introduced with a function *G* (geometric counting efficiency) given by:

$$G = \begin{cases} 0 & \text{for } E' < E^{*'}, \\ \text{const} = 1 & \text{for } E' \geq E^{*'}. \end{cases}$$

With (6) it is therefore possible to evaluate *m* when the lower limits of the integrals are set equal to E_{lim} , this being the minimum energy at which the μ -meson may transfer the energy $E^{*'}$ to the knock-on electron.

The calculation of E_{lim} (see Appendix) has been carried out according to ANNIS and coll. (17), obtaining for trays *C* and *E* a value of about 2 GeV. The evaluation of *m* by the above methods, gives, e.g. at 50 m.w.e.:

$$m = 1.5,$$

in agreement with the experimental datum at the same depth.

4'2. *Experiment C.* — The values of *m* obtained under the experimental conditions of hodoscope *C* (§ 3), are presented in Table IV.

(17) M. ANNIS, H. C. WILKINS and J. D. MILLER: *Phys. Rev.*, **94**, 1038 (1954).

TABLE IV.

Experiment	Al α	Pb	
		β	γ
m	1.20 ± 0.10	1.04 ± 0.16	1.07 ± 0.15

As was to be expected, given the geometry of the telescope, the values are, within the errors, very close to unity. This result is clearly explainable in the framework of the conclusions deducible from (7). In fact, in the limiting case of a geometrical knock-on detection efficiency which is constant for all energies above the experimental cut-off E_c (a situation possible with good approximation in the Wilson chamber) equation (6) gives a value of m only a few percent greater than unity.

5. - Conclusions.

Summarizing the various considerations discussed in this work, we believe that we have clarified the reasons for the disagreement between counter hodoscope and cloud chamber measurements on secondary electrons. Therefore we conclude that

1) The ratio

$$m = \frac{p_{Hh}}{p_H \cdot p_K}$$

is by definition greater than unity.

2) The departure from this value is sensible only when the experimental apparatus has a geometry such as to operate a strong cut-off in the registration of the electronic secondaries in the sense of accepting only those having an energy not less than a certain limiting value. This is the case when the counters of the hodoscope are separated from each other by slats. Particular care should therefore be used in the interpretation of results of hodoscope experiments set up, e.g., for the study of penetrating showers produced by μ -mesons.

3) The conclusions to which WOLFENDALE⁽⁷⁾ and LOVATI and coll.⁽⁹⁾ have arrived should be modified since these authors have directly compared the mean numbers per incident meson of their events of type Σes and Σdes with the corresponding ones of the type es and des obtained by AMALDI and coll.⁽³⁾ (*).

(*) For example: if the results of WOLFENDALE are treated with the same limiting criteria adopted in the above cited work, one obtains a value of about 1.3 against 0.91 found by this Author.

Further, a comparison between measurements carried out with counters separated by lead slats, and a Wilson chamber can only be made with particular caution.

4) The geometrical and physical situation given by hodoscope U is to be considered as intermediate between that of hodoscope A and that of the cloud chamber, and thus the values of m in Table IV lead to a further clarification of the problem.

Acknowledgements.

The authors wish to express thanks to Prof. E. AMALDI for helpful discussions. They wish also to thank Prof. E. AMALDI and Prof. E. PANCINI for having made the collaboration possible.

The underground measurements A_2 and U were made possible by the kindness of the « Società Romana di Elettività » which provided space and power: the authors are particularly grateful to Ing. A. ROVELLI and his staff for their friendly cooperation.

It is also our pleasure to express thanks to Miss L. MAIOLO, Mr. C. ZANGHI and Mr. R. MASCI for assistance in taking the data.

APPENDIX

The calculation of the energy E_{lim} is carried out by calculating the probability $p(E' > E^{*'})$, per incident meson, of the generation of a knock-on electron of energy E' greater than a prefixed value $E^{*'} (17)$. From the graph of $p(E' > E^{*'})$ as a function of $E^{*'}$, and from the weighted mean of the experimental values of p_c and p_E , one gets the energy $E^{*'}$ starting from which the knock-on detection efficiency G can be considered equal to one.

From the known relation (to be resolved in terms of the kinetic energy E of the μ -meson):

$$E'_{max} = E^{*' } = 2m_e c^2 \frac{p^2 c^2}{(m_e c^2)^2 + (m_\mu c^2)^2 + 2m_e c^2 (p^2 c^2 + m_\mu^2 c^4)^{\frac{1}{2}}},$$

one thus determines the value of E_{lim} corresponding to the prefixed $E^{*'}$; m is therefore given by:

$$m = \frac{\int_{E_{lim}}^{\infty} N(E) \sigma^2(E) dE}{\left[\int_{E_{lim}}^{\infty} N(E) \sigma(E) dE \right]^{\frac{1}{2}} \int_{E_t}^{\infty} N(E) dE},$$

where ⁽¹⁸⁾

$$N(E) = \frac{2E_0^2}{(E + E_0)^3}$$

and

$$\int_0^{\infty} N(E) dE = 1.$$

(¹⁸) E. P. GEORGE: in *Progress in Cosmic Ray Physics* (New York, 1952).

RIASSUNTO

Con un odoscopio espressamente progettato per lo studio dei secondari elettronici e sfruttando i dati di esperimenti con odoscopio, in parte già pubblicati, viene studiata la generazione dei secondari elettronici in successivi strati di materiale condensato (Al o Pb) da parte dello stesso mesone μ . L'esame dei risultati mostra che la discrepanza tra le misure con odoscopio e quelle in camere a nebbia può essere esaurientemente chiarita.

Proton Relaxation in Pure Liquids and in Liquids Containing Paramagnetic Gases in Solution.

G. CHIAROTTI, G. CRISTIANI, and L. GIULOTTO

Istituto di Fisica dell'Università - Pavia

(ricevuto il 10 Marzo 1955)

Summary. — Some data on proton relaxation times in pure liquids completely free of oxygen in solution are reported. The observed values of T_1 (Table I) are generally greater than those found by other authors. The value we find for water agrees well with the value predicted by the theory of Purcell and coworkers. The experimental values of T_1 for benzene, chlorobenzene and nitrobenzene seem to be somewhat longer than those we evaluate following Purcell's theory. The possible causes of the observed deviations (quasi-crystalline structure of liquids, microviscosity effect and molecular associations) are discussed. The influence of dissolved paramagnetic gases O_2 and NO is also studied. The magnetic moment of O_2 effective for the relaxation is of the same order of magnitude of the one derived from susceptibility measurements in the gas and is independent from the solvent. The μ_{eff} of NO on the contrary is considerably smaller than that resulting from susceptibility measurements and decreases with increasing polarity of the solvent (Table II). This behaviour of μ_{eff} of NO is attributed to interactions of the orbital magnetic moment with non uniform local electric fields of the solvent.

The thermal motions of the molecules in a liquid are responsible for the nuclear magnetic relaxation. Such motions generate local magnetic fields variable with time which cause transitions between the nuclear magnetic levels. Measurements of nuclear relaxation times therefore represent a method to obtain some information on the structure of the liquids.

The movements of the molecules in a liquid can be described with a certain approximation by means of the model assumed by Debye in his theory on

dispersion and absorption of polar liquids at radiofrequencies ⁽¹⁾. This model treats a molecule as a rigid sphere executing brownian motions in a viscous medium. BLOEMBERGEN, POUND and PURCELL adopt the same model in their theory of nuclear relaxation in liquids ⁽²⁻⁴⁾. The experimental results so far known ^(2,5-11) show that the theory of Purcell and cow. is able to predict the right order of magnitude of the nuclear relaxation times in liquids. In particular the dependence of relaxation time upon the viscosity agrees satisfactorily with the theory. However, the measurements of relaxation times in liquids have been mostly carried out neglecting the influence of oxygen in solution which changes considerably the results. Therefore we thought it suitable to perform measurements of relaxation times in various pure liquids completely free of oxygen in solution. The obtained results are discussed on the basis of the theory.

Moreover the theory of Purcell and cow. enables one to evaluate the influence of paramagnetic impurities in solution on the relaxation time. The experimental measurements performed so far concern the effect of paramagnetic ions ^(2,12-15). The magnetic moment effective for the relaxation is in some cases of the order of magnitude of that we can obtain from susceptibility measurements; in other cases considerably smaller. We have extended the study to the influence of the paramagnetic O₂ and NO gases in solution. Owing to the comparable solubility of O₂ and NO in polar and non polar liquids, the study of their influence on relaxation can give some information on « quenching » processes of magnetic moments in liquids.

1. - Experimental Results.

The measurements of thermal relaxation times of pure liquids and of liquids containing paramagnetic gases in solution have been carried out with

⁽¹⁾ P. DEBYE: *Polar Molecules* (New York, 1945), chapter 5.

⁽²⁾ N. BLOEMBERGEN, R. V. POUND and E. M. PURCELL: *Phys. Rev.*, **71**, 466 (1947).

⁽³⁾ N. BLOEMBERGEN, E. M. PURCELL and R. V. POUND: *Nature*, **160**, 475 (1947).

⁽⁴⁾ N. BLOEMBERGEN: *Nuclear Magnetic Relaxation* (The Hague, 1948).

⁽⁵⁾ F. BLOCH, W. W. HANSEN and M. PACKARD: *Phys. Rev.*, **70**, 474 (1946).

⁽⁶⁾ L. E. DRAIN: *Proc. Phys. Soc.*, A **62**, 301 (1949).

⁽⁷⁾ E. L. HAHN: *Phys. Rev.*, **76**, 149 (1949); E. L. HAHN: *Phys. Rev.*, **80**, 580 (1950).

⁽⁸⁾ G. CHIAROTTI and L. GIULOTTO: *Phys. Rev.*, **93**, 1241 (1954).

⁽⁹⁾ E. M. PURCELL: *Journ. Phys. et Rad.*, **15**, 758 (1954).

⁽¹⁰⁾ G. B. BENEDEK and E. M. PURCELL: *Journ. Chem. Phys.*, **22**, 2003 (1954).

⁽¹¹⁾ A. GANSSEN: *Zeits. Naturfor.*, **10a**, 54 (1955).

⁽¹²⁾ G. CHIAROTTI and L. GIULOTTO: *Nuovo Cimento*, **10**, 54 (1953).

⁽¹³⁾ R. L. CONGER and P. W. SELWOOD: *Journ. Chem. Phys.*, **20**, 383 (1952).

⁽¹⁴⁾ R. L. CONGER: *Journ. Chem. Phys.*, **21**, 937 (1953).

⁽¹⁵⁾ J. R. ZIMMERMANN: *Journ. Chem. Phys.*, **21**, 1605 (1953).

a method described in a previous work ⁽¹⁶⁾. This method is based on the record of «in phase» nuclear signals due to the total reversal of the magnetization. This method enables us to perform readily measurements of relaxation times of liquids with good accuracy. Some results obtained for pure liquids completely free of oxygen in solution, at a temperature of 20 °C are shown in Table I. The liquids have been freed of oxygen by means of prolonged boiling in vacuo and then closed in phials. The error in the measurements is in general less than 10%.

TABLE I.

Liquid	Relaxation time in s	Liquid	Relaxation time in s
Water	3.6	Benzene	19
Ethyl alcohol	3.5	Chlorobenzene	15
Methyl alcohol	8	Nitrobenzene	6.5
Ethyl ether	14.5	Aniline	2.4
Acetone	15	Toluene	12.5
Cyclohexane	6.5	Glycerin	0.025
Acetic acid	3.8	Formic acid	8

The value found by PURCELL and cow. and by others ^(6,7) for water is somewhat different from the one we find, but coincides with the value we find for water in the presence of air. For ethyl alcohol, ethyl ether, and benzene we find values of relaxation times longer than those reported in the literature. In some cases the presence of air can have considerable influence: e.g. the relaxation time we find for pure benzene is 2.7 s. and for benzene in the presence of air it is 2.7 s. This latter value is about the same as Ganssen finds for pure benzene ⁽¹¹⁾.

The influence of O₂ and NO in solution on the relaxation time of some liquids was studied by saturating the liquid with the gas at various pressures. The contribution

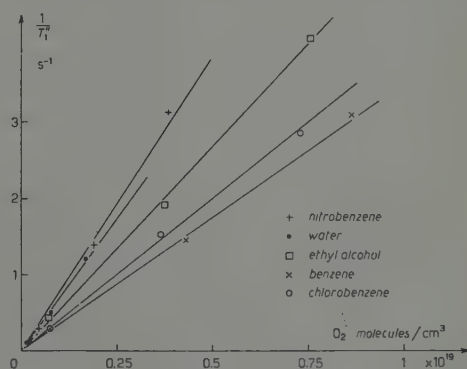


Fig. 1. — $1/T_1''$ as a function of the number of dissolved O₂ molecules per cm³ for various liquids at a temperature of 20 °C (measured at 7 MHz).

⁽¹⁶⁾ G. CHIAROTTI, G. CRISTIANI, L. GIULOTTO and G. LANZI: *Nuovo Cimento*, **12**, 519 (1954); L. GIULOTTO: *Rendiconti Seminari Mat. Fis. Milano*, vol. XXIV (1953).

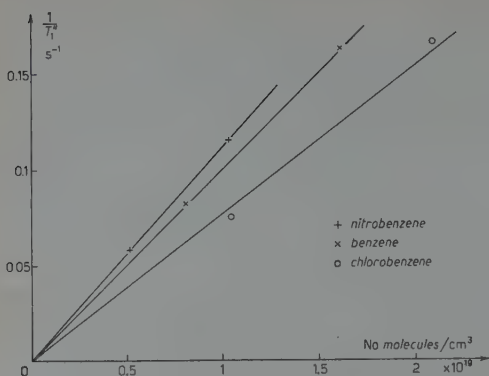


Fig. 2. — $1/T_1''$ as a function of the number of dissolved NO molecules per cm^3 for various liquids at a temperature of 20°C (measured at 7 MHz).

of a paramagnetic impurity to the relaxation time of a liquid is given by:

$$(1) \quad 1/T_1'' = 1/T_1 - 1/T_1',$$

where T_1 is the relaxation time of the liquid containing the impurity and T_1' that of the pure liquid. In Fig. 1 and 2 are plotted the values of $1/T_1''$ for O_2 and NO in various liquids as a function of the concentration of the dissolved gas. The solubility coefficients have been taken from the Landolt-Börnstein Tables with the exception of those

for chlorobenzene which have been determined by us ($\alpha_{\text{O}_2} = 0.136$, $\alpha_{\text{NO}} = 0.390$ at the temperature of 20°C ; α is the Ostwald solubility coefficient).

2. — Discussion of the Results.

2.1. Pure liquids. — The theory of Purcell and cow. shows that the nuclear thermal relaxation is determined by the intensity of the square of the local field at the Larmor frequency and at twice this frequency. In order to evaluate the spectrum of the square of the local field in a liquid, the molecular motions are identified with the brownian motions of rigid spheres of radius a in a medium of viscosity η . The contributions of the motions of translation and rotation are considered separately. In order to evaluate the contribution of the rotation PURCELL and cow. take into account only the field generated by the other nuclei of the same molecule. The spectrum of the square of the local field in the case of the rotation is similar to that shown in Fig. 3: it is constant at low frequencies and goes to zero at frequencies greater than $1/\tau_c$ where τ_c is the correlation time for the rotation. τ_c represents the time in which the local field is considerably changed owing to the rotation of the molecule.

For molecules as water containing only two nuclei with magnetic moments it is:

$$(2) \quad \tau_c = \tau/3 = 4\pi\eta a^3/3kT,$$

τ being Debye's relaxation time. In the case of water the contribution of the

rotation to the proton relaxation results in:

$$(3) \quad \left(\frac{1}{T_1} \right)_{\text{rot}} = 0.9 \gamma^4 \hbar^2 b^{-6} \tau_c,$$

where γ is the gyromagnetic ratio of protons and b their distance in the water molecule.

PURCELL and coll. assume for the spectrum of the local field due to translational motions a behaviour similar to that of Fig. 3. They take as correlation time for two molecules separated by a distance r the time a molecule takes to travel over a distance r . With this hypothesis one obtains, still in the case of water:

$$(4) \quad \left(\frac{1}{T_1} \right)_{\text{trans}} = 9\pi^2 \gamma^4 \hbar^2 \eta N / 5kT,$$

N being the number of molecules per cm^3 . By substitution of numerical values in eq. (3) and (4) one obtains for water:

$$(T_1)_{\text{rot}} = 5.2 \text{ s}, \quad (T_1)_{\text{trans}} = 10 \text{ s}.$$

For the proton relaxation in water it results therefore:

$$\frac{1}{T_1} = \left(\frac{1}{T_1} \right)_{\text{rot}} + \left(\frac{1}{T_1} \right)_{\text{trans}}; \quad T_1 = 3.4 \text{ s}.$$

In the case of water the agreement between the value of the time we find (3.6 s) and the theoretical value is better than one could reasonably expect. The agreement, however, does not seem to be so good in other cases.

In general a rigorous calculation following Purcell's theory is practically impossible for molecules more complicated than water. We have made an attempt to evaluate approximately with Purcell's theory the relaxation time of benzene.

A rough approximation consists in taking into account only the two protons nearest to the one we consider and in supposing them collinear with it. With this hypothesis the nearest protons influence the relaxation only if their spins are parallel. We can easily calculate the probability that this may occur and we find a value of 0.76. We obtain thus for the contribution of the rotation a relaxation time of about 8 s. In order to evaluate the order of magnitude

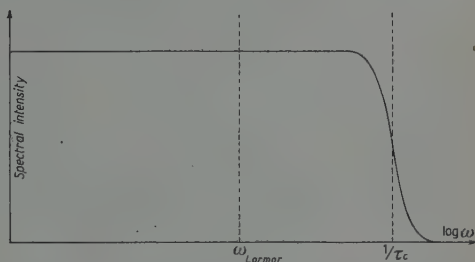


Fig. 3. - The behaviour of the intensity of the square of the local field as a function of frequency.

of the error we make with these simplifications, we compared the value of the local field in the case of the simplified molecule with that of the real molecule. To do this we considered various suitably chosen positions of the two molecules taking into account the different possibilities of orientation of the spins. The square of the local field can be considerably different in the two cases. In particular in the case of the real molecule the nearest protons contribute to the relaxation even if they have antiparallel spins. A comparison between the correlation times in the two cases can be made by considering the rotation around particular axes. On the basis of an evaluation of this kind we conclude that a time of 8 s should not be very different from that we could obtain with a rigorous calculation. In order to evaluate the contribution of the translational motions we attribute to each molecule a resulting moment applied at the centre. The value of the relaxation time due to translation we found is about 23 s. The relaxation time we evaluate for benzene taking into account both the rotation and translation is thus about 6 s, i.e. one third of the experimental value. A similar evaluation of the relaxation time gives for chlorobenzene a value of about 5.5 s and for nitrobenzene a value of about 2 s, while the experimental values are respectively 15 s and 6.5 s. We can, however, observe that the experimental values of the times of benzene, chlorobenzene and nitrobenzene are about inversely proportional to their respective viscosity, in accordance with the theory.

An experimental value of the thermal relaxation time of a liquid longer than the value we calculate following Purcell's theory can be explained assuming that the spectrum of the square of the local field for frequencies in the range of the Larmor frequency (in our case 7 MHz) is less intense than we could expect from Debye's picture.

The causes that can produce a deviation from Debye's model can be:

a) *The existence of orienting fields in the liquid.* This hypothesis was introduced by DEBYE himself in a later improvement of his theory of dispersion and absorption at radiofrequencies⁽¹⁷⁾. Owing to the orienting field the liquid assumes a quasi-crystalline structure. The molecules execute angular oscillations around their equilibrium positions with a frequency much greater than the Larmor frequency. The spectrum of the square of the local field can thus be different from that of Fig. 3. In particular several correlation times could occur and the intensity of the spectrum be increased at high frequencies and decreased at frequencies of the order of the Larmor frequency⁽¹⁸⁾. The existence of orienting fields in the liquid can therefore cause an increase in

(17) P. DEBYE and W. RAMM: *Ann. Phys.*, **23**, 28 (1937).

(18) L. GIULOTTO, G. CHIAROTTI and G. CRISTIANI: *Journ. Chem. Phys.*, **22**, 1143 (1954).

the relaxation time with respect to the time we can calculate with Debye's model.

b) The effect of microviscosity. Stokes' formulas giving the values of the friction coefficients for the rotation and translation of a sphere moving in a viscous medium are valid only if the radius of the sphere is much greater than the molecular radius. With geometrical considerations GIERER and WIRTZ⁽¹⁹⁾ show that for a sphere of molecular size the viscosity in Stokes' formulas must be multiplied by a microviscosity coefficient $f < 1$. In particular if the sphere has the same radius as the neighbouring molecules GIERER and WIRTZ find $f_{\text{rot}} \cong 0.15$ and $f_{\text{trans}} \cong 0.57$. By introducing these microviscosity corrections we find the correlation time decreased and the nuclear relaxation time increased.

c) The presence of molecular associations. It is well known that some liquids show molecular associations. In this case, neglecting the relative movements of the molecules within the complex, we can think that each molecule moves as a sphere of radius equal to that of the complex. The correlation time for the rotation is therefore increased with consequent decreasing of the nuclear relaxation time.

To conclude, of the three reported causes of deviation from Debye's model, *a)* and *b)* lead to an increase in the relaxation time while *c)* leads to a decrease. The causes *b)* and *c)*, however are not independent. It is obvious indeed that in the presence of conspicuous phenomena of association the effect of microviscosity becomes negligible.

The fact that, as in water, the experimental value of the relaxation time agrees well with the theoretical one, does not allow us to conclude that Debye's model gives a satisfactory picture of the molecular motions. It is indeed well known⁽²⁰⁾ that water presents a marked quasi-crystalline structure and shows a considerable molecular association. It is thus quite possible that these two effects counterbalance in such a way that the relaxation time is in accordance with the theory.

It is interesting to compare the experimental results on nuclear relaxation for water with those on dispersion and absorption at radiofrequencies. It is well known that the values of τ derived from the experimental results on the dispersion at radiofrequencies applying the primitive Debye's theory are smaller than those foreseen by eq. (2)⁽²¹⁾. On the other hand COLLIE, HASTED and RITSON⁽²²⁾ showed that a value of τ in a rather good accordance with eq. (2)

(19) A. GIERER and K. WIRTZ: *Zeits. Naturfor.*, **8a**, 532 (1953).

(20) See f. i. L. GRUNBERG and A. H. NISSAN: *Trans. Faraday Soc.*, **45**, 125 (1949).

(21) F. H. MÜLLER: *Eig. Exact Naturwiss.*, **17**, 164 (1938).

(22) C. H. COLLIE, J. B. HASTED and D. M. RITSON: *Proc. Phys. Soc.*, A **60**, 145 (1948).

can be derived by applying to Debye's theory Onsager's correction⁽²³⁾. However even this agreement could be due to the fortuitous compensation of the effects a) and c). This interpretation seems to be confirmed by the fact that the shape of the reflection spectrum in the far infrared is different from that we can foresee with the primitive of Debye. Indeed CARTWRIGHT and ERRERA⁽²⁴⁾ found in this spectral region two bands at 20 and 60 μ which HETTNER⁽²⁵⁾ attributes to pendular oscillations of the molecule.

In the case of benzene the difference between experimental and calculated value of the relaxation time could be due to a quasi-crystalline structure of the liquid. The diffraction patterns with X rays show indeed that the liquid benzene has a marked quasi-crystalline structure⁽²⁶⁾. From the data on molecular refraction, on light scattering and on Kerr effect, MUELLER⁽²⁷⁾ and PETERLIN and STUART⁽²⁸⁾ evaluate for benzene a hindrance potential for the rotation of the order of $8kT$. On the other hand following the point of view b) the relatively great value of the relaxation time could be interpreted as due to the effect of microviscosity. GIERER and WIRTZ correction for the microviscosity could just by itself explain the observed deviation. However the theory of Gierer and Wirtz seems to agree well with the experimental results on diffusion and on dispersion at radiofrequencies in the cases of diluted solutions⁽²⁹⁾, while it is not clear what changes would be introduced by the microviscosity correction for a liquid with quasi-crystalline structure. To conclude, it does not seem thus possible to state the relative weights of causes a) and b) in determining the observed deviation in the relaxation time of benzene.

2.2. *Liquids containing paramagnetic gases in solution.* — Eq. (4) can be adapted to the case in which the contribution to the relaxation is due to the motion of paramagnetic ions in solution. PURCELL and cow. find:

$$(5) \quad \frac{1}{T_1} = \frac{12}{5} \pi^2 \gamma^2 N \mu_{\text{eff}}^2 \frac{\eta}{kT},$$

N being the number of paramagnetic ions dissolved in a cm^3 and μ_{eff} the magnetic moment of the ion effective for the relaxation processes. The formula (5)

⁽²³⁾ L. ONSAGER: *Journ. Amer. Chem. Soc.*, **58**, 1486 (1936); see also: E. FISCHER: *Ann. Phys.*, **6**, 117 (1949).

⁽²⁴⁾ C. H. CARTWRIGHT and J. ERRERA: *Proc. Royal Soc.*, **154**, 138 (1936); *Phys. Rev.*, **49**, 70 (1936).

⁽²⁵⁾ G. HETTNER: *Phys. Zeits.*, **38**, 771 (1937).

⁽²⁶⁾ W. C. PIERCE: *Journ. Chem. Phys.*, **5**, 717 (1937); P. W. DAVEY and P. H. BELL: *Phys. Rev.*, **58**, 207 (1940).

⁽²⁷⁾ H. MUELLER: *Phys. Rev.*, **50**, 547 (1936).

⁽²⁸⁾ A. PETERLIN and H. A. STUART: *Zeits. f. Phys.*, **113**, 628 (1939).

⁽²⁹⁾ A. SPERNOL and K. WIRTZ: *Zeits. Naturfor.*, **8a**, 522 (1953).

was derived with the hypothesis that the ions have the same mobility as the molecules of the solvent and that the radii of the ions are small with respect to those of the solvent molecules. In the case of paramagnetic molecules in solution the latter hypothesis is not justified. Assuming as the distance of closest approach $a+A$ (a =radius of solvent molecule; A =radius of dissolved paramagnetic molecule) and taking into account the different diffusion velocities of the two molecules, we obtain:

$$(6) \quad \frac{1}{T_1} = \frac{12}{5} \pi^2 \gamma^2 \mu_{\text{eff}}^2 N \frac{\eta}{kT} \frac{2aA}{(a+A)^2}.$$

A further correction can be introduced in order to take into account the effect of the microviscosity following the data of SPERNOL and WIRTZ⁽²⁹⁾.

In Table II are reported the values of μ_{eff} for O_2 and NO dissolved in various solvents. These values are derived from the data of Fig. 1 and 2 and are calculated following eq. (5), (6) and again eq. (6) and taking into account the microviscosity corrections.

TABLE II.

Solvent	μ_{eff} in Bohr magnetons of					
	O_2			NO		
	after eq. (5)	after eq. (6)	after eq (6) with microviscosity correction	after eq. (5)	after eq. (6)	after eq. (6) with microviscosity correction
Water	1.36	1.94	2.50	—	—	—
Benzene	1.10	1.52	2.35	0.215	0.314	0.466
Chlorobenzene . .	1.15	1.67	2.46	0.168	0.244	0.360
Nitrobenzene . .	1.10	1.57	2.41	0.127	0.187	0.274
Ethyl alcohol . .	1.20	1.73	2.45	—	—	—

From Table II it appears that the μ_{eff} of O_2 is practically independent of the solvent and is of the same order of magnitude as the one we derive from susceptibility measurements in the gas. In particular the values of μ_{eff} for O_2 calculated with eq. (6) and taking into account the microviscosity corrections are very near to the value of the moment of the gaseous O_2 (2.82 Bohr magnetons).

In the case of NO on the contrary the magnetic moment effective in the relaxation processes depends upon the solvent and is considerably smaller than that of the NO gas (1.83 Bohr magnetons). By comparison of the values of μ_{eff} of NO dissolved in benzene, chlorobenzene and nitrobenzene we can observe that μ_{eff} decreases with the increasing of the polarity of the solvent.

Because the μ_{eff} 's are independent of the concentration it is not probable that the relatively small values of μ_{eff} of NO are due to association phenomena. An explanation of the different behaviour of O₂ and NO could be the following. The normal state of O₂ is a $^3\Sigma$ state. Its moment is therefore caused only by electronic spins. Non uniform local electric fields present in the liquid have therefore a weak influence on the magnetic moment. The normal state of NO is instead a $^2\Pi$ state. Its magnetic moment is therefore caused by the spin and angular moment of the unpaired electron. In this case non uniform local electric fields can interact with the orbit of the unpaired electron. These interactions can cause, following VAN VLECK⁽³⁰⁾, a quenching of the orbital moment and also a quenching of the spin through the spin-orbit coupling. The coupling energy is indeed for NO of the order of kT . Another effect that could contribute to a diminution of the magnetic moment effective in the nuclear relaxation is the influence of very short electronic relaxation time on the correlation time^(2,14). For both these effects one must expect a dependence on the solvent polarity in the sense we observe experimentally.

It is interesting to compare the values of μ_{eff} we find for the paramagnetic molecules with those PURCELL and COW. and CONGER and SELWOOD⁽¹³⁾ found from some paramagnetic ions in aqueous solutions. Indeed one can observe that for those ions which are in a S state or for those that through quenching of the orbital moment are « effectively » in a S state (ions of the iron group), the value of μ_{eff} is of the order of the magnetic moment derived from susceptibility measurements. For those ions which are not in a S state (ions of the rare earths) the μ_{eff} is much smaller than that we can derive from susceptibility measurements. Our results for O₂ and NO are in accordance with this rule.

The dependence of μ_{eff} on the polarity of the solvent we observe in the case of NO confirms that the cause of the great diminution of the μ_{eff} must be attributed to the action of the electric field of the solvent. The different behaviour of NO in liquids of different polarity can give some information on the influence of non uniform local electric fields on the magnetic moment. The result that also in benzene the μ_{eff} of NO is considerably smaller than the magnetic moment of the gas, allows us to conclude that interactions of this kind occur also in non polar liquids.

We wish to thank Drs. G. LANZI and L. TOSCA for their efficient help in performing the measurements. This research was supported by the C.N.R.. One of us (G. CHIAROTTI) would like to thank the C.N.R. for its grant.

⁽³⁰⁾ J. A. VAN VLECK: *The Theory of Electric and Magnetic Susceptibilities* (Oxford, 1932), p. 287.

RIASSUNTO

Vengono riportati alcuni dati sul tempo di rilassamento dei protoni in liquidi puri liberati completamente dall'ossigeno in soluzione. I valori osservati di T_1 (Tab. I) sono in genere più grandi di quelli riportati da altri autori. Il valore da noi trovato per l'acqua è in buon accordo con quello previsto dalla teoria di Purcell e coll. I valori sperimentali di T_1 per benzolo, clorobenzolo e nitrobenzolo sembrano invece alquanto più grandi di quelli che si possono valutare in base alla teoria di Purcell. Vengono discusse le possibili cause delle deviazioni osservate (struttura quasi cristallina del liquido, effetto della microviscosità e fenomeni di associazione molecolare). È stata pure studiata l'influenza dei gas paramagnetici O_2 e NO in soluzione. Il momento magnetico di O_2 efficace nei processi di rilassamento risulta dello stesso ordine di grandezza di quello ottenibile da misure di suscettività nel gas ed è indipendente dal solvente. Il μ_{eff} di NO invece risulta considerevolmente più piccolo di quello ottenibile da misure di suscettività e diminuisce al crescere della polarità del solvente (Tab. II). Il comportamento del μ_{eff} di NO è attribuito a interazioni del momento magnetico orbitale con i campi elettrici non uniformi del solvente.

Evidence for Heavy Mesons with The Decay Processes $K_{\pi 2} \rightarrow \pi + \pi^0$ and $K_{\mu 2} \rightarrow \mu + \nu$ from Observations with a Multiplate Cloud Chamber (*).

H. S. BRIDGE, H. DESTAEBLER Jr., B. ROSSI and B. V. SREEKANTAN (+)

*Department of Physics and Laboratory for Nuclear Science
Massachusetts Institute of Technology - Cambridge, Massachusetts*

(ricevuto il 18 Marzo 1955)

Summary. — Analysis of the data on S-events observed in the M.I.T. multiplate cloud chamber shows that these events represent the decay processes of two kinds of heavy mesons. The decay processes are of the type: $K_{\mu 2} \rightarrow \mu + \nu$ and $K_{\pi 2} \rightarrow \pi + \pi^0$.

1. — Experimental Data.

Analysis of the pictures obtained with a multiplate cloud chamber at 3260 m altitude has yielded 67 examples of S-events, that are interpreted as showing the stopping of heavy mesons and their subsequent decay into light mesons.

We cannot make accurate direct measurements of the masses of the primary S-particles. However, in most cases we can estimate the mass from relative specific ionization, scattering, and residual range. In these cases the primary mass is probably less than the proton mass. Thus we can say that most of the primary particles are heavy mesons and not hyperons.

Tables I and II present a summary of the observations made, respectively, with a lead and with a brass plate assembly in the chamber. Some of these data have appeared in previous publications, where one will find the details

(*) This work was supported in part by the joint program of the U.S. Office of Naval Research and the U.S. Atomic Energy Commission.

(+) On leave from Tata Institute of Fundamental Research, Bombay, India.

of the experimental arrangement ^(1,2). The lead plate assembly has been previously described. The brass plate assembly consisted of 11 plates whose thickness, composition, and density are accurately known. The composition of the brass by actual analysis was 85 percent copper and 15 percent zinc; the plates were 11.08 g cm^{-2} thick. We obtained the density by weighing small accurately machined samples and checked the result by weighing one finished plate. The values of these independent determinations agreed to better than 0.1 percent.

In most cases the secondary particle leaves the chamber with practically minimum ionization. It is then known that its initial range exceeds a certain minimum value, to be called here *potential range*. The potential range equals the actual amount of matter traversed plus the maximum residual range of a light meson whose specific ionization is appreciably greater than minimum. For this residual range we have taken 5 g cm^{-2} Pb for the events in lead and 5 g cm^{-2} brass for the events in brass; this corresponds to an ionization in the neighborhood of 2.5 times minimum for a π^- or a μ -meson.

When the secondary particle stops in the chamber or leaves the chamber with an ionization appreciably greater than minimum, then one can determine its *actual range at production* as well as its potential range, which in this case is defined as the minimum value of the initial range that would have allowed the particle to escape from the chamber at minimum ionization if it had continued in the direction of the last visible track segment.

Potential ranges and actual ranges of the secondary particles are listed in Tables I and II. For a comparison of the lead and brass data one can assume that 1 g cm^{-2} Pb is approximately equivalent to 0.75 g cm^{-2} brass.

The range limits are derived from the total amount of material that the charged secondary is seen to penetrate in the chamber. The penetration in one plate was calculated under the assumption that the trajectory within the plate consists of two rectilinear portions, the extensions into the plate of the two adjacent track segments, which intersect at a point of effective single scattering. In the reconstruction of the track segments we took into account the conical projection, and we corrected approximately for the gas motion during expansion.

We determined the maximum possible amount of material penetrated in the last plate under the assumption that the particle stopped at the far side of the last plate and did not scatter in this plate. Thus, in the case of stopped secondaries, we derived two penetration limits, a minimum value which corresponds to the amount of material traversed by the particle up to the point

(1) H. S. BRIDGE, C. PEYROU, B. ROSSI and R. SAFFORD: *Phys. Rev.*, **90**, 921 (1953).

(2) H. S. BRIDGE, H. COURANT, B. DAYTON, H. C. DE STAEBLER JR., B. ROSSI, R. SAFFORD and D. WILLARD: *Nuovo Cimento*, **12**, 81 (1954).

of entry into the last plate and a maximum value obtained by adding to the minimum penetration the thickness of the last plate in the direction of motion of the particle.

From these data, we then obtained the range limits shown in Tables I and II with the

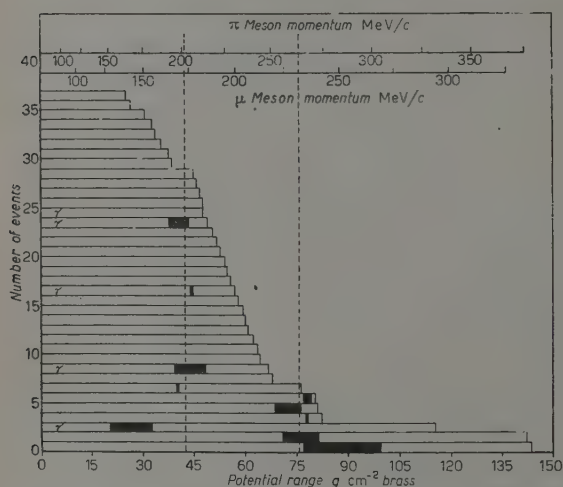
Fig. 1. — Distribution of Potential and Actual Ranges of the Charged Secondaries Observed with the Lead Plate Assembly. The solid area indicate limits of the actual range of the stopped secondaries. γ indicates an associated shower. The

dotted lines are drawn at the ranges of 57.4 g cm^{-2} and 102 g cm^{-2} .

following procedure: (a) by a visual estimate, taking into account the inclination of the track segment, we determined conservative limits for the specific ionization of the secondary particle above the plate where it stopped;

(b) from these limits, we computed the corresponding limits of the residual range of the secondary particle in the last plate (*); (c) we then combined these limits with the penetration limits determined previously to obtain the range limits.

A single range value is given for each of the events No. 92136



Brass Plate Assembly. The dotted lines are drawn at the ranges of 43.1 g cm^{-2} and 76.5 g cm^{-2} .

(*) The secondary particles which belong to the 60 g cm^{-2} Pb range group were assumed to be π -mesons and those belonging to the 100 g cm^{-2} Pb range group were assumed to be μ -mesons; see below.

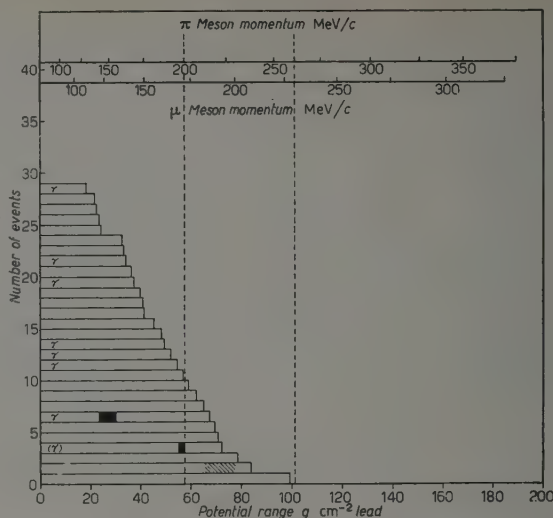


TABLE I. - S-events observed with the lead plate assembly. In the second column *a*, *b* and *c* indicate respectively that the origin of the S-particles was *a*) undetermined and outside the chamber, *b*) a nuclear interaction outside the chamber, or *c*) a nuclear interaction inside the chamber. — *Charged Secondary*. The letters *f* and *b* in the third column indicate whether the secondary particle has been emitted in the forward or backward hemisphere with respect to the direction of the primary particle. Ranges are given in g cm⁻² of lead. — *Photon Secondary*. The sixth column indicates whether or not there is a non-ionizing link between the point of stopping of the S-particle and the origin of the shower. ϑ is the angle between the axis of the shower and the trajectory of the charged secondary particle. *N* is the total number of visible electron tracks in the shower. The last column lists estimated values of the individual π^0 -detection probabilities. (These are calculated on the assumption of two body decay giving rise to a π^0 -meson of 200 MeV/c momentum).

Event	Origin of S	Charged Secondary		Photon Secondary			
		Direction	Pot. Range	Actual Range	n.i.l.	ϑ	π^0 det. prob.
			g cm ⁻² Pb				
H-1	<i>a</i>	<i>f</i>	67	23 ÷ 29.5	yes	180°	.87
TR-2	<i>a</i>	<i>b</i>	99		—	—	.1
S-1	<i>a</i>	<i>f</i>	41		—	—	.63
S-2	<i>a</i>	<i>f</i>	33		—	—	.82
02877	<i>b</i>	<i>b</i>	50		yes	127°	.69
03246	<i>b</i>	<i>f</i>	18		no	147°	.38
12668 (S3) *	<i>a</i>	<i>f</i>	83	66.4 ÷ 78.2	—	—	.38
25178	<i>a</i>	<i>f</i>	34		no	180°	.1
26049	<i>a</i>	<i>f</i>	52		no	157°	.48
26110 (S4)	?	<i>b</i>	72	55.2 ÷ 57.5	yes	163°	.19
26653	<i>b</i>	<i>b</i>	79		—	—	.75
29428	<i>c</i>	<i>f</i>	59		—	—	.74
30122 (S5)	<i>c</i>	<i>f</i>	41		—	—	.29
30654	<i>b</i>	<i>b</i>	22		—	—	.67
32531	<i>a</i>	<i>b</i>	5		yes	180°	.52
39567	<i>a</i>	<i>b</i>	65		—	—	0.0
42166 (S8)	<i>a</i>	<i>f</i>	48		—	—	.66
46796	<i>a</i>	<i>b</i>	36		—	—	.51
53688	<i>a</i>	<i>b</i>	57		—	—	.69
56409	<i>a</i>	<i>b</i>	62		—	—	.20
58070	<i>a</i>	<i>b</i>	24		—	—	.38
58649	<i>a</i>	<i>b</i>	71		—	—	.39
61641	<i>c</i>	<i>f</i>	33		—	—	.55
64228	<i>a</i>	<i>f</i>	22		—	—	.77
64700	<i>c</i>	<i>f</i>	37		no	—	.39
64888	<i>a</i>	<i>f</i>	54		yes	123°	.75
65479	<i>c</i>	<i>f</i>	69		—	—	.06
66672	<i>a</i>	<i>b</i>	46		—	—	.87
70557	<i>a</i>	<i>b</i>	40		—	—	.51
70589	<i>a</i>	<i>b</i>	24		—	—	—

* Stopping questionable.

TABLE II.

S-events observed with the brass plate assembly. Ranges are given in g cm^{-2} of brass.

Event	Origin of S	Charged Secondary			Photon Secondary			
		Direct- ion	Pot. Range	Actual Range g cm^{-2} Brass	n.i.l.	θ	N	π^0 det. prob.
76734	<i>b</i>	<i>b</i>	47		—	—	—	.62
77039	<i>b</i>	<i>b</i>	61		—	—	—	.79
77074	<i>b</i>	<i>f</i>	34		—	—	—	.60
77509	<i>b</i>	<i>f</i>	46		—	—	—	.58
78003	<i>c</i>	<i>f</i>	48		—	—	—	.53
78405	<i>b</i>	<i>f</i>	26		—	—	—	.66
78475	<i>a</i>	<i>b</i>	49		—	—	—	.62
80015	<i>c</i>	<i>f</i>	65		—	—	—	.73
81558	<i>b</i>	<i>f</i>	144	$77.0 \div 107.2$	—	—	—	.02
82203	<i>b</i>	<i>f</i>	50	$39.2 \div 46.6$	yes	170°	7*	.72
84965	<i>a</i>	<i>f</i>	56		—	—	—	.73
85380	<i>a</i>	<i>b</i>	143	$70.9 \div 81.7$	—	—	—	.20
85415	<i>a</i>	<i>f</i>	68		—	—	—	.56
85494	<i>c</i>	<i>f</i>	27		—	—	—	.69
85751	<i>b</i>	<i>f</i>	53		—	—	—	.73
87415	<i>b</i>	<i>b</i>	61		—	—	—	.62
87981	<i>c</i>	<i>f</i>	67	$40.2 \div 49.2$	yes	151°	3	.55
88405	<i>c</i>	<i>f</i>	55		—	—	—	.82
88515	<i>a</i>	<i>b</i>	62		—	—	—	.73
90713	<i>b</i>	<i>b</i>	57		—	—	—	.65
90912	<i>a</i>	<i>b</i>	116	$20.5 \div 33.0$	no	—	4	.70
91256	<i>c</i>	<i>f</i>	54		—	—	—	.73
91829	<i>b</i>	<i>b</i>	39		—	—	—	.30
92136	<i>c</i>	<i>f</i>	76	40.7	—	—	—	.50
92329	<i>c</i>	<i>f</i>	81	$76.4 \div 79.4$	—	—	—	.72
96787	<i>c</i>	<i>f</i>	81	$68.6 \div 75.9$	—	—	—	.80
98367	<i>c</i>	<i>f</i>	64		—	—	—	.76
98529	<i>a</i>	<i>b</i>	59		—	—	—	.40
99319	<i>b</i>	<i>f</i>	38		—	—	—	.28
99705	<i>b</i>	<i>b</i>	51		—	—	—	.40
100846	<i>a</i>	<i>f</i>	45		no	112°	3	.72
102209	<i>b</i>	<i>b</i>	82	$77.1 \div 77.6$	—	—	—	.56
102565	<i>c</i>	<i>b</i>	33		—	—	—	.82
105345	<i>b</i>	<i>b</i>	31		—	—	—	.68
105596	<i>a</i>	<i>f</i>	58	44.8	yes	166°	3	.69
105711	<i>a</i>	<i>f</i>	66		—	—	—	.40
106168	<i>c</i>	<i>f</i>	36		—	—	—	.66

* A second shower was apparently associated with this event.

and 105596. In these events the electron arising from the $\pi \rightarrow \mu \rightarrow e$ or from the $\mu \rightarrow e$ decay is visible, and affords a more accurate determination of the point of stopping of the secondary particle.

In 14 cases an electron shower appears to be associated with an S-event. In over half of these cases the shower originates in one of the plates next to that in which the primary particle stops, with no ionizing track appearing between the point of stopping and the origin of the shower. This is taken as evidence that the showers are initiated by photons. The general appearance of the showers indicates that these photons have energies of the order of 100 MeV. The pertinent data concerning the electron showers are given in Tables I and II.

Figs. 1 and 2 illustrate the data relative to the charged secondaries. The events are arranged from top to bottom in order of increasing potential range. Each event is represented by a rectangle of unit height with a base equal to the potential range. Black areas represent the actual range limits when these are known. The letter γ indicates events with associated showers.

It is convenient to define the function $P(R)$, which, for a given plate assembly, represents the *a priori* probability that the secondary particle of an S-event taken at random has a potential range greater than R . We notice that the outer profiles of the graphs in Figs. 1 and 2 are the histograms of the function $P(R)$ for the lead and for the brass plate assembly respectively, as determined from our experimental data.

One should point out that we list as S-decays only those events in which the secondary charged particle traverses an amount of matter at least equivalent to about 20 g cm^{-2} Pb, or in which an electron shower appears in addition to the secondary product (only events 03246 and 32531 fall in the second category). Therefore, our criteria of selection strongly discriminate against decay processes yielding secondaries with ranges less than 20 g cm^{-2} Pb.

2. - Interpretation of the Data.

Examination of the tables and of the figures brings out the following significant facts.

All secondary particles whose potential ranges are greater than 100 g cm^{-2} Pb stop in the chamber. Most stopped secondaries have ranges in the neighborhood of either 100 g cm^{-2} Pb or 60 g cm^{-2} Pb. The only exceptions are two short-range cases (H-1 and 90912) and one case (12668) where the range appears to lie between 66.4 and 78.2 g cm^{-2} Pb. This particular picture was taken at a time when the chamber was underexpanded, and it is not possible to decide whether or not the particle came to rest before leaving the chamber.

The interpretation is therefore questionable, and the event will be disregarded in the following analysis.

This marked grouping of the secondary ranges immediately suggests that two different two-body decay processes are involved.

This view is greatly strengthened if one investigates the potential range distribution in more detail since it then becomes obvious that particles undergoing a three-body decay and therefore producing charged secondaries with a continuous energy distribution cannot figure prominently among our S-events. For if they did, and if the range spectrum were such that most secondary particles traversed more than $100 \text{ g cm}^{-2} \text{ Pb}$, then one should expect that some of the particles with potential range greater than $100 \text{ g cm}^{-2} \text{ Pb}$ (6 in our sample) should escape from the chamber. If, on the other hand, the bulk of the secondary range spectrum lay below $100 \text{ g cm}^{-2} \text{ Pb}$, the number of stopped secondaries should be much greater than was found. Moreover, the ranges of the stopped secondaries should not cluster around any particular value. Indeed, the function $f(R)$ describing the differential range spectrum of the secondary particles from the three-body decay and the function $n(R)$ describing the differential range distribution of those among them that are actually *seen to stop* in the chamber, are related by the equation: $n(R) = f(R)P(R)$, where $P(R)$ is the potential range distribution defined previously. With the help of this equation one could estimate quantitatively an upper limit for the number of particles undergoing a three-body decay in our sample of S-events, if one knew the differential range spectrum, $f(R)$, of the secondaries arising from this decay. A calculation of this kind shows that, barring extreme assumptions concerning the form of $f(R)$, this upper limit is only a small fraction of the total. We therefore disregard the possible existence of a small number of events which may originate in a three-body decay process *and discuss our results on the assumption of two different two-body decay processes, one producing secondaries of about $100 \text{ g cm}^{-2} \text{ Pb}$ range and one producing secondaries of about $60 \text{ g cm}^{-2} \text{ Pb}$ range and one producing secondaries of about $60 \text{ g cm}^{-2} \text{ Pb}$ range.*

If we take this view, it immediately becomes apparent that the secondary photons are associated with the 60 g cm^{-2} group and not with the 100 g cm^{-2} group. Indeed we note the following: (a) of the five events in which the secondary particle stops with a range of about $60 \text{ g cm}^{-2} \text{ Pb}$, four have associated showers; (b) there are eight events in which photons appear and the secondary charged particles fail to stop in the chamber. In all of these cases the potential range is less than $60 \text{ g cm}^{-2} \text{ Pb}$; (c) there are 24 events in which the secondary particle is known to have a range greater than $60 \text{ g cm}^{-2} \text{ Pb}$. In none of these events do photons appear.

From our observations, it is also clear that the photons do not arise directly from a two-body decay process. For if this were so, the photon would always

be emitted in the direction opposite to that of the charged decay product, which is not the case. It is thus natural to assume that the neutral particle in the 60 g cm^{-2} decay process is a π^0 -meson, which subsequently decays into photons. A careful analysis by H. COURANT⁽³⁾ shows that this assumption is perfectly consistent with our observations.

As already noted, there are two cases in which the secondary particle stops in the chamber after traversing considerably less than 60 g cm^{-2} Pb. In both events there is an associated electron shower. It appears therefore natural to assume that these events belong to the 60 g cm^{-2} group, in which case one must invoke nuclear interactions to explain the anomalously short ranges of the charged secondaries. It then follows that the charged secondary particles are π -mesons and not μ -mesons and one is led to interpret the events of the 60 g cm^{-2} Pb group as decay processes of the following type:



Notice that in both short-range cases the charged secondary enters the last plate at minimum ionization, as one would expect if the stopping were due to a nuclear encounter rather than to the gradual energy loss by ionization.

One may mention, too, that the secondary particles which were associated with electron cascades traversed an amount of material equal to 2.6 geometric mean free paths. In this distance the expected number of nuclear stoppings is 1.3 as against two actually observed (*).

Let us now consider the S-events producing secondaries with about 100 g cm^{-2} Pb range. Absence of associated showers rules out the possibility that here the neutral secondary particles are photons or π^0 -mesons.

Since there can be only a small number of hyperons in our sample the neutral secondary cannot be a neutron or Λ^0 -particle. A θ^0 -meson is not ruled out by this argument but the detection probability of a θ^0 -meson (or a Λ^0 -particle) is high and frequent emission of such particles as the neutral decay product is impossible. By elimination it is thus probable that the neutral decay product is a neutrino.

(3) H. COURANT: *Associated Photons in K-Particle Decays Observed in a Multiplate Cloud Chamber*, submitted for publication in the *Phys. Rev.* (see also *M.I.T. Thesis*, 1954).

(*) The cross-sections for the various inelastic processes which would result in the apparent absorption of a π^+ -meson in one of the cloud chamber plates are known roughly in the region of interest 40-100 MeV kinetic energy. Over this energy range the absorption cross-section for π^+ -mesons in heavy elements varies from about one-half geometric to geometric. As a conservative lower limit we take the mean absorption cross-section as one half geometric. One then arrives at the quoted figures by subtracting 20 g cm^{-2} lead equivalent from the total track length available in each event this being the thickness required for the identification of the event as an S-particle.

As for the charged decay products, they appear to be μ -mesons for none of them was found to undergo nuclear interaction. One can make a quantitative argument by noting that the charged secondaries of all events in which no associated electron cascade was detected traversed 15 geometric mean free paths of material without an interaction. If all the secondaries were π -mesons we would expect at least 7.5 nuclear stoppings (*). Since no certain case was observed, we conclude that (a) most of the events without associated showers represent decay processes different from $K_{\pi 2}$ -decay, and (b) these decay processes produce μ -mesons rather than π -mesons.

In conclusion it appears that the events of the 100 g cm⁻² Pb group must be interpreted as decay processes of the following type:

$$(2) \quad K_{\mu 2} \rightarrow \mu + \nu.$$

3. - Properties of the $K_{\pi 2}$ and $K_{\mu 2}$ Particles.

Tables III and IV present in greater detail the data relative to the five S-events in which the secondary particle stops in the cloud chamber with a range of about 45 g cm⁻² brass (60 g cm⁻² Pb equivalent), and to the five events in which the secondary particle comes to rest with a range of about 75 g cm⁻² brass (100 g cm⁻² lead).

The values of the primary mass given in column five are computed from the values of the secondary momenta in column four for the assumed decay process $K_{\pi 2} \rightarrow \pi + \pi^0$.

In order to convert the range limits into momentum limits, we used the range energy relations for lead and copper calculated by ARON, HOFFMANN, and WILLIAMS (4). The statistical errors in the range and momentum limits shown in Tables III and IV result from three independent statistical errors: a) 2.7 percent from range straggling, b) an average of about 1 percent from the reconstruction of the angles along the trajectory, and c) 1.6 mm uncertainty in the location of the point of decay. This figure is an estimate of the error due to scattering of the primary and secondary tracks, and to the relative displacement of the track segments due to gas motion.

In events 92136 and 105596 there is an additional uncertainty in locating the actual point of stopping of the secondary particle. This arises from the scattering of the decay electron and (for an assumed electron energy of 35 MeV) amounts to 2.6 mm and 0.7 mm respectively.

In converting the observed ranges into momenta, one must consider the possibility of an additional systematic error due to the uncertainty in the

(*) V. nota a pag. 881.

(4) W. A. ARON, B. G. HOFFMAN and F. C. WILLIAMS: AECU 663, unpublished.

TABLE III. - Experimental data concerning five S-events interpreted as K_{π^2} decays.

Event Number	Origin of S-particle	Charged Secondary Particle		
		Range Limits $g\text{ cm}^{-2}$ Brass	Momentum Limits for a π -meson MeV/c	Primary Mass $M(\pi, \pi^0)$ m_e
26110	1 prong star from neutral primary	$(41.4 \div 43.1)^* \pm 3.1$	$(197 \div 201) \pm 6$	$(941 \div 952) \pm 20$
82203	outside chamber	$(39.2 \div 46.6) \pm 1.9$	$(193 \div 208) \pm 4$	$(926 \div 975) \pm 12$
87981	2 prong star from charged primary	$(40.2 \div 49.2) \pm 2.0$	$(195 \div 213) \pm 4$	$(933 \div 992) \pm 13$
92136	3 prong star from charged primary	40.7 ± 2.7	196 ± 6	936 ± 18
105596	outside chamber	44.8 ± 2.1	204 ± 4	963 ± 14
Average of 92136 and 105596	—	43.0 ± 1.6	201 ± 3	952 ± 11

* This event occurred in lead, but the range is given in brass equivalent.

TABLE IV. - Experimental data concerning five S-events interpreted as K_{μ^2} decays.

Event Number	Origin of S-Particle	Charged Secondary Particle		
		Range Limits $g\text{ cm}^{-2}$ Brass	Momentum Limits for a μ -meson MeV/c	Primary Mass $M(\mu, \nu)$ m_e
81558	outside chamber	$(77.0 \div 107.2) \pm 3.2$	$(232 \div 280) \pm 5$	$(953 \div 1135) \pm 19$
85380	outside chamber	$(70.9 \div 81.7) \pm 2.7$	$(222 \div 239) \pm 4$	$(917 \div 982) \pm 16$
92329	2 prong star from charged primary	$(76.4 \div 79.4) \pm 2.8$	$(231 \div 236) \pm 5$	$(950 \div 968) \pm 17$
96787	5 prong star from charged primary. A Λ^0 is also emitted from this star.	$(68.6 \div 75.9) \pm 2.5$	$(218 \div 230) \pm 4$	$(903 \div 947) \pm 15$
102209	outside chamber	$(77.1 \div 77.6) \pm 2.7$	$(232 \div 233) \pm 4$	$(954 \div 957) \pm 16$

momentum-range relation. One may note that the momentum-range relation here used was obtained under the assumption of an average ionization potential for copper, $I = 333.5$ eV. For π -mesons with a range of 45 g cm^{-2} copper an increase in I of 10 percent increases the momentum by about 0.4 percent and the primary $K_{\pi 2}$ mass by about 0.25 percent.

The two « best » examples of $K_{\pi 2}$ -decay (events No. 92136 and 105596) yield secondary ranges of 40.7 ± 2.7 and $44.8 \pm 2.1 \text{ g cm}^{-2}$ brass (54.2 ± 3.6 and $59.7 \pm 2.8 \text{ g cm}^{-2}$ Pb) respectively. We take, as an average, a range value of $43.0 \pm 1.6 \text{ g cm}^{-2}$ brass ($57.3 \pm 2.1 \text{ g cm}^{-2}$ Pb) and note that all of the other secondary ranges of $K_{\pi 2}$ -particles are consistent with this value. We then obtain a value $p = 201 \pm 3 \text{ MeV/c}$ for the secondary momentum of the π -meson in the $K_{\pi 2}$ -decay. The corresponding value for the mass of the primary particle is:

$$m_{K_{\pi 2}} = 952 \pm 11 \text{ electron masses.}$$

Turning our attention to the $K_{\mu 2}$ -decay, we find for the range of the secondary μ -meson: from events 81558 and 102209 an upper limit of $77.0 \pm 2.7 \text{ g cm}^{-2}$ brass ($102.6 \pm 3.6 \text{ g cm}^{-2}$ Pb), and from event 96787 a lower limit of $75.9 \pm 2.5 \text{ g cm}^{-2}$ brass ($101.1 \pm 3.3 \text{ g cm}^{-2}$ Pb). We thus choose $76.5 \pm 2.5 \text{ g cm}^{-2}$ brass ($102 \pm 3 \text{ g cm}^{-2}$ Pb) as our present best *estimate* of the range in question. The corresponding μ -meson momentum is $p = 230 \pm 5 \text{ MeV/c}$, from which we obtain the following value for the mass of the $K_{\mu 2}$ -particle:

$$m_{K_{\mu 2}} = 950 \pm 15 \text{ electron masses.}$$

It should be emphasized that the errors quoted above result from a preliminary calculation and may require some revision.

In our sample of S-events, the primary particle travels in the chamber for times between 10^{-9} and $2 \cdot 10^{-9}$ s before coming to rest. It is thus clear that the mean life $K_{\pi 2}$ - and of the $K_{\mu 2}$ -particles cannot be much shorter than about 10^{-9} s, while it could be considerably longer.

With the brass plate assembly we observe comparable numbers of events in which the secondary particles of $K_{\pi 2}$ -decays and $K_{\mu 2}$ -decays come to rest in the chamber. On the other hand, the former have about four times the probability of stopping as the latter. We thus conclude that, in our sample of S-particles, $K_{\mu 2}$ -particles are about four times more abundant than $K_{\pi 2}$ -particles. Because of the small statistical sample, this is, of course, only an order of magnitude estimate.

4. - Comparison with Other Experimental Results.

a) *The $K_{\mu 2}$ -decays.* - The existence of heavy mesons disintegrating into light mesons with ranges greater than about $85 \text{ g cm}^{-2} \text{ Pb}$ was first established by the M.I.T. group ⁽⁵⁾. Further examples of long-range secondaries were later reported by this group ^(2,6) and by the group at the École Polytechnique ^(6,7). Moreover, from a simultaneous measurement of the primary mass and of the secondary range, the French group reached the conclusion that the charged decay product was a μ -meson, and that the mass of the neutral product was much smaller than the π^0 -mass. The French group also concluded that the events observed by them probably represented a two-body decay process: $K_{\mu} \rightarrow \mu + \nu$.

There seemed at first to be some difficulty in reconciling the results of both groups with this assumption because the first two events found by the French group yielded a secondary range of about $90 \text{ g cm}^{-2} \text{ Pb}$ ⁽⁷⁾ while the first three events found by the M.I.T. group yielded a secondary range of about $102 \text{ g cm}^{-2} \text{ Pb}$ ⁽²⁾. This discrepancy, however, has disappeared as a consequence of new observations and of a re-evaluation of the old data ⁽⁸⁾.

b) *The $K_{\pi 2}$ -decay.* - Observations with photoemulsions by the Bristol group first suggested the possible existence of charged heavy mesons (χ -particles) undergoing a two-body decay with a π -meson as the charged secondary product ⁽⁹⁾. However, only in a small number of recently reported examples does one find any substantial confirming evidence for this decay scheme ⁽¹⁰⁾.

There is little doubt that these events are identical to our $K_{\pi 2}$ -decays. The Padua group ⁽¹⁰⁾ reported a value of $197 \pm 7 \text{ MeV/c}$ for the momentum of the secondary π -meson, in good agreement with our range data. From a comparison between the values of the primary mass and of the secondary momentum, the same group obtained evidence that the neutral decay product is a π^0 -meson, in agreement with our direct observations.

Finally one may recall the event observed by the Princeton group, showing

⁽⁵⁾ H. S. BRIDGE, H. COURANT, H. C. DESTAEBLER Jr. and B. ROSSI: *Phys. Rev.*, **91**, 1024 (1953).

⁽⁶⁾ *Proceedings of the Duke Conference*, 1953, unpublished.

⁽⁷⁾ B. GREGORY, A. LAGARRIGUE, L. LEPRINCE-RINGUET, F. MULLER and C. PEYROU: *Nuovo Cimento*, **11**, 292 (1954).

⁽⁸⁾ *Proceedings of the Rochester Conference*, 1955, unpublished.

⁽⁹⁾ M. G. K. MENON and C. O'CEALLAIGH: *Proc. Roy. Soc., A* **221** 292 (1954).

⁽¹⁰⁾ See reports of M. CECCARELLI and N. DALLAPORTA at the 1954 Varenna Summer School (*Nuovo Cimento*, in press), see also R. D. HILL, E. O. SALANT and M. WIDGOFF: *Bull. Am. Phys. Soc.*, **29**, no. 7, 32 (1954).

the decay in flight of a charged particle into a light meson and two electron pairs ⁽¹¹⁾. This event has also been interpreted as a decay process of the $K_{\pi 2}$ -type, with a direct conversion of the π^0 -meson into two electron pairs. Under this assumption the primary mass is $954^{+30}_{-20} m_e$.

5. - Further Remarks.

Since our method of detection strongly discriminates against decay processes giving rise to short-range charged secondaries, one can easily understand why τ -mesons undergoing either one of the two possible decay processes ($\tau^+ \rightarrow 2\pi^+ + \pi^-$ or $\tau^+ \rightarrow 2\pi^0 + \pi^+$) do not appear among our S-events. Indeed the maximum range of the secondary π -mesons from these processes is only about $20 \text{ g cm}^{-2} \text{ Pb}$.

It is more difficult to understand our failure to observe any example of κ -particles of the kind found in photoemulsions, where they are seen to decay into μ -mesons with a continuous energy distribution ⁽⁹⁾. It is conceivable that in our observations κ -particles are discriminated against on account of their mean life, or of their energy distribution at production, or of the particular shape of their secondary momentum spectrum. Notice that our range cut-off of about $20 \text{ g cm}^{-2} \text{ Pb}$ corresponds to a momentum cut-off of about 100 MeV/c for μ -mesons.

It is interesting to speculate about the possible relationship between the various kinds of decay processes that have been detected so far.

The $K_{\pi 2}$ -particle has a mass very similar to that of the τ -meson. However, arguments have been presented showing that the τ -meson is probably a particle with zero spin and odd parity ⁽¹²⁾. If this is so, the τ -meson cannot decay into a charged and a neutral π -meson, and the $K_{\pi 2}$ -decay cannot be regarded as an alternate mode of decay of the τ -meson.

The $K_{\pi 2}$ -particle has a mass very similar to that of the θ^0 -particle ($966 \pm 10 m_e$) ⁽¹³⁾ and the decay schemes of the two particles bear a close resemblance to one another:

$$\theta^0 \rightarrow \pi^+ + \pi^-, \quad K_{\pi 2}^{\pm} \rightarrow \pi^{\pm} + \pi^0.$$

For these reasons it has been repeatedly pointed out that the $K_{\pi 2}$ -particles is perhaps the charged counterpart of the θ^0 -particle.

⁽¹¹⁾ A. L. HODSON J. BALLAM W. H. ARNOLD, D. R. HARRIS, R. RONALD RAU, GEO. T. REYNOLDS and S. B. TREIMAN: *Phys. Rev.* **96**, 1089 (1954).

⁽¹²⁾ R. H. DALITZ: *Proceedings of the Rochester Conference*, 1955, unpublished.

⁽¹³⁾ R. W. THOMPSON: *Progress in Cosmic Ray Physics* vol. **3**, edited by J. G. WILSON (Amsterdam), in press.

If the τ -meson is actually a pseudoscalar particle, it is very similar to the π -meson except for the greater mass. One might therefore suspect the existence of a decay mode $\tau \rightarrow \mu + \nu$, similar to the π -meson decay process: $\pi \rightarrow \mu + \nu$, and one might be led to interpret the $K_{\mu 2}$ -decay as an alternate mode of decay of the τ -meson. In this connection, it is very important to decide whether or not the mean lives and the masses of the $K_{\mu 2}$ - and of the τ -meson are the same. No evidence for a difference in the mean lives exists so far. As for the masses, our data may indicate that the $K_{\mu 2}$ -mass is somewhat smaller than the τ -mass, but the difference does not lie outside the statistical and the possible systematic errors. However, the French group has reported stronger evidence for a mass difference between the τ - and the $K_{\mu 2}$ -mesons. It is to be hoped that this question will soon be unambiguously decided.

It is a pleasure to acknowledge the assistance of Mr. R. A. HEWITT in the operation of the cloud chamber, and that of Mr. E. BOLDT in the calculation of the detection probabilities for the π^0 -meson secondaries. The experiment was carried out with the cooperation of the Inter-University High Altitude Laboratories.

RIASSUNTO

L'analisi delle fotografie ottenute colla camera di Wilson a setti del Massachusetts Institute of Technology mostra che i cosiddetti «eventi S» rappresentano processi di disintegrazione di due diversi tipi di mesoni pesanti, secondo gli schemi: $K_{\mu 2} \rightarrow \mu + \nu$ e $K_{\pi 2} \rightarrow \pi + \pi^0$.

On Heavy Unstable Particles Produced in High Energy Nuclear Disintegrations.

C. DAHANAYAKE (*), P. E. FRANCOIS, Y. FUJIMOTO (+), P. IREDALE,
C. J. WADDINGTON and M. YASIN

H. H. Wills Physical Laboratory, University of Bristol

(ricevuto il 28 Marzo 1955)

Summary. — The results of a systematic investigation into the production of heavy unstable particles in energetic nuclear disintegrations is reported. Mass measurements by the grain density-range method have been made in order to detect K-mesons independently of any secondary effects. Measurements were made on tracks which satisfied certain geometrical criteria and which originated in disintegrations of energy greater than ~ 2 GeV. The velocity range studied for K-mesons was from $0.25c$ to $0.56c$. Ten K-mesons and two hyperons were found. The two hyperons and one of the K-mesons decayed in flight. All the particles decayed into single charged secondaries. Both hyperons were emitted from disintegrations which also produced K-mesons. These associated pairs have been reported previously ⁽¹⁾. The results are consistent with the view that hyperons and heavy mesons are mainly produced in association, and that, in the energy range considered, K-mesons show a large charge disparity. Two additional hyperons were found one of which appears to be an example of the decay scheme $Y^\pm \rightarrow \Lambda^0 + \pi^\pm + \sim 60$ MeV. A value for the lifetime of the hyperons is estimated from six suitable examples found in this laboratory. Mass measurements have been made on the tracks of 17 K-mesons. The mean value obtained is $985 \pm 16 m_e$.

Introduction.

During the past few years many observations of heavy mesons have been reported. In nuclear emulsions most of these particles have been detected by

(*) On leave of absence from the University of Ceylon.

(+) On leave of absence from the University of Kyoto.

⁽¹⁾ C. DAHANAYAKE, P. E. FRANCOIS, Y. FUJIMOTO, P. IREDALE, C. J. WADDINGTON and M. YASIN: *Phil. Mag.* **7**, 45, 855 (1954).

the recognition of their characteristic secondary effects. The information on the relative frequencies of the different types of events found is difficult to interpret because of the varying modes of search adopted and because of the uncertain scanning efficiencies for the various types of secondary effects. There is, however, strong evidence that heavy mesons which interact producing visible stars when arrested in emulsions are produced with a much lower frequency than those which decay ⁽²⁾. This apparent charge disparity could be due to a disparity at production or to the existence of a considerable number of negative mesons which, upon coming to rest, undergo decay or do not produce observable secondary effects. To investigate this last possibility, and also to obtain information free from scanning bias on the relative proportions of particles with different modes of decay, it appeared necessary to identify particles by making measurements on tracks selected without reference to any secondary effects. We have done this by making mass measurements, using the grain density-range method, on the tracks of particles emitted from energetic nuclear disintegrations observed in stacks of stripped emulsions. These measurements were designed to distinguish a mass ratio of approximately 2:1 thus making it possible to detect particles of mass $\sim 1000 m_p$ from the background of protons. As the tracks considered were followed out from their parent stars, decays in flight of short lived particles, which would often be missed in conventional scanning, would be detected.

The rest of this paper has been divided into two parts. The first contains the experimental details and the results of the systematic investigation. A discussion of the properties of the hyperons found and details of the accurate mass measurements made on the K-mesons are given in Part II.

PART I. — Experimental Details.

Two stacks of G5 stripped emulsions were used. Both were flown on balloons at high altitudes with the planes of the emulsions vertical. Details are given in Table I.

In order to keep both the ratio of unstable to stable particles and the mass resolution as high as possible, it was necessary to impose selection criteria on the types of stars selected and on the types of tracks accepted from these stars.

To ensure that a large majority of the disintegrations studied should have

⁽²⁾ M. W. FRIEDLANDER, G. G. HARRIS and M. G. K. MENON: *Proc. Roy. Soc.*, **221**, 394 (1954).

TABLE I. - *Details of the stacks and their exposures. Stack HA.54 was exposed in England in May 1953. S.35 was exposed in the 1953 Sardinian Expedition.*

Stack	Dimensions of Emulsions	Numbers of Emulsions	Exposure	
			Duration (hours)	Height (ft)
HA.54	15 cm \times 15 cm \times 600 μ	46	3	80 000
S.35	15 cm \times 10 cm \times 600 μ	40	8	80 000

been capable of producing heavy unstable particles an approximate energy selection was imposed by considering only stars with two or more shower particles. There is a great variation in the energy of disintegration for a given number of shower particles (³) but this selection served to eliminate a very large proportion of the low energy disintegrations. No selection was introduced in the value of N_h accepted, as this would have implied a selection in the atomic numbers of the target nuclei and could thus have introduced a bias against the production of particular types of particles.

From the suitable stars the tracks selected for measurement were chosen so that there was a very large probability that a K-meson accepted would come to rest within the stack. Consequently only tracks with a grain density greater than twice the plateau value were considered (i.e. those with $\beta \leq .56$ for singly charged particles). In order to exclude a large proportion of the evaporation particles and to avoid the difficulties of making ionization measurements on short tracks, the minimum range accepted was 2 mm. This procedure was adopted as it was easy to apply although it meant that the minimum velocity accepted varied with the different types of particles.

Particles emitted at large angles to the planes of the emulsions were excluded because of the difficulties of grain counting and because of the short lengths available to them in the stack. The selection was imposed by fixing a certain minimum length which a particle had to traverse in either the plate of origin or the adjacent plate. These conditions were varied from plate to plate to ensure that a particle accepted had a potential length of at least 5.4 cm, the residual range of a K-meson with a grain density equal to twice the plateau value. A small proportion of the shorter tracks, though emitted in the defined solid angle, were excluded because they did not achieve the required length in either the plate of origin or its neighbour. A correction factor has been applied to allow for this discrimination against the shorter tracks.

(⁶) U. CAMERINI, J. H. DAVIES, P. H. FOWLER, C. FRANZINETTI, H. MUIRHEAD, W. O. LOCK, D. H. PERKINS and G. YEKUTIELI: *Phil. Mag.*, **7**, 42, 1241 (1951).

No selection was made in the angle of the track in the plane of the emulsion and, as a result, some particles emitted from stars near to an edge of the emulsion had a potential stack length of less than 5.4 cm. The number of tracks affected in this manner was kept to a minimum by scanning areas near the top of the stack, so that the higher energy particles which are, in general, emitted downwards would have longer stack lengths.

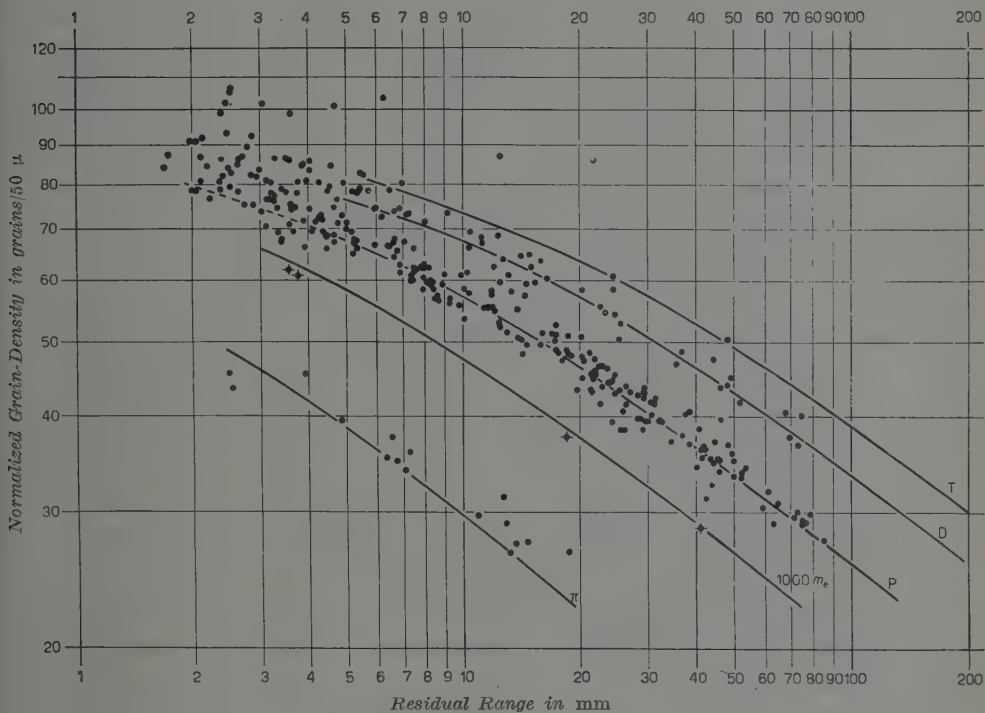


Fig. 1. — A typical grain density-range curve.

An estimate of the mass of each particle satisfying these criteria was made by measurements of the grain density and the residual range. The grain density was measured by counting 600 grains of the track at some convenient point near to the parent star. This estimate was corrected for the different degrees of development of the plates and for the effect of the inclination of the track to the plane of the emulsion. The track was then followed from emulsion to emulsion until the particle either came to rest, left the stack or interacted. For particles which did not come to rest a second grain count was made as far as was convenient from the first, in order to estimate the mass from the change in grain density. The ends of all the tracks of particles arrested in the emulsion were scrutinised for any secondary effects.

In those cases where a heavy unstable particle was detected all other tracks

emitted from the parent star with a grain density above 1.4 times the plateau value were traced as far as possible through the stack in an attempt to find any associated heavy unstable particles.

A typical grain density-range curve is shown in Fig. 1.

In Fig. 2 is shown the mass distribution obtained for all singly charged particles, other than π -mesons, which had residual ranges greater than 4 mm s

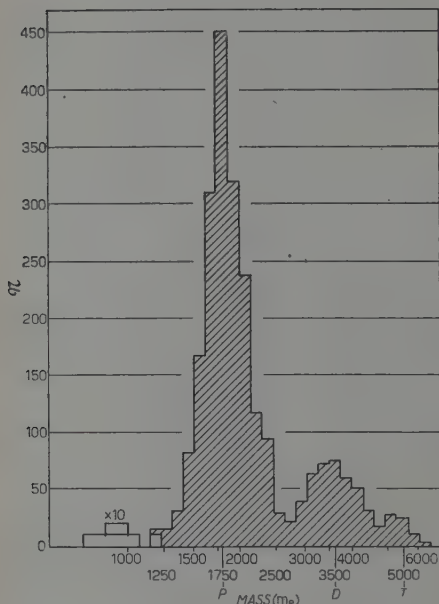


Fig. 2. — The mass distribution obtained for all particles, other than π -mesons, having residual ranges greater than 4 mm. The area shown in white represents the K-mesons, the scale for these has been increased by a factor of ten.

have equal accuracy we estimate from the observed spread in masses of the protons that the probability that a ϱ K-meson⁽⁴⁾ of mass 1000 m_e is classified as a proton is $\sim 0.2\%$ and that even for particles of mass 1200 m_e this probability is only $\sim 5\%$. For particles with total ranges of less than one centimetre it was impracticable to re-examine the tracks and so in this case the probability of missing a ϱ K-particle of mass $\sim 1000 m_e$ is $\sim 12\%$.

⁽⁴⁾ Throughout this paper we have adopted the nomenclature used in the *Report of the Committee on K-Particles, Padova Conference Report*, in *Suppl. Nuovo Cimento*, **12**, 433 (1954).

and came to rest in the stack. This figure shows that the K-mesons were not completely resolved from the protons. In order to reduce the possibility that a particle of mass $\sim 1000 m_e$ which came to rest and produced no observed secondary effect had been classified as a proton, all those tracks having total ranges greater than 1 cm and apparent masses of less than 1500 m_e were re-examined by making further grain density measurements on different parts of the tracks. Because of the greater accuracy of the range measurements compared with that of the ionization estimates, the subsequent measurements provided effectively independent mass values. No particles other than protons were found among the tracks re-examined.

In order that a K-meson having a total range of greater than 1 cm should be classified as a proton it must have had an apparent mass greater than 1500 m_e . By assuming that all points

As the ends of all tracks were carefully examined the above probabilities will be reduced by a large factor for all K-particles having observable secondary effects.

The mass measurements were not sufficiently precise to detect a K-meson among the particles not coming to rest in the emulsion and we must consider the possibility that this group contains such a particle. Of the 621 particles not coming to rest in the stack, 429 have been observed for more than the distance that a K-meson with the same initial velocity would have traversed. There is a very small probability that there is a K-meson in this group, for even in the limiting case where the distance observed was just that expected for a heavy meson the large change in grain density and the high scattering would have been apparent. Of the remaining particles 88 leave the stack. These are tracks which have unfavourable geometry and may fairly be considered as a random sample of particles. There is therefore a probability of only $\sim .4$ that there is a K-meson among them. There remain 104 particles which interacted before traversing the distance expected for a K-meson. It is very unlikely that there is more than one K-particle in this sample of tracks since we have observed for the identified K-mesons a total path length which is only ~ 0.7 of a mean free path, even if we assume that this is geometrical. In addition K-particles have been observed to re-emerge from interactions ⁽⁵⁾. Since we have examined the products of the observed secondary interactions and have found no K-particles and have noticed no lack of balance of energy, the probability that there is such a particle in this group is reduced.

Due to the lack of resolution it is not possible to identify hyperons by our mass measurements alone and we are dependent upon observing secondary effects. The probability of detection will vary with the type of decay. All those decaying at rest into a proton should have been observed since the secondary would have had a high grain density, but for decays into a relativistic π -meson the probability of detection will be a little smaller. Owing to their short lifetime a large number of hyperons decay in flight and it should be possible to detect all these except for a fraction of about 10 % which decay in the gaps between the emulsions, and for those which decay into a proton emitted with such a velocity that there is no noticeable decrease in ionization. In these latter cases the event has to be distinguished from the many nuclear scatterings of stable particles where a track is seen to be deviated through a large angle and to have an increase, or no change, in grain density. In an attempt to see where there is an appreciable number of such hyperons we have analysed 38 of the observed large angle deflections as if they were examples of the decay process $Y \rightarrow p + \pi^0 + Q$. In making this analysis we have

⁽⁵⁾ R. R. DANIEL and D. LAL: *Proc. Ind. Acad. Sci.*, **41**, 1, 15 (1955).

taken only events which have satisfied the following criteria:

- a) the «secondary particle» came to rest within the stack;
- b) the angle of deflection was greater than 5 degrees;
- c) there was no apparently associated track or «blob» at the «decay point».

A plot of the Q -values obtained is shown in Fig. 3. From this it can be seen that there is no significant peak. This is not surprising for if this sample

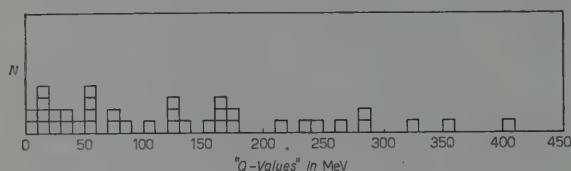


Fig. 3.

contained many hyperons we would have expected to observe some decays in which the proton had a lower ionization than its parent. We have to conclude that unless accurate mass measurements are made on the primary

track, it is not possible to detect this decay mode with an efficiency of more than about one half.

There remain the possibilities that a hyperon may have interacted in flight, or left the stack before decaying. If it interacted the excess energy may have revealed itself in a distinctive manner. Also, assuming a geometrical cross-section, for a given path length of hyperon track, the probability of decay in flight is much greater than that of interaction.

Those hyperons which leave the stack will not be detected, but we can calculate from time of flight considerations, assuming the lifetime given in Part II, that the probability that one hyperon would remain undetected among this sample is $\sim 4\%$.

From the foregoing considerations, we conclude that the figures given for the numbers of heavy unstable particles produced in the disintegrations we have examined cannot be seriously in error.

Results.

Of the 4323 tracks examined, 3031 lie within the velocity range accepted for K-mesons, i.e. between $0.25c$ and $0.56c$. Details of these are given in Table II.

Two hyperons were found. The parent disintegrations of both of these also emitted K-mesons. These events are consistent with the process



TABLE II. — Details of the tracks examined which had velocities between $0.25c$ and $0.56c$, at their origins. It was not possible to identify unambiguously the particles which did not come to rest in the emulsion. They have, however, been analysed in a statistical manner.

	Protons	Deuterons and Tritons	π -mesons (*)		K-mesons	Hyperons
			Positive	Negative		
Uncorrected	2203	691	33	87	10	2
Corrected	2320	691	33	90	10	2

(*) There are five π -mesons not included in this table. Three interacted in flight, one left the stack and one decayed in flight.

The second line of the table shows the numbers of particles after corrections have been made for geometrical losses. The total numbers of particles in the energy range considered emitted from the 4742 stars examined can be estimated by multiplying the figures in the second line of this table' by the factor 4.7.

first reported by FOWLER *et al.* ⁽⁶⁾, and have been described in a previous communication ⁽¹⁾. The details of these hyperons both of which decayed in flight into single charged particles are given in Table III.

Altogether, eleven K-mesons were observed. One of these, K_{42} , had a velocity outside the range accepted in this experiment and was found during the re-examination of the parent disintegration of Y_6 . Only one, K_{43} , decayed in flight. The total time of flight of K-mesons observed was $2.1 \cdot 10^{-9}$ s. Details of these particles are given in Table IV.

All the heavy mesons found in this investigation decayed into single charged particles. The secondaries of the ten which came to rest all have blob densities which are not significantly different from the plateau value. It appears therefore, that there are among them no examples of the alternative mode of decay of the τ -meson:

$$\tau^{\pm} \rightarrow \pi^{\pm} + 2\pi^0 \quad (7).$$

An analysis of the decay in flight shows that it also is inconsistent with this mode of decay.

⁽⁶⁾ W. B. FOWLER, R. P. SHUTT, A. M. THORNDIKE and W. L. WHITEMORE: *Phys. Rev.*, **93**, 861 (1954).

⁽⁷⁾ J. CRUSSARD, M. F. KAPLON, J. KLARMANN and J. H. NOON: *Phys. Rev.*, **93**, 253 (1954).

TABLE III. - Details of the hyperons and their secondaries. Y_4 and Y_{14} lay

Y	Stack	Parent star	Angle to Primary Direction	Length (mm)	Number of plates traversed	PRIMARY	
						Mass (m_e)	at d
5	S.35	$19 + 3n$	—	9.60	3	$2\,350 \pm 350$	0.518
6	HA.54	$13 + 3p$	35°	17.5	7	$1\,850 \pm 250$	0.548
4	HA.54	$9 + 8p$	9°	4.40	2	$2\,500 \pm 500$	0.59
14	S.35	$5 + 3p$	14°	10.2	2	$2\,400 \pm 300$	0.55

(*) With the exception of Y_4 the Q values are calculated assuming the decay scheme $Y^\pm \rightarrow \pi^\pm$

TABLE IV. - Details

IV-a.

K	Stack	Parent Star	Angle to Primary Direction	Range (mm)	No. of plates traversed	PRIMARY	
						Mass in m_e	α
25	HA.54	$26 + 4n$	—	3.77	1	—	1 150
26	HA.54	$18 + 19\alpha$	15°	42.10	3	886 ± 39	960
32	HA.54	$28 + 2p$	42°	19.18	10	$1\,020 \pm 60$	
33	HA.54	$8 + 4p$	17°	4.03	2	$1\,100 \pm 120$	
35	HA.54	$15 + 4p$	6°	40.36	6	977 ± 29	
38	S.35	$11 + 4p$	8°	18.81	5	$1\,095 \pm 90$	
41	S.35	$19 + 3n$	—	38.30	12	989 ± 50	940
44	HA.54	$12 + 3p$	39°	11.49	4	$1\,139 \pm 100$	
46	HA.54	$19 + 6p$	120°	11.79	5	961 ± 70	760
42	HA.54	$13 + 3p$	17°	70.90	7	983 ± 24	900 ($\bar{\alpha}$ -

IV-b.

K	Stack	Parent star	Angle to Primary Directoin	Length (mm)	No. of plates traversed	PRIMARY	
						β at emission	Mass in m_e $g^* - \bar{\alpha}$
43	HA.54	$22 + 3p$	62°	4.77	2	.56	$1\,180 \pm 100$

velocity range considered. These are discussed in Part II of the paper.

S E C O N D A R Y							
ne ight rved)	Total observable time of flight (s)	Length (mm)	No. of plates traversed	Angle between primary and secondary tracks	$p\beta$ (MeV/c)	Normalised blob density	Q (*) (MeV)
10^{-10}	$5.53 \cdot 10^{-10}$	13.3	12	46°	—	1.02 ± 0.04	> 85
10^{-10}	$4.26 \cdot 10^{-10}$	44.3	12	50°	190 ± 10	1.05 ± 0.04	116 ± 15
10^{-10}	$0.42 \cdot 10^{-10}$	23.73	9	26.2°	227 ± 31	0.97 ± 0.04	63 ± 27
10^{-10}	$1.67 \cdot 10^{-10}$	16.3	14	45.5°	—	0.95 ± 0.04	> 80

+ Q . For Y_4 the decay scheme $Y^\pm \rightarrow \Lambda^0 + \pi^\pm + Q$ was assumed.

resons and their secondaries.

S E C O N D A R Y				
gth (m)	No. of plates traversed	Normalised blob-density	$p\beta$ (MeV/c)	R e m a r k s
3	33	0.97 ± 0.03	—	—
9	29	0.94 ± 0.04	> 120	—
0	18	~ 1.0	—	—
8	20	0.95 ± 0.06	> 115	—
37	12	1.00 ± 0.07	—	—
9	9	~ 1.0	—	—
6	13	0.98 ± 0.04	—	Produced in association with Y_5
2	25	0.98 ± 0.02	155 ± 10	—
1	23	1.00 ± 0.04	49 ± 4	Electron secondary
27	30	0.9	—	Produced in association with Y_6

S E C O N D A R Y				
gth (m)	No. of plates traversed	Normalised blob-density	$p\beta$ MeV/c	R e m a r k s
8	43	1.00 ± 0.03	—	Decays in flight.

It was possible to make reliable scattering measurements on only four of the secondary particles, the remainder being too steeply inclined to the planes of the emulsions. The secondary of K_{46} was identified as an electron ⁽⁸⁾. The measurements on the secondaries of K_{26} , K_{33} , and K_{44} are consistent with their being either electrons or L-mesons.

We can combine with these results those of FOWLER and PERKINS ⁽⁹⁾ who identified by grain density-scattering measurements two K-mesons which were subsequently found to have stopped in the emulsion. One of these was a τ^+ -meson; the other decayed into a single charged particle. Thus of the twelve K-mesons identified without reference to their secondary effects all decayed. One was a τ -meson, and at least one decayed into an electron.

Discussion.

The principal features of the results of this experiment are that within the velocity range concerned K-mesons are often produced in association with hyperons, and that among the K-mesons which come to rest in emulsion there are few which do not decay.

That σ K's are much rarer than K-mesons which decay is suggested by the results of direct scanning. In the present experiment the ten K-mesons which came to rest all decayed, and if we include with these the two examples found by FOWLER and PERKINS the ratio of the number of K-mesons which decayed to number which interacted when at rest becomes 12 to 0. The agreement between the results of these experiments and those of direct scanning indicates that the apparent charge disparity among the K-mesons coming to rest in emulsion cannot be due to the existence of a large proportion of ϱ K particles.

The two examples of associated production found in this experiment are consistent with the reaction (A). Several other examples of associated production have been reported but not all of them have energies and angles of emission which are consistent with this scheme. This may be due to the interaction of the particles in the parent nucleus after production, or to the particles in the parent nucleus after production, or to the creation of additional particles. Because a heavy meson or hyperon may be neutral and, because the stacks used are of limited size, there is a large probability that a thorough examination of the products of a disintegration which produces one unstable

⁽⁸⁾ C. DAHANAYAKE, P. E. FRANCOIS, Y. FUJIMOTO, P. IREDALE, C. J. WADDINGTON and M. YASIN: *Phil. Mag.*, **7**, 45, 1219 (1954).

⁽⁹⁾ P. H. FOWLER and D. H. PERKINS: *Report of Padova Conference*, in *Suppl. Nuovo Cimento*, **12**, 236 (1954).

particle would fail to detect an associated particle. The present result is therefore not inconsistent with all the observed K-mesons being produced in association, and from other results reported it appears probable that a large proportion of all K-mesons found in emulsions are so produced.

As was stated previously, a large majority of the K-mesons, when arrested in emulsion, are observed to decay. This may be due to an intrinsic charge disparity or to the presence of negative K-mesons which do not interact upon coming to rest. It would be expected that the negative counterpart of a positive K-meson produced in a reaction of the type (A) would interact according to the scheme



and several events which appear to represent this reaction have in fact been observed. Since this reaction should be very fast the negative K-meson should interact before decaying. The products of this process are highly interacting and in a large majority of the cases we would expect a visible disintegration to be produced. It appears therefore that the predominance of decaying K-particles indicates a real positive excess among K-particles produced in this manner.

PART II. - Accurate Mass Measurements on K-Mesons.

The tracks of the K-mesons found in this experiment are suitable for accurate grain density measurements and together with suitable events found by other methods they have been used for mass measurements by the ionisation-range method. Ionisation estimates were made by the blob-gap method of FOWLER and PERKINS ⁽¹⁰⁾ which is less subjective than the grain density measurements made elsewhere in this experiment. As the majority of the suitable K-particles were in stack HA.54 the more accurate measurements were confined to this stack. Similar but less extensive measurements were carried out in stack S.35.

Measurements were made at as many points as possible, both along the tracks of the K-mesons and along those of suitable protons identified in the main experiment. The measurements made on K-mesons and those on protons were distributed throughout the stack and thus any normalising errors which may have occurred affected the protons and K-mesons alike. A large majority of the points have a similar statistical weight; in most cases 400 blobs and

⁽¹⁰⁾ P. H. FOWLER and D. H. PERKINS: in press (1955).

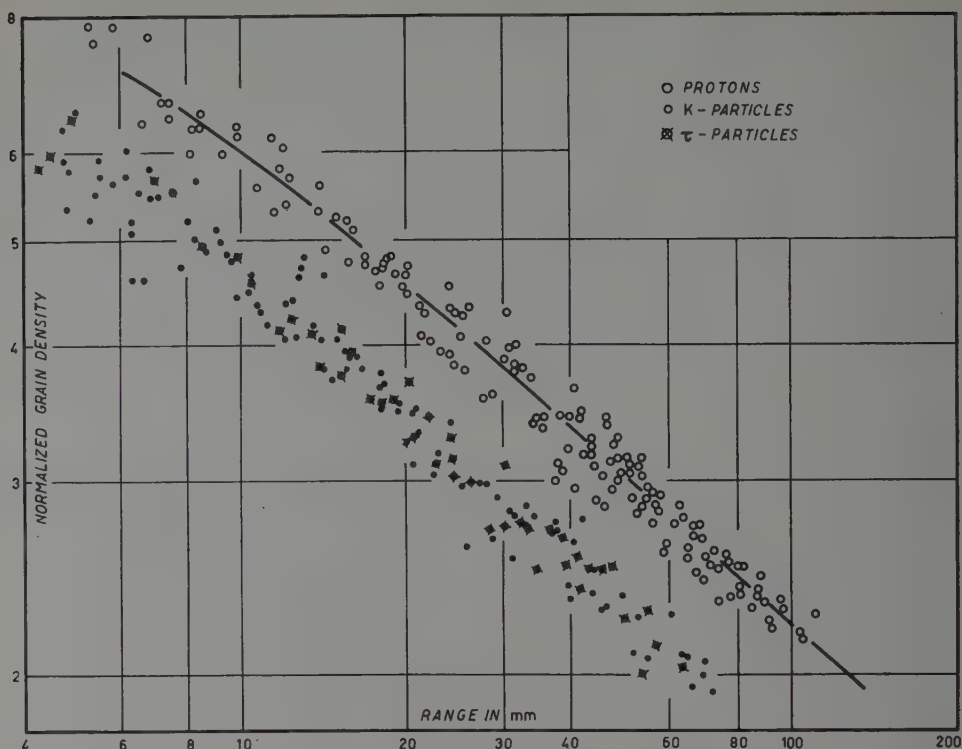


Fig. 4. - The grain density-range curve for the measurements made on the tracks of K-particles and calibration protons measured in stack HA.54.

100 gaps of length greater than a value between two and three times the mean gap size were counted. The results for tracks measured in HA.54 are shown in Fig. 4. The mass distribution obtained from these results is shown in Fig. 5.

The mean mass obtained for the K-particles observed in HA.54 and which decayed into single charged secondaries is $983 \pm 17 m_e$ which is not significantly different from the mass of the τ -meson. For the τ -mesons the

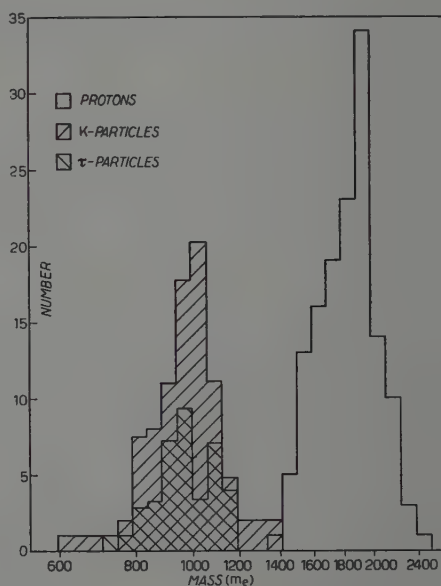


Fig. 5. - The mass distribution obtained from the measurements shown in Fig. 4.

mean mass obtained is $972 \pm 20 m_e$. The errors quoted, which are standard deviations, can be compared with values of $\pm 16 m_e$ and $\pm 21 m_e$, for K and τ -mesons respectively, calculated from the observed spread in the proton masses, and with $\pm 16 m_e$ and $\pm 10 m_e$ calculated from the statistical weight of each measurement. It was possible to make only a small number of measurements in stack S.35. When the results of these are included with those of HA.54 the mean mass of the K-mesons measured becomes $985 \pm 16 m_e$.

Fig. 6 shows the results obtained for the individual K-mesons. The χ^2 test indicates that these results are not inconsistent with a unique mass.

Hyperons.

In addition to the two hyperons found within the velocity range accepted, two other examples have been identified in the course of this investigation. One of these, Y_4 , was found upon grain counting to be just outside the velocity range accepted and was detected only because it decayed in the plate in which its grain density was measured. The track of the other, Y_{11} , was originally accepted on the basis of a grain count made in an incompletely normalised plate, and had subsequently to be rejected. Details of these two hyperons are given in Table III.

Y_4 appears inconsistent with the decay scheme

$$Y^\pm \rightarrow \pi^\pm + \text{Neutron} + Q$$

for the Q value obtained assuming this decay mode is 66 ± 28 MeV which is inconsistent with the accepted value of 115 MeV. It may however be an example of the process

$$Y^\pm \rightarrow \Lambda^0 + \pi^\pm + Q \quad (11)$$

(11) R. ARMENTEROS, K. H. BARKER, C. C. BUTLER, A. CACHON and C. M. YORK: *Phil. Mag.*, 43, 597 (1952). See also, R. B. LEIGHTON: *Bagnères Report*, p. 97 (1953).

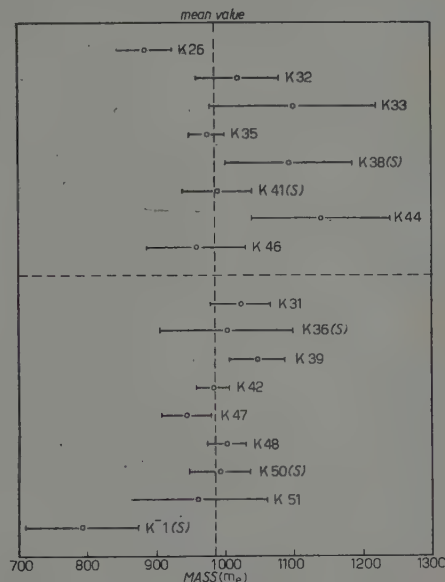


Fig. 6. — The masses of the individual K-mesons measured. Those points shown above the line represent the particles found in the systematic search. The K-mesons measured in stack S.35 are distinguished by the symbol (S).

for the « Q value» obtained for this scheme is 63 ± 27 MeV. This is in agreement with the value 67 ± 12 MeV reported by COWAN ⁽¹²⁾ which is the most precise value published to date.

A search has been made along the expected line of flight of the Λ^0 for the available distance of 3.0 cm. This length corresponds to a time of flight of $1.4 \cdot 10^{-10}$ s. No event which could be interpreted as the decay of this particle has been found.

Lifetime of the Hyperon.

The lifetime of the hyperon is difficult to estimate from examples found by direct scanning because of the uncertainty in determining the efficiencies of detection of decay in flight. AMALDI *et al.* ⁽¹³⁾ have estimated these efficiencies and concluded that the lifetime of the hyperon probably lies between $0.5 \cdot 10^{-10}$ s and $3 \cdot 10^{-10}$ s. For hyperons which are detected by following tracks out from stars no such uncertainties exist. Six examples have been found in this manner in this laboratory: four in the present experiment and two others, Y_3 and Y_{13} , which have been reported by FRIEDLANDER *et al.* ⁽¹⁴⁾. Using the maximum likelihood method ⁽¹⁵⁾ we estimate from these six examples that the mean lifetime of the hyperons is

$$\tau = 0.5^{+2.5}_{-.32} \cdot 10^{-10} \text{ s.}$$

The «errors» given are 90% confidence limits. In making this estimate we have assumed that 2 mm of track were necessary in order to establish the identity of a particle.

These six events probably consist of a mixed sample. Only four are consistent with the decay into a neutron and a π -meson with an energy release of ~ 115 MeV. The mean lifetime calculated for these four is

$$\tau = 0.5^{+3.3}_{-.0.33} \cdot 10^{-10} \text{ s.}$$

The other two, Y_3 and Y_4 , are inconsistent with the above scheme and are probably examples of the decay

$$Y^\pm \rightarrow \pi^\pm + \Lambda^0 + Q.$$

The best estimate of lifetime from these two is $1 \cdot 10^{-10}$ s.

⁽¹²⁾ E. W. COWAN: *Phys. Rev.*, **94**, 161 (1954).

⁽¹³⁾ E. AMALDI, C. CASTAGNOLI, G. CORTINI and C. FRANZINETTI: *Nuovo Cimento*, **12**, 5, 668 (1954).

⁽¹⁴⁾ M. W. FRIEDLANDER, T. D. KEEFE and M. G. K. MENON: *Nuovo Cimento*, **1**, 3, 482 (1955).

⁽¹⁵⁾ M. S. BARTLETT: *Phil. Mag.*, **7**, 44, 249 (1953).

* * *

We wish to thank P. H. FOWLER and Dr. D. H. PERKINS, who initiated this experiment; Dr. M. G. K. MENON for reading the draft, and other members of this laboratory for useful discussions. We are deeply indebted to Professor C. F. POWELL, for his continued help and encouragement.

Three of us (P.E.F., P.I., and C.J.W.) wish to thank the Department of Scientific and Industrial Research for maintenance grants. C.D. wishes to thank the Government of Ceylon; Y.F. the British Council, and M.Y. the Government of India and the Muslim University of Aligarh, for maintenance grants.

RIASSUNTO (*)

Si riferisce il risultato di un esame sistematico della produzione di particelle pesanti instabili nelle disintegrazioni nucleari di alta energia. Sono state eseguite misure di massa col metodo densità di grani-range onde rilevare i mesoni K indipendentemente dai loro effetti secondari. Si sono eseguite misure su tracce soddisfacenti determinati criteri geometrici e che traevano origine da disintegrazioni di energia superiore a ~ 2 GeV. L'intervallo di velocità studiato per i mesoni K è stato da $0,25c$ a $0,56c$. Sono stati trovati 10 mesoni K e 2 iperoni. I due iperoni e uno dei K decadono in volo. Tutte le particelle decadono in secondari a carica semplice. I due iperoni sono emessi in disintegrazioni che producono anche mesoni K. Su queste coppie associate fu già riferito in precedenza ⁽¹⁾. I risultati sono compatibili con l'ipotesi che iperoni e mesoni pesanti siano prodotti prevalentemente in associazione, e che, nell'intervallo di energie considerato, i mesoni K mostrino una grande disparità di carica. Si trovarono due ulteriori iperoni, uno dei quali appare essere un esempio dello schema di decadimento $Y^\pm \rightarrow \Lambda^0 + \pi^\pm + \sim 60$ MeV. Il tempo di vita degli iperoni è stato stimato in base a sei esempi adatti trovati in questo laboratorio. Misure di massa sono state eseguite sulle tracce di 17 mesoni K. Il valore medio ottenuto è $985 \pm 16 m_p$.

(*) Traduzione a cura della Redazione.

Results on Some Secondary Particles of K-Mesons from the Stacks Flown in Sardinia 1953.

A. BONETTI, R. LEVI SETTI and B. LOCATELLI

Istituto di Scienze Fisiche dell'Università - Milano
Istituto Nazionale di Fisica Nucleare - Sezione di Milano

G. TOMASINI

Istituto di Fisica dell'Università - Genova

(ricevuto il 30 Marzo 1955)

Summary. — In this paper are given the results of measurements on secondaries of K-particles found in stacks of stripped emulsions exposed at high altitude from Sardinia 1953. Among the 8 secondaries, one has been identified as a π -meson, one as a μ -meson. The other 6 form a group whose ionization is near the plateau and whose $p\beta$ is about 200 MeV/c. The K-particle with π -meson secondary can be classed as a χ -meson, that with an identified μ secondary is probably a κ . The remaining 6 secondaries can be interpreted as the products of the K_μ decay, and the mass of the K_μ can be determined from their mean $p\beta$. The methods of measurement and some possible sources of error are discussed critically.

1. — Introduction.

We give here the results of measurements on secondaries of K-particles found in stacks of stripped emulsions exposed during the Sardinian Expedition 1953. Results on preliminary measurements were given at the Padua Meeting April 1954 ⁽¹⁾. In these stacks, of dimensions $(10 \times 15 \times 2.4)$ cm³ in 40 (600 μ) stripped emulsions, the major part of the secondaries of the heavy mesons could not be brought to rest. Their identification had therefore to be

⁽¹⁾ A. BONETTI, R. LEVI SETTI, B. LOCATELLI and G. TOMASINI: *Suppl. Nuovo Cimento*, 12, 222 (1954).

made by measurements on scattering and ionization for which several centimetres of track were available.

The results discussed in this paper are given in Table II and Fig. 1.

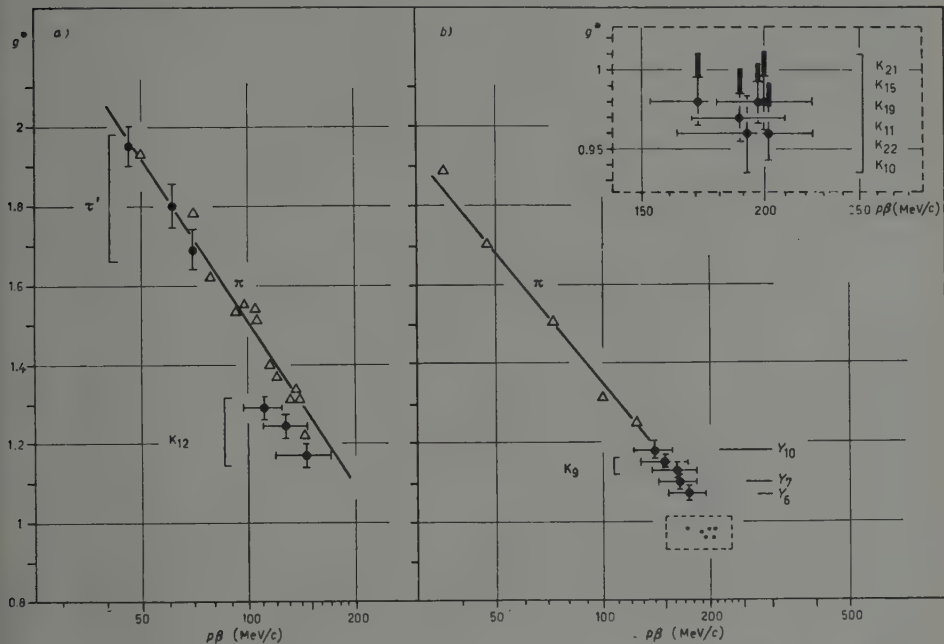


Fig. 1. — $(p\beta, g^*)$ plot for the secondaries of K-mesons. a) Calibration on stack 9; τ' refers to the secondary of the $(\tau)K_{\mu}^+$ -meson described by ⁽²⁾; b) Calibration on stack 31; the curve is that obtained by ⁽³⁾. Points Y_5 , Y_7 and Y_{10} refer to the secondaries of hyperons found in the same stack. — The triangles refer to our measurements on π -mesons ending in the emulsion. — In the upper right hand corner is an enlargement giving detail of the region enclosed in the dotted rectangle. The points corresponding to K's 21, 15, 19, 11, 22, 10, are found by reading from left to right, and downwards.

2. — Methods of Measurement (*).

a) *Scattering*. — In the calculation of the mean sagitta, the 4-times cut-off was used and the noise eliminated between two different cell lengths. The

(*) In what follows we indicate by a star * those points in which we employ methods differing from those suggested by the Bureau of Standards ⁽⁴⁾.

⁽²⁾ M. DI CORATO, C. C. DILWORTH and L. SCARSI, *Suppl. Nuovo Cimento*, **12**, 202 (1954).

⁽³⁾ M. DI CORATO, C. DILWORTH, D. HIRSCHBERG, L. HIRSCHBERG, L. SCARSI and G. TOMASINI: Private communication.

⁽⁴⁾ *Recommendations etc.*, in *Suppl. Nuovo Cimento*, **11**, 228 (1954); *Recommendations etc.*, in *Suppl. Nuovo Cimento*, **12**, 474 (1954).

basic cell and the cell of measurement were chosen so as to keep as near as possible in the optimum conditions.

* Following the results of the Brussels-Milan Scattering Group ⁽⁺⁾ ⁽⁵⁾, we used complete overlapping of the multiple cells and obtained the error from the curves calculated by them on the basis of the theory of MOLIÈRE-D'ESPAGNAT ⁽⁶⁾ and HUYBRECHTS ⁽⁷⁾ and checked by them against the experimental dispersion of the mean sagittas on slow particles.

Distortion was eliminated by the method of third differences. That the distortion in our plates was mainly of the 2nd order and the use of third differences sufficient to eliminate it, was checked by direct measurement of the distortion vector.

* We used the value of the ratio of third to second differences

$$\bar{D}'''/\bar{D}'' = 1.06\sqrt{3/2}$$

given by calibrations both on slow ⁽⁵⁾ and fast ⁽³⁾ particles. We note that this value is equal to that given by Bombay ⁽⁸⁾.

As a further check on the validity of the third difference method we used two of the longest secondary tracks to compare directly the results of the third differences and of the second differences corrected by the use of the distortion vector (see Table I, K₁₅ and K₂₁). The effect of the longitudinal component of distortion on cell length has been taken into account for the secondary of K₂₁ and found to be negligible (bracketed $p\beta$'s in Table I), the distortion vectors being oriented at random in the various plates.

TABLE I. — *Distortion correction on two tracks of secondaries of K-mesons.*

Particle	$(p\beta)''$ (MeV/c)	$(p\beta)'''$ (MeV/c)	$(p\beta)''$ (*) (MeV/c)
K ₁₅	174 ± 17	197 ± 20	181 ± 18
K ₂₁	160 ± 16	171 ± 18	184 ± 18
		(173 ± 18) (**)	(186 ± 18) (**)

(*) Corrected with direct measurement of the distortion vector.

(**) Longitudinal component of the distortion vector taken into account.

⁽⁺⁾ We are very indebted to our colleagues ⁽⁵⁾ for having made available to us the results of their measurements and calculations.

⁽⁵⁾ M. DI CORATO, D. HIRSCHBERG and B. LOCATELLI: *Suppl. Nuovo Cimento*, **12**, 381 (1954) and private communication.

⁽⁶⁾ B. D'ESPAGNAT: *Compt. Rend., Ac. Sci.*, **232**, 800 (1951) and *Journ. Phys. et Rad.*, **13**, 74 (1952).

⁽⁷⁾ H. HUYBRECHTS: Private communication.

⁽⁸⁾ S. BISWAS, E. C. GEORGE, B. PETERS and M. S. SWAMY: *Suppl. Nuovo Cimento*, **12**, 369 (1954).

The component of distortion transversal to the track varied from a few microns up to about $50\ \mu$. In those few plates in which it reached an anomalously high value, around $100\ \mu$, the corresponding section of track was rejected.

The scattering «constant» was taken from the curves of PICKUP and VOJVODIC⁽⁹⁾. The error on the $p\beta$ takes into account the 8% experimental spread in the various determinations of the «constant», as suggested by DILWORTH *et al.*⁽¹⁰⁾ and⁽⁴⁾.

b) *Ionization.* — The ionization was determined by blob counting on $100\ \mu$ cells. The relative error on the blob density g was obtained from the frequency distribution of blobs in counting on fast electrons, and was found to be $(0.91 \pm 0.05)/\sqrt{N}$, where N is the total number of blobs counted on the track. The error has been increased in order to take into account our incertitude of the original thickness of the emulsion, supposing the mean thickness to be $(600 \pm 50)\ \mu$; this increase reaches $0.006\ g$ for our steepest tracks. The internal consistency of the measurements on individual tracks was good. As for the scattering, the effect of the longitudinal component of distortion was negligible.

The plateau grain density g_0 was determined by counting on tracks of electrons from cascades crossing the whole thickness of the emulsion so that the effect of development gradient and of corrosion should be the same as for the K secondary particles. The values of g_0 for the various plates were equal within the experimental errors and therefore we felt justified in comparing the mean value of g for each track with the average g_0 for the whole stack.

Such a comparison will be rigorous only if the tracks both of calibration and of measurement have the same dip. Since our calibration tracks were flatter than those of the K secondaries (4° against 12° in average), this led to a possible underestimate of $g/g_0 = g^*$ ⁽¹¹⁾; so we calculated the order of magnitude of the error involved. The vertical heavy bars in Fig. 1b represent the possible displacement of the upper limit of the error on 5 of 6 of our tracks having $g^* \sim 1$. An individual calibration had to be made for K_{22} , which was in corner of the stack. The absence of the correction for shadowing effect⁽¹¹⁾

⁽⁹⁾ E. PICKUP and L. VOJVODIC: *Phys. Rev.*, **80**, 89 (1950).

⁽¹⁰⁾ C. DILWORTH, G. P. S. OCCHIALINI and L. SCARSI: *Annual Rev. of Nucl. Sci.*, **4**, 271 (1954).

⁽¹¹⁾ The variation with dip of blob or gap density is one of the problems of the Ionization Group of Milan. They suggest that the shadowing effect on small gaps pointed out by DELLA CORTE⁽¹²⁾ should lead to a loss of the smallest gaps which can be estimated if the frequency distribution of the gaps and the optical cut-off is known. A precise correction cannot of course be given until it has been verified experimentally.

⁽¹²⁾ M. DELLA CORTE: *Nuovo Cimento*, **12**, 28 (1954).

TABLE II. — Data on K-

a) PRIMARY PARTICLES

Particle K-GeMi	Stack	Range	N. of plates (μ)	\bar{D}'' ⁽¹⁾ standard	Mass'' (m_e)	\bar{D}''' ⁽¹⁾ (μ) standard	Mass''' (m_e)	Parent star
1	2	3	4	5	6	7	8	9
9	31	19.24	2	$0.276 \pm .022$	980 ± 180	$0.274 \pm .023$	990 ± 200	7+0p (6)
10	"	18.50	17	$0.278 \pm .026$	960 ± 210	$0.286 \pm .029$	910 ± 220	—
11	"	18.33	5	$0.282 \pm .022$	930 ± 175	$0.270 \pm .023$	1030 ± 210	14+2p
12	9	15.85	5	$0.269 \pm .023$	1040 ± 210	$0.310 \pm .028$	750 ± 160	4+2p
15	31	8.15	2	$0.275 \pm .028$	980 ± 250	$0.309 \pm .033$	750 ± 190	31+9p
19 ⁽⁴⁾	"	3	2	$0.270 \pm .042$	1030 ± 400	$0.276 \pm .045$	990 ± 390	22+7p
21	"	18.9	21	$0.370 \pm .048$	490 ± 150	$0.352 \pm .054$	550 ± 200	18+5p
22	"	8.8	7	$0.230 \pm .025$	1500 ± 400	$0.230 \pm .029$	1690 ± 510	17+7p

⁽¹⁾ $\bar{D}_{\text{standard}}$ (protons) = $(0.212 \pm .004) \mu$.

⁽²⁾ Measured length in brackets.

⁽³⁾ Star produced by a shower-particle from a (24+11p) star.

⁽⁴⁾ From an analysis of 2-branch stars (6).

is due to the fact that the calibration tracks were of the same mean dip as the secondary tracks.

c) *Curves relating $p\beta$ and g^* .* — We have used for the identification of the K secondaries in stack 31 a ($p\beta, g^*$) curve obtained from measurements on π -mesons and protons by our colleagues ⁽³⁾. Our blob counts on π -mesons ending in the stack, carried out up to the range corresponding to $p\beta=140$ MeV/c show good agreement with this curve. For stack 9 we constructed a similar curve with measurements on stopping π -mesons. These curves are shown in Figs. 1a and 1b, together with the experimental points corresponding to the mean value of $p\beta$ and g^* over the whole track length for the K secondaries and for three secondaries of hyperons decaying in flight (Fig. 1b). The effect of shadowing ⁽¹¹⁾ on the mass determination of the secondaries with $g^* > 1$, if existing, is certainly small, since the calibration tracks had the same average dip as the secondary tracks.

3. — Experimental Results.

Complete data on the height and duration of flight of our stacks (n. 9 and 31) are given in the Report of the 1953 Sardinian Expedition ⁽¹³⁾.

⁽¹³⁾ J. DAVIES and C. FRANZINETTI: *Suppl. Nuovo Cimento*, **12**, 480 (1954).

measurable secondaries.

b) SECONDARY PARTICLES							
ht (2) (m)	N. of plates	Dip	g^*	$p\beta''$ (MeV/c)	$p\beta'''$ (MeV/c)	Mass or Identity	$p\beta_{\text{emission}}$ (MeV/c)
1	12	13	14	15	16	17	18
45)	20	10°	$1.14 \pm .014$	146 ± 16	155 ± 17	$(278 \pm 31) m_0$ assumed π	174 ± 16
37.5)	17	16°	$0.96 \pm .017$	176 ± 19	202 ± 24	assumed μ	216 ± 22
49.3)	21	9°	$0.97 \pm .015$	154 ± 17	189 ± 20	assumed μ	207 ± 18
46)	13	7°	$1.25 \pm .020$	124 ± 13	124 ± 13	$(222 \pm 23) m_0$ assumed μ	144 ± 12
56.6)	19	11°	$0.98 \pm .013$	174 ± 17	197 ± 20	assumed μ	216 ± 18
47.6)	24	17°	$0.98 \pm .016$	188 ± 20	200 ± 23	assumed μ	217 ± 21
64.3)	29	11°	$0.98 \pm .015$	160 ± 16	171 ± 18	assumed μ	195 ± 17
18.3)	6	10°	$0.96 \pm .024$	215 ± 30	192 ± 29	assumed μ	200 ± 27

B. — The results on $K_{9,10,11,12}$ given here substitute the preliminary results published in ⁽¹⁰⁾, ⁽¹⁴⁾ and ⁽¹⁾. In ⁽¹⁾ the errors on $p\beta$ are larger than in ⁽¹⁰⁾ and ⁽¹⁴⁾ since they were recalculated by use of the relations employed in this paper.

20 particles heavier than the π -meson and decaying at rest were found in the total volume explored, i.e. 56 cm³ in stack 31 and 16 cm³ in stack 9. Of these, 16 were K_L , 2 were SY_L and 2 were unidentified.

a) *Primaries.* — The mass of all the primaries was determined by the Constant Sagitta Method using as calibration the measurements on flat slow protons referred to above ⁽⁵⁾. The same standard cell set was used as in these calibration measurements and the correction factors recalculated by ⁽⁵⁾ on the basis of the latest range energy relation ⁽¹⁵⁾. The results on dipping tracks can be considered only as indicative, even when the normal correction for dip is applied, unless a calibration on tracks of the same inclination is made ⁽⁸⁾. The results of mass measurements on those primaries whose secondaries were suitable for measurement (see later), are given in Table IIa. Two values, obtained on very dipping tracks (K_{21} and K_{22}), lie somewhat far from the mean value. That of K_{22} leaves in doubt whether the particle is a μ -meson or a K-particle, but this doubt is resolved by measurements of $p\beta$ of the secondary, which gives a value well above the maximum for the μ -e decay. K_{22} could be a hyperon: the ratio of probability P_K/P_Y is about 5 on the basis of our statistics ⁽¹⁶⁾. Provisionally we leave it in the group of K-particles.

⁽¹⁴⁾ Report of the Committee on K-mesons, in *Suppl. Nuovo Cimento*, 12, 433 (1954).

⁽¹⁵⁾ G. BARONI *et al.*: Bureau of Standard CERN, Bull. no. 9.

⁽¹⁶⁾ C. C. DILWORTH, G. GOLDSACK and L. HIRSCHBERG: *Nuovo Cimento*, 11, 113 (1954).

b) *Secondaries*. — We followed and measured the 8 tracks which had an angle of dip less than 20° . On a total length of about 39 cm no interaction was found. The results on $p\beta$ and g^* are given in Table IIb and Fig. 1a, b. The $p\beta$ values from second and third differences are given in the table, columns 15 and 16 respectively, to give an idea of the order of magnitude of the effect of distortion. The values of g^* both for K_9 and K_{12} lie significantly above the plateau, and a consistent increase of g^* and decrease of $p\beta$ was observed as measurements progressed along the track away from the decay point. This is indicated in Fig. 1 and Table III, in which are given the results on successive sections of the tracks.

TABLE III. — *Secondaries of K_9 and K_{12} .*

Particle	Partial Length (mm)	g^*	$(p\beta)'''$ (MeV/c)	Mass (m_e)
K_9	0-20	$1.13 \pm .020$	161 ± 23	282 ± 41
	20-45	$1.15 \pm .018$	150 ± 22	273 ± 41
K_{12}	0-11.8	1.17 ± 0.30	145 ± 25	227 ± 41
	11.8-26.3	1.25 ± 0.30	129 ± 18	228 ± 33
	26.3-42.0	1.29 ± 0.30	111 ± 14	214 ± 28

The points representing the two secondaries fall in a region in which it is still possible to try to determine on a single track whether the particle is a π^- or a μ^- -meson (⁹).

The value of the mass obtained from the mean $p\beta$ and g^* for the whole track is $(278 \pm 31) m_e$ for the secondary of K_9 .

From this value and from the internal consistency of the measurements shown in Fig. 1b and Table III we are led to identify this particle with a π^- -meson: the identification is further supported by the fact that the corresponding point is bracketed by those of three hyperon secondaries. Taking into account the energy loss along the track, the $p\beta$ of emission turns out to be (174 ± 16) MeV/c.

In the same way (Fig. 1a and Table III), we obtain a value of $(222 \pm 23) m_e$ for the mass of the secondary of K_{12} . If we identify this particle with a μ^- -meson, we find a $p\beta$ of emission of (144 ± 12) MeV/c.

The g^* 's corresponding to the other 6 secondaries are in the region of the plateau. There is no detectable variation of either the blob density or the mean angle of scattering along these tracks. They appear to form a group characterized by:

- i) g^* close to 1,
- ii) $p\beta$ lying between 170 and 200 MeV/c.

In these conditions and on this evidence alone, the identification of the particles is difficult if not impossible, as stressed by ⁽¹⁰⁾. On the other hand the absence of detectable energy losses of radiative origin in the 5 tracks longer than 4 cm implies that the presence of electrons in this group is very improbable. Similarly the absence of interactions on a total length of about 29 cm makes it unlikely that the 6 particles should be all π -mesons. So, either these particles do not form a unique group, or they are probably μ -mesons. We calculated the $p\beta$ at emission on the second assumption. (Table IIb, column 18). As seen in Fig. 2, these values of $p\beta$ lie even closer together, in fact in such

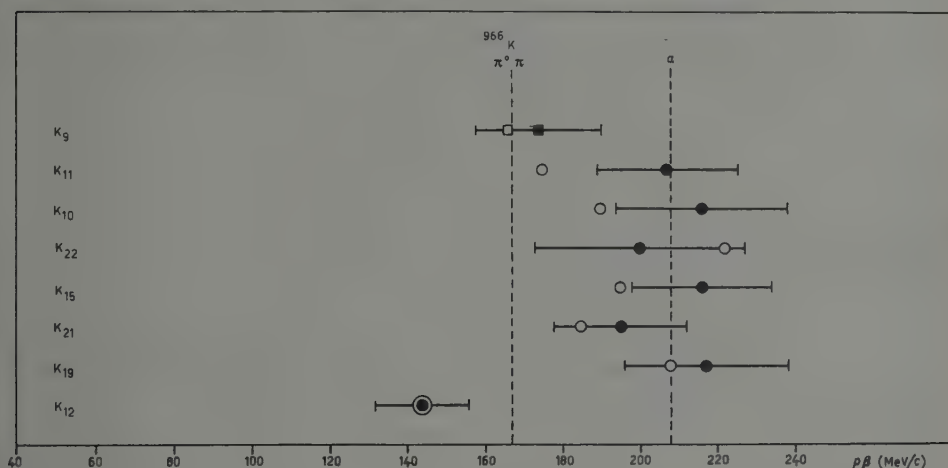


Fig. 2. - $p\beta$ of emission of the secondaries of K-mesons. Full circles: values from third differences. Empty circles: values from second differences.

α indicates the mean $p\beta$ of the group of low ionization secondaries.

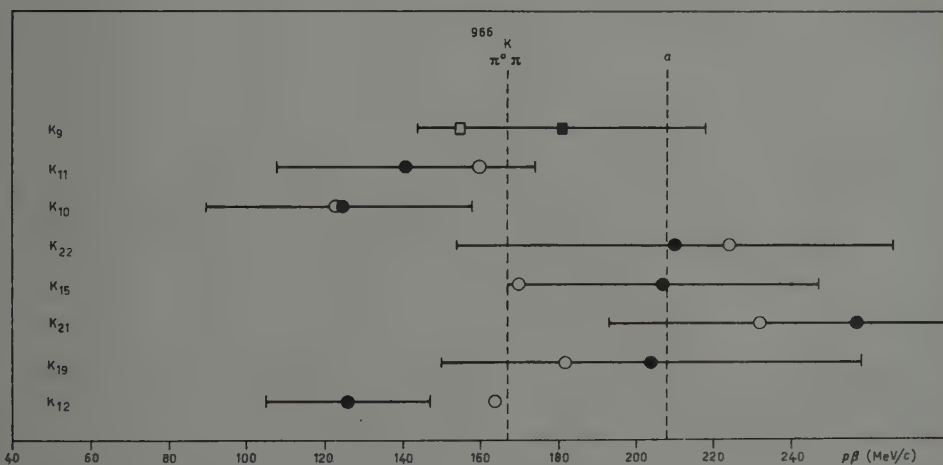


Fig. 3. - $p\beta$ of the secondaries of K-mesons on the first 4-6 mm of track from the decay. Full circles: values from third differences. Empty circles: values from second differences.

α : see Fig. 2.

a way as to suggest that they are products of a two-body decay. The mean value of the $p\beta$ of emission is (208 ± 8) MeV/c. (If we take out from the group the secondary of K_{22} on account of the doubts as to the nature of its primary ((section 3a), we find a mean $p\beta$ of (209 ± 9) MeV/c).

4. - Discussions and Conclusions.

a) From the $p\beta$ of emission $((174 \pm 16)$ MeV/c) of the π -meson arising from the decay of K_9 , we are led to the conclusion that this particle is probably a χ -meson ⁽¹⁷⁾, which decays following the scheme

$$\chi \rightarrow \pi + \pi_0.$$

The possibility of its being a hyperon Y_L decaying at rest is ruled out by the value of the primary mass.

b) The properties of the group of 6 secondaries of low ionisation and high $p\beta$ are similar to those of the K_μ -meson, whose existence, proposed by E. P. ⁽¹⁸⁾, has been confirmed by E.P. ⁽¹⁹⁾ and M.I.T. ⁽²⁰⁾.

On the basis of the two body decay scheme

$$K_\mu \rightarrow \mu + \nu,$$

the mass of the primary deduced from our mean $p\beta$ is $(943 \pm 23) m_e$ (or $(945 \pm 25) m_e$ excluding K_{22}), in good agreement with those found by E.P. and M.I.T..

c) The secondary of K_{12} is very probably a μ -meson. Its $p\beta$ of emission $((144 \pm 12)$ MeV/c) is such as to exclude K_{12} from the group of K_μ 's. It seems to enter into the class of κ -mesons ⁽²¹⁾.

d) The relative frequencies of χ -, K_μ - and κ -mesons in emulsions re-

⁽¹⁷⁾ M. G. K. MENON and C. O'CEALLAIGH: *Proc. Roy. Soc.*, **221**, 292 (1954).

⁽¹⁸⁾ R. ARMENTEROS, B. GREGORY, A. LAGARRIGUE, L. LEPRINCE-RINGUET, F. MULLER and C. PEYROU: *Nuovo Cimento*, **11**, 242 (1954).

⁽¹⁹⁾ ÉCOLE POLYTECHNIQUE GROUP - *Rochester Conference* (1955)

⁽²⁰⁾ M.I.T. GROUP: *Rochester Conference* (1955).

⁽²¹⁾ C. O'CEALLAIGH: *Phil. Mag.*, **32**, 1033 (1951).

present a problem which is difficult to solve given the diverse conditions under which the measurements have been made in the various laboratories. Our statistics alone is of course too small to allow us to give an answer.

We seem to have a preponderance of low ionisation secondaries, which might be accounted for by the excellent condition of the plates of stack 31. This stack, developed by the Group of Rome, had a high grain density at the minimum and was very transparent, so that low ionisation secondaries were easily detected.

The material which we obtained here has been examined together with our colleagues C. C. DILWORTH and L. SCARSI, and we have used it to look for some of the possible causes, in scattering measurements, of blurring or displacement of a line spectrum at high energies. Such causes are e. g.:

1) The precision of measurements may be exaggerated by the use of an incorrect formula for the calculation of the error (see (3)).

2) Overconfidence in the lack of distortion of plates might be responsible for a lowering and a spread of the $p\beta$ values. Such an effect is illustrated in Fig. 2 in which the empty circles represent our $p\beta$ values not corrected for distortion. Also, ignorance of distortion leads to an underestimate of the error.

3) Measurements on short tracks with their correspondingly high statistical errors will certainly tend to spread a line. We tried to get an idea of the magnitude of this effect by calculating the $p\beta$ of the tracks of Table II *b* from the measurements of the first 4 to 6 mm of secondary from the decay point. The results are given in Fig. 3 which can be compared with Fig. 2: the increased dispersion tends to blur the evidence for a line spectrum.

Such sources of ambiguity in measurements as those outlined above might have led to an underestimate of the number of high energy K_μ -secondaries in nuclear emulsions.

* * *

We are very grateful to our colleagues and in particular to C. C. DILWORTH and L. SCARSI who gave a substantial contribution to the discussion of these results.

We wish to express our sincere gratitude to Prof. G. P. S. OCCHIALINI who directed and criticized our work.

RIASSUNTO

Si presentano i risultati di misure su secondari di mesoni K trovati nei pacchi di emulsioni pellicolate esposte ad alta quota in Sardegna nel 1953. Tra gli 8 secondari uno è stato identificato come un mesone π , uno come mesone μ e gli altri 6 formano un gruppo avente ionizzazione vicina al plateau e $p\beta$ intorno a 200 MeV/c. La particella K avente come secondario un mesone π si può attribuire al tipo χ , quella avente come secondario un mesone μ identificato, appartiene probabilmente al tipo κ . Gli altri 6 secondari si possono interpretare come i prodotti della disintegrazione del mesone K_μ e dal loro $p\beta$ medio si può determinare la massa di questa particella. Nel corso del lavoro vengono discussi criticamente i metodi di misura e alcune possibilità di errore e ambiguità.

Further Discussion of the K_μ Decay Mode (*).

R. ARMENTEROS, B. GREGORY, A. HENDEL (+), A. LAGARRIGUE,
L. LEPRINCE-RINGUET, F. MULLER and C. PEYROU (×)

Laboratoire de Physique, École Polytechnique - Paris.

(ricevuto il 12 Aprile 1955)

Summary. — After a description of the methods used in the measurements of momentum and range, the data on 46 S-events obtained with a double cloud-chamber experiment are examined. Momentum-range measurements on 22 positive S's give a mass consistent with a single value at $(928 \pm 13) m_e$. The analysis of the ranges of the secondaries shows, however, that not all S-events can be explained by a single decay mode. A large proportion of the secondaries correspond to a light meson of unique range $(75.7 \pm 1.7) g \cdot cm^{-2} Cu$. The comparison of this range with the measured masses of the primary particles proves that these secondaries are μ -mesons. The accompanying neutral secondary is shown at the same time to be a particle of zero mass. The absence of cascade showers associated with S-events with long-range secondaries shows that the neutral secondary is a neutrino. The decay mode $K_\mu \rightarrow \mu + \nu$ previously proposed is more firmly established. Two independent mass estimates are obtained for the K_μ -particle. One—from momentum-range measurements—gives directly $(906 \pm 27) m_e$. Another—from the mode of decay and the range of the μ -secondary—gives indirectly $(941 \pm 11) m_e$. A final best mass of $(935 \pm 15) m_e$ is obtained by the combination of the two estimates after taking into account possible additional errors. The K_μ -particle is then shown to be essentially positive and to constitute $(66 \pm 18)\%$ of the S's which passed through the top chamber. No precise information can be obtained as to the mode of decay of S-particles which are known not to belong to the K_μ -decay mode.

(*) The cost of the experiment has been shared by le Commissariat à l'Energie Atomique and l'Enseignement Supérieur.

(+) On leave of absence from the C.B.P.F. (Brazil).

(×) Now at Berne University.

Introduction.

In this article we report the results of a study of S-events made with the double cloud-chamber arrangement operating at the Pic du Midi.

The 45 events whose analysis we now publish have been obtained in the scanning of approximately 38 000 photographs. Some of them have been presented either in an article published in *Nuovo Cimento* (GREGORY *et al.*, 1953) or at the Padua Conference (1954). We will refer to these two publications as N and P, respectively.

The apparatus has already been briefly described in N. Events with reference numbers below 20 000 were obtained with a plate assembly consisting of 9 lead and 6 graphite plates. For all other events, the multiplate chamber contained 15 copper plates of 1 cm thickness each.

29 of the S-particles passed through the top chamber. Their signs were therefore known and their masses could be measured. Each of these particles lived for about $5 \cdot 10^{-9}$ s before being brought to rest.

The remaining 16 particles were produced either inside the multiplate chamber or in the material in its neighbourhood. We will refer to them as «locally produced S-particles». Their sign and mass are not known. On the average these particles lived for about $2 \cdot 10^{-9}$ s before coming to rest.

In order to recognize it as the decay of a heavy particle, an S-event should be clearly different from a $\pi \rightarrow \mu \rightarrow e$ decay. For locally produced S's this separation can, in general, only be made if the secondary traverses at least two plates without multiplication. For S-events with measured primary mass, this restriction is not necessary; this class can, therefore, include S's with short-range secondaries and even without a visible secondary.

1. — Measurements and Errors.

Essentially, two sets of measurements are made on S-particles; one leading to the mass of the primary, the other to the range of the secondary.

For the mass-measurement, the momentum and the range of the primary have to be known.

1.1. Momentum Determination. — All curvature measurements have been made by fitting circular arcs of known curvature to nearly full size projections of the views obtained by 3 cameras. The usual corrections were then applied to obtain the actual curvature in space of the particle.

Three sources of non-systematic error have been considered in the curvature measurements:

- i) multiple scattering in the gas filling the cloud-chamber (argon at a total pressure of 70 cm Hg in our experiment);
- ii) inaccuracy in the fitting of the standard circles to the track, and
- iii) random chamber distortions.

The result of i) can be calculated (BETHE, 1946). For an individual trajectory the influence of ii) can be estimated in the measuring operation and depends on the length and quality of the track. To determine statistically the influence of ii) and iii) measurements were made on tracks which appeared due to protons. These 52 tracks were selected in photographs taken from the same runs in which S-particles had been observed. The individual masses obtained for the 52 particles are displayed in Fig. 1.

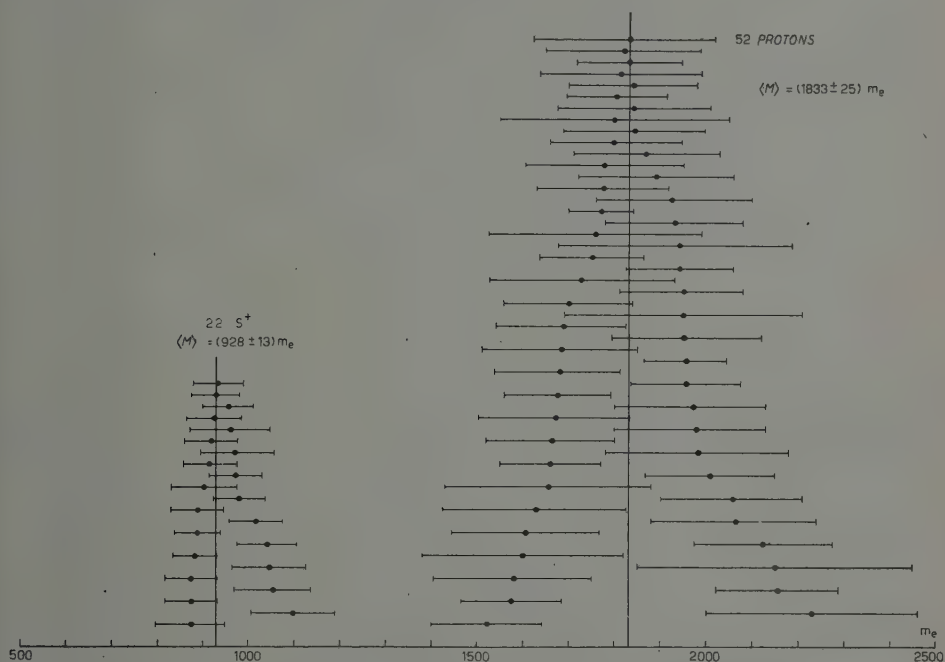


Fig. 1. — The measured masses of 52 protons and 22 S-events are individually displayed in this diagram.

The mean mass in $(1833 \pm 25) m_e$. From the dispersion of the masses and after correcting for the known effect of the multiple scattering and for the error in mass introduced by the uncertainty in the individual ranges, we have arrived at the result that the 'spurious sagitta due to ii) and iii) has a r.m.s. deviation of 15/100 mm. This corresponds to a M.D.M. of 15 GeV/c for track-lengths of the order of 48 cm. The magnetic field was of the order of 25 000 gauss.

On the average, the primaries of the S-events we have measured had the same value of P/M as the calibration protons. If, as it was generally the case, the length and quality of the track were similar to those of the calibration protons, the error in its sagitta was obtained by combining quadratically the error due to multiple scattering and the 15/100 mm found for the minimum detectable sagitta. In seven examples the primary track appeared in the top chamber under conditions such that we could not use the reference protons to estimate the precision of the measurement. The average sagitta of these seven trajectories was, nevertheless, sufficiently large (2-3 mm) to decide quite unambiguously on the signs of the corresponding particles.

In the measurement of mass by far the largest error came from the momentum determination. The error in range made only a small contribution especially when, as it most frequently happened, the stopping point could be well determined. To find the error in the mass the errors due to the measurements of momentum and range were added quadratically.

Systematic errors are also possible. They could arise from:

- i) the calibration of the magnetic field,
- ii) systematic distortion in the cloud-chamber (as we shall see later most of the S-particles we have observed are positive),
- iii) uncertainty in the range-momentum relation used (*).

The influence of these errors will be discussed later (see § 4).

1.2. *Range Measurements.* — The estimation of the amount of matter traversed by a particle in a plate chamber appears at first sight as a simple geometrical problem. Its exact solution, however, is not straightforward since the scattering of the particles has to be considered besides the errors in the reconstruction of the paths. We will now describe qualitatively the way we have solved this problem. The analytical treatment is explained in Appendix II.

On a given secondary we define three quantities:

R_1 — or *minimum range* — is the amount of matter it traverses before disappearing,

R_3 — or *available range* — is the amount of matter it would have traversed before leaving the illuminated volume of the chamber.

If R_1 and R_3 do not coincide, this means that the particle stopped in one of the plates. In this case we define a quantity R_2 given by $R_2 = R_1 + (h/\cos \vartheta)$.

(*) Throughout this paper we have used the Marvin Rich and Richard Madey Range-Energy tables (1954).

$(1 + k^2)$ (h being the thickness of the plate, ϑ the angle with the normal at which the particle entered it and k^2 a correction factor due to Coulomb scattering (*) at the end of the range and which is of the order of 4% for μ -mesons in copper). We call R_2 the *maximum range* of the particle since it would correspond to the case in which the particle stopped at the bottom of the plate.

R_1 , R_2 and R_3 are geometrical quantities. What we are interested in obtaining, however, is the *actual range*, R , of the secondary, since this is the quantity that corresponds to the momentum of the particle at emission. If the particle stops, the actual range, R , can be obtained from the two values R_1 and R_2 . Before we can find the best value of R and its error we have to analyse the errors in R_1 and R_2 .

Errors in R_1 arise from:

a) spatial reconstruction;

b) the location of the decay point (this depends mainly on the precision in the determination of the angle between the primary and secondary particles and also on their scattering). To a very good approximation this error has a Gaussian distribution.

c) the uncertainty, due to Coulomb scattering, about the actual path followed by the particle in the plate traversals.

d) range straggling (+).

For each observed secondary, R_1 was measured in a uniform way which involved only the knowledge of the angles at which the particle entered and left each plate. The error in the measurement of angles was determined statistically from the precision with which the position of a track could be localized in the spaces between the plates.

The error in R_1 is, of course, transferred to R_2 , but it is clear that R_2 is not an absolute maximum of the range of the particle. Because of the effect of multiple scattering at the end of the range, R_2 has fluctuations which are independent of those in R_1 . The problem then is to combine R_1 and R_2 with all their uncertainties to obtain the range, R , of the particle and its error.

In the absence of errors in R_1 and of multiple scattering in the last plate, each range would be distributed with equal probability between R_1 and R_2 (×).

(*) Coulomb scattering introduces not only fluctuations in range but also increases slightly the geometrically measured values of R_2 .

(+) This was taken as 3%. Strictly, the straggling should only be included when we transform range into momentum, once we have assumed or determined the mass of the particle. We have, however, included it for convenience in the total error of R_1 .

(×) We assume that for any R , all values of R_1 are *a priori* equally probable. This assumption is justified for our events in Appendix II.

If we first take into account the scattering in the last plate the probability distribution will have a «tail» beyond R_2 . The distribution of R is finally obtained by combining with this new probability law the errors in R_1 . It turns out that for angles ϑ less than 45° the errors in R_1 are predominant while for angles greater than 45° the «tail» effect begins to be appreciable.

Typical R -distributions are shown in Fig. 2 where they are compared both to the corresponding rectangular distribution and the best adapted Gaussian.

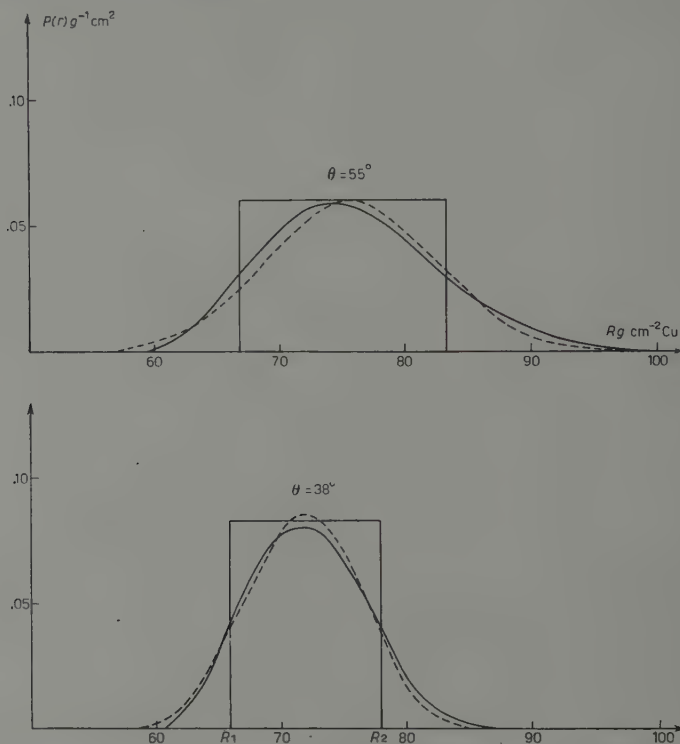


Fig. 2. - Two typical distributions of R are given for angles, ϑ , of entry into the last plate of 38 and 55 degrees. The bold bell-shaped curves are the actually calculated distributions. The broken curves are the gaussians best adapted to the calculated curves. The rectangular distributions, with limits at R_1 and R_2 , are also shown.

2. - Results.

In the following sections we will take up and develop the arguments already put forward in N and P. The increased statistics will be shown to confirm the conclusions then reached. Namely, that a large proportion of our S-events are most satisfactorily explained in terms of a K-particle decaying into a μ -meson and a neutrino. This particle was called K_μ . We shall show at the same time that not all S-events can be explained in the same way.

2.1. *Measured Masses.* — Meaningful measurements of mass were possible on 24 of the 29 primaries which passed through the top chamber. Their individual masses and signs are given in Table I; of the 29 particles, 27 were positive and 2 negative. This remarkable charge asymmetry will be discussed in § 6. Until then the analysis will not take into account the 2 negative particles.

TABLE I. — *General results on S-events.*

The measurements on the 46 S-events are summarized in this table.

The event have been divided into 3 groups. Group A contains 27 events with positive primaries. Group B consists of 16 events locally produced, i.e. events whose primaries did not pass through the top chamber. Group C is composed of 2 negative S-events.

The angle θ^* is the angle at which the secondary was emitted with respect to the direction of the primary.

The quantities R_1 , R_2 , R_3 are defined in § 1.2 and also in Appendix II. They represent respectively the minimum, the maximum and the available ranges of the secondaries. ΔR_1 is the error in R_1 .

I/I_n indicates the estimated ionisation of the secondary in the last interval in which it was seen.

θ is the angle with respect to the normal at which the secondary entered the plate in which it stopped.

In the column 'Presence of γ -rays', the observation of cascade showers produced by γ -rays which were probably associated with some of the S-events is indicated. When they were observed, the figures in the brackets indicate the number of electrons which constituted the shower in successive plates.

The last column indicated the successive amounts of matter (in radiation lengths) after which the materialization of a γ -ray could have been observed if emitted in a direction opposite to that of the charged secondary. The angle between the γ -ray and the charged secondary is also indicated in this column.

ϵ denotes a very small quantity. In the column R_3 it means that although the secondary would have been seen in the next interval, its direction was such that it would not have crossed the next plate.

For group B the type of interaction in which the S-particle was produced is shown. The symbol before the arrow indicates the charge of the particle which produced the interaction. The particles which were observed to come out of the interaction are indicated within the brackets. When the S-particle originated outside the chamber its possible origin is indicated.

Note. — For some events, slight differences will be noted between the data now given and those already published. There are three reasons for this:

a) A new measurement of the mean thickness of each plate has shown a defect of nearly 3% in the values previously assumed.

b) The energy-range tables of RICH and MADEY (1954) are now used instead of those given in ARON's Thesis (1951).

c) The transformation of the geometrical measurements into range measurements was not properly understood at the time. The treatment described in Appendix II has been developed since.

TABLE I (continued)

GROUP A: Positive S's.

Event N.	Primary Mass (m _c)	θ^* (Deg.)	R_1	ΔR_1 (g·cm ⁻² Cu)	R_2	I/I_0	θ (Deg.)	R_3 (g·cm ⁻² Cu)	Presence of γ -rays	Possible Observation of γ -rays (Radiation length)
16192	888 ± 57	95	8.66	1.9	41.4	1	79	ϵ	—	ϵ
16197	916 ± 58	85	28	3	—	1	—	—	—	4.5
16307	979 ± 57	50	8.4	+1.5 -1.0	12.6	> 2	30	ϵ	—	2.3/
16569	874 ± 57	—	—	—	—	—	—	—	—	0/
18094	1040 ± 65	55	40	3.5	—	—	—	—	—	1.0/2.5
18805	928 ± 53	45	7.3	1.9	15.5	> 4	38	28.3	—	2.6
19231	872 ± 76	45	50.6	2.25	—	1	—	—	—	0.7
22964	902 ± 73	65	56.9	3.5	—	1	—	—	(3e)(2e)(1e)	—
23473	955 ± 56	—	0	—	—	—	—	—	—	—
25679	970 ± 75	—	—	—	—	—	—	—	—	—
25845	—	180	70.9	2.8	81.15	1	22	100.95	—	0.5
25933	882 ± 47 (1)	85	28.8	3.3	—	1	—	—	—	—
26320	917 ± 58 (2)	25	59.8	—	—	1	—	—	—	0.5(1.2/1.9/2.6/
27170	933 ± 54	100	54.5	5	—	1	—	—	—	3.8/
28222	1052 ± 84	40	14.4	1.8	—	1	—	—	—	0.6(1.4/2.1/2.9/3.7/etc.
30174	925 ± 59	60	12.6	1.7	37.8	1	69	112.8	Possible	—
30248	—	180	66.0	2.8	78.0	1	38	101.1	—	0.15/0.9/1.7/2.5/3.3/4.1/
30433	—	80	37.9	3.8	—	1	—	—	—	1.6/4.0/6.1/
32232	888 ± 50	90	ϵ	—	—	—	—	—	—	—
32515	1045 ± 80	45	40.28	2.5	—	1	—	—	—	0.2(1.3/2.5/
39306	—	150	8.7	1.1	20.6	1	40	56.6	(6e)(5e)(1e)	~ 155°
40804	1096 ± 91	90	36.1	2.4	—	> 1	—	—	(4e)	~ 180°
40823	—	135	16.1	1.5	—	1	—	—	—	0.7(1.7/2.6/
42868	959 ± 87	180	46.85	3.1	—	1	—	—	—	1.4/2.9/
46348	971 ± 58	135	30.74	1.54	—	1	—	—	(5e)	~ 110°
47644	1016 ± 58	180	31.93	2.37	—	1	—	—	—	4.7/6.0/
48813	874 ± 57	80	48.5	3.4	76.5	1	71	131.5	—	ϵ

(1) This event appeared as decay of a very slow charged V-particle.

(2) Only one photograph was available for the last part of the secondary of this event.

Event N.	Nature and Products of Interaction	θ^* (Deg.)	R_1 ($\text{g}\cdot\text{cm}^{-2}$ Cu)		I/I_0	θ (Deg.)	R_3 ($\text{g}\cdot\text{cm}^{-2}$ Cu)	Presence of γ -rays	Possible Observation of γ -rays (Radiation length)
			R_1	ΔR_1					
17804	$0 \rightarrow (2\text{pp}, \text{S})$	30	47.61	1.9	—	—	—	—	1.45/2.9/
21073	Coil	150	61.5	2.5	71.6	20	100.68	—	0.4/1.15/1.9/2.7/
21162	$+ \rightarrow (\text{lpp}, 3\gamma, \text{S})^1$	30	43.2	3.6	$\begin{cases} > \\ < \end{cases} \begin{matrix} 1 \\ 10 \end{matrix}$	—	—	—	0.18/
21242	$\pm \rightarrow (3\text{pp}, 2\text{P}, 2\gamma, \text{V})^{(1)}$	76	63.3	2.4	—	—	—	—	1.4/2.8/4.1/
22854	— ⁽¹⁾	102	17.3	1.0	—	—	—	—	1.3/
27924	$+ \rightarrow (\text{lpp}, \text{S})$	30	53.67	2.2	—	—	—	—	0.6/1.4/2.2/
28093	Coil	120	30.84	2.1	—	—	—	—	1.5/3.7/6/8.3/etc.
29321	$+ \rightarrow (\text{lP}, \text{S})$	90	41.35	2.5	—	—	—	—	0.9/2.3/3.7/5/
38275	Coil	63	66.8	3.7	83.3	55	141.0	—	1.4/
38797	Between Chambers	120	64.6	4.2	84.2	61	ε	—	2.24/
40359	$- \rightarrow (\text{V}, \text{S})$	135	27.6	1.3	—	—	—	—	1.5/2.5/3.8/
40896	$\pm \rightarrow (4\text{pp}, 2\gamma)$	160	75.7	3.0	$\begin{cases} > 1 \\ < 3 \end{cases}$	12	135.6	—	0.4/1.1/
	$\text{pp} \rightarrow (\text{P}, \Lambda^0, \text{S})$	—	94.7	3.5	105.6	29.5	—	—	—
41676	$- \rightarrow (\text{lpp}, \gamma, \Lambda^0, \text{S})$	50	41.1	2.0	—	—	—	—	0.05/1.1/2.3/3.4/4.5/
43599	$\pm \rightarrow (\text{lpp}, \Lambda^0)$	155	72.36	2.4	—	—	—	—	0.75/1.5/2.4/3.1/4/etc.
	$\text{pp} \rightarrow (\text{S})$								
47066	$+ \rightarrow (\text{S})$	45	73.3	3.1	$\begin{cases} > 1 \\ < 3 \end{cases}$	37	108.2	—	0.02/1.0/
47438	Coil	48	68.5	3.4	83.6	51	—	—	1.4/3/

GROUP C: Negative S's.

Event N.	Primary Mass (m.)	θ^* (Deg.)	R_1 ($\text{g}\cdot\text{cm}^{-2}$ Cu)		I/I_0	θ (Deg.)	R_3 ($\text{g}\cdot\text{cm}^{-2}$ Cu)	Presence of γ -rays	Possible Observation of γ -rays (radiation length)
			R_1	ΔR_1					
26945	1240 ± 87	—	—	—	—	—	—	—	—
41930	1050 ± 69	45	11.47	—	22.94	38	80.29	(2e)(1e)	0.88/1.76/2.64/3.52/4.4/

⁽¹⁾ This event appeared as decay of a very slow, charged V-particle.

In Fig. 1 the individual masses and errors of the 22 positive particles are displayed.

The weighted mean mass is $(928 \pm 13 (\pm 14)) m_e$, where the two errors (without and within brackets), have been obtained respectively from the individual calculated errors (see 1.1) and from the distribution of the masses about the mean value. The agreement between the two errors shows that the results are compatible with a unique mass. It is possible, however, that the results represent an admixture of several particles with masses close together and/or particles with fairly dissimilar masses. If the latter is true, then one of the particles must be predominantly abundant. Thus, for instance, if particles of mass $1050 m_e$ contribute, their proportion cannot be greater than those indicated below for different levels of probability.

TABLE II. — *Proportion of particles of mass $1050 m_e$.*

N. S's of Mass = $1050 m_e$	Upper limit of Probability level
N. S's of Measured Mass	
27%	1%
18%	5%
11%	16%

No more information can be derived from mass considerations alone about the possible decay schemes applying to S-particles. To proceed with the analysis, the ranges of the secondaries are next considered.

§ 2.2. *Secondary Ranges.* — The results of the range measurements are given in Table I and shown graphically in Fig. 3. The S-events have been separated into 2 groups. The first group consists of 29 positive K-particles and the second of 16 locally produced S-particles. We shall refer to these two groups as *A* and *B* respectively, in what follows.

The results show clearly several interesting features:

The proportion of long-range secondaries is apparently greater for the locally produced S's than for those which passed through the top chamber. Indeed no secondaries with ranges in the vicinity of $20 \text{ g} \cdot \text{cm}^{-2} \text{ Cu}$ have been observed amongst locally produced S's. This is probably due to the observational bias mentioned in the Introduction. None of the short range secondaries in Group *A* traversed 2 plates, therefore similar events which should appear in Group *B* have most probably been missed or not identified unambiguously.

The second and most important feature, however, is the non-random distribution of the stopping points. Restricting ourselves to the more accurately

known ranges, say those for which the average plate traversals corresponded to less than $20 \text{ g}\cdot\text{cm}^{-2} \text{ Cu}$, we notice (see Fig. 3) that three secondaries stopped at about $12 \text{ g}\cdot\text{cm}^{-2} \text{ Cu}$, one at about $43 \text{ g}\cdot\text{cm}^{-2} \text{ Cu}$ and 8 at about $75 \text{ g}\cdot\text{cm}^{-2} \text{ Cu}$.

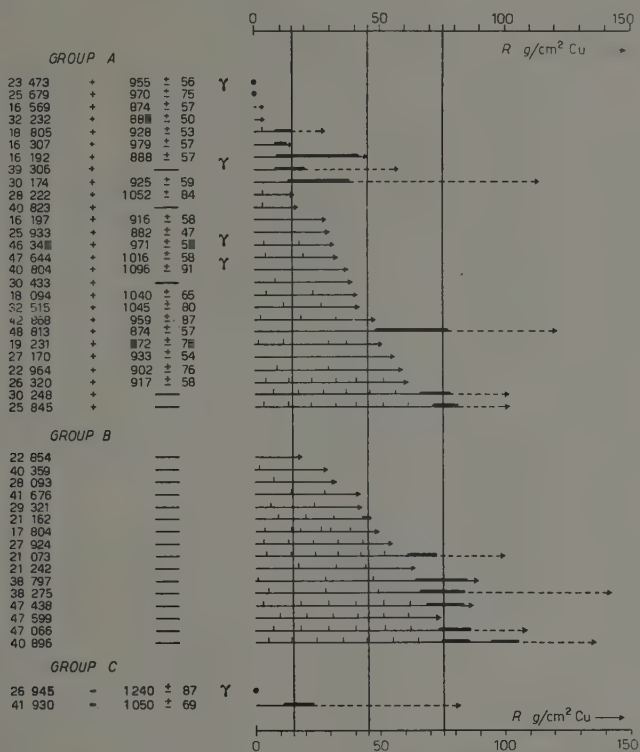


Fig. 3. — In this diagram the information about the ranges of the secondary particles is displayed. The events have been divided into three groups. The positive S's constitute group A, in group B appear the S's locally produced, while group C contains the negative events. The solid lines indicate the amount of matter traversed by the secondary before it disappeared. The dotted lines indicate the available range, R_3 . If the secondary disappeared because it left the illuminated region, the solid line is terminated by an arrow and, of course, $R_1 = R_3$. On the other hand, when the secondary stopped in a plate, the solid line has been made bolder between the two limits R_1 and R_2 . In each case the observed ranges are divided into segments which correspond to the ranges in the different plates traversed. The observation of γ -rays possibly associated with the stopping of S-particles is also indicated.

This distribution is hardly compatible with a spectrum of a single particle, especially, if we take into account the geometrical bias that discriminates strongly against the observation of high ranges. Ranges below $20 \text{ g}\cdot\text{cm}^{-2} \text{ Cu}$ could correspond to secondaries of known particles (τ or κ). We will therefore study the form of the spectrum that can be adapted to the observations above

20 g·cm⁻² Cu. This is done by an analysis which, to take into account the effect of the geometrical bias, considers the distribution of stopping points along the available ranges. If we represent the hypothetical range spectrum above 20 g·cm⁻² Cu by:

$$\begin{aligned} f(R) dR &= (\gamma + 1) \frac{R^\gamma}{R^{\gamma+1}} dR && \text{for } R < R' \\ f(R) dR &= 0 && \text{for } R > R' \end{aligned}$$

and set the upper limit, R' , of the range at 85 g·cm⁻² Cu, we find that there is only a 10% chance of observing only one stopping secondary at less than 60 g·cm⁻² Cu if the exponent γ be 2.7. We can, therefore, state that the results are barely in agreement with a spectrum rising as $R^{2.7}$ between 20 and 85 g·cm⁻² Cu. In terms of momentum this means that the spectrum of the secondaries would have to be sharper than $P^{5.5}$ between roughly 130 and 240 MeV/c. This seems a most implausible form of spectrum and we are forced to conclude that all events with $R > 60$ g·cm⁻² Cu correspond to secondaries of unique range. This conclusion — which is further verified in the next section — confirms the need for at least two different decay schemes to explain our observations. In § 5 it will be shown that from our results alone not very precise conclusions can be reached as to the decay scheme(s) applying to the secondaries whose ranges do not fit the unique value just indicated.

2.3. *Study of the Long Secondary Ranges.* — In 1.2 and in Appendix II, it is shown how the stopping of a particle constitutes a measurement of its range with a given probability distribution. These probability distributions can be used to see if all measurements above 60 g·cm⁻² Cu are consistent with a unique range. This will clearly not be the case if for event 40896 (*) we take the higher of the two possible limits of range. Taking for this event the lower limits, we obtain for the weighted mean value of the 9 events stopping above 60 g·cm⁻² Cu, and whose individual data are shown in Table III:

$$\langle R \rangle = (74.4 \pm 1.7) \text{ g·cm}^{-2} \text{ Cu.}$$

If we exclude event 40896, the best value is:

$$\langle R \rangle = (73.4 \pm 1.9) \text{ g·cm}^{-2} \text{ Cu.}$$

The quoted errors are the standard deviations deduced from the errors in the individual ranges. The standard deviations derived from the dispersion

(*) In this case it is possible, if not probable, that a decay electron extended the range of the secondary (see Appendix I).

TABLE III. - *Data on the 9 secondary particles constituting the long-range group.*

Event N.	R_1	ΔR_1 ($\text{g}\cdot\text{cm}^{-2}$ Cu)	R_2	ϑ (Deg.)	R ($\text{g}\cdot\text{cm}^{-2}$ Cu)	p for μ -meson (MeV/c)
21073	61.5	2.5	71.6	20	66.55+ 3.9	213.6+ 6.5
25845	70.9	2.8	81.15	22	76.0 + 4.1	229.4+ 6.8
30248	66.0	2.8	78.05	38	72.0 + 4.7	222.7+ 7.8
38275	66.8	3.7	83.3	55	75.6 + 6.8	227.3+11.3
38797	64.6	4.2	84.2	61	75.6 + 8.5	227.3+14.1
40896	75.7	3.0	85.4	12	80.55+ 4.1	237.0+ 6.8
	94.7	3.5	105.6	30	100.15+ 4.7	—
47066	73.3	3.1	85.2	37	79.25+ 4.8	235.1+ 8.0
47438	68.5	3.4	83.6	51	76.35+ 6.1	229.9+10.2
48813	48.5	3.4	76.5	71	67.2 +13.8	214.7+ 2.3

R_1 , R_2 (the minimum and maximum ranges), and ϑ (angle at which the secondary enters the last plate) have been defined in 1'2. How R (the best value of the range) is calculated from these is shown in Appendix II.

of the ranges about the mean are $1.7 \text{ g}\cdot\text{cm}^{-2}$ Cu and $1.6 \text{ g}\cdot\text{cm}^{-2}$ Cu respectively, which shows the compatibility of these results with a unique range.

In these evaluations no account has been taken of the ionization of the secondaries in the interval before the plate in which they stopped. For a sufficiently large sample this additional information would not increase the precision of the best range estimate. For our small sample, however, the fact that none of the secondaries has an ionization estimated at above three times the minimum can usefully be taken into account. In each of the nine cases, the minimum values of the ranges, R_1 , have to be increased by $2 \text{ g}\cdot\text{cm}^{-2}$ Cu. As a result the mean value of the range increases to $(75.7 \pm 1.7) \text{ g}\cdot\text{cm}^{-2}$ Cu.

We can, therefore, conclude that the best interpretation of our results is provided by the existence of an S-particle which undergoes a two-body decay emitting a secondary of range $(75.7 \pm 1.7) \text{ g}\cdot\text{cm}^{-2}$ Cu. (According to the suggestion made in N we call this particle K_μ ; the index μ will be justified in the next section). We must then assume that the ranges at approximately 12 and $43 \text{ g}\cdot\text{cm}^{-2}$ Cu belong to other decay schemes.

This conclusion has been reached using two main arguments: the paucity of intermediate ranges between 20 and $60 \text{ g}\cdot\text{cm}^{-2}$ Cu — which excludes any reasonably smooth spectrum — and the grouping of ranges at about $75 \text{ g}\cdot\text{cm}^{-2}$ Cu. To arrive at it the two groups (A and B) of S-particles were considered together. It could be argued that this is not a justifiable procedure. Indeed, as it has already been mentioned, the times of flight of the primaries in the two groups are different. Consequently, in the group of locally produced

S's, certain types of particles can be present which do not appear in group A. It is clear, however, that if the study of the combined ranges has reached a definitive conclusion, this cannot be explained as an accident brought about by the combination of the two groups. Also the same conclusion could have been reached with a smaller degree of precision had we considered the two groups independently.

3. - Decay Scheme Producing the Long Range Secondaries.

The complete mode of decay of the particle disintegrating into a charged secondary of range $(75.7 \pm 1.7) \text{ g} \cdot \text{cm}^{-2} \text{ Cu}$ will be obtained by comparing the directly measured primary mass with those that correspond to different decay modes assumed a priori.

TABLE IV. - *Calculated Primary Mass for Various Decay Schemes.*

$$R_{\text{sec}} = (75.7 \pm 1.7) \text{ g} \cdot \text{cm}^{-2} \text{ Cu.}$$

Decay Scheme	$\text{K} \rightarrow \mu + \nu \text{ (or } \gamma \text{)}$	$\text{K} \rightarrow \mu + \pi^0$	$\text{K} \rightarrow \pi + \nu \text{ (or } \gamma \text{)}$	$\text{K} \rightarrow \pi + \pi^0$
Primary Mass (m_0)	941 ± 11	1012 ± 12	1090 ± 13	1150 ± 14

In Table IV, are given the masses which would correspond to possible two-particle decays giving a charged secondary of range $(75.7 \pm 1.7) \text{ g} \cdot \text{cm}^{-2} \text{ Cu}$. Only known particles are assumed as secondaries. From these, only μ and π -mesons have been considered as charged secondaries since the observed behaviour of the secondaries, while indicating that they are light particles, excludes the possibility of their being electrons.

From the Table it is seen that the only mode of decay which fits the directly measured mean mass of $(928 \pm 13 m_0)$ is that involving as secondaries a μ -meson and a zero mass neutral particle (γ -ray or neutrino).

The study of the secondary ranges has shown, however, that S-events have to be explained by at least two different decay modes. The analysis of the distribution of masses made in 2.1 (see Table II) showed that the presence of a large contamination of high masses in our sample was quite improbable. A closer investigation is now required before we are able to draw a conclusion as to the mode of decay of the long range group.

Only one decay with a stopping secondary of long range had its primary mass measured (event No. 48813). Five other events however had lower limits of range above $47 \text{ g} \cdot \text{cm}^{-2} \text{ Cu}$ and thus belong most probably to the long range group. The mean mass of the six corresponding primaries is $(906 \pm 27) m_0$. This is in good agreement with the general mean and clearly incompatible

with the minimum mass of about $1000 m_e$ which would be required if one of the secondaries (neutral or charged) were a pion. We see, therefore, that any possible contamination of our sample by masses significantly above $(928 \pm 13) m_e$ cannot be attributed to those S-particles which give the long range secondaries. Consequently, we conclude that the secondary of range $(75.7 \pm 1.7) \text{ g} \cdot \text{cm}^{-2} \text{ Cu}$ is a μ -meson and that the accompanying neutral secondary has zero mass. We can establish, furthermore, that this neutral secondary is a neutrino and not a γ -ray. Indeed, the momentum of the K_μ -secondaries is of the order of $225 \text{ MeV}/c$. γ -rays of this momentum produce cascade showers which are easily detectable (*). In Table I, we have given (in radiation-length units) the possible traversals of the plates by γ -rays emitted in a direction opposite to that of the charged secondary. Although in four cases an electronic shower appeared in association with an S-event, none was observed in association with a secondary of range greater than $45 \text{ g} \cdot \text{cm}^{-2} \text{ Cu}$. In 13 of the 17 events for which R_1 was greater than $45 \text{ g} \cdot \text{cm}^{-2} \text{ Cu}$ the geometry of the decay was such that the probability of observing the electron showers of $225 \text{ MeV}/c$ γ -rays was equal or greater than 50%. Therefore, the neutral secondary cannot be a γ -ray, and the decay of the K_μ -particle can finally be established as: $K_\mu \rightarrow \mu + \nu$.

4. - The Mass of the K_μ -Particle.

Two independent values have been obtained for the mass of the K_μ -particle. Direct measurements on six events with lower limits of range, R_1 , greater than $45 \text{ g} \cdot \text{cm}^{-2} \text{ Cu}$ yielded a mean value of $(906 \pm 27) m_e$. An indirect value of $(941 \pm 11) m_e$ was obtained from the range of the μ -meson secondary and the nature of the neutral secondary.

The agreement between the two values is good. In principle they can be combined to yield a statistically more accurate mass. Care, however, has to be applied in the interpretation of these values since they can be affected by errors, statistical or systematic, others than those so far considered. In the direct mass estimate, the additional errors arise from the uncertainty in the magnetic field measurement and in the momentum-range correspondence used. In the indirect estimate besides the last mentioned uncertainty (+), there is another important source of error arising from what may be called « wrong

(*) Professor HAZEN has carried out a study of this question with the help of our apparatus. He has shown that, in the momentum region we are directly concerned with, the average cascade shower is composed of 8 electrons.

(+) An error in the momentum-range relationship affects the two mass estimates in opposite directions.

interpretation of events ». An event may be wrongly interpreted in different ways; the assumption that the S-particle came to rest before decaying may not always be fulfilled; the secondary itself may decay in such a way that its own secondary escapes detection as such and apparently increases the range of the S-secondary. It is also possible, of course, to mistake for an S-particle some kind of fortuitous event.

In Table V, we indicate the estimated magnitudes of the above errors and the corresponding uncertainties in primary mass. The influences of the possible « wrong interpretation » has been estimated by eliminating from the sample of 9 events both the event with the highest and that with the lowest mean range.

TABLE V. — *Estimates of possible additional errors in the K_μ -mass.*

Cause of Error	Estimated % Uncertainty	Error in Primary Mass	
		Direct (m_e)	Indirect (m_e)
Magnetic field	± 1	± 15	—
Momentum-range	± 2	± 11	± 10
« Wrong interpretation »	—	—	± 10

To a first approximation new errors in the two estimates of mass can be obtained by combining quadratically those previously quoted and those given in Table V. In this way we obtain:

$$\text{Mean direct mass: } (906 \pm 30) m_e$$

$$\text{Mean indirect mass: } (941 \pm 17) m_e$$

Combining these two values after taking into account that the uncertainty in the range-energy tables affects them simultaneously although in opposite sense, we finally obtain as best estimate of the K_μ -mass: $(935 \pm 15) m_e$. To this corresponds a momentum (*) of the secondaries in the C.M. given by $P^* = (228 \pm 4) \text{ MeV}/c$.

It is to be noticed that the direct and the indirect estimates give values of mass which are both almost two standard deviations lower than that of

(*) In N the existence and properties of the K_μ -particle had been established using essentially the same arguments as those followed in the last 3 sections. The momentum of the μ -secondary was given as $(220 \pm 3) \text{ MeV}/c$. The difference between this and the new value is due partly to the reasons exposed at the foot of Table I, but mainly also to the fact that one of the first long range secondaries observed (event n. 21073) is that which gives the shortest of the individual mean values of range.

the τ -meson. The presence of errors whose influence can only be ascertained approximately, does not allow us, however, to go beyond saying that the mass of the K_μ -particle appears to be lower or at most equal to that of the τ -meson.

5. - Particles which are not K_μ -Particles. Their Relative Frequency.

We have already mentioned that some of our S-events do not represent the decay of a K_μ -particle. These are the events in which either the secondary had a range incompatible with $75 \text{ g}\cdot\text{cm}^{-2}$ Cu or γ -rays appeared associated with the decay.

We have, however, an a priori knowledge of other types of K-particles. There is the κ -particle, which emits a μ -meson with what appears as a rather smooth spectrum although very little is known about its shape or its high energy limit (O'CEALLAIGH, 1951, see also DILWORTH *et al.*, 1954). The χ -particle emitting a monoenergetic π -meson secondary of $p^* \sim 200 \text{ MeV}/c$ (MENON and O'CEALLAIGH, 1954). The decay of this particle is most probably associated with γ -rays resulting from the decay of a π^0 -meson (BRIDGE *et al.*, 1954; HODSON *et al.*, 1954). There is the K_e -particle emitting an electron and probably two neutral secondaries (FRIEDLANDER *et al.*, 1954); there is the τ -meson (BROWN *et al.*, 1949) with its two alternate modes of decay.

All our events which are not K_μ -particles can be fitted into these categories. But in almost every case it is impossible to ascribe an individual event to a definite mode of decay. Events with secondaries shorter than $15 \text{ g}\cdot\text{cm}^{-2}$ Cu represent the decay of τ - or κ -particles and in some cases of K_e -particles. Ranges between 20 and $45 \text{ g}\cdot\text{cm}^{-2}$ Cu can be due to the decay of κ 's or χ 's. Particles with associated γ -rays can be τ -, χ -, K_e or even κ -particles depending on the observed range of the charged secondary.

One thing can be stated, however: from all the known particles only the κ could possibly emit a secondary with a range above $45 \text{ g}\cdot\text{cm}^{-2}$ Cu and as large as $75 \text{ g}\cdot\text{cm}^{-2}$ Cu and escape recognition as such. The almost complete lack of these intermediate ranges, which has helped us in establishing the existence of the K_μ -meson, shows that either the range spectrum of the κ -secondary does not extend much beyond $20 \text{ g}\cdot\text{cm}^{-2}$ Cu or that the number of κ 's amongst our S's is very small indeed.

In either case we are justified in identifying as K_μ -particles all the S's whose secondaries went beyond $45 \text{ g}\cdot\text{cm}^{-2}$ Cu. Use of this has already been made in the direct determination of the K_μ -mass and in the identification of its secondary as a μ -meson. The criterion also provides us with a simple way of establishing the proportion of K_μ 's in our S-events. We consider the proportion of K_μ -particles (ranges greater than $45 \text{ g}\cdot\text{cm}^{-2}$ Cu) amongst all the K_μ -particles which had available ranges, R_3 , greater than $45 \text{ g}\cdot\text{cm}^{-2}$ Cu and

could thus have been identified as K_μ or not K_μ . From the statistics we eliminate, however, all the K_μ -particles which have been recognized as such only from the ranges of their secondaries. This restricts us to the events with measured masses in group A. Of the 9 K-particles satisfying this condition six could be identified as K_μ -particles. This gives $(66 \pm 18)\%$ for the proportion of K_μ 's amongst K-particles with a time of flight of about $5 \cdot 10^{-9}$ s. The $\pm 18\%$ is calculated making use of the binomial distribution since what we are testing in each event is whether or not it is compatible with a K_μ -decay. The probability of finding a ratio of 6/9 when the expected proportion is 3/9, is less than 3%.

There are other ways of calculating this proportion. One could, for instance, find an upper limit by eliminating from the whole of group A all those events which, either because they gave short range secondaries or had associated γ -rays, are certainly not K_μ -particles. Seven (*) events are thus classified as not K_μ -decays and the upper limit to the proportion becomes 15/22 or $(68 \pm 12)\%$. The closeness of this upper limit and the probable value obtained previously depends on the detection efficiency of γ -rays which can be rather large.

Finally we notice that in group B — locally produced S-particles — only one event of range compatible with that of the secondary of the γ -particle was found in 11 cases in which it could have been observed.

6. — The Sign of K-Particles.

As indicated in 2.1. one of the outstanding results is the very strong charge asymmetry in the K-particles we have observed. This result has already been commented on in P. Since then the scanning of the photographs has been completed and only one more negative S (catalogue number 41930) has been observed. The characteristics of this event both in the top and in the bottom chamber are those of a typical S. The measured mass of the primary is $(1050 \pm 69) m_e$. The secondary, which is at an ionization of, or near, the minimum, stops in the first plate it encounters; its range is between 11.5 and 23 $\text{g} \cdot \text{cm}^{-2}$ Cu and can therefore be a light meson or an electron.

To obtain the best value of the ratio of negative to positive K-particles we can only consider those primaries whose masses could be well measured. In this way we will not discriminate against possible negative particles which if they did not produce visible secondaries could only be identified as S's through an accurate mass measurement. Applying this criterion we are left

(*) The mean mass of these events is $(948 \pm 22) m_e$.

with 22 positive and at most (*) two negative K-particles. Taking into account the statistical fluctuations in these numbers (REGENER, 1951) we find that there is a 95% probability that negative K-particles constitute less than 22% of the S-particles passing through the top chamber i.e. of K-particles with an average time of flight of $5 \cdot 10^{-9}$ s.

7. - Summary and Discussion.

An analysis has been presented of 45 S-particle: 29 of them passed through the top chamber and the remaining 16 were locally produced. The average times of flight of the two groups were $5 \cdot 10^{-9}$ s and $2 \cdot 10^{-9}$ s, respectively.

All particles in the long time of flight group had their signs established unambiguously. 24 had their masses measured: 22 were positive and 2 negative. Negative particles can therefore constitute no more than about 20% of the S-particles in this group.

The masses of the positive K-particles were consistent with a unique value of $(928 \pm 13) m_e$.

The decay products of the S-particles in both groups were then examined and the conclusion reached that S-particles have to be explained by at least two different decay schemes. One is a two-body decay giving a charged secondary of range $(75.7 \pm 1.7) \text{ g} \cdot \text{cm}^{-2} \text{ Cu}$. Not very definite evidence could be obtained about the other mode or modes of decay.

From the comparison of the primary masses and the secondary ranges, it was then shown that the range of $(75.7 \pm 1.7) \text{ g} \cdot \text{cm}^{-2} \text{ Cu}$ corresponds to a μ -meson and that the accompanying neutral secondary is massless. The absence of associated showers indicates that it is a neutrino. The existence of decay $K_\mu \rightarrow \mu + \nu$ first proposed in N is thus confirmed.

The best mass obtained for the K_μ -particle is $(935 \pm 15) m_e$. It appears to be smaller than that of the τ -meson, but the possible existence of systematic errors does not allow us to say that the difference in mass is firmly established.

K_μ -particles were then shown to constitute $(66 \pm 18)\%$ of the S-particles passing through the top chamber.

The comparison (+) of our results with those obtained by the MIT group with a multiplate chamber shows a striking analogy respecting the lack of intermediate ranges and the grouping of long ranges at a value of approximately $76 \text{ g} \cdot \text{cm}^{-2} \text{ Cu}$. The MIT group have also found that no γ -rays are

(*) See P for comments on event 26945.

(+) This comparison was already made by Rossi at the Varenna Summer School (1954). From the confrontation of the independently obtained results, the existence of the K_μ -mode of decay could then be firmly established.

associated with the long range secondaries. They have shown (COURANT, 1954), however, that γ -rays produced by the decay of neutral π -mesons are frequently associated with secondaries whose ranges appear grouped at a unique value of about $45 \text{ g} \cdot \text{cm}^{-2} \text{ Cu}$. This constitutes very strong evidence in favour of the decay scheme $\chi \rightarrow \pi + \pi^0$. Some of the secondary ranges we have observed could well belong to this decay scheme. Our results, however, do not allow us to say anything about the homogeneity of the particles which are not K_μ -particles.

The comparison with photographic emulsion data is more difficult. Recent mass measurements by the Paris group (HOANG *et al.*, 1955) are in close agreement with our direct measurements. A certain number of $p\beta$ -values of K-secondaries found in several laboratories agree with the K_μ -line. The total $p\beta$ -spectrum in emulsions, however, indicates (DILWORTH *et al.*, 1954) a much stronger proportion of particles which are not K_μ than those observed in multi-plate chambers. Whether the discrepancy can be explained in terms of difference in lifetime or in production, we cannot say.

Acknowledgements.

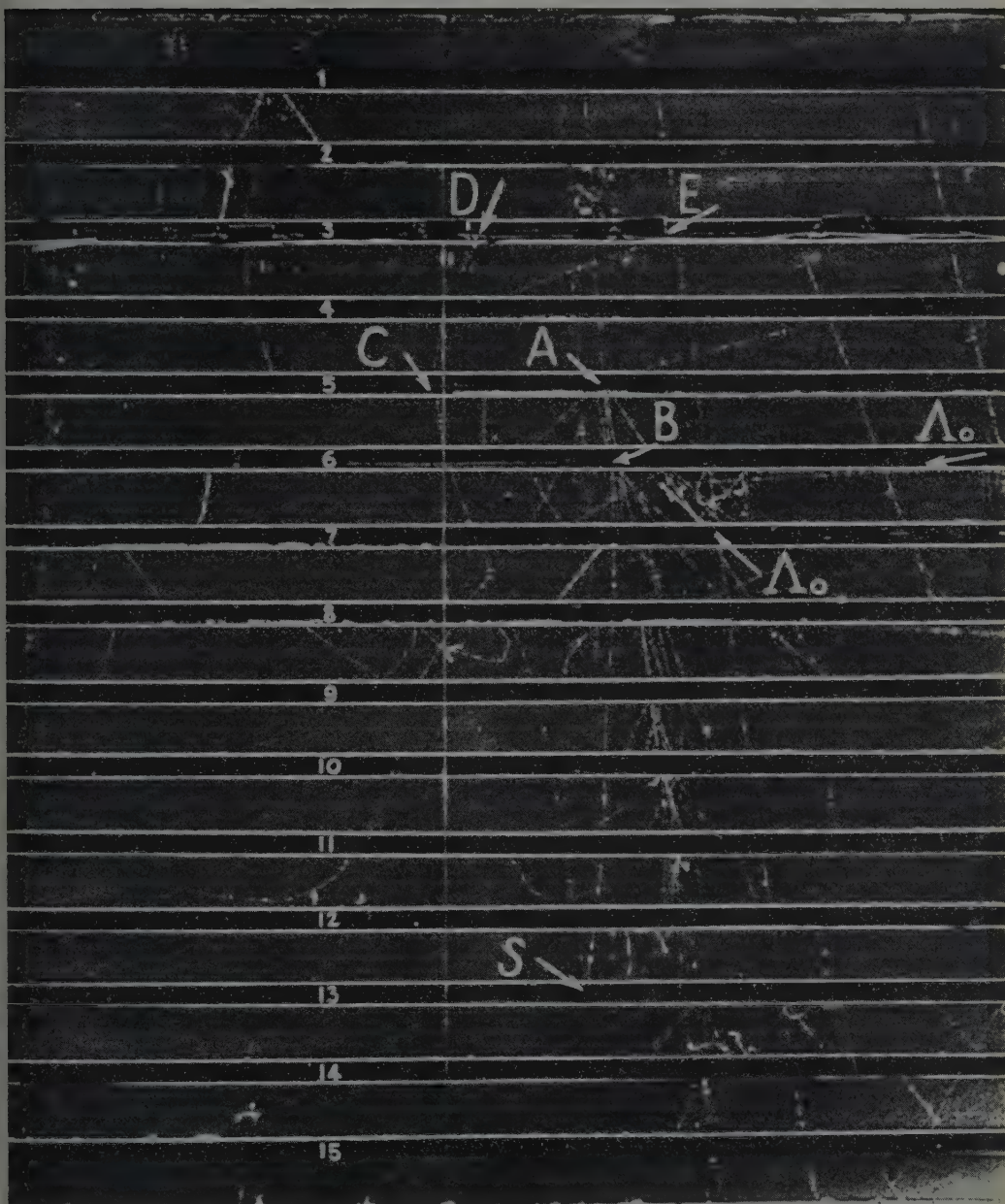
It is with pleasure that we thank Professor R. R. RAU for the many discussions we have had with him during the preparation of this paper. We are also very much indebted to Dr. J. ROSCH, the Director of the Observatoire du Pic du Midi, and his staff for the valuable help they have given us during the experimental work.

APPENDIX I

Discussion of Event 40896.

Event 40896. — The S-particle is probably produced in a nuclear interaction at *B* in plate 6. This interaction appears as a nuclear scattering (in a plane perpendicular to the front glass) of a secondary produced in the nuclear interaction at *A* in plate 5. It is therefore not certain that the S-particle was produced at *B*. It could have been produced at *A* and have suffered a nuclear scattering at *B*. It should be noted, however, that the V-track observed between plates 6 and 7 is due most likely to the decay of a Λ^0 -particle which originated at the point *B*. It is more reasonable to assume therefore that the nuclear event at *B* is not a simple nuclear scattering but an interaction in which an S-particle and a Λ^0 -particle were produced. As shown in Table I, similar associated events appear fairly frequently when the S's have been produced in the multiplate chamber.

R. ARMENTEROS, B. GREGORY, A. HENDEL, A. LAGARRIGUE,
L. LEPRINCE-RINGUET, F. MULLER and C. PEYROU



Event N. 40896.

The S-particle stops in plate 13 at S. The secondary is emitted backwards and between plates 6 and 5 it appears to have an ionization definitely above the minimum: $1 < I/I_0 < 3$. However, the possible fluctuations in ionization connected with the short interval between the plates does not allow us to assert that the secondary stopped in plate 5 (C). Above plate 5 a track can be seen almost in the prolongation of that below. This track is at the minimum of ionization; the corresponding particle crosses plate 4 and stops in plate 3 (D). The most likely interpretation of this S-event is that the secondary stopped in plate 5 (C). The range would then be: $\langle R \rangle = (80.5 \pm 4.1) \text{ g} \cdot \text{cm}^{-2} \text{ Cu}$. The track above plate 5 would then correspond to an electron from the disintegration of a μ -meson. Track E between plates 4 and 5 could then result from the multiplication of this electron in plate 4. It is also possible, however, that this track is that of a knock-on electron produced by the fast particle which traverses the whole chamber.

If the ionization estimate between plates 6 and 5 is wrong, it is possible that the S-secondary stopped in plate 3. The range of the secondary would then be: $\langle R \rangle = (100.1 \pm 4.7) \text{ g} \cdot \text{cm}^{-2} \text{ Cu}$, which is significantly larger than the K_μ -secondary.

APPENDIX II

The Determination of the Ranges of S-Secondaries.

The problem of determining the amount of matter traversed by a particle in a plate chamber is primarily a geometrical one. We will not describe in this section the method used in the reconstruction of the path in the intervals between the plates, nor the errors involved in this operation. We will restrict the discussion to the following problems:

1) Determination of the amount of matter traversed by a particle entering a plate at an angle ϑ_1 and emerging at an angle ϑ_2 . It will be found that the fluctuations due to multiple scattering introduce errors which for large angles constitute the major contribution to the total error in range.

2) Determination of the residual range of a particle entering a plate at an angle ϑ and assumed to stop at a given depth Z . The formulae obtained for the mean and the fluctuations about the mean of this residual range are found to be useful in the following problem.

3) Determination of a likelihood function $G(R)dR$, when the values of the minimum range, R_1 , and its error, ΔR_1 , are known together with the angle ϑ at which the particle entered the plate in which it appeared to stop. It will be found that this function can be approximated by a gaussian in the case we are immediately interested.

4) Comparison of our results on the long range group of secondaries with a line spectrum. This can be solved by a simple analysis of the set of values $\langle R_i \rangle$ — or mean value of the function $G(R)$ — and ΔR_i —, the standard deviation of $G(R)$.

A.1. *Measurement of Range in the Traversal of a Plate.* — In order to minimize the errors due to possible displacements of the tracks in adjoining plate intervals, we have used a formula for the range which depends only on angles. These angles are the ones obtained by the reconstruction in space of the tracks.

Let us consider the actual path of a particle which enters a plate at an angle ϑ_1 and leaves it at an angle ϑ_2 , the angles being measured with respect to the normal to the plate. If we divide the actual range r into $(2n+1)$ intervals, we can define in each one two projected angles of scattering: φ_i in the plane defined by the incoming particle and the normal to the plate, and ψ_i in a plane orthogonal to the first plane. For each interval the projected length, z_i , on the normal to the plate is given by:

$$(1) \quad z_i = \frac{r}{2n+1} \cos \left[\vartheta_1 + \varphi_1 + \varphi_2 + \dots + \varphi_{i-1} + \frac{\varphi_i}{2} \right] \cos \left[\psi_1 + \psi_2 + \dots + \frac{\psi_i}{2} \right].$$

If we call ϑ_2^* the projection of the angle ϑ_2 on to the plane defined by the incoming particle and the normal to the plate, we see that:

$$\vartheta_2^* = \vartheta_1 + \sum_1^{2n+1} \varphi_i.$$

Introducing ϑ_2^* into formula (1) and summing all z_i 's over the total thickness, h , of the plate we have:

$$\frac{h}{r} = \frac{1}{2n+1} \sum_1^{2n+1} \cos \left[\frac{\vartheta_1 + \vartheta_2^*}{2} + \frac{1}{2} \sum_1^{i-1} \varphi_i - \frac{1}{2} \sum_{i+1}^{2n+1} \varphi_i \right] \cos \left[\psi_1 + \dots + \psi_{i-1} + \frac{\psi_i}{2} \right].$$

If we call Φ the r.m.s. projected angle of scattering in the plate, we see that:

$$\sqrt{\langle \varphi_i^2 \rangle} = \sqrt{\langle \psi_i^2 \rangle} = \frac{\Phi}{\sqrt{2n+1}}.$$

A series expansion of the cosines gives then:

$$(A) \quad \left\{ \begin{array}{l} \left\langle \frac{h}{r} \right\rangle = \frac{h}{\cos(\vartheta_1 + \vartheta_2^*)/2} \sim \frac{h}{\cos(\vartheta_1 + \vartheta_2)/2} \\ \text{and} \\ \sqrt{\left\langle \left(\frac{h}{r} - \left\langle \frac{h}{r} \right\rangle \right)^2 \right\rangle} = \sin \frac{\vartheta_1 + \vartheta_2^*}{2} \cdot \frac{\Phi}{\sqrt{12}} \sim \sin \frac{\vartheta_1 + \vartheta_2}{2} \cdot \frac{\Phi}{\sqrt{12}} \end{array} \right.$$

where only terms of the first order have been kept.

It was found that, even when the residual range is small, the influence of second order terms is negligible. In fact, the formula using the more easily measurable angle ϑ_1 instead of ϑ_2^* is a better approximation to the actual mean range.

An important point to notice is the large value which the standard deviation attains for steeply inclined angles.

One can calculate this error for each plate traversal after assuming the

nature of the particle and estimating its energy. The total error due to scattering was obtained by adding quadratically the errors in each plate traversal. This contribution of multiple scattering to the error ΔR_1 of R_1 is, for μ -mesons of range near to $75 \text{ g}\cdot\text{cm}^{-2}$ Cu and angles ϑ_i larger than 45° , larger than $1 \text{ g}\cdot\text{cm}^{-2}$ Cu and turns out to be larger than that due to errors in spatial reconstruction.

A.2. Determination of the Range in the Last Plate. — We first suppose that the particle stops in a layer of arbitrary depth, z , in the plate. Neglecting scattering the residual range would be:

$$S = z/\cos \vartheta,$$

where ϑ is the angle, w.r.t. the normal, at which the particle entered the last plate.

Scattering at the end of the range will have two effects: the mean range will be greater than the geometrical one. The range will fluctuate around this mean value. These effects are bigger than those found in A.1. The calculation is very similar, however. We divide the residual range in intervals in which the r.m.s. angle of scattering is constant. This can be done making use of the well-known empirical formula $p\beta \propto S^{1/2}$. Since $d\langle\Phi^2\rangle \propto dS/(p\beta)^2$, we have, for a finite interval ΔS :

$$\langle\Phi^2\rangle = \propto \log \frac{S + \Delta S}{S}.$$

Dividing the residual range S into intervals $xS, x(1-x)S, \dots, x(1-x)^nS, \dots$, we obtain for each interval, if x is very small:

$$\langle\Phi^2\rangle = k^2 \frac{x}{1-x/2},$$

where k is a constant which depends only on the mass of the particle and the material traversed. For μ -mesons in copper $k = 0.2$ radians.

We may apply the same kind of calculations as in A.1. Using the same notation we have:

$$z = \sum_{n=0}^{\infty} Sx(1-x)^n \cos [\vartheta + \varphi_0 + \varphi_1 + \dots + \varphi_{n/2}] \cos [\psi_0 + \psi_1 + \dots + \psi_{n/2}].$$

Developping up to the second order terms the cosines in terms of the small angles φ_i and ψ_i and averaging over them, we find:

$$(B) \quad \left\{ \begin{aligned} \left\langle \frac{z}{S} \right\rangle &= \cos \vartheta (1 - k^2) \\ \left\langle \left(\frac{z}{S} - \left\langle \frac{z}{S} \right\rangle \right)^2 \right\rangle &= \frac{k^2}{2} \sin^2 \vartheta + \left[\frac{k^4}{4} \cos^2 \vartheta + \dots \right] \end{aligned} \right.$$

for the mean value and standard deviation, respectively, of z/S .

Formulae (B) are independent of x , as they should be.

a) If we assume that a particle stops at a certain depth z , the mean value of the reciprocal of the range is: $\langle 1/S \rangle = (\cos \vartheta / z)(1 - k^2)$.

The maximum ranges, R_2 , given in Table I were obtained from:

$$R_2 = R_1 + S = R_1 + \frac{h}{\cos \vartheta} (1 + k^2),$$

with $k^2 = 0.04$ for μ -mesons in copper.

b) Inversely if the actual residual range is S , the depth, z , of the stopping point is distributed according to a gaussian law with a mean value: $\langle z \rangle = S \cos \vartheta [1 - k^2]$ and relative standard deviation:

$$\sigma = \sqrt{\left\langle \left(\frac{z}{\langle z \rangle} - 1 \right)^2 \right\rangle} = \frac{k \operatorname{tg} \vartheta}{\sqrt{2} (1 - k^2)} \sim 0.15 \operatorname{tg} \vartheta,$$

for μ -mesons in copper.

In other words, the distribution of z for a given range S and a given angle ϑ is gaussian. We denote it by:

$$P(z) dz = g \left[\frac{z - S \cos \vartheta (1 - k^2)}{\sigma S \cos \vartheta (1 - k^2)} \right] \frac{dz}{\sigma S \cos \vartheta (1 - k^2)}.$$

A.3. *The Likelihood Function for the Range.* — From the reconstruction in space of the path of a stopping particle, we have been able to measure R_1 — or minimum range — and its standard error, ΔR_1 . We have also measured the angle, ϑ , of entry into the last plate. We look now for the likelihood function, $G(R) dR$, for the range to be actually R when the measurements yield R_1 , ΔR_1 and ϑ .

If we consider a given partition of the range: $R = R_0 + S$, where R_0 is the true value of R_1 , the probability of the whole observation (R_1 , ΔR_1 , ϑ) for *this particular partition* is:

$$(C) \quad g \left[\frac{R_1 - R_0}{\Delta R_1} \right] \cdot \frac{dR_1}{\Delta R_1} \int_0^h P(z) dz = g \left[\frac{R_1 - R_0}{\Delta R_1} \right] \cdot \frac{dR_1}{\Delta R_1} f(S).$$

The first term corresponds to the gaussian probability of observing R_1 when the actual value is R_0 , the second is the probability that the particle has stopped within the plate.

We are not interested, however, in a given partition but in the probability law for R . A complete treatment requires the knowledge of the a priori probability law of partition (ANNIS *et al.*, 1953). In our case, however, the random distribution of the starting points in a plate and the apparent randomness of the emission angles indicate that a flat a priori law may be taken for R_0 in an interval $(R - A; R)$ with R in the neighbourhood of $75 \text{ g} \cdot \text{cm}^{-2} \text{ Cu}$ and A of the order of $20 \text{ g} \cdot \text{cm}^{-2} \text{ Cu}$. We therefore integrate (C) over all possible

values (*) of S and obtain the likelihood function for R :

$$(D) \quad G(R; R_1, \Delta R_1, \vartheta) = \frac{1}{A} \int_0^A f(S) g \left(\frac{S' - (R - R_1)}{\Delta R_1} \right) \frac{dS'}{\Delta R_1}.$$

This formula yields our best information on R . If ΔR_1 and σ are small, we find a flat probability law for R between R_1 and R_2 . For values of $\Delta R_1 \sim 3 \text{ g} \cdot \text{cm}^{-2} \text{ Cu}$ and for small angles ϑ ($\leq 45^\circ$) scattering introduces practically no skewness, the two sides of the curve join in the middle without any noticeable flattening of, or angular point at, the top and $G(R)$ is very well approximated by a gaussian curve. (See Fig. 2 in the text).

For bigger angles, the fluctuation due to the scattering at the end of the range introduces a skewness in the probability curve. Even then, and up to angles $\vartheta \sim 60^\circ$, the approximation given by a gaussian distribution is surprisingly good.

A numerical integration of equation (D) applied to all our important cases shows that the best adapted gaussians are defined by:

$$(E) \quad \begin{cases} \langle R \rangle = \frac{R_1 + R_2}{2} + f(\vartheta) \\ \langle (R - \langle R \rangle)^2 \rangle = \Delta R_1^2 + \frac{(\langle R \rangle - R_1)^2}{3} + \sigma^2 (\langle R \rangle - R_1)^2 \end{cases}$$

where σ is the standard deviation defined in A.2 and $f(\vartheta)$ a correction term which is negligible for $\vartheta \leq 45^\circ$. The calculated values of $f(\vartheta)$ for four angles were:

ϑ (Deg.)	51	55	61	71
$f(\vartheta) \text{ g} \cdot \text{cm}^{-2} \text{ Cu}$	0.3	0.5	1.2	5

Formulae (E) were those used for calculating the values listed in Tables I and III.

A.4. *Determination of the Mean Range of a Group of Events.* — We have now found the individual likelihood functions $G_i(R)$. The hypothesis of a unique range is expressed by the a priori probability law:

$$P(R) dR = \frac{\exp \left[-\frac{1}{2} \left(\frac{R - \langle R \rangle}{\lambda} \right)^2 \right]}{\sqrt{2\pi}} \cdot \frac{dR}{\lambda},$$

λ being the dispersion due to straggling and $\langle R \rangle$ the mean range. In our case λ is small (about $2 \text{ g} \cdot \text{cm}^{-2} \text{ Cu}$) compared with the standard deviation

(*) In fact the limit A may be taken arbitrarily large since for large values of S the relative smallness of ΔR_1 will make the integrand to vanish.

of each $G_i(R)$; $P(R)$ may then be approximated by a delta function. The best value of the range is then given by the maximum likelihood equation:

$$\sum_i \frac{\partial G_i / \partial R}{G_i} = 0.$$

When all the G_i 's are gaussian this equation leads to the usual ponderation methods for the mean and standard deviation.

If the functions $G_i(R)$ cannot be approximated by gaussians, the final analysis may still be carried out using the methods described by ANNIS *et al.* (1953).

BIBLIOGRAPHY

- M. ANNIS, W. CHESTON and H. PRIMAKOFF: *Rev. Mod. Phys.*, **25**, 818 (1953).
 R. ARMENTEROS, B. GREGORY, A. LAGARRIGUE, L. LEPRINCE-RINGUET, F. MULLER and C. PEYROU: *Suppl. Nuovo Cimento*, **12**, 327 (1954).
 W. A. ARON: University of California, Thesis. UCRL 1325 (1951) (not published).
 H. A. BETHE: *Phys. Rev.*, **70**, 821 (1946).
 H. BRIDGE, H. COURANT, B. DAYTON, H. C. DESTAEELER, B. ROSSI, R. SAFFORD and D. WILLARD: *Nuovo Cimento*, **12**, 81 (1954).
 R. H. BROWN, U. CAMERINI, P. H. FOWLER, H. MUIRHEAD, C. F. POWELL and D. M. RITSON: *Nature*, **163**, 82 (1949).
 H. COURANT: MIT, Thesis (1954) (not published).
 C. C. DILWORTH, L. SCARSI and G. P. S. OCCHIALINI: *Annual Reviews of Nuclear Science*, vol. **4** (1954).
 W. FRIEDLANDER, D. KEEFE, M. G. K. MENON and L. VAN ROSSUM: *Phil. Mag.*, **45**, 1043 (1954).
 B. GREGORY, A. LAGARRIGUE, L. LEPRINCE-RINGUET, F. MULLER and C. PEYROU: *Nuovo Cimento*, **11**, 292 (1954).
 T. F. HOANG, L. JAUNEAU, J. JOUVIN, G. KAYAS, L. LEPRINCE-RINGUET, D. MORELLET, A. ORKIN-LECOURTOIS and J. TREMBLEY: *Suppl. Nuovo Cimento* (1955).
 A. L. HODSON, J. BALLAM, W. H. ARNOLD, D. R. HARRIS, R. R. RAU, G. T. REYNOLDS and S. B. TREIMAN: *Phys. Rev.*, **96**, 1089 (1954).
 M. G. K. MENON and C. O'CEALLAIGH: *Proc. Roy. Soc.*, A **221**, 292 (1954).
 C. O'CEALLAIGH: *Phil. Mag.*, **42**, 1032 (1951).
 V. A. REGENER: *Phys. Rev.* **84**, 161 (1951).
 M. RICH and R. MADEY: University of California, UCRL 2301 (1954) (not published).
 B. ROSSI: Varenna Summer School (1954) (MS. kindly sent to us by Prof. Rossi).

RIASSUNTO (*)

Dopo una descrizione dei metodi usati nelle misure di momento e di percorso si esaminano i dati di 46 eventi S ottenuti da un'esperienza eseguita con una doppia

(*) Traduzione a cura della Redazione.

camera a nebbia. Misure di momento-percorso eseguite su 22 S positivi danno una massa compatibile con un valore unico a $(928 \pm 13) m_e$. L'analisi dei percorsi dei secondari mostra, tuttavia, che non tutti gli eventi S si possono spiegare con un unico tipo di decadimento. Una forte proporzione di secondari corrisponde a un mesone leggero con p rcorso residuo unico $(75,7 \pm 1,7) g \cdot cm^2 Cu$. Il confronto di questo percorso con le masse misurate delle particelle primarie prova che questi secondari sono mesoni μ . Contemporaneamente si dimostra che il secondario neutro che li accompagna è una particella di massa zero. L'assenza di sciami in cascata associati ad eventi S con secondari di lungo percorso dimostra che il secondario neutro è un neutrino. Il processo di decadimento $K_\mu \rightarrow \mu + \nu$ precedentemente proposto risulta maggiormente confermato. Si ottengono per la particella K_μ due valutazioni di massa indipendenti. Una, da misure di momento-percorso, dà direttamente $(960 \pm 27) m_e$. Un'altra, dal processo di decadimento, e dal percorso del μ secondario, dà indirettamente $(941 \pm 11) m_e$. Infine, dalla combinazione dei due precedenti valori, dopo aver tenuto conto dei possibili errori addizionali, si ottiene per la massa un valore più probabile finale di $(935 \pm 15) m_e$. Si mostra poi che la particella K_μ è essenzialmente positiva e costituisce il $(66 \pm 17)\%$ degli S passati attraverso la camera superiore. Non si possono ottenere dati precisi sul decadimento delle particelle S che risultano non seguire il processo di decadimento delle particelle K_μ .

Sui circuiti di somma.

M. CERVASI e G. FIDECARO

Istituto di Fisica dell'Università - Roma
Istituto Nazionale di Fisica Nucleare - Sezione di Roma

(ricevuto il 25 Febbraio 1955)

Riassunto. — Vengono descritti due circuiti di somma, facenti parte di un grande odoscopio per Raggi Cosmici e costruiti con particolare riguardo alle condizioni di stabilità nel tempo e precisione dell'ampiezza degli impulsi addendi. In uno dei due circuiti le condizioni sono diverse dalle usuali per il fatto che le valvole formatrici degli impulsi lavorano in regime di tranconduttanza negativa griglia controllo-placca. Viene discusso l'effetto di questa circostanza sulle condizioni di stabilità del circuito stesso.

1. — Nella presente nota vengono descritti due circuiti di somma ⁽¹⁾ impiegati in una esperienza sui Raggi Cosmici ⁽²⁾ in cui è necessario conoscere quanti contatori di Geiger sono stati scattati contemporaneamente su un numero totale n ($n = 20 \div 30$). Riferiamo in particolare alcune osservazioni sulla precisione e sulla stabilità a lungo termine degli impulsi addendi. Le ampiezze e le durate degli impulsi possono essere rapidamente controllate con un dispositivo elettronico che viene pure descritto. Il tempo di salita è di qualche $0,1 \mu s$ e la durata è regolabile da un minimo di circa $3 \mu s$ fino a $10 \div 15 \mu s$.

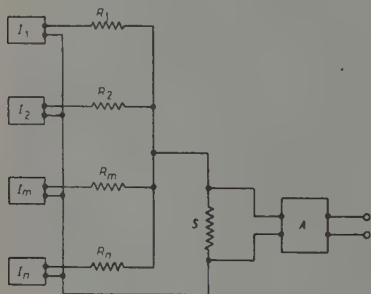


Fig. 1.

2. — Lo schema di principio è rappresentato in fig. 1, dove I sono i formatori degli « addendi » e A è un amplificatore a controreazione che amplifica linearmente i segnali di somma in vista della successiva discriminazione.

⁽¹⁾ Considerazioni generali sui circuiti di somma si trovano in *Waveforms*, vol. 19 della Radiation Laboratory Series M.I.T., cap. 18.

⁽²⁾ M. CERVASI, G. FIDECARO e L. MEZZETTI: *Nuovo Cimento*, 1, 300 (1955).

È facile vedere che per la somma di k impulsi v_m si ha:

$$(1) \quad V_k = \frac{\sum_m v_m (1/r_e + 1/r_m)}{1/r_e + \sum_m 1/r_m}.$$

La Σ va estesa ai k canali azionati che possono essere k qualsiasi fra gli n canali esistenti; v_m è l'ampiezza dell'addendo m -mo, cioè del segnale che si osserva fra gli estremi della resistenza di somma S quando è azionato il formatore m -mo (e solo quello). Inoltre:

$$1/r_e = \frac{1}{s} + \Sigma_m \frac{1}{R_m^0 + R_m}$$

$$1/r_m = \frac{1}{R_m^0 + R_m} - \frac{1}{R_m^0 + R_m}$$

dove R_m^0 e R_m^0 sono l'impedenza interna del formatore m -mo, rispettivamente in assenza e in presenza di impulso. Se $r_e |\Sigma_m 1/r_m| \ll 1$ e se i parametri dipendono poco dall'indice m la (1) diviene:

$$(2) \quad V_k = [1 - (r_e/r)(k-1)]kv,$$

dove r è il valore medio di r_m e v il valore medio di v_m , le medie essendo fatte su tutti gli n canali a un dato istante.

Dalla (2) risulta che il segnale di uscita non dipende linearmente dal numero k dei segnali addizionati; lo scostamento dalla linearità è tanto maggiore quanto maggiore è il rapporto r_e/r e può essere rilevante anche se r_e/r è molto piccolo, per valori grandi di k . Nel seguito ammetteremo tuttavia, per semplificare la discussione, che valga con approssimazione sufficiente la:

$$V_k = \Sigma_m v_m.$$

Vogliamo considerare separatamente la precisione e la stabilità del circuito di somma, intendendo per precisione una misura dello scostarsi delle n ampiezze dal loro valore medio v , a un dato istante, e per stabilità a lungo termine una misura della variazione nel tempo dell'ampiezza del singolo canale. Per quel che riguarda la precisione è facile stabilire quale deve essere la tolleranza per Δv_{\max} , il massimo valore di $v_m - v$, al variare di v_m . È ragionevole pensare che a causa dello scostarsi dei v_m da v , V_k si scosti dal suo valore medio (la media essendo fatta su tutte le possibili combinazioni di k canali su n) per una quantità che cresce con k fino a $k \sim n/2$, e quindi decresce riducendosi a zero per $k = n$. Si può scrivere allora:

$$(\Delta V_k)_{\max} = (n/2) \Delta v_{\max},$$

da cui segue che la discriminazione può essere effettuata senza errore se

$$\frac{\Delta v_{\max}}{v} < 2/n.$$

Con $n = 20$ basta pertanto una tolleranza di $\pm 10\%$. Il $\pm 5\%$ dovrebbe rappresentare un buon margine di sicurezza.

Considerazioni analoghe valgono ovviamente anche per la stabilità a lungo termine; in questo caso, però, occorre tener conto della eventuale deriva del valore medio di V_k (dovuta all'invecchiamento delle valvole o delle altre componenti). Essa può essere compensata mediante un opportuno aggiustamento del taglio dei discriminatori.

3. - Nelle soluzioni adottate per i circuiti di formazicne degli « addendi » si è dovuto tenere conto dell'elevato numero di canali e delle notevoli fluttuazioni nel tempo di salita dei contatori impiegati, che erano lunghi fino a 135 cm. Per queste ragioni, per esempio, abbiamo scartato a priori la possibilità di impiegare degli univibratori, dato che la esigenza di una sicura stabilità dell'intero sistema appariva in contrasto con quella di un taglio il più possibile ridotto sul segnale fornito dal contatore di Geiger.

In fig. 2 è dato lo schema del formatore di tipo a). Quando il contatore di Geiger viene scaricato, in B si ha un impulso la cui ampiezza (nell'ipotesi che il tempo di salita sia piccolo in confronto alla durata e $S \ll (r + R)$) è:

$$\Delta V = \frac{V_0}{r + R} R - V_a,$$

dove V_a è la tensione anodica della valvola in condizioni di riposo. Per quanto riguarda la valvola, la precisione dell'ampiezza dell'impulso di uscita dipende solo dalla precisione di V_a . Se si scelgono le condizioni di lavoro del tubo nel tratto in cui la caratteristica di placca sale molto rapidamente, è ragionevole pensare che le fluttuazioni di V_a dovute a variazioni nella tensione del filamento V_f o all'invecchiamento del tubo siano, al massimo, dell'ordine di grandezza di V_a . Introducendo pertanto un parametro di precisione $p = V_a / \Delta V$, è facile vedere che per p esiste una limitazione dipendente dalla costante di tempo τ del circuito di placca. Infatti: $p\tau = CR_i$, con R_i = resistenza interna della valvola, C = capacità parassita di placca. Si può allora fissare p e scegliere il tubo: per questioni di potere risolutivo conviene un tubo a interdizione netta, cioè con R_i piccolo. Si ricava quindi τ . Il valore di τ determina la scelta di R e r , insieme con il criterio di avere il massimo segnale ΔV compatibile con un assorbimento totale di corrente (inclusa la corrente di griglia schermo) ragionevolmente piccolo e con un punto di lavoro che si trovi nella

parte iniziale della caratteristica di placca del pentodo. In fig. 2 sono indicati i valori da noi scelti.

Per quel che riguarda R e r , ove basti una precisione degli impulsi non superiore al 5% si possono usare resistenze chimiche selezionate con una tolleranza del $\pm 1\%$. Le variazioni di ciascuna, se ci si mantiene sufficientemente lontani dai

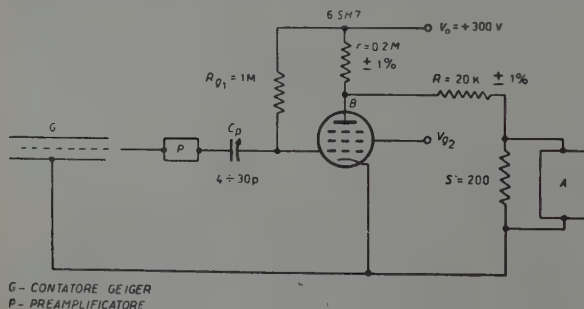


Fig. 2.

limiti di dissipazione massima, non superano il 3%, anche su periodi di impiego di alcune settimane, almeno per i tipi S.E.C.I. da noi usati.

Le variazioni di V_a che si riscontrano sostituendo la valvola a parità di altre condizioni, sono alquanto maggiori di quelle dipendenti da invecchiamento e da fluttuazioni nell'alimentazione dei filamenti. Su un gruppo di 17 valvole lo scarto massimo è stato di $\pm 1,2$ V su un valore medio di 4,4 V. Ciò non ha però una eccessiva importanza pratica, perchè le differenze fra le resistenze interne dei diversi tubi possono essere compensate sfruttando le piccole differenze residue fra le resistenze r ed R dei diversi circuiti (anche dopo averle selezionate con tolleranze ristrette): in pratica basta quasi sempre scambiare fra loro le valvole dei diversi canali finchè gli impulsi di uscita non sono uguali.

4. - Le condizioni di lavoro imposte al pentodo nel circuito di fig. 2 sono piuttosto inusuali per un tubo commerciale (tensione di placca dell'ordine di pochi volt). Le curve caratteristiche riportate nei cataloghi omettono spesso la regione delle basse tensioni anodiche; abbiamo perciò esaminato il comportamento di un certo numero di pentodi in queste condizioni, soffermandoci maggiormente sul tipo 6SH7 RCA. In fig. 3 è riportata la tensione anodica V_a in funzione della tensione di griglia controllo V_{g1} per una 6SH7, montata come indicato nella figura stessa. La curva *a*) si riferisce a una tensione di griglia schermo $V_{g2} = \text{cost} = 75$ V. Le curve *b*) e *c*) sono state ricavate con lo schermo polarizzato per caduta su una resistenza R_s rispettivamente di 40 k Ω e 80 k Ω . Al crescere di V_{g1} , V_a risale dopo avere raggiunto un minimo: la corrente anodica i_a presenta un massimo; al di là di questo si trova una regione in cui la

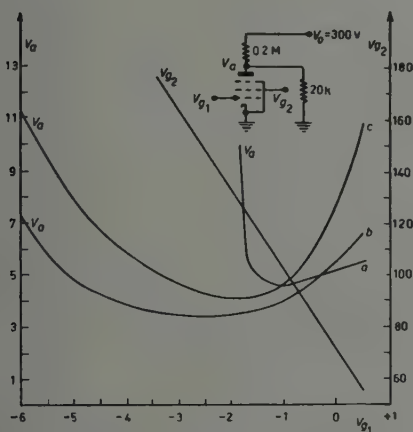


Fig. 3.

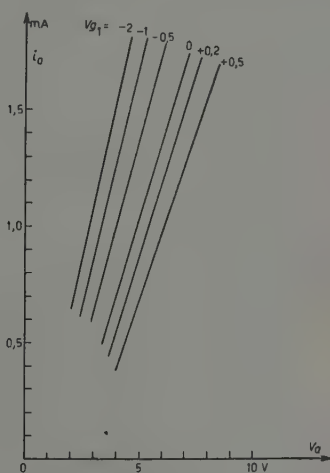


Fig. 4.

trasconduttanza griglia-controllo-placca è negativa. L'effetto appare più pronunciato se la griglia schermo non è mantenuta a una tensione fissa ma è polarizzata per caduta. In fig. 4 sono riportate le caratteristiche $i_a = i_a(V_a)$ con $R_s = 40$ k Ω per alcuni valori di V_{g1} compresi nella regione a trasconduttanza negativa. V_{g2} rimane costante su ciascuna delle rette di fig. 4 a un valore che

dipende da V_{g1} . In fig. 3 è mostrata la dipendenza di V_{g2} da V_{g1} per $R_s = 40 \text{ k}\Omega$.

Dalle fig. 3 e 4 si ricava che per $V_{g1} = 0$ il coefficiente di amplificazione del tubo cresce con R_s e vale 0,7; 2; 6; rispettivamente con $R_s \sim 0$ ($V_{g2} = \text{cost}$); $R_s = 40 \text{ k}\Omega$; $R_s = 80 \text{ k}\Omega$. Se si riducono gli effetti dovuti alle fluttuazioni dell'alimentazione dei filamenti ed all'invecchiamento del tubo a variazioni di V_{g1} , dall'esame dei diagrammi si conclude che le fluttuazioni di V_a decrescono con R_s e che pertanto, ai fini della stabilità, la polarizzazione fissa dello schermo è preferibile alla polarizzazione per caduta, contrariamente a ciò che accade per un pentodo usato in condizioni di lavoro normali. Per verificare la validità di queste considerazioni, è stata misurata V_a in funzione di V_f per un gruppo di 6SH7 montate come in fig. 2. La dipendenza di V_a da V_f nel circuito di fig. 2 con $V_{g2} = \text{cost}$ (curva *a*) e con griglia schermo polarizzata con $R_s = 40 \text{ k}\Omega$ (curva *b*) è mostrata in fig. 5. I risultati confermano, almeno qualitativamente, le conclusioni precedenti. Gli effetti dell'invecchiamento sono stati studiati su un circuito montato con resistenze di precisione a filo, e con tensione di griglia schermo stabilizzata: su un periodo di funzionamento continuo di parecchie centinaia di ore le variazioni massime osservate per la tensione V_a sono state di $\pm 0,2 \text{ V}$, corrispondenti a una precisione migliore dell'1% per l'ampiezza degli impulsi.

Il presentarsi di una regione a trasconduttanza negativa nelle nostre condizioni di lavoro non appare di semplice spiegazione né ci risulta essere stato specificamente descritto nei trattati sulle valvole termoioniche e nelle riviste tecniche a nostra disposizione (*RCA Review*, *P.I.R.E.*, *Bell System Technical Journal*). La possibilità che esso sia da attribuirsi a qualche tipo di autooscillazione della valvola su frequenze molto elevate non può essere completamente esclusa, per quanto ci sembri poco probabile, dati i controlli eseguiti. Fenomeni analoghi, dovuti a complessi effetti di carica spaziale, sono descritti

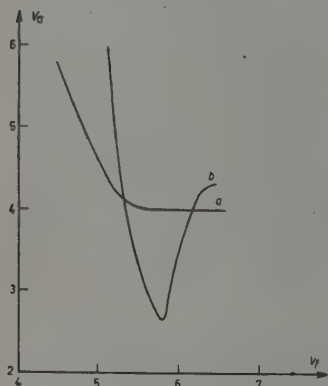


Fig. 5.

nel trattato di SPANGENBERG ⁽³⁾ ma l'applicabilità di quella analisi al caso qui in discussione non appare immediata: date le basse tensioni anodiche in gioco, è plausibile che alla creazione delle cariche spaziali contribuiscano sostanzialmente anche fenomeni di riflessione elastica degli elettroni sulla superficie dell'anodo, eventualmente contaminata dai vapori catodici ⁽⁴⁾. Non essendo convenientemente attrezzati per un più accurato studio sperimentale dell'effetto, ci limitiamo a segnalarlo, e ad osservare contemporaneamente che la sua presenza non appare compromettere la stabilità di funzionamento del circuito formatore di impulsi qui descritto.

5. - In fig. 6 è mostrato il formatore di impulsi di tipo *b*). In esso la precisione dell'impulso dipende evidentemente dalla precisione del taglio del diodo

do e della resistenza R . La variazione dei tagli dei diodi usati (6AL5) relativamente alle ampiezze degli impulsi che si possono ottenere, sono così ridotte, anche per quel che riguarda la sostituzione di un diodo con un altro, che la precisione e la stabilità del circuito risultano indipendenti dalle caratteristiche della valvola precedente e restano pertanto affidate essenzialmente a quelle

della resistenza R . Come preamplificatrice è stata scelta la 6U8 perchè riunisce, entro l'ingombro di un tubo in miniatura, un pentodo ad elevata trasconduttanza con un triodo di notevole amplificazione e bassa resistenza interna; ciò permette di realizzare una amplificazione molto grande del segnale di ingresso (cfr. 3, in principio) e una durata e tempo di salita notevolmente ridotti^(b). La durata dell'impulso è regolabile (come anche nel formatore di tipo a) da $\sim 3 \mu s$ a $\sim 15 \mu s$ mediante il compensatore C_p . Il tempo di salita non è indipendente dalla durata ed aumenta con il diminuire di questa: con la durata di $7 \mu s$ si ottiene un tempo di salita di $\sim 0,2 \mu s$.

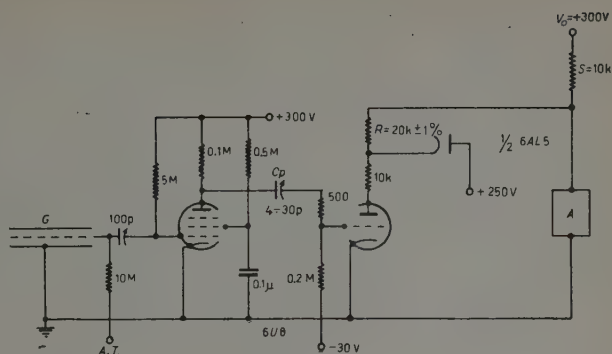


Fig. 6.

6. - Per il rapido controllo degli impulsi addendi, si è dimostrato di grande utilità un commutatore elettronico in cui l'elemento fondamentale è costituito

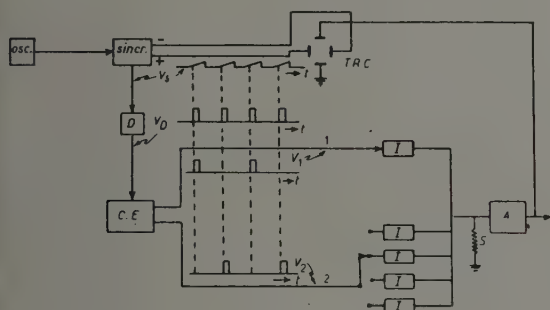


Fig. 7.

da un circuito a due posizioni di equilibrio stabile. Il principio di funzionamento è rappresentato in fig. 7. Un oscillatore comanda l'asse dei tempi di un sincroscopio, e un impulso viene trasmesso su questo comando dal sincroscopio al commutatore elettronico CE attraverso un discriminatore D . Il commutatore elettronico commuta l'impulso alternativamente sul canale campione e sul canale da confrontare. In tal modo, se la

frequenza dell'oscillatore è sufficientemente alta, sullo schermo dell'oscillografo si osservano sovrapposti i due impulsi addendi. Ogni piccola differenza, sia in tempo sia in ampiezza, è messa così facilmente in risalto.

È nostro dovere ringraziare il Dott. L. MEZZETTI per la collaborazione data nell'esecuzione del presente lavoro.

(³) K. R. SPANGENBERG: *Vacuum Tubes* (New York, 1948), pag. 259.

(⁴) H. BRUNINGS: *Physics and Applications of Secondary Electron Emission* (New York, 1954), pag. 107.

(⁵) Ringraziamo il sig. A. FERRERO per averci segnalato questa valvola.

SUMMARY

Two types of adding circuits used in a Cosmic Ray experiment in connection with a large Geiger counters hodoscope are described. Precision and long range stability of the output pulses are discussed. In one of the two circuits, the operating conditions of the pulse shaping tubes are rather unusual. As a consequence of the very low plate voltages used, the tubes exhibit a negative transconductance over a certain range of control grid voltages. This effect and its influence on the stability of the circuit are also discussed.

Un accélérateur à cavité.

J. POTTIER

C.E.A. - Division des Constructions Électriques - Centre d'Études Nucléaires de Saclay.

(ricevuto il 16 Marzo 1955)

Résumé. — On décrit rapidement un petit accélérateur à une seule cavité. Il permet d'accélérer à des énergies de 200 à 300 keV des particules relativement légères, électrons, protons et deutons. Ses utilisations principales sont la production de neutrons par réaction (d, n) et la production par impulsions de rayons X par freinage des électrons accélérés.

La construction de cette machine vise un double but:

1) réaliser une machine susceptible de délivrer un faisceau d'ions de basse énergie (quelques centaines de keV) mais d'assez forte intensité.

2) étudier quelques problèmes posés par la construction d'accélérateurs linéaires d'ions.

1. — Principe.

Pour obtenir un champ électrique intense, on utilise la résonance d'une cavité « réentrante » (schéma fig. 1).

Les ions issus de la source *S* située dans le cylindre intérieur de la cavité sont accélérés dans l'intervalle *I* avant d'atteindre la cible *C*.

Un oscillateur *O* fournit l'énergie H.F..

Le modulateur *M* l'alimente par impulsions en tension anodique.

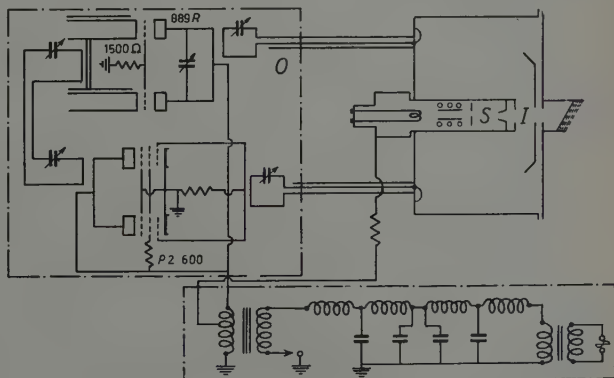


Fig. 1.

2. - Description sommaire des éléments.

La cavité. - Le choix d'un intervalle d'accélération I étroit présente les avantages suivants: *a)* on est dispensé de tout problème de focalisation, *b)* on peut utiliser une fréquence d'oscillation plus élevée, ce qui permet d'obtenir un meilleur rendement, *c)* la cavité a des dimensions plus petites et on peut utiliser des impulsions plus courtes.

En effet, pour une accélération à une énergie E_e donnée, la période de la H.F. doit être au moins le double du temps de transit pour que le champ reste accélérateur tout le long de la trajectoire de l'ion. La période minimum de la H.F. est alors approximativement proportionnelle à la longueur l de l'intervalle d'accélération.

Cependant, l est limité inférieurement par les claquages qui se produisent si le champ (approximativement proportionnel à E/l) est trop grand.

On a choisi comme longueur de l'intervalle d'accélération $l = 2,5$ cm et comme fréquence d'oscillation $f = 50$ MHz.

La longueur de la cavité et son diamètre mesurent environ 90 cm, tandis que le cylindre intérieur, qui doit contenir la source d'ions, a un diamètre de 32 cm.

Le choix de cette dernière dimension permet de n'employer aucun dispositif focalisant tout en ayant une cible extérieure.

La cavité est construite en tôle d'acier roulée et soudée, puis cuivrée intérieurement par électrolyse.

La surtension à vide mesurée est environ 18500.

L'oscillateur. - L'oscillateur est constitué par un amplificateur dont l'entrée et la sortie, reliées par deux câbles coaxiaux à deux boucles placées dans la cavité, sont couplées entre elles par le champ qui règne dans celle-ci. On obtient ainsi une oscillation stable à la fréquence de résonance de la cavité et une bonne adaptation des impédances.

L'amplificateur comprend un étage de puissance constitué par un push-pull sur lignes de triodes R.C.A. 889-R en montage inversé, et un étage d'attaque constitué par un push-pull sur lignes équipé d'une double pentode P.2.-600 S.F.R..

L'amplificateur de puissance, dont la puissance en régime continu est de 20 kW environ, peut fournir en régime pulsé (durée des impulsions 350 μ s, fréquence de répétition 50 Hz) une puissance crête de 150 kW.

Le modulateur. - C'est un modulateur à ligne à retard à charge résonante. A 50 Hz, la ligne se comporte comme une capacité. Une self est connectée en série avec celle-ci, de façon à former un circuit résonant sur 50 Hz. Ce circuit est alimenté par le secteur à travers un transformateur.

Un éclateur tournant mû par un moteur synchrone décharge périodiquement la ligne dans le primaire d'un transformateur d'impulsions qui adapte l'impédance du circuit d'anode de l'oscillateur à la résistance caractéristique de la ligne.

Ce modulateur délivre des impulsions de 350 μ s à une fréquence de répétition de 50 Hz.

Au cours des essais du modulateur débitant sur une charge résistive, on a obtenu une puissance de crête de 500 kW.

La source d'ions. — C'est une source du type Finkelstein. L'intensité maximum du faisceau d'ions frappant la cible est de 2,5 mA.

3. — Mise au point de la machine.

Dès les premiers essais on a obtenu un fonctionnement correct de chaque élément séparé. Toutefois, il n'en a pas été de même pour le fonctionnement de l'ensemble où on a rencontré de nombreuses difficultés, dont la plus importante était l'« Effet multipactor ».

Pour un fonctionnement à faible puissance, en régime continu et sans faisceau on a obtenu des troubles, dus au gaz résiduel, qui disparaissaient pour une pression inférieure à $5 \cdot 10^{-5}$ mm de mercure environ. Toutefois l'« effet multipactor » se manifestait dès qu'on cherchait à obtenir plus de 2 à 3000 V dans l'intervalle d'accélération, empêchant ainsi toute montée du champ à une valeur supérieure.

Ce phénomène (effet multipactor) est dû à la multiplication des électrons d'une paroi sur l'autre de l'intervalle d'accélération; il peut se produire quand le champ H.F. est tel que le temps de transit des électrons dans cet intervalle correspond à environ une demi-période de la H.F..

Pour l'éviter on a placé dans l'intervalle d'accélération un disque, percé d'un trou pour le passage du faisceau, porté à un potentiel d'environ 2000 V par rapport à la cavité, et qui rend différents, dans chaque sens, les temps de transit des électrons accélérés par le champ H.F..

Ce disque n'a pratiquement pas modifié la fréquence de résonance de la cavité, mais a diminué très sensiblement sa surtension.

4. — Résultats obtenus.

L'énergie maximum du faisceau est limitée par les claquages qui se produisent quand la tension dans l'intervalle d'accélération atteint 300 kV crête environ.

On peut alors accélérer des électrons, des protons ou des deutons à des énergies maxima respectives de 300, 240 ou 220 keV (à cause des temps de transit).

Le calcul montre que le spectre d'énergie des particules doit être très étroit au voisinage de l'énergie maximum. Ceci a été vérifié de façon qualitative. En utilisant un petit spectrographe magnétique muni d'un écran fluorescent, on voit une lueur beaucoup plus vive au voisinage immédiat de la raie correspondant à l'énergie maximum (*).

L'intensité moyenne du faisceau accéléré (de l'ordre de 20 μ A) est limitée par le débit crête de la source d'ions.

(*) Cette mesure est critiquable car:

- 1) la quantité de lumière émise croît avec l'énergie de la particule incidente;
- 2) le spectre d'un tel appareil se resserre vers les énergies élevées.

5. - Utilisation de la machine.

La machine paraît intéressante comme accélérateur de deutons. On l'emploie comme générateur de neutrons rapides en utilisant du deutérium comme cible, réaction (d-n).

On obtient 10^7 neutrons rapides par seconde.

Actuellement on étudie les possibilités de cette machine de produire la réaction (d-n) sur le tritium.

Enfin, le faisceau sortant est utilisé pour faire des études de dispositifs focalisants.

RIASSUNTO (*)

Si descrive brevemente un piccolo acceleratore a una sola cavità. Questa permette di accelerare fino a $200 \div 300$ keV le particelle relativamente leggere: elettroni, protoni e deutoni. I suoi principali impieghi sono: la produzione di neutroni sfruttando la reazione (d, n) e la produzione per impulso di raggi X per frenamento degli elettroni accelerati.

(*) Traduzione a cura della Redazione.

LETTERE ALLA REDAZIONE

(La responsabilità scientifica degli scritti inseriti in questa rubrica è completamente lasciata dalla Direzione del periodico ai singoli autori)

On the Cosmological Implication of Galactic Magnetic Fields (*).

R. L. BRAHMACHARY

Khaira Laboratory of Physics, Science College - Calcutta

(ricevuto il 15 Febbraio 1955)

The existence of a galactic magnetic field has been recently suggested by FERMI (1) in order to explain the high acceleration of cosmic-ray particles. Observations by HILTNER and HALL (2) of an appreciable polarization of light coming from distant stars have been interpreted as due to orientation of non-spherical dust grains by a magnetic field. This suggestion also supports the existence of a galactic magnetic field. We shall investigate the influence of this magnetic field on models of relativistic cosmology.

A spherically symmetric solution is concordant with a monopole only. Following the method employed by NORDSTRÖM and JEFFERY (for a charged particle) we consider a magnetic monopole at the origin. The only surviving component of the static field (F_{12} , F_{13} , F_{23}) is F_{23} or H_z . Assuming the metric to be

$$g_{\mu\nu} = \begin{pmatrix} -e^\lambda & 0 & 0 & 0 \\ 0 & -r^2 & 0 & 0 \\ 0 & 0 & -r^2 \sin^2 \theta & 0 \\ 0 & 0 & 0 & e^\nu \end{pmatrix}$$

(*) DE SITTER: *in Memoriam*.

(1) E. FERMI: *The Astrophysical Journal*, **119**, 1 (1954).

(2) Quoted by H. FERMI: *ibid.*

we obtain

$$\mathcal{J}^{23} = F^{23} \sqrt{-g} = [e^{\frac{1}{2}(\lambda+\nu)} / r^2 \sin \theta] M$$

where

$$M = (\partial K_2 / \partial x_3 - \partial K_3 / \partial x_2)$$

and K_i = four-potential.

We further impose the condition of no charge and current:

$$\partial \mathcal{J}^{23} / \partial x_3 = \frac{1}{r^2 \sin^2 \theta} \frac{\partial}{\partial \varphi} [e^{\frac{1}{2}(\lambda+\nu)} M] = 0.$$

We then have

$$M = e^{-\frac{1}{2}(\lambda+\nu)} c.$$

Again, from the relation

$$t_\mu^\nu = -F^{\nu\alpha} F_{\mu\alpha} + \frac{1}{4} g_\mu^\nu F^{\alpha\beta} F_{\alpha\beta}$$

we find

$$(1) \quad 8\pi t_1^1 = -8\pi t_2^2 = 4\pi M^2 / r^4 \sin^2 \theta$$

and

$$\lambda = -\nu; \quad M = c.$$

Assuming the well known equation (3)

$$8\pi T_1^1 = -e^\lambda (\nu'/r + 1/r^2) + 1/r^2$$

(3) R. C. TOLMAN: *Relativity Thermodynamics and Cosmology* (Oxford, 1934) pag. 242.

with

$$ds^2 = -e^{-\lambda} dr^2 - \dots + e^{\nu} dt^2$$

we have from (1):

$$(2) \quad c_1/r^4 = -e^{\lambda} \nu'/r - e^{\lambda}/r^2 + 1/r^2$$

$$[c_1 = 4\pi M^2; \lambda = \nu]$$

provided we choose such a plane that $\sin^2 \theta = 1$.

The solution of (2) is

$$e^{\nu} = (1 + c_2/r + c_1/r^2).$$

Also

$$ds^2 = -e^{-\nu} dr^2 - \dots + e^{\nu} dt^2.$$

This solution is exactly like that of NORDSTRÖM and JEFFERY.

We shall now attempt to find the non-local i.e., cosmological form of the line-element. In order to avoid the special difficulties of a spatially finite model containing a magnetic field, we shall work with an open model. The following method based on TOLMAN's presentation (4) will clearly show how this model differs from that of EINSTEIN.

Without imposing the restriction $\lambda = -\nu$ for the line element

$$ds^2 = -e^{\lambda} dr^2 - \dots + e^{\nu} dt^2$$

TOLMAN obtained the relation

$$(3) \quad dp/dr = -(\rho + p)\nu'/2.$$

Similarly we shall have

$$(i) \quad T_1^1 = T_2^2 = T_3^3 = -p = 0; \quad T_4^4 = \rho = 0$$

(4) R. C. TOLMAN: *ibid.*, p. 243.

or

$$(ii) \quad p \neq 0; \quad \rho \neq 0$$

and

$$8\pi t_1^1 - 8\pi t_2^2 = 2c_1/r^4.$$

$$\text{CASE 1. } 8\pi T_1^1 = 0; \quad 8\pi t_1^1 \neq 0.$$

We have the line-element (3) if the cosmological constant be zero.

CASE 2. The non-static flat model of Einstein and De Sitter (5).

If \mathcal{T}_1^1 is the general energy tensor, which can be split up into t_1^1 and T_1^1 , and knowing (5) that

$$8\pi T_1^1 = \ddot{g} + \frac{3}{4}(\dot{g})^2,$$

we have:

$$(4) \quad 8\pi \mathcal{T}_1^1 = 8\pi t_1^1 + \ddot{g} + \frac{3}{4}(\dot{g})^2 \\ = -e^{-\lambda_E} e^{-g} (\nu_E'/r + 1/r^2) + 1/r^2$$

where $\dot{g} = dg/dt$ and $\partial \lambda_E, \nu_E$ are the contributions due to the t_μ^ν .

From (4) we obtain the relation

$$(5) \quad e^{-\lambda_E} = e^{\nu_E} = e^g 2c_1/r^2 + e^g - \\ - e^g/3[\ddot{g} + \frac{3}{4}(\dot{g})^2]r^2 + e^g c_2/r$$

where c_2 is a constant of integration. The form of the line-element is then

$$(6) \quad ds^2 = -e^{\lambda+\lambda_E} dr^2 - \dots + e^{\nu+\nu_E} dt^2 \\ = -(e^g/e^{\nu_E}) dr^2 - \dots + e^{\nu_E} dt^2.$$

Discussion on the line element shall form the second part of our treatment.

I take this opportunity of thanking Dr. T. ROY for his discussion on a certain point.

(5) R. C. TOLMAN: *ibid.*, p. 451.

An Improved Approximate Analytic Solution of the Tomas-Fermi Equation for Atoms.

T. TIETZ

Nicolas Copernicus University - Toruń (Poland)

(ricevuto il 14 Marzo 1955)

The solution of the Thomas-Fermi (F-T) equation for free neutral atom is reducible ⁽¹⁾ to the solution of the equation

$$(1) \quad \frac{d^2 \Phi}{dx^2} = x^{-1} \Phi^{\frac{5}{2}},$$

subject to the boundary conditions

$$(2) \quad \Phi(0) = 1, \quad \Phi(\infty) = 0.$$

There have been given the approximate solutions (denoted simply by A-S) of the (F-T) equation previously by SOMMERFELD ⁽²⁾ and ROZENTAL ⁽³⁾ as well as by MARCH ⁽⁴⁾ and KERNER ⁽⁵⁾ and recently by BRINKMAN ⁽⁶⁾ and the author ⁽⁷⁾. The comparison of these different A-S and the further derivation of prospective A-S would be facilitated if there existed a measure for the approximation degree of any A-S. For this measure UMEDA ⁽⁸⁾ has proposed to employ the numerical value of the variational integral

$$(3) \quad I(\Phi) = \int_0^{\infty} [(\Phi')^2 + \frac{4}{5} \Phi^{\frac{5}{2}}/x^{\frac{1}{2}}] dx,$$

evaluated by putting the given A-S in place of Φ . Since the minimization of I is equivalent to the integration of the F-T equation, the best A-S should give as result

⁽¹⁾ E. U. CONDON and G. H. SHORTLEY: *The theory of atomic spectra* (Cambridge, 1935), p. 335.

⁽²⁾ A. SOMMERFELD: *Zeits. f. Phys.*, **78**, 283 (1932).

⁽³⁾ S. ROZENTAL: *Zeits. f. Phys.*, **98**, 742 (1935).

⁽⁴⁾ N. H. MARCH: *Proc. Camb. Phil. Soc.*, **46**, 336 (1950).

⁽⁵⁾ E. H. KERNER: *Phys. Rev.*, **83**, 71 (1951).

⁽⁶⁾ H. C. BRINKMAN: *Physica*, **20**, 44 (1954).

⁽⁷⁾ T. TIETZ: *Journ. of Chem. Phys.*, **22**, 2094 (1955); *Ann. d. Phys.*, **15**, 186 (1955).

⁽⁸⁾ K. UMEDA: *Journ. Phys. Soc. Japan.*, **9**, 290 (1954).

the smallest numerical value of I . For MIRANDA'S ⁽⁹⁾ exact solution, direct numerical quadrature of (3) gives the value

$$I = 1,3625,$$

which should be of course the limiting minimum value of I . Using the equation (3) UMEDA has determined the disposable parameters for the A-S of SOMMERFELD ⁽²⁾

$$(4) \quad \Phi(x) = [1 + (x/12^{\frac{2}{3}})^{\frac{1}{2}}]^{-3/\lambda}$$

and for the A-S of KERNER

$$(5) \quad \Phi(x) = 1/(1 + Cx),$$

UMEDA has found

TABLE I.

A-S of KERNER		A-S of SOMMERFELD	
$\frac{dI}{dC} = 0$	$C = 1,3679$ $I = 1,3679$	$\frac{dI}{d\lambda} = 0$	$\lambda = 0,8371$ $I = 1,3670$

For the A-S of the author

$$(6) \quad \Phi(x) = \frac{a^2}{(x + a)^2},$$

the constant a being considered as a disposable parameter. Equation (3) is reduced to single function of a

$$(7) \quad I(\Phi) = \frac{4}{5a} + \frac{4}{5} \int_0^{\infty} \frac{x^{-\frac{1}{2}}}{(1 + x/a)^5} dx = \frac{4}{5a} + \frac{7\pi a^{\frac{1}{2}}}{2^5},$$

for $dI/da = 0$ we find

$$(8) \quad a = 2^{\frac{1}{2}} \left(\frac{4}{35 \cdot \pi} \right)^{\frac{2}{5}},$$

also

$$(9) \quad I = 0,15 \cdot (\pi \cdot 8,75)^{\frac{2}{5}}.$$

We obtain in our case

$$(10) \quad a = 1,7566, \quad I = 1,3662.$$

According to the Table I and (10) we see that our A-S is capable of extensive application by virtue of its simplicity and higher degree of approximation.

The author thanks to Prof. Dr. KWAI UMEDA for his precious advice.

⁽⁹⁾ C. MIRANDA: *Mem. R. Accad. d'Italia*, 5 (1934).

^(*) We have determined the values of a and I with the sevenplace logarithms.

Coulomb Effects in the ${}^6\text{Li}(n, \alpha){}^3\text{H}$ and ${}^6\text{Li}(p, \alpha){}^3\text{He}$ Reactions.

J. SAWICKI

Institute of Theoretical Physics, University of Warsaw - Warsaw

(ricevuto il 21 Marzo 1955)

Recently ⁽¹⁾ Coulomb corrections to the Butler cross-section for the (d, p) and (d, n) reactions were discussed with the help of the « zero-range » Horowitz-Messiah approximation for the n-p interaction. The integrations in the matrix elements were performed with the help of complicated numerical computations.

It appears that on applying the H.-M. approximation and the asymptotical exponential form of the wave function of the particle captured in the particular case of the *S*-state in the one-particle model (e.g. for the ${}^{29}\text{Si}$ -nucleus) one can calculate analitically the matrix element for a (d, p) or (d, n) reaction with the Coulomb wave functions. The calculations for this case are in preparation.

A somewhat similar situation is in the case of the ${}^6\text{Li}(n, \alpha){}^3\text{H}$ reaction. This reaction was recently ⁽²⁾ investigated from the point of view of the « α -particle + + deuteron » model with the assumption that the « α +d » system is in *S*-state.

The Born approximation differential cross-section in the c.m. system for this reaction was obtained in ref. ⁽²⁾ in the form:

$$(1) \quad \sigma(\theta) = \frac{M_t^x M_{n_0}^x}{(2\pi\hbar^2)^2} \frac{k_t}{k_{n_0}} \left[\frac{1}{2 \cdot 3} \sum_{\mu_0, \mu_d, \mu_t} |\langle \chi_\alpha \cdot \chi_t \exp [i\mathbf{k}_t(\mathbf{r} - \mathbf{s})/3] | V_{n_0 d} | \psi_0 \rangle|^2 \right],$$

where: $M_t^x = (12/7)M$, $M_{n_0}^x = (6/7)M$ are resp. the triton and the neutron reduced masses; k_t and k_{n_0} are the resp. momenta in the c.m. system; μ_i are the resp. magnetic quantum numbers, $\chi_\alpha = \chi_\alpha(\xi)$ is the internal wave function of the α -particle, $\chi_t = S_{\mu_t}(\sigma_0 \sigma_n \sigma_p) R_t(s, u)$ of the triton, σ_i being the resp. spin variables; $\mathbf{s} = [(\mathbf{r}_n + \mathbf{r}_p)/2]p - \mathbf{r}_{n_0}$, $\mathbf{u} = (\sqrt{3}/2)(\mathbf{r}_n - \mathbf{r}_p)$ are the internal coordinates of the triton, \mathbf{r} is the vector from the α -particle to the deuteron: $V_{n_0 d}$ is the incident neutron-deuteron interaction. ψ_0 is defined by:

$$\psi_0 = \chi_{\mu_0}(\sigma_0) \exp \left[i\mathbf{k}_0 \left(\frac{2}{3} \mathbf{r} - \mathbf{s} \right) \right] \chi_\alpha(\xi) S_{\mu_d}(\sigma_n \sigma_p) \psi \left(\frac{2}{\sqrt{3}} u \right) \Phi(r),$$

χ_{μ_0} and S_{μ_d} are the neutron and the deuteron spin functions; $\psi(q)$ is the unperturbed deuteron internal function and $\Phi(r)$ is the *S*-state « α +d » system internal function.

⁽¹⁾ J. Yoccoz: *Proc. Phys. Soc.*, A **67**, 813 (1954).

⁽²⁾ J. DĄBROWSKI and J. SAWICKI: *Phys. Rev.*, **97**, 1002 (1955).

Now we shall not apply the transformation of the matrix element as done in ref. (2), but the «zero range» interaction $V_{nd} = -(3\pi a_{nd}\hbar^2/M)\delta(\mathbf{s})$, where $a_{nd} = \sqrt{(2/3)a_1^2 + (1/3)a_2^2} = 5.08 \cdot 10^{-13}$ cm the n-d «scattering length» given by CRISTIAN and GAMMEL (3) as done in ref. (4) (*). As a result we have:

$$(2) \quad \frac{1}{2 \cdot 3} \sum |\langle \rangle|^2 = \frac{1}{4} \left(\frac{3\pi a_{nd}\hbar^2}{M} \right)^2 |b_k|^2 |I_t|^2,$$

where $b_k = \int R_t(u, 0) \psi \left(\frac{2}{\sqrt{3}} u \right) du$ and $I_t = \int \Phi(r) \exp [i\mathbf{K}\mathbf{r}] d\mathbf{r}$ where $\mathbf{K} = \frac{2}{3} \mathbf{k}_{n_0} - \mathbf{k}_t$.

Similarly as in ref. (5) on applying for $\Phi(r)$ the asymptotical form $\sqrt{\frac{\tilde{\alpha}}{2\pi}} \frac{\exp [-\tilde{\alpha}r]}{r}$

where $\tilde{\alpha} = \sqrt{(8/3) M \tilde{\epsilon}} / \hbar^2$ ($\tilde{\epsilon} = 1.477$ MeV = the binding energy of the deuteron in the

^6Li nucleus). We obtain: $I_t = \sqrt{\frac{\tilde{\alpha}}{2\pi}} \frac{4\pi}{K^2 + \tilde{\alpha}^2}$. The last assumption for $\Phi(r)$ increases, however, too much the absolute values of the cross section, but does not alter considerably the angular distribution similarly as the analogically widely used assumption for the deuteron function in stripping.

Let us now discuss the Coulomb effect of the outgoing triton wave in (1). The Coulomb polarization of the strongly bound structure of the triton is negligible.

On putting the Coulomb wave function in the place of the triton plane wave in (1) we obtain instead of I_t :

$$(3) \quad I_t^c = \int \Phi(r) \exp \left[i \frac{2}{3} \mathbf{k}_{n_0} \mathbf{r} \right] \cdot F_t^c(\mathbf{r}) d\mathbf{r},$$

where:

$$F_t^c(\mathbf{r}) = \exp \left[-\frac{\pi n}{2} t \right] \Gamma(1 + in_t) \exp [-i\mathbf{k}_t \mathbf{r}] {}_1F(-in_t; 1; i(k_t r + \mathbf{k}_t \cdot \mathbf{r})),$$

$n_t = 2e^2 M_t / \hbar^2 K_t$; ${}_1F$ is the confluent hypergeometrical function.

The last integral may be evaluated by a straightforward generalisation of the Sommerfeld method (6) for the case $\tilde{\alpha} \neq 0$:

$$I_t^c = \exp \left[-\frac{\pi n}{2} t \right] \Gamma(1 + in_t) I_t \left\{ \frac{(4/9)k_{n_0}^2 - k_t^2 + \tilde{\alpha}^2 - i2\tilde{\alpha}k_t}{K^2 + \tilde{\alpha}^2} \right\}^{in_t}.$$

The ratio of the cross-section resulting from (3) to $\sigma(\theta)$ is:

$$(4) \quad \frac{\sigma^c(\theta)}{\sigma(\theta)} = \frac{|I_t^c|^2}{|I_t|^2} = \exp [-\pi n_t] \cdot \frac{\pi n_t}{\text{sh } \pi n_t} \cdot \exp \left[-2n_t \arctg \frac{2\tilde{\alpha}k_t}{k_t^2 - (4/9)k_{n_0}^2 - \tilde{\alpha}^2} \right].$$

(3) J. DĄBROWSKI et J. SAWICKI: *Bull. Acad. Pol. Sci.*, **3** (1955).

(4) R. CHRISTIAN et J. GAMMEL: *Phys. Rev.*, **91**, 100 (1953).

(*) The «zero-range» approximation is reasonable for neutron energies considerably less than 10 MeV; here it is equivalent mathematically to the H.-M. approximation.

(5) I. WASZAKIDZE et G. CZILASZWILI: *Journ. Phys. USSR*, **28**, 254 (1954).

(6) A. SOMMERFELD: *Wellenmechanik*, p. 502.

We observe that in our approximation this ratio is independent of $\theta (= \angle(\mathbf{k}_{n_0}, \mathbf{k}_t))$ i.e. that the angular distribution remains unchanged. However, as it is seen from Fig. 1 the agreement of the angular distribution with experiment for 1.5 MeV neutrons is quite good (considerably better than that in ref. (2)).

It is then concluded, that the « zero-range » interaction « wiping out » the factor I_k from ref. (2) is even a better approximation for small energies.

Similarly as in ref. (1) the absolute values of $\sigma(\theta=0)$ and $\sigma^c(\theta=0)$ are more important. The values of these quantities for 1.5 MeV neutron energy are shown in Table I for 3 cases:

- 1) R_t , the gaussian function used in ref. (7) and ψ , the usual square well deuteron function,
- 2) R_t , the same as in (1) and ψ , the Hulthén function with the parameter values given by CHEW and GOLDBERGER (8),
- 3) R_t , the Irving's function defined in ref. (9) and ψ , the same as in (2).

TABLE I.

	(1)	(2)	(3)
$\sigma(\theta=0)$	215.3	222.1	196.1
$\sigma^c(\theta=0)$	94.7	97.7	86.3

$\sigma(\theta=0)$ and $\sigma^c(\theta=0)$ in $\mu\text{b/ster}$ for 1.5 MeV neutrons. The ratio σ^c/σ is equal respectively for neutron energies: 1.5; 2 and 14 MeV: 0.44; 0.43 and 0.62. As it was mentioned the use of $\Phi(r) = \sqrt{\tilde{\alpha}/2\pi} \exp[-\tilde{\alpha}r]/r$ gives too great $\sigma(\theta=0)$. In ref. (2) the best value $\sigma(\theta=0) = 72 \mu\text{b/ster}$ for 1.5 MeV neutrons was obtained for small energies « α -d » interaction radius $R_0 = 4 \cdot 10^{-13} \text{ cm}$, R_t —gaussian and ψ —Hulthén. Since the resp. experimental value (10) is $\sigma(\theta=0) = 46 \mu\text{b/ster}$, on extrapolating our result $\sigma^c/\sigma \cong 0.44$ to the approximation of ref. (2) we would obtain a better agreement with experiment.

Further we see that σ^c/σ increases together with the neutron energy. In ref. (2)

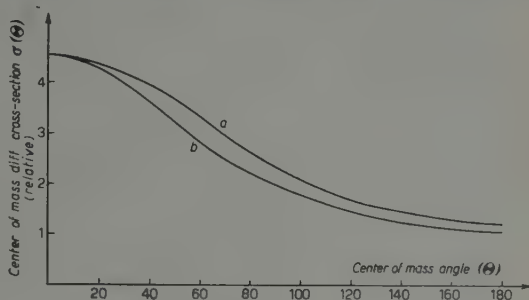


Fig. 1. — Angular distribution of tritons from ${}^6\text{Li}(n, \alpha){}^3\text{H}$ for incident neutron energy = 1.5 MeV: a) experimental (WEDDEL and ROBERTS (10)), b) theoretical.

(7) H. NEWNS: *Proc. Phys. Soc.*, A **65**, 916 (1952).

(8) G. CHEW and M. GOLDBERGER: *Phys. Rev.*, **77**, 470 (1950).

(9) J. IRVING: *Phil. Mag.*, **42**, 338 (1951).

(10) I. WEDDEL and J. ROBERTS: *Phys. Rev.*, **95**, 117 (1954).

too low values of $\sigma(\theta=0)$ were obtained for 14 MeV neutrons. A much better (greater) value of $[\sigma]_{14}/[\sigma]_{1.5}$ is hoped to result due to the Coulomb effect.

On assuming the same « zero range » nuclear interaction nucleon-deuteron as done previously we shall now discuss the Coulomb effect of the incoming proton and outgoing ${}^3\text{He}$ -nucleus wave for the ${}^6\text{Li}(p, \alpha){}^3\text{He}$ reaction (*). In the place of I_i in (2) we shall have:

$$(5) \quad I_3^c = \int \Phi(r) F_{p_0} \left(\frac{2}{3} \mathbf{r} \right) F_3^x(\mathbf{r}) d\mathbf{r},$$

where:

$$F_{p_0} \left(\frac{2}{3} \mathbf{r} \right) = \exp \left[-\frac{\pi n_0}{2} \right] \Gamma(1 + in_0) \exp \left[i \frac{2}{3} \mathbf{k}_{p_0} \mathbf{r} \right] {}_1F(-in_0, 1; i \frac{2}{3} (k_{p_0} r - \mathbf{k}_{p_0} \cdot \mathbf{r})),$$

$$F_3^x(\mathbf{r}) = \exp \left[-\frac{\pi n_3}{2} \right] \Gamma(1 + in_3) \exp [-i \mathbf{k}_3 \mathbf{r}] {}_1F(-in_3, 1; i(k_3 r + \mathbf{k}_3 \cdot \mathbf{r})),$$

$n_0 = \frac{3e^2 M_{p_0}^x}{\hbar^2 k_{p_0}}$, $n_3 = \frac{4e^2 M_3^x}{\hbar^2 k_3}$ and k_{p_0} , k_3 are the proton and ${}^3\text{He}$ momenta in the c.m. system.

On integrating (5) on Sommerfeld method we find:

$$I_3^c = \exp \left[-\frac{\pi}{2} (n_0 + n_3) \right] \Gamma(1 + in_0) \Gamma(1 + in_3) \cdot I_3 \cdot \left\{ \frac{k_3^2 - (4/9)k_{p_0}^2 + \tilde{\alpha}^2 - i(4/3)\tilde{\alpha}k_{p_0}}{\sigma^2 + \tilde{\alpha}^2} \right\}^{in_0} \cdot \left\{ \frac{(4/9)k_{p_0}^2 - k_3^2 + \tilde{\alpha}^2 - i2\tilde{\alpha}k_3}{\sigma^2 + \tilde{\alpha}^2} \right\}^{in_3} {}_2F_1 \left(-in_0, -in_3, 1; \lambda \sin^2 \frac{\theta}{2} \right),$$

where: $\sigma = (2/3)\mathbf{k}_{p_0} - \mathbf{k}_3$, $I_3 = \sqrt{\tilde{\alpha}/2\pi} \cdot 4\pi/(\sigma^2 + \tilde{\alpha}^2)$ is the hypergeometrical function and

$$\lambda = \frac{(8/3)k_{p_0}k_3\{((2/3)k_{p_0} + k_3)^2 - \tilde{\alpha}^2 + i2\tilde{\alpha}((2/3)k_{p_0} + k_3)\}}{(k_3^2 - (4/9)k_{p_0}^2 + \tilde{\alpha}^2 - i(4/3)\tilde{\alpha}k_{p_0})((4/9)k_{p_0}^2 - k_3^2 + \tilde{\alpha}^2 - i2\tilde{\alpha}k_3)}.$$

The respective ratio $\sigma^c(\theta)/(\sigma(\theta))$ is:

$$(6) \quad \frac{\sigma^c(\theta)}{\sigma(\theta)} = \frac{|I_3^c|^2}{|I_3|^2} = \exp [-\pi(n_0 + n_3)] \frac{\pi n_0}{\text{sh } \pi n_0} \cdot \frac{\pi n_3}{\text{sh } \pi n_3} \exp \left[2n_0 \text{arctg } \frac{(4/3)\tilde{\alpha}k_{p_0}}{k_3^2 - (4/9)k_{p_0}^2 + \tilde{\alpha}^2} \right] \cdot \exp \left[-2n_3 \text{arctg } \frac{2\tilde{\alpha}k_3}{k_3^2 - (4/9)k_{p_0}^2 - \tilde{\alpha}^2} \right] \cdot \left| {}_2F_1 \left(-in_0, -in_3, 1; \lambda \sin^2 \frac{\theta}{2} \right) \right|^2.$$

(*) Since the Coulomb barrier is \sim the « α -d » binding energy, the Coulomb polarization of the « α -d » system is negligible (see ref. (1)).

The numerical computations were performed for the incident proton energy = 6 MeV. Similar to the results of ref. (1) for (d, p) reactions the angular distribution is only very slightly flattened due to the Coulomb field (Fig. 2), but the

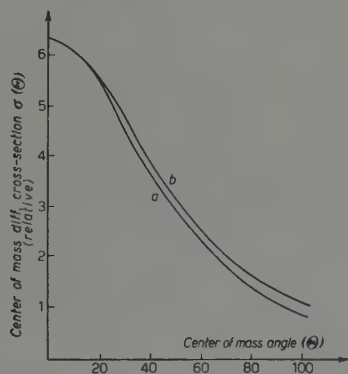


Fig. 2. - Theoretical angular distribution of ${}^3\text{He}$ -nuclei from ${}^6\text{Li}(\text{p}, \alpha){}^3\text{He}$ for incident proton energy = 6 MeV: a) without Coulomb effect; b) including Coulomb effect.

absolute values are very distinctly lowered: $\sigma^e(\theta=0)/\sigma(\theta=0) \cong 0.136$. Due to the Coulomb effect of the incoming proton wave the cross-section for ${}^6\text{Li}(\text{p}, \alpha){}^3\text{He}$ reaction is for 6 MeV protons several times smaller than that for ${}^6\text{Li}(\text{n}, \alpha){}^3\text{H}$ for MeV 6 neutrons.

My thanks are due to Dr. J. DĄBROWSKI and Dr. M. SUFFCZYŃSKI for interesting discussions.

On the Mean Lives of Heavy Unstable Particles.

N. DALLAPORTA

Istituto di Fisica dell'Università - Padova

Istituto Nazionale di Fisica Nucleare - Sezione di Padova

(ricevuto il 24 Marzo 1955)

It is well known that one of the greatest difficulties in interpreting the properties of heavy unstable particles, which in these last years have been detected in a continuously increasing number of different types either in the cosmic radiation or in nuclear disintegrations artificially produced, consists in reconciling their relatively abundant production in the nuclear events, which is compatible with an interaction of the same order of magnitude as the interaction for π production, with their long mean life, which should instead require a very weak interaction. This peculiar feature which is common to all unstable particles known up to date has recently been tentatively explained by GELL-MANN and PAIS ⁽¹⁾ in the following way: the strong interaction from which these « strange » particles originate (and also their electromagnetic interaction) are subject to special selection rules, which are correlated to conservation theorems imposed to a new internal coordinate of these particles, specially introduced for this purpose, and which act in such a way that they allow only those reactions in which two « strange » particles are produced together, while they forbid those reactions in which they should be produced singly.

These selection rules are supposed to act only on the strong nuclear and electromagnetic interactions, and not on other possible weak interactions, which could be responsible only in a very secondary way for exceptional cases of single production, and would instead be the only ones responsible for those decay processes, which are forbidden by the selection rules for the strong interactions. Some possible classification schemes and additional new quantum numbers attributed to the strange particles are proposed by the authors, from which, in the spirit of charge independence, it is possible to formulate those additional conservation theorem responsible for the new desired selection rules.

The aim of the present considerations is only to show how, in the framework of the GELL-MANN and PAIS hypothesis, it is easy to deduce the right order of magnitude for the mean lives of the different kinds of « strange » particles by the

⁽¹⁾ M. GELL-MANN and A. PAIS: *Proceedings of the Glasgow Conference on Nuclear Physics*, (London, 1954), p. 342.

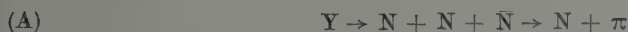
exclusive use of interaction constants already known from interactions of « normal » particles.

Let us consider first the group of forbidden reactions which can take place only through the weak interaction, and let us choose among them as representative the reaction: (N = nucleons, Y = hyperons)



As the Gell-Mann Pais selection rules forbid that forces other than weak ones may act between two nucleons for the creation of a single hyperon, and as this reaction takes place between 4 fermions, it seems rather natural to assume that in this case the weak interaction should be the universal Fermi interaction between fermions, with interaction constant $G \sim 2 \cdot 10^{-49} \text{ erg} \cdot \text{cm}^3$.

The virtual inversion of this reaction allows us then to interpret the decay of an hyperon according to the following two-step process:



which may be then described with the use of only the Fermi interaction constant and the g interaction constant between pions and nucleons.

For the sake of evaluating only the order of magnitude, it is sufficient to use scalar interactions with $g^2/4\pi\hbar c = 0.25$ and the drastic simplifications used by FERMI ⁽²⁾ for the sums on the intermediate states. We get in this way for the transition probability per unit times w_Y :

$$(1) \quad w_L = \frac{0.1}{8\pi^4} \frac{1}{\hbar} \frac{G^2 M^4 c^2}{\hbar^6} \frac{g^2}{4\pi\hbar c} \frac{c^3 p^2}{w(v_1 + v_2)}$$

where M is the mass of the nucleon, p and w the momentum and total energy of the final pion, and v_1 and v_2 the velocities of the decay products.

For the Λ_0 we obtain:

$$(2) \quad \frac{1}{w_\Lambda} \sim 6.7 \cdot 10^{-10} \text{ s.}$$

The same calculation for the Σ and Ξ particles, according to a similar scheme, would have given very similar results.

Let us take now as representative for the allowed strong interaction the process (K = heavy boson)



and let us suppose that in this case the interaction constant is the same as the g constant of the pions. This of course implies that the associated production of the heavy unstable particles will be of the same order of magnitude as the production of pions.

By inverting the reaction, we can now try to interpret the decay of the different K by the following 3rd order process:

⁽²⁾ E. FERMI: *Elementary Particles* (Oxford, 1951).

for the θ -decay:

$$(B) \quad \theta \rightarrow Y + \bar{N} \rightarrow Y + N + \pi \rightarrow \pi + \pi$$

and for the τ decay:

$$(C) \quad \tau \rightarrow Y + \bar{N} \rightarrow Y + \bar{N} + \pi + \pi \rightarrow \pi + \pi + \pi.$$

In both cases the transition $Y + N \rightarrow \pi$ is to be considered as equivalent to process (A) and defined by the constant:

$$\frac{1}{2\pi} \frac{\gamma^2}{\hbar c} = \frac{0.1}{8\pi^4} \frac{G^2 M^4 c^2}{\hbar^6} \frac{g^2}{4\pi\hbar c}.$$

In case of the τ -decay the emission of two pions in a single act is assumed to be more probable than and equivalent two step process in which the two π -mesons should be emitted in succession, according to the experimental Brookhaven evidence⁽³⁾ on production of pions by 3 GeV energy protons.

In the same approximation as before, we get for the θ -decay:

$$(3) \quad w_\theta = \frac{0.044}{16\pi^2} \frac{1}{\hbar} \left(\frac{g^2}{4\pi\hbar c} \right)^2 \frac{\gamma^2}{2\pi\hbar c} \frac{M}{\mu_k} M c^2 \frac{c^2 p^2}{w^2} \frac{c}{v_1 + v_2}$$

with μ_k mass of the θ , w and p energy and momentum of final π ; which compared with (2) gives us:

$$(4) \quad \frac{w_\theta}{w_\pi} \sim 1,08 \cdot 10^{-3} \quad \text{hence} \quad \frac{1}{w_\theta} \sim 6,2 \cdot 10^{-7} \text{ s.}$$

For the τ -decay, let us first try to form a tentative evaluation of the interaction constant for double pion production:

According to the statistical theory of FERMI⁽⁴⁾ the ratio of the production cross-sections σ_2 and σ_1 for two and one pion in nucleon-nucleon collision, should be:

$$\frac{\sigma_2}{\sigma_1} = \frac{V}{\Omega} \frac{g(4)}{g(3)} \sim \frac{3}{20},$$

V = Fermi volume, Ω = normalization volume; $g(3)$ and $g(4)$ statistical factors for 3 and 4 final reaction products.

According to Brookhaven data, this ratio is instead:

$$\frac{\sigma_2}{\sigma_1} = \frac{V'}{\Omega} \frac{g(4)}{g(3)} = \frac{3}{1} \quad \text{hence} \quad \frac{V'}{V} \sim 20.$$

Therefore we can interpret the creation of the second pion as if the interaction constant g' in this case should be $g'^2 \simeq 20 g^2$.

(3) W. B. FOWLER, R. P. SHUTT, A. M. THORNDIKE and W. L. WHITEMORE: *Phys. Rev.*, **95**, 1026 (1954).

(4) E. FERMI: *Prog. Theor. Phys.*, **5**, 570 (1950).

In the usual way we can then obtain for the mean life of the τ :

$$(5) \quad w_{\tau} = \frac{0,0044}{32\pi^3} \frac{1}{\hbar} \left(\frac{g^2}{4\pi\hbar c} \right)^2 \frac{g'^2}{4\pi\hbar c} \frac{\gamma^2}{2\pi\hbar c} \frac{M^2}{\mu_{\pi}\mu_{\pi}} \mu_{\pi} c^2$$

and therefore

$$(6) \quad \frac{w_{\tau}}{w_0} \sim 0,2, \quad \frac{1}{w_{\tau}} \sim 3 \cdot 10^{-8} \text{ s.}$$

If we had treated the problem by supposing that the three pions were produced in successive independent acts, we should have obtained a longer mean life by a factor of about 10^3 .

The formulae (2), (4), (6) do not represent as yet the true mean lives, as we have to sum over all the different intermediate states corresponding to different distributions of the charge between the different virtual particles and eventually also between the final states. For example, for the Λ^0 , we have also to consider the possibility of the decay $\Lambda^0 \rightarrow N + \pi^0$, which can take place through 3 different ways of intermediate states, so that the lifetime turns out to be:

$$\tau_{\Lambda} \sim \frac{1}{10} \frac{1}{w_{\Lambda}} \sim 0,67 \cdot 10^{-10} \text{ s.}$$

For the θ and τ -particles it is more difficult to decide (as we are not yet sure how many of the hyperons we know are to be considered as intermediate states) the number of ways of decay over which we have to sum. Tentative estimates seem to indicate that we have to divide formula (3), (5) by factors of the order of 10^2 . These factors may have to be increased if we also try to apply isotopic spin formalism and consider the different possible charge states depending on it.

For example we obtain in this way for the order of magnitude of the θ and τ mean lives assuming Λ^0 and Σ^{\pm} particles in intermediate states:

$$\tau_{\theta} \sim 10^{-8} \text{ s}, \quad \tau_{\tau} \sim 4,5 \cdot 10^{-8} \text{ s.}$$

These figures, though somewhat too large may be considered in rough agreement with the probable experimental values, owing to the very simplified procedure of calculation. These examples seem therefore to indicate that the Gell-Mann Pais theory should be able to fit the experimental data as concerns the mean lives of the particles without the introduction of any new type of interaction.

Remarques sur les Interactions Électromagnétiques Multiples des Mésons μ .

D. KESSLER et R. MAZE

École Normale Supérieure - Paris

(ricevuto il 31 Marzo 1955)

Dans un travail précédent ⁽¹⁾, nous avons signalé que les effets secondaires électromagnétiques des mésons μ détectés au moyen de dispositifs de compteurs à gerbes pénétrantes ne sont pas indépendants et nous avons interprété cet effet comme étant dû à une sélection en énergie des mésons incidents. AMALDI *et al.* ⁽²⁾ ont abouti à la même conclusion. Cette opinion est cependant démentie par WOLFENDALE ⁽³⁾ et LOVATI *et al.* ⁽⁴⁾, qui se basent sur des expériences effectuées à la chambre de Wilson.

Nous avons étudié ce phénomène au cours des dernières années, en raison de son importance dans l'interprétation des expériences de compteurs sur les gerbes pénétrantes produites par les mésons μ . Les détails des expériences et les calculs sont en voie de publication ⁽⁵⁾:

Soit α le rapport entre le nombre d'évènement doubles observés et le nombre d'évènements doubles prévus (à partir du nombre d'évènements simples, comme si ces derniers étaient indépendants). Le calcul basé uniquement sur la probabilité de production d'électrons de choc (knock-on) donne alors: $\alpha(\text{sol})=1,09$; $\alpha(10 \text{ mwe})=1,10$ et $\alpha(65 \text{ mwe})=1,07$ et ces résultats sont confirmés par une expérience comportant des compteurs en verre mince et accolés. On a obtenu $(1,05 \pm 0,07)$, $(1,10 \pm 0,05)$ et $(1,19 \pm 0,10)$ respectivement. L'effet de sélection est donc faible, mais non négligeable. Ces résultats ne sont pas en désaccord avec ceux de WOLFENDALE et LOVATI *et al.* Il en est de même pour le rapport β relatif aux triples effets, pour lequel le calcul donne $\beta(65 \text{ mwe})=1,20$.

L'effet de sélection est cependant beaucoup plus accentué dès qu'on intercale des cloisons de plomb entre les compteurs, contrairement à l'opinion de WOLFENDALE ⁽³⁾. Nous avons en effet montré dans le travail cité qu'à partir de 8 mm de plomb, les compteurs sont surtout touchés par des photons dans la bande de $2 \div 7$ MeV pour lesquels le rendement des compteurs est faible. Les

⁽¹⁾ D. KESSLER et R. MAZE: *Physica*, **18**, 528 (1952).

⁽²⁾ E. AMALDI, C. CASTAGNOLI, A. GIGLI et S. SCIUTI: *Nuovo Cimento*, **9**, 969 (1952).

⁽³⁾ A. W. WOLFENDALE: *Nuovo Cimento*, **10**, 1493 (1953).

⁽⁴⁾ A. LOVATI, A. MURA et C. SUCCI: *Nuovo Cimento*, **11**, 92 (1954).

⁽⁵⁾ D. KESSLER et R. MAZE: *Physica* (1025), sous presse.

compteurs seront donc rarement saturés, ce qui conduit à considérer non pas le nombre d'interactions, mais l'énergie totale dépensée et à tenir compte également des interactions radiatives et la production directe de paires d'électrons. Le calcul donne alors $\alpha(65 \text{ mwe}) = 1,51$ et l'expérience, utilisant des cloisons de 12 mm de plomb entre les compteurs, et après déduction des interactions nucléaires qu'on a pu identifier, $\alpha(65 \text{ mwe}) = (1,73 \pm 0,21)$. Pour les événements triples, le β calculé diverge, ce qui indique un effet de sélection très prononcé que l'expérience semble confirmer avec $\beta(65 \text{ mwe}) \sim 12$. Ceci s'explique par

l'élévation de l'énergie moyenne des mésons détectés: Elle passe de 17 GeV, énergie moyenne des mésons à 65 mwe, à 90 GeV pour les mésons ayant déjà produit 2 effets. A cette énergie les effets radiatifs commencent à dominer ce qui augmente considérablement la probabilité d'obtenir des effets supplémentaires.

En conclusion, l'importance de l'effet de sélection dépend beaucoup du montage utilisé, surtout à partir des effets triples. On est donc obligé de procéder à une analyse détaillée dans les expériences destinées à mettre en évidence les gerbes pénétrantes produites par les mésons μ au moyen de dispositifs de compteurs.

ERRATA-CORRIGE

G. PLACZEK and L. VAN HOVE: **Interference Effects in the Total Neutron Scattering Cross-Section of Crystals**, *Nuovo Cimento*, 1, 233 (1955).

Errata

pag. 233 - « ricevuto il 29 Novembre 1951 »

pag. 238 - in eq. (2.14) « I_0 »

pag. 238 - on line following eq. (2.14):
« I_1 and I_2 »

pag. 238 - third line of last paragraph:
« expanding (2.13) »

pag. 240 - in third line from bottom:
« $\langle \delta S_i \rangle | \langle S_{ii} \rangle$ »

pag. 245 - left hand side of eq. (4.5):

$$\left(\frac{\delta S_i}{S_{ii}} \right)_{k_0 \rightarrow 0}$$

pag. 247 - fifth line of second paragraph:
« computation »

pag. 251 - two lines above eq. (5.22):
« $\delta S_i / S_{ii}$ »

Corrige

« ricevuto il 29 Novembre 1954 »

« $I^{(0)}$ »

« $I^{(1)}$ and $I^{(2)}$ »

« expanding (2.14) »

« $\langle \delta S_i \rangle | \langle S_{ii} \rangle$ »

$$\left(\frac{\delta S_i}{S_{ii}} \right)_{k_0 \rightarrow 0}$$

« computations »

« $5S_i / S_{ii}$ »

Über eine Approximation der Fermischen Verteilungsfunktion für positive freie Ionen.

T. TIETZ

Theoretisch-Physikalisches Institut der Universität - Lodz, Polen

(ricevuto il 12 Aprile 1955)

Für freie positive Ionen hängt die Lösung der Thomas-Fermischen Differentialgleichung ⁽¹⁾

$$(1) \quad \Phi'' = x^{-\frac{1}{2}} \Phi^{\frac{3}{2}}$$

nur vom Ionisationsgrad q ab. Die Lösung der Differentialgleichung (1) muß folgenden Randbedingungen genügen.

$$(2) \quad \Phi(0) = 1; \quad \Phi(x_0) = 0; \quad x_0 \Phi(x_0) = -q.$$

Aus der Randbedingung $\Phi(x_0) = 0$ folgt, daß die x -Achse bei $x = x_0$ geschnitten wird. Weiter aus der Randbedingung $x_0 \Phi'(x_0) = -q$ folgt nämlich, daß q die Strecke der Ordinatenachse bedeutet, welche die zum Schnittpunkt $(x_0, 0)$ gezogene und nach rückwärts verlängerte Tangente von der Ordinatenachse abschneidet. Um Φ zu bestimmen, kann man nach Fermi folgendermassen verfahren. Man setzt

$$(3) \quad \Phi(x) = \Phi_0(x) + \delta(x),$$

wo $\Phi_0(x)$ die Lösung des neutralen Atoms bedeutet und $\delta(x)$, für die x -Werte die mit x_0 verglichen genügend klein sind, eine kleine Korrektur von $\Phi_0(x)$ darstellt. Die Gleichung (3) zeigt, daß wegen der Randbedingungen

$$(4) \quad \Phi(0) = 1; \quad \Phi_0(0) = 1$$

$\delta(0) = 0$ sein muß. Fermi setzt Φ in die D-Gl (1) und entwickelt die rechte Seite nach δ/Φ_0 in einer Reihe die er nach dem zweiten Gliede abbricht, und bekommt so für δ folgende lineare Differentialgleichung

$$(5) \quad \delta'' = \frac{3}{2} \left(\frac{\Phi_0}{x} \right)^{\frac{1}{2}} \delta.$$

⁽¹⁾ E. FERMI: *Mens. Acc. Italia*, **1**, 1 (1930); P. GOMBAS: *Die statistische Theorie des Atoms und ihre Anwendungen* (Wien, 1949), S. 47-54.

Fermi setzt weiter

$$(6) \quad \delta(x) = K \eta_0(x),$$

wo K eine von q abhängige Konstante bedeutet; die Funktion η_0 genügt dann folgender Differential-Gleichung

$$(7) \quad \eta_0'' = \frac{3}{2} \left(\frac{\Phi_0}{x} \right)^{\frac{1}{2}} \eta_0,$$

und die Anfangsbedingungen

$$(8) \quad \eta_0(0) = 0; \quad \eta_0'(0) = 1.$$

Im folgenden wird eine Approximation für die Funktion η_0 gegeben. Es ist bekannt, daß die Funktion ⁽²⁾

$$\eta_0(x) = \frac{b^2}{(b+x)^2} = \frac{1}{(1+ax)^2} \quad \begin{matrix} b = 1,75661, \\ a = 0,569272. \end{matrix}$$

ziemlich gut die Differential-Gleichung des neutralen Atoms erfüllt (*) und damit können wir (9) verwenden um (7) zu lösen. Zuerst schreiben wir (7) in folgender Form

$$(10) \quad \eta_0'' = \frac{3}{2} \left(\frac{\Phi_0}{x} \right)^{\frac{1}{2}} \eta_0 = \frac{3}{2} \left(\frac{\Phi_0''}{\Phi_0} \right)^{\frac{1}{2}} \eta_0,$$

und setzen für Φ_0 die Funktion (9) ein; wir bekommen so folgende Differential-Gleichung für η_0

$$(11) \quad \eta_0'' - \frac{9a^2}{(1+ax)^2} \eta_0 = 0.$$

Die allgemeine Lösung der Differential-Gleichung (11) ist, wie eine leichte Rechnung zeigt, die folgende

$$(12) \quad \eta_0(x) = \left[-\frac{C_1}{\sqrt{37}} \left(\frac{a}{1+ax} \right)^{-\sqrt{37}} + C_2 \right] \left(\frac{a}{1+ax} \right)^{-\frac{1}{2} + \frac{1}{2}\sqrt{37}}.$$

Weiter müssen wir die Konstanten C_1 , C_2 so bestimmen, daß die Anfangsbedin-

(*) T. TIEZ: *Journ. Chem. Phys.*, **22**, 2094 (1954); *Ann. der Phys.* **15**, (1955).

(*) Der Wert von $b = 1,86478$ wurde nach dem Vorschlag von Prof. Dr. K. UMEMA zu $b = 1,75661$ abgeändert.

gungen (8) erfüllt werden. Die Bestimmung der Konstanten gibt uns folgende Lösung

$$(13) \quad \eta_0(x) = \frac{1}{a\sqrt{37}} \frac{(1+ax)^{\frac{1}{2}}}{(1+ax)^{\frac{1}{2}\sqrt{37}}} [(1+ax)^{\sqrt{37}} - 1].$$

Wenn wir uns für die Funktion η_0 auf zwei Dezimale beschränken, so zeigt uns die folgende Tabelle wie unsere Approximation verläuft.

TABELLE I. — Werte von η_0 .

x	η_0		x	η_0	
	FERMI	TIETZ		FERMI	TIETZ
0,0	0,00	0,00	0,9	1,18	1,15
0,1	0,10	0,10	1,0	1,36	1,33
0,2	0,21	0,22	1,2	1,76	1,75
0,3	0,32	0,31	2,0	4,04	4,25
0,4	0,44	0,44	4,0	16,7	19,3
0,5	0,56	0,55	5,0	28,6	30,2
0,6	0,70	0,68	8,0	103,0	118
0,7	0,85	0,82	15,0	755,0	758
0,8	1,01	0,96	20,0	2080	2142

A. SOMMERFELD⁽³⁾ hat eine Näherungslösung für positive Ionen abgeleitet. Die Sommerfeldsche Approximation $_{80}\Phi$ die der Randbedingung $\Phi(x_0) = 0$ genügt hat die Form

$$(14) \quad \Phi(x) = \frac{1}{(1+z)^{\lambda_1/\lambda_2}} \left[1 - \left(\frac{1+z}{1+z_0} \right)^{\lambda_1/\lambda_2} \right],$$

wo z , λ_1 , λ_2 folgende Bedeutung haben

$$(15) \quad z = \left(\frac{x}{144^{\frac{1}{2}}} \right)^{\lambda_2}; \quad \lambda_1 = 8; \quad \lambda_1 \cdot \lambda_2 = 6.$$

Die Sommerfeldsche Näherungslösung $_{80}\Phi$ genügt nicht genau der Randbedingung $\Phi(0)=1$. Die Bestimmung von x_0 geschieht mit Hilfe der Nebenbedingung $x_0 \Phi'(x_0) = -q$, die wegen der Randbedingung $\Phi(x_0) = 0$ uns folgende Gleichung gibt:

$$(16) \quad q = \frac{ax_0}{(1+ax)^3} \left[\frac{1}{2} (5 + \sqrt{37}) + \frac{\sqrt{37}}{[(1+ax_0)^{\sqrt{37}} - 1]} \right].$$

Zum Schluss gebe ich eine Tabelle für x_0 für verschiedene Ionisationsgrade q

(³) A. SOMMERFELD: *Zeits f. Phys.*, **78**, 283 (1932).

TABELLE II. — Werte von x_0 für verschiedene Werte von q .

q nach FERMI und SOMMERFELD	q nach TIETZ	x_0 nach FERMI und TIETZ	x_0 nach SOMMERFELD
0,10	0,88	11,2	10,64
0,08	0,07	12,9	12,18
0,05	0,048	16,2	15,81
0,03	0,03	21,1	20,54

Der Vergleich zeigt, daß in unserer Approximation Gl. (2) genügend gute Werte gibt

$$(17) \quad \tau_1 \Phi(x) = \frac{1}{(1+ax)^3} + \frac{K}{a\sqrt{37}} \frac{(1+ax)^{\frac{1}{2}}}{(1+ax)^{\frac{1}{2}\sqrt{37}}} [(1+ax)^{\frac{1}{2}\sqrt{37}} - 1],$$

$$K = - \frac{a\sqrt{37}(1+ax_0)^{-\frac{5}{2}+\frac{1}{2}\sqrt{37}}}{[(1+ax_0)^{\frac{1}{2}\sqrt{37}} - 1]}.$$

Weitere Untersuchungen für die Näherungslösung für freie positive Ionen sind im Gange. Es steht fest, daß man für

$$(18) \quad \Phi_0(x) = \frac{1}{(1+ax)^\alpha} \quad \begin{array}{ll} \alpha = 9/5 & a = 0,645996 \\ \alpha = 7/5 & a = 0,881206 \end{array}$$

bessere Resultate bekommt.

Diese Arbeit widme ich meinem Lehrer Prof. Dr. F. J. WIŚNIEWSKI zu seinem 65. Geburtstage für sein menschliches Entgegenkommen.

Decay of ^{103}Ru .

H. H. FORSTER and A. ROSEN

Department of Physics, University of Southern California - Los Angeles, California

(ricevuto il 15 Aprile 1955)

In recent studies of Coulomb excitation of ^{103}Rh HEYDENBURG and TEMMER⁽¹⁾ observed γ -rays of energies 295 and 357 keV, corresponding to transitions from energy levels at 295 and 357 keV to the ground state. Studies on the decay of $^{103}\text{Pd} \rightarrow ^{103}\text{Rh}$ by RIETJENS *et al.*⁽²⁾ have revealed that energy levels at 300 and 365 keV, presumably identical with the above, are excited in the ^{103}Pd decay. Since ^{103}Ru decays to the same residual nucleus an excitation of the same energy levels is to be expected. However, although the decay of ^{103}Ru has been intensively investigated^(3,10) no indication of such

an excitation has been found. Under these circumstances further studies of the decay scheme of ^{103}Ru seemed indicated.

The β -spectrum of ^{103}Ru was observed with a double thin lens β -ray spectrometer described in more detail elsewhere⁽¹¹⁾. ^{103}Ru was obtained from the Isotope Division at Oak Ridge and from Chalk River, Canada; the former as ruthenium trichloride in hydrochloride acid solution, the latter in solid form. The detector was a conventional type Geiger-Müller counter with replaceable end window, pressure sealed by O-rings; thin nylon films, $10 \div 50 \mu\text{g}/\text{cm}^2$ thick, were used as counter windows. The counting circuit was a modified model No. 200 pulse counter⁽¹²⁾. Thin uniform sources were deposited on nylon or tygon films (sources $\sim 20 \mu\text{g}/\text{cm}^2$, films $\sim 10 \mu\text{g}/\text{cm}^2$ thick) and the films supported by a lucite cylinder the sides of which had been milled so as to leave only a narrow ring held by four thin strips. The resolution of the instrument varied between 1% and 2.5%.

(¹) N. P. HEYDENBURG and G. M. TEMMER: *Phys. Rev.*, **95**, 861 (1954).

(²) L. H. TH. RIETJENS, H. J. VAN DEN BOLD, and P. M. ENDT: *Physica*, **20**, 107 (1954).

(³) E. BOHR and N. HOLE: *Ark. Mat. Astr. fys.*, **32A**, 15 (1945).

(⁴) N. HOLE: *Ark. Mat. Astr. fys.*, **36A**, 2 (1948).

(⁵) C. MANDEVILLE and E. SHAPIRO: *Phys. Rev.*, **77**, 439 (1950).

(⁶) MEI, HUDDLESTON, and MITCHELL: *Phys. Rev.*, **79**, 429 (1950).

(⁷) E. KONDIAR: *Phys. Rev.*, **79**, 891 (1950).

(⁸) A. W. KNUDSEN, *Phys. Rev.*, **86**, 571 (1952).

(⁹) J. M. CORK, J. M. LEBLANC, F. B. STUMPF, and W. H. NESTER: *Phys. Rev.*, **86**, 575 (1952).

(¹⁰) B. SARAF: *Phys. Rev.*, **97**, 715 (1955).

(¹¹) C. M. VAN ATTA, S. D. WARSHAW, J. J. L. CHEN, and S. I. TAIMUTY: *Rev. Sci. Instr.*, **21**, 985 (1950).

(¹²) W. A. HIGINBOTHAM: *Rev. Sci. Instr.*, **18**, 1706 (1947).

A Fermi Plot of the β -spectrum of ^{103}Ru is shown in fig. 1; an analysis of the β -spectrum reveals the presence of

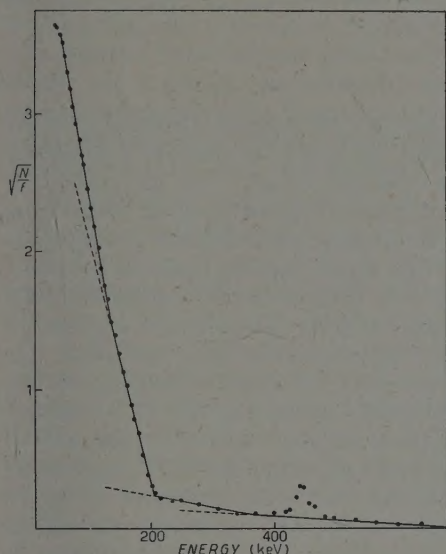


Fig. 1.

three β -groups with endpoint energies of 128 ± 4 keV (28%), 202 ± 2 keV (70%), and 695 ± 15 keV ($\sim 1\%$). The Fermi plot of the first two groups is straight, indicating allowed transitions ($\log ft \sim 4$). The Fermi plot of the high energy, β -group appears to be curved; however the low ft value of the transition ($\log ft \sim 5$) leads one to expect an allowed transition. While the possibility that spurious counts give the illusion of curvature cannot definitely be ruled out a different interpretation should be

considered; namely that the experimental results are compatible with the existence of a fourth β -group of maximum energy 374 ± 20 keV (1%).

The γ -spectrum of ^{103}Ru obtained with a NaI crystal spectrometer with a single channel pulse height analyzer showed γ -lines of 55, 498 and 610 keV. However, the photoelectron spectrum obtained with the β -ray spectrometer by placing a 30 mg/cm^2 Pb converter in front of the radioactive source produced additional lines. Photoelectron peaks were found at 210, 236 and 279 keV, corresponding to γ -ray energies of 297, 323 and 366 keV respectively.

The results of this experiment indicate that the energy levels at 295 and 365 keV which have been interpreted ⁽¹⁾ as rotational levels of the collective model of the nucleus are excited through the decay of ^{103}Ru . The 295 keV γ -seems to correspond to a transition from the 295 keV level to the ground state, the 325 and 365 keV gammas to transitions from the 365 keV level to the isomeric state and the ground state respectively.

No β transitions to the rotational levels have definitely been identified. A 374 keV β -group, postulated because of a better fit to the Fermi plot, would excite an energy level at ~ 365 keV; however, the small ft value of the transition makes the required change in parity rather doubtful. A β -transition to the 295 keV level has not been found; but such a transition would be difficult to detect due to the presence of the 498 keV γ conversion line.

A. PERUSSIA e coll. - *Medicina Nucleare*, un vol. in 8° di XII+877 p., 143 fig. e XXIII tab. « Il pensiero Scientifico Editore, Roma, 1954. L. 7000.

Mentre l'elenco dei libri italiani di fisica pura continua ad essere brevissimo, comprendendo, è vero, alcuni ottimi trattati, ma praticamente nessun lavoro di carattere monografico, quello dei libri dedicati alle applicazioni medico-biologiche della fisica nucleare si arricchisce ogni anno di qualche nuovo volume. È da notare per altro che questi volumi non sono di solito dovuti alla penna di un fisico, oppure i fisici contribuiscono ad essi solo in veste di collaboratori, per alcune ristrette parti a carattere generale e introduttivo.

Ciò è vero anche per il libro di cui dobbiamo oggi occuparci, il quale per altro si distingue dai precedenti innanzi tutto per la mole e l'impegno. Esso è stato diretto e per la massima parte scritto dal Prof. A. PERUSSIA, nella sua qualità di capo del gruppo medico-biologico del Centro Informazioni Studi Esperimenti di Milano. Egli, che ricopre la carica di assistente all'Istituto Nazionale per lo studio e la cura dei tumori di Milano, e quella di incaricato presso la Facoltà di Medicina Veterinaria dell'Università di quella città, si è valso, per la compilazione di alcuni capitoli di carattere generale o strumentale, della collaborazione di un gruppo di eminenti fisici, chimici e ingegneri del suddetto Centro, dell'Università e del Politecnico (U. FACCHINI, E. GATTI, L. MALATESTA, C. SALVETTI, M. SILVESTRI).

Dopo tre « Prefazioni », una « Premessa » dell'Autore (5 pagine) e una « Intro-

duzione » (18 pagine) dichiarante le ragioni dell'opera, la materia è suddivisa in quattro « Parti » ed un gruppo di « Appendici » (costituenti in realtà una quinta parte) per complessive 843 pagine.

La prima parte ha carattere introduttivo e propedeutico. Comprende: elementi di fisica nucleare (SALVETTI); principi di dosimetria delle radiazioni (A. PERUSSIA); produzione artificiale di radiazioni (macchine acceleratrici: GATTI; reattori nucleari: SALVETTI); elementi di radiochimica (MALATESTA); osservazioni generali sul comportamento biologico degli isotopi (A. PERUSSIA). La vastità della materia, trattata in 113 pagine, fa sì che molti argomenti siano appena sfiorati, con vantaggio assai dubbio per il lettore, biologo o fisico che sia. Probabilmente sarebbe meglio omettere certi capitoli generali e generici, che, scritti spesso con evidente malavoglia dal collaboratore non medico per dover dire troppo e troppo poco a un tempo, non sono esenti da mende, e rinviare francamente il lettore ad altri testi.

La seconda parte, di 92 pagine, è dedicata alle tecniche, per la rivelazione e la misura di radiazioni, limitatamente a quelle che si basano sul potere ionizzante delle radiazioni, ai contatori a scintillazione e ai metodi fotografici. Ad essa hanno collaborato con PERUSSIA, GATTI e FACCHINI. Non molto felice la suddivisione della materia in due capitoli. Nel primo si descrivono i vari mezzi strumentali e nel secondo se ne discute l'impiego ai fini della misura: la distinzione tra i due punti di vista, concettualmente chiara, nella pratica sfuma e causa indecisione e tortuosità nel filo conduttore dell'opera. In un terzo capitolo sono raccolti i dati relativi ai radio-

isotopi più importanti dal punto di vista biofisico. È spiacevole che gli schemi di decadimento siano qui presentati in modo non convenzionale. Ciò genererà certamente confusione nella mente del lettore non pratico. Non bisogna dimenticare infatti che i grafici convenzionali (numero atomico in ascisse, energia in ordinate) visualizzano e distinguono tra loro in modo assai chiaro i vari processi.

Le parti terza (93 pagine) e quarta (418 pagine) costituiscono il nucleo centrale dell'opera e sono dedicate l'una all'impiego dei radioisotopi nella ricerca biologica e nell'indagine clinica, l'altra alle applicazioni della fisica nucleare in terapia. Salta immediatamente agli occhi il peso enormemente maggiore dato alla terapia, nei confronti della ricerca e della diagnostica. Questa sproporzione che pensiamo sia conseguenza della formazione dell'Autore, radiologo, non corrisponde certamente all'importanza relativa delle due branche. Tanto più grave essa risulta, se si pensa che mentre il metodo dei traccianti ha assunto una sua fisiologia definitiva e portato innumerevoli frutti in tutti i campi e in particolare nella ricerca biofisica, aprendo alla diagnostica possibilità inaspettate, gli effetti biologici delle radiazioni (che stanno alla base delle applicazioni di carattere terapeutico) costituiscono ancor oggi materia estremamente fluida, non sistemata e in gran parte non capita: argomento che quindi, almeno per la maggior parte, non è ancora da trattato a carattere istituzionale, ma da ricerca ed eventualmente da monografia specializzata.

Nella terza parte, si espone dapprima la teoria generale del metodo dei traccianti, venendo a un compromesso, non sappiamo quanto vantaggioso, tra matematica e divulgazione. Segue una rapida rassegna informativa delle principali applicazioni del metodo alla ricerca biologica.

La quarta parte è a sua volta suddivisa in quattro capitoli, il primo dei quali (61 pagine) è dedicato alla radio-

terapia tradizionale, il secondo (80 pagine) alla radioterapia esterna con radiazioni di elevatissima energia e con neutroni, il terzo (63 pagine) alla radioterapia esterna con radionuclidi artificiali e il quarto (214 pagine) alla radioterapia interna pure con radionuclidi artificiali. Una tale suddivisione della materia, parzialmente basata su criteri (origine delle radiazioni) estranei al fatto biologico, non è certamente molto soddisfacente. I principi dei metodi, i risultati di carattere generale e orientativo, le applicazioni di carattere particolare non risultano così sufficientemente distinti e in questa, più ancora che nelle precedenti parti del volume, la mancanza di sintesi e la prolissità addirittura eccessiva del discorso appesantiscono l'esposizione, tanto che spesso lasciano al lettore una impressione confusa.

Le appendici (123 pagine) sono dedicate ai rischi biologici da radiazioni ionizzanti, a una tabella di isotopi stabili e radioattivi e ad un breve avviamento bibliografico, per ulteriori studi. L'esame dei libri citati in quest'ultimo elenco lascia spesso, a dire il vero, alquanto perplessi: se infatti si considera che opere di alta fisica teorica vengono allineate con altre di divulgazione, e che libri di vent'anni fa, ormai superati, sono ricordati a fianco di pubblicazioni recentissime e specializzate, vien fatto di dubitare che esso, in tutti i casi, sia il frutto di conoscenza ed esame critico personale.

Concludendo, nonostante le critiche da noi fatte fin qui (e le numerose sviste, inesattezze, ecc., forse inevitabili in una pubblicazione del genere, sulle quali per brevità abbiamo sorvolato) fa piacere riconoscere che la fatica sostenuta dagli Autori è veramente encomiabile per impegno e intendimento, e che il volume può essere utile (chi scrive l'ha già adoperato più d'una volta) anche se poi non costituisce intrinsecamente un deciso progresso rispetto alle precedenti pubblicazioni italiane sullo stesso argomento.

M. AGENO

N. F. RAMSEY - *Nuclear Moments*
x+169 pag., 38 fig., J. Wiley &
Sons Inc. New York; Chapman
& Hall, lim. London 1953.

Le ricerche sui momenti nucleari, che fino a una decina d'anni fa costituivano il monopolio di pochi laboratori specializzati, hanno avuto recentemente un grande sviluppo. Ciò è dovuto soprattutto alla rapida diffusione delle tecniche fondate sull'induzione e sull'assorbimento paramagnetico nucleare di risonanza e sulla spettroscopia con microonde.

Il libro di N. F. RAMSEY offre una sintesi del lavoro compiuto in questo campo. I primi quattro capitoli sono una riedizione dell'articolo dello stesso autore *Nuclear Moments and Statistics* facente parte del primo volume dell'*Experimental Nuclear Physics*, edito da E. SEGRÈ. A quell'articolo è stato aggiunto un quinto capitolo, di interesse non predominante per la fisica nucleare, riguardante

le applicazioni alla chimica e alla fisica dello stato solido.

Per quanto riguarda la parte comune al trattato di SEGRÈ il lettore può confrontare la recensione del trattato stesso fatta da M. AGENO (*Nuovo Cimento*, 11, 332 (1954)).

Il 5° capitolo tratta delle interazioni di spin e di quadrupolo nelle molecole e nei cristalli, dell'effetto dello schermaggio elettronico sulle risonanze nucleari, dei momenti magnetici rotazionali delle molecole, della spettroscopia con microonde e delle risonanze paramagnetiche e ferromagnetiche. Vi è infine un'appendice sulla struttura a shell dei nuclei.

L'esposizione è molto sintetica, ma concettualmente chiara. Il volume di RAMSEY, che è corredato di una sufficientemente ampia bibliografia, può quindi fornire un primo utile orientamento a chi voglia approfondire qualcuno degli argomenti in esso trattati.

L. GIULOTTO

PROPRIETÀ LETTERARIA RISERVATA

Direttore responsabile: G. POLVANI

Tipografia Compositori - Bologna

Questo fascicolo è stato licenziato dai torchi il 26-IV-1955